ADVANCED ONLINE BATTERY STATES CO-ESTIMATION USING KALMAN FILTER FOR ELECTRIC VEHICLE APPLICATIONS

PRASHANT SHRIVASTAVA

FACULTY OF COMPUTER SCIENCE AND INFORMATION TECHNOLOGY
UNIVERSITY OF MALAYA
KUALA LUMPUR

2021

ADAVANCED ONLINE BATTERY STATES CO-ESTIMATION USING KALMAN FILTER FOR ELECTRIC VEHICLE APPLICATIONS

PRASHANT SHRIVASTAVA

THESIS SUBMITTED IN FULFILMENT OF THE REQUIREMENTS FOR THE DEGREE OF DOCTOR OF PHILOSOPHY

FACULTY OF COMPUTER SCIENCE AND INFORMATION TECHNOLOGY
UNIVERSITY OF MALAYA
KUALA LUMPUR

2021

UNIVERSITY OF MALAYA

ORIGINAL LITERARY WORK DECLARATION

Name of Candidate: Prashant Shrivastava

Matric No: 17006320/1/WVA170058

Name of Degree: Doctor of Philosophy

Title of Thesis: Advanced online battery states co-estimation using Kalman filter for electric vehicle applications

Field of Study: Modelling, Simulation and Systems Performance

I do solemnly and sincerely declare that:

(1) I am the sole author/writer of this Work;
(2) This Work is original;
(3) Any use of any work in which copyright exists was done by way of fair dealing and for permitted purposes and any excerpt or extract from, or reference to or reproduction of any copyright work has been disclosed expressly and sufficiently and the title of the Work and its authorship have been acknowledged in this Work;
(4) I do not have any actual knowledge nor do I ought reasonably to know that the making of this work constitutes an infringement of any copyright work;
(5) I hereby assign all and every rights in the copyright to this Work to the University of Malaya ("UM"), who henceforth shall be owner of the copyright in this Work and that any reproduction or use in any form or by any means whatsoever is prohibited without the written consent of UM having been first had and obtained;
(6) I am fully aware that if in the course of making this Work I have infringed any copyright whether intentionally or otherwise, I may be subject to legal action or any other action as may be determined by UM.

Candidate's Signature Date: 12/10/2021

Subscribed and solemnly declared before,

Witness's Signature Date: 13/10/2021

Name:

Designation:

UNIVERSITI MALAYA

PERAKUAN KEASLIAN PENULISAN

Nama: Prashant Shrivastava

No. Matrik: 17006320/1/WVA170058

Nama Ijazah: Doktor Falsafah

Tajuk Tesis : Penganggaran Bersama Keadaan Bateri Atas Talian Termaju Menggunakan Penuras Kalman Untuk Aplikasi Kenderaan Elektrik

Bidang Penyelidikan: Pemodelan, Simulasi dan Prestasi Sistem

Saya dengan sesungguhnya dan sebenarnya mengaku bahawa:

(1) Saya adalah satu-satunya pengarang/penulis Hasil Kerja ini;
(2) Hasil Kerja ini adalah asli;
(3) Apa-apa penggunaan mana-mana hasil kerja yang mengandungi hakcipta telah dilakukan secara urusan yang wajar dan bagi maksud yang dibenarkan dan apa-apa petikan, ekstrak, rujukan atau pengeluaran semula daripada atau kepada mana-mana hasil kerja yang mengandungi hakcipta telah dinyatakan dengan sejelasnya dan secukupnya dan satu pengiktirafan tajuk hasil kerja tersebut dan pengarang/penulisnya telah dilakukan di dalam Hasil Kerja ini;
(4) Saya tidak mempunyai apa-apa pengetahuan sebenar atau patut semunasabahnya tahu bahawa penghasilan Hasil Kerja ini melanggar suatu hakcipta hasil kerja yang lain;
(5) Saya dengan ini menyerahkan kesemua dan tiap-tiap hak yang terkandung di dalam hakcipta Hasil Kerja ini kepada Universiti Malaya ("UM") yang seterusnya mula dari sekarang adalah tuan punya kepada hakcipta di dalam Hasil Kerja ini dan apa-apa pengeluaran semula atau penggunaan dalam apa jua bentuk atau dengan apa juga cara sekalipun adalah dilarang tanpa terlebih dahulu mendapat kebenaran bertulis dari UM;
(6) Saya sedar sepenuhnya sekiranya dalam masa penghasilan Hasil Kerja ini saya telah melanggar suatu hakcipta hasil kerja yang lain sama ada dengan niat atau sebaliknya, saya boleh dikenakan tindakan undang-undang atau apa-apa tindakan lain sebagaimana yang diputuskan oleh UM.

Tandatangan Calon Tarikh: 12/10/2021

Diperbuat dan sesungguhnya diakui di hadapan,

Tandatangan Saksi Tarikh: 13/10/2021

Nama:

Jawatan:

ADVANCED ONLINE BATTERY STATES CO-ESTIMATION USING KALMAN FILTER FOR ELECTRIC VEHICLE APPLICATIONS

ABSTRACT

Carbon impression and the growing reliance on fossil fuels are two unique concerns for world emission regulatory agencies. These issues have placed electric vehicles (EVs) powered by lithium-ion batteries (LIBs) on the forefront as alternative vehicles. The LIB has noticeable features, including high energy and power density, compared with other accessible electrochemical energy storage systems. However, LIB is exceedingly nonlinear and dynamic; therefore, it requires an accurate state estimation technique in a battery management system (BMS). Due to the existing correlation between the battery states, the co-estimation method for different battery states estimation is preferred over individual state estimation. Though, the trade-off between accuracy and computational burden of the co-estimation method is difficult to maintain in real-time application. This thesis focuses on the development of the co-estimation methods of lithium-ion battery states of interest, which are capable to improve the efficiency of BMS, especially for EV applications.

To achieve high estimation accuracy at a low cost, the co-estimation method for state of charge (SOC) and state of energy (SOE) is investigated in the first phase of the thesis. A new dual forgetting factor-based adaptive extended Kalman filter (DFFAEKF) algorithm to concurrently estimate the electrical equivalent circuit model parameters and SOC at high accuracy is first developed. The DFFAEKF algorithm has the feature to reduce the possibility of battery model parameter divergence from the true value under different dynamic conditions with the same order of big O notation complexity as DEKF. Thereafter, with the credible SOC estimation by using DFFAEKF, a co-estimation method for SOC and SOE using a quantitative relationship between SOC and SOE is

developed. The simplicity of the proposed co-estimation method can avoid the heavy computational burden required by the individual state estimation of SOC and SOE.

Finally, to effectively utilize the correlation amongst battery states and reduce the computational burden of the BMS, a unified frame of co-estimation method for battery states including SOC, SOE, state of power (SOP). actual capacity and maximum available energy is developed. In addition to co-estimation of SOC and SOE in the first method, the SOP estimation is performed by using identified Rint battery model parameters using the forgetting factor recursive least square (FFRLS) algorithm. Next, the actual capacity and maximum available energy estimation are performed by using a new sliding window-approximate weighted total least square (SW-AWTLS) algorithm at a low computational burden. The performance of the proposed co-estimation methods are experimentally verified with battery cells of different chemistries and dynamic load profiles which suitable for EV. Besides, the low computational burden of the proposed co-estimation, the results demonstrate the high accuracy of the battery states estimation irrespective of the change in battery chemistry under-considered dynamic operating conditions.

With the effective utilization of battery states correlation and high estimation accuracy of the battery states co-estimation methods, the performance of the BMS can be significantly improved. Furthermore, the proposed co-estimation methods in this thesis can contribute to the safe, reliable, and efficient utilization of the LIBs used in EV applications.

Keywords: Battery State; Electrical equivalent circuit model (EECM); Kalman Filter (KF); Lithium-ion battery (LIB); Electric Vehicle (EV).

PENGANGGARAN BERSAMA KEADAAN BATERI ATAS TALIAN TERMAJU MENGGUNAKAN PENURAS KALMAN UNTUK APLIKASI KENDERAAN ELEKTRIK

ABSTRAK

Kesan karbon dan pergantungan yang semakin meningkat pada bahan bakar fosil adalah dua keprihatinan unik bagi agensi pengawalan pelepasan dunia. Isu-isu ini telah meletakkan kenderaan elektrik (EV) yang dikuasakan oleh bateri lithium-ion (LIB) di barisan hadapan sebagai kenderaan alternatif. LIB mempunyai ciri-ciri yang ketara, termasuk ketumpatan tenaga dan tenaga yang tinggi, berbanding dengan sistem penyimpanan tenaga elektrokimia yang lain. Walau bagaimanapun, LIB sangat tidak linear dan dinamik; oleh itu, secara amnya memerlukan teknik anggaran keadaan yang tepat dalam sistem pengurusan bateri (BMS). Oleh kerana terdapat hubungan antara keadaan bateri, kaedah anggaran bersama untuk anggaran keadaan bateri yang berbeza lebih disukai daripada anggaran keadaan individu. Walaupun begitu, keseimbangan antara ketepatan dan beban komputasi kaedah pengiraan bersama sukar dikekalkan dalam aplikasi sebenar. Tesis ini memfokuskan kepada pengembangan kaedah anggaran bersama keadaan bateri lithium-ion yang menarik, yang mampu meningkatkan kecekapan BMS, terutamanya untuk aplikasi EV.

Untuk mencapai ketepatan anggaran yang tinggi dengan kos rendah, kaedah anggaran bersama untuk keadaan cas (SOC) dan keadaan tenaga (SOE) disiasat pada fasa pertama tesis. Algoritma penapis Kalman (DFFAEKF) pelengkap adaptif berasaskan faktor lupa dua yang baru untuk secara bersamaan menganggarkan parameter model litar setara elektrik dan SOC pada ketepatan tinggi mula-mula diperkembangkan. Algoritma DFFAEKF mempunyai ciri untuk mengurangkan kemungkinan perbezaan parameter model bateri dari nilai sebenarnya dalam keadaan dinamik yang berbeza dengan kerumitan notasi O susunan yang sama dengan DEKF. Selepas itu, dengan perkiraan SOC

yang boleh dipercayai dengan menggunakan DFFAEKF, kaedah perkiraan bersama untuk SOC dan SOE menggunakan hubungan kuantitatif antara SOC dan SOE diperkembangkan. Keberkesanan kaedah penganggaran bersama yang dicadangkan dapat mengelakkan beban komputasi berat yang diperlukan oleh anggaran keadaan individu untuk SOC dan SOE.

Akhirnya, untuk memanfaatkan korelasi antara keadaan bateri dengan berkesan dan mengurangkan beban komputasi BMS, satu kaedah taksiran bersama bagi keadaan bateri termasuk SOC, SOE, state of power (SOP), kapasiti sebenar, dan tenaga maksimum yang ada diperkembangkan. Sebagai tambahan kepada pengiraan bersama SOC dan SOE dalam kaedah pertama, anggaran SOP dilakukan dengan menggunakan parameter model bateri Rint yang dikenal pasti dengan menggunakan algoritma faktor terlupa rekursif kuasa dua terkecil (FFRLS). Seterusnya, kapasiti sebenar dan anggaran tenaga maksimum yang ada dilakukan dengan menggunakan algoritma slaid tingkap-perkiraan jumlah paling sedikit persegi (SW-AWTLS) baru dengan beban pengiraan yang rendah. Prestasi kaedah penganggaran bersama yang dicadangkan disahkan secara eksperimen dengan sel kimia bateri yang berbeza dan profil beban dinamik yang sesuai untuk EV. Selain itu, beban komputasi yang rendah dari penganggaran bersama yang dicadangkan, hasilnya menunjukkan ketepatan anggaran tinggi dari keadaan bateri tanpa mengira perubahan kimia bateri dalam keadaan operasi dinamik yang dipertimbangkan.

Dengan penggunaan korelasi keadaan bateri yang berkesan dan ketepatan anggaran yang tinggi bagi kaedah pengiraan bersama keadaan, prestasi BMS dapat meningkat dengan ketara. Selanjutnya, kaedah penganggaran bersama yang dicadangkan dalam tesis ini dapat menyumbang kepada penggunaan LIB yang selamat, boleh dipercayai, dan efisien yang digunakan dalam aplikasi EV.

Keywords: Keadaan Bateri; Model litar setara elektrik (EECM); Penapis Kalman (KF); Bateri ion litium (LIB); Kenderaan Elektrik (EV).

ACKNOWLEDGEMENTS

All praises to God for the strengths and blessing in completing this thesis.

With the sincerest gratitude in my heart, I would like to thank my academic supervisors Dr. Tey Kok Soon, Dr. Mohd Yamani Idna Bin Idris, Professor Saad Mekhilef, and Dr. Syed Bahari Ramadzan Syed Adnan, for their support and encouragement throughout my candidature. It is a great honor for me to have the opportunity to learn from and with them.

I would like to thank Mrs. Noor Fhadzilah Binti Mansur, Assistant Science Officer, Physics Division, Centre for Foundation Studies in Science, University Malaya for her valuable support in the battery testing.

I greatly appreciate the helpful advice and technical support from my colleagues and friends in the Power Electronics and Renewable Energy Research Laboratory, Faculty of Engineering, University of Malaya (UM), etc., in particular, Mr. Marif Dual Siddique, Mr. Asif Mustafa, Mr. Immad Shams, Mr. Shameem Ahmad, and Mr. Leong Wen Chek.

I wish to give special thanks to my family and my wife for their everlasting moral support and encouragement, without whom, this journey would have not been possible.

In addition, I also would like to thank my beloved daughter, who joined us when I was writing my thesis, for giving me unlimited happiness and pleasure. Remembering her wonderful and gentle soul will forever remain in our hearts. May she rest in peace!

TABLE OF CONTENTS

LIST OF FIGURES

LIST OF TABLES

LIST OF SYMBOLS AND ABBREVIATIONS

AEKF	:	Adaptive extended Kalman filter
AWTLS	:	Approximate weighted total least square
BMS	:	Battery management system
DAEKF	:	Dual adaptive extended Kalman filter
DEKF	:	Dual extended Kalman filter
DFFAEKF	:	Dual forgetting factor-based adaptive extended Kalman filter
DST	:	Dynamic stress test
E_n	:	Actual energy or maximum available energy in Wh
ECM	:	Electrochemical model
EECM	:	Electrical equivalent circuit model
EKF	:	Extended Kalman filter
EV	:	Electric vehicle
FFAEKF	:	Forgetting factor-based adaptive extended Kalman filter
FFRLS	:	Forgetting factor recursive least square
FUDS	:	Federal urban drive schedule
HPPC	:	Hybrid pule power characterization
KF	:	Kalman filter
LIB	:	Lithium-ion battery
MAE	:	Mean absolute error
MaxAE	:	Maximum absolute error
MBM	:	Model-based method
MET	:	Mean execution time
$O(.)$	:	Big O notation

OCV	:	Open circuit voltage
Q_n	:	Actual capacity in Ah
RLS		Recursive least square
RMSE	:	Root mean square error
SOC	:	State of Charge
SOE	:	State of Energy
SOH	:	State of Health
SOP	:	State of Power
SW-AWTLS	:	Sliding window-approximate weighted total least square
$T(.)$	:	Running time

LIST OF APPENDICES

CHAPTER 1: INTRODUCTION

1.1 Background and Motivation

The efficient deployment of Electric Vehicles (EVs) in the world transportation system is one of the appealing solutions to decrease greenhouse gases emission and boost energy efficiency. As per the Global EV outlook 2018 (IEA International Energy Agency, 2018), the worldwide automobile market will be successfully deploy 117.6 million EVs on the road, and that will contribute to reducing 262 Mt CO_2 emission by 2030. The potential advantages of Lithium-ion batteries (LIBs) intrigue the EVs manufacturer companies to utilize them as the primary source of an energy storage system (Peters et al., 2017; Zubi et al., 2018). However, high cost, low production capacity, and highly dynamic nature are the real worries that confine its successive application in EV (Hannan, Hoque, et al., 2017a). According to data collected by Bloomberg (*This Is the Dawning of the Age of the Battery - Bloomberg*, n.d.), the cumulative demand of LIB expected to tough the unthinkable number 9,300 GWh by 2030, as presented in Figure 1.1. Also, the worldwide cost and production capacity of the LIB pack are improving continuously, as shown in Figure 1.2. As reported by Bloomberg, the worldwide LIB pack cost will drop to nearly 90 % as compared to 2010 and reached 73 USD/kWh by 2030.

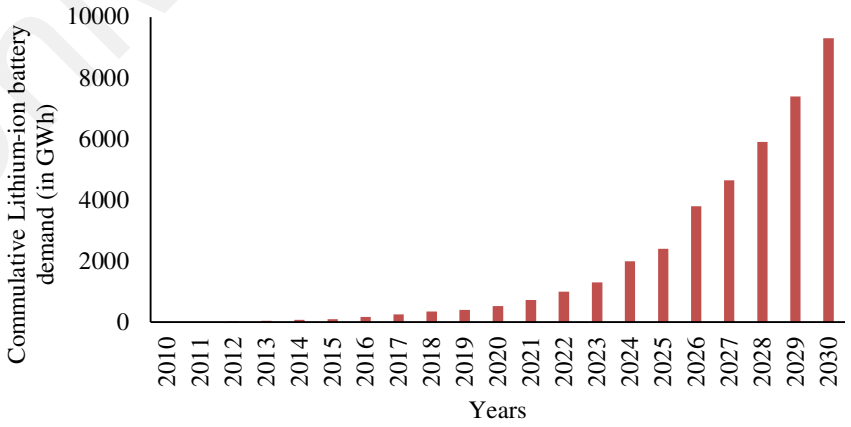

Figure 1.1: Expected worldwide cumulative lithium-ion battery demand by 2030 in GWh (*This Is the Dawning of the Age of the Battery - Bloomberg*, n.d.)

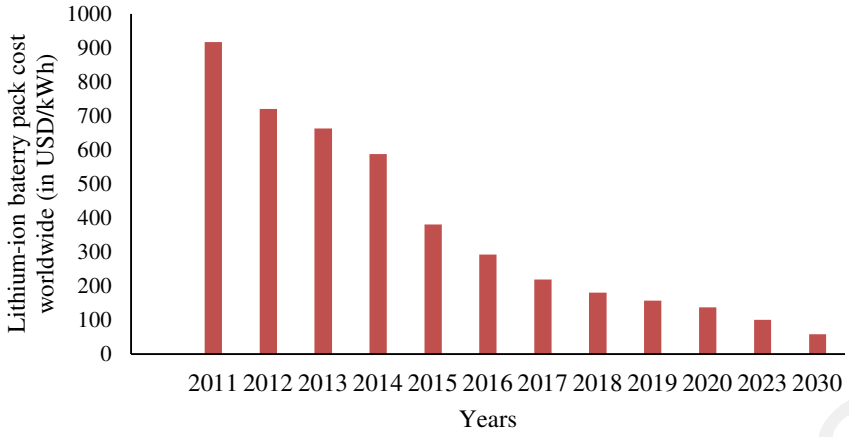

Figure 1.2: Worldwide lithium-ion battery pack cost by 2030 in USD/kWh (*This Is the Dawning of the Age of the Battery - Bloomberg*, n.d.)

Due to the highly nonlinear and dynamic nature of LIB, an effective battery management system (BMS) is constantly required to work LIB in the safe operating area. Protection from overcharging/discharging, cell balancing, and monitoring the battery states are the key roles of BMS.

Figure 1.3: Example of failed BMS in Chevrolet Bolt EV model 2017-2019 (*General Motors Recalling Nearly 69,000 Bolt EVs for Fire Risks - The Economic Times*, n.d.)

Figure 1.3 shows a fire-damaged Chevrolet Bolt EV, whose failure is strongly linked to a defective BMS software that led to the thermal runaway. From this photograph, it can be seen

that a reliable and robust BMS is the utmost priority for the EV manufacturer to provide a safe driving experience to EV users. Other benefits of the robust BMS are to maximize the energy and power delivery capabilities of the battery pack and prolong the overall service life by accurately monitoring the battery states. Different battery states such as state of charge (SOC) (Z. Li et al., 2017a), state of energy (SOE) (HongWen He et al., 2015), state of health (SOH) (Lin et al., 2015), and state of power (SOP) (Farmann & Sauer, 2016) are estimated by using estimation algorithm in BMS.

Generally, there are two types of estimation methods available in the literature such as the single/individual state estimation method and the combined states estimation or states co-estimation method. In the single/individual estimation, any one of the states is estimated by using a dedicated estimation method. In the last couple of years, there is plenty of research that has been done on the individual estimation method (Y. Wang et al., 2020). However, the individual estimation method may not be accurate due to the high dependency and correlation of the states on each other. To overcome this issue, the co-estimation method has been employed for the accurate battery states estimation especially for EV applications (X. Hu et al., 2018; P. Shen, Ouyang, Lu, et al., 2018). Based on the different states involved in the co-estimation method, the existing co-estimation method can be classified into several categories such as 1) SOC and SOH, 2) SOC and SOE, 3) SOC and SOP, and 4) others. These categories are described in detail in chapter 2.

This thesis aims to expand upon the current state-of-the-art of advanced LIB states estimation algorithms, by preparing a novel body of work on battery states co-estimation method, with a view to improve the accuracy and reduce the computational cost of the BMS used in EV. This chapter provides an overview of research motivations answering the question of the proposed research work. Also, a summary of previous work found in

the literature is presented. The problem statement, research questions, and objectives are described here.

1.2 Problem Statement

The battery states co-estimation method plays a vital role in improving the efficiency and reducing the computation of BMS (Hossain Lipu et al., 2021). Remarkably, the battery states co-estimation method continuously requires accurate SOC along with the other relevant battery parameters. Hence, to proceed with the battery states co-estimation method, the initial requirement is to estimate the SOC accurately. A large number of SOC estimation methods have been developed by the researchers so it is crucial to select a suitable algorithm for EV applications (Hannan, Lipu, et al., 2017).

In recent years, the Kalman filter (KF) algorithm and its variants are most favored by researchers for model-based SOC estimation due to its prominent features such as the capability to adaptively decrease the impact of noise and wide operating range. Especially, the extended Kalman filter (EKF) is the most suitable algorithm for real-time SOC estimation (C. Huang et al., 2018). In model-based SOC estimation using EKF, the SOC estimation accuracy directly depends on the accuracy of identified battery model parameters and the prior knowledge of the system noise variables. To address this, the dual extended Kalman filter (DEKF) is extensively utilized by the researchers to concurrently update the battery model parameters and SOC. However, the problem of battery model parameter divergence from the true value greatly affects the estimation accuracy under realistic dynamic loading conditions (Wassiliadis et al., 2018). Thus, there is a need to develop an accurate SOC estimation algorithm to work effectively in the presence of uncertain disturbances and erroneous initial conditions under real-time applications.

Nowadays, the co-estimation method which estimates two or more battery states concurrently is gaining popularity due to the existing high correlation between the different states. Also, the co-estimation method helps to improve the battery states estimation accuracy (Y. Wang et al., 2020). In the literature, different co-estimation methods have been presented by researchers using KF family algorithms (X. Li et al., 2019; Song et al., 2020; S. Zhang & Zhang, 2021b; Yongzhi Zhang et al., 2017). As the computational burden of the co-estimation algorithm proportionally increases the cost and size of the controller used in BMS, there is a need to develop an accurate comprehensive co-estimation method with the low computational burden that acquires the benefits of correlation between the battery states (Y. Wang et al., 2020).

The problem statement of the thesis can be summarized as follows:

i. With the advancement of EV battery technology, it is always crucial to select the more appropriate battery SOC estimation method for an EV application.
ii. Subject to the uncertain disturbances and erroneous initial conditions, the accuracy of the SOC estimation process varies over the wide range of operating conditions.
iii. Due to the high correlation between the states, it is critical to improve the overall performance of the BMS in the absence of any state information in real-time dynamic conditions.

1.3 Research Objectives

There are three main research objectives in this thesis and all of them are geared toward enhancing the overall performance of the BMS.

i. To analyze the existing online SOC estimation methods suitable for EV application.
ii. To develop online SOC estimation with high accuarcy and robustness under uncertain disturbances and erroneous initial conditions.
iii. To develop an accurate and computationally efficient co-estimation method with proper utilization of the correlation among the different battery states.

1.4 Research Questions

To achieve the objectives of this research, the following research questions need to be answered

i. Which type of algorithm is well suited for online SOC estimation method performance in an EV application?
ii. How can we improve the accuracy of the online SOC estimation method under under uncertain disturbances and erroneous initial conditions?
iii. How can we estimate the different states of the battery under the influence of real-time dynamic load by using the correlation among them with minimum computation effort?

1.5 The importance and Relevance of the Study

This research provides highly accurate, strongly robust to measurement noise uncertainties and computationally less expensive states co-estimation method for online estimation of different states, including SOC, SOE, SOP, actual capacity, and maximum available energy. With the proposed battery states co-estimation method, the existing

correlation between different states of LIB will be effectively utilized hence it would be implemented in limited computation capability microprocessor used in BMS. The output of this research will benefit EV users by providing more accurate information about the available charge, driving range, and safe driving experience. Furthermore, this research output will help to extend battery life, efficient energy management system to regulate the power flow with EV more precisely, optimize battery performance, protects from premature failures and safety hazards.

1.6 Layout of Thesis

This thesis is organized into several chapters. In this chapter, the background, objectives, research methodology, and relevance of the study are discussed. A brief explanation of the rest of the chapters are as follows:

1.6.1 Chapter 2

This chapter provides a state-of-the-art review on battery states estimation methods, for instance, individual state estimation method and battery states co-estimation method. It begins with a review of the suitable LIB technologies for EV applications. The key functions of the BMS are also discussed. Thereafter, a comprehensive review on the battery modeling method suitable for online battery states estimation is provided. A review on state-of-the-art of battery states including SOC, SOE, SOP, SOH, actual capacity, and maximum available energy estimation algorithms reported in the literature is undertaken. Also, a review on existing co-estimation methods is given. Finally, the recent studies in the existing literature on online SOC estimation using KF family algorithms are discussed.

1.6.2 Chapter 3

In this chapter, the experimental setting used to validate the proposed estimation methods in this thesis is discussed. The specification of the considered different

chemistries commercial battery cells, temperature chamber, and battery tester are provided. The battery testing methods involved in the development of the useful dataset and the evaluation matrices considered for the validation of the proposed methods are explained. After this, the proposed research methodology to achieve the objectives of the thesis is discussed.

1.6.3 Chapter 4

This chapter discusses the importance of the accurate and low computational burden co-estimation method for battery SOC and SOE is developed for EV applications. The mathematical model of the proposed dual forgetting factor-based adaptive extended Kalman filter (DFFAEKF) algorithm and its implementation for the SOC estimation method are provided. The benefits of DFFAEKF over DEKF in terms of estimation accuracy and fast convergence are given. Thereafter, the concept of the proposed co-estimation method for SOC and SOE estimation and mathematics behind the implementation are also discussed. In addition, the experimental setting and battery test involved in the validation of the proposed method under dynamic operating conditions are explained.

1.6.4 Chapter 5

This chapter discusses the proposed unified frame of battery states co-estimation method for the estimation of SOC, SOE, SOP, actual capacity, and maximum available energy. The correlation between different battery states is effectively utilized to reduce the computational burden. The mathematical model of the proposed unified frame of the battery states co-estimation method is also discussed. Considered different algorithms for the battery SOP, actual capacity, and maximum available energy estimation are presented. In addition, the experimental setting and battery test involved in the validation of the proposed method under dynamic operating conditions are explained.

1.6.5 Chapter 6

This chapter discusses the results of the proposed co-estimation method for SOC and SOE estimation using DFFAEKF under-considered dynamic operating conditions. Also, the identified battery 2RC model parameters using DFFAEKF and DEKF are presented for DST and US06 drive cycles. The accuracy and the robustness of the proposed co-estimation method for SOC and SOE estimation under-considered dynamic operating conditions are analyzed. Thereafter, the results of the proposed unified frame of battery states co-estimation method for battery states (SOC, SOE, SOP), actual capacity, and maximum available energy are explained. The results analysis of the proposed unified frame of battery states co-estimation method under-considered dynamic operating conditions are also presented.

1.6.6 Chapter 7

This chapter contains the re-examination of the thesis objectives, conclusion, and suggestions for future work.

CHAPTER 2: BACKGROUND AND STATE OF THE ART LITERATURE REVIEW

2.1 Introduction

The LIB technologies are becoming a favorite choice for energy storage for EV applications. However, without significant improvement in the battery management system, LIBs will not be considered a safe and reliable choice for EV users. Therefore, this chapter initial aim to provide a review on LIB chemistries for EV and BMS. Thereafter, a comprehensive review on the battery modeling method suitable online states estimation is performed. A review on state-of-the-art of battery states, actual capacity, and maximum available energy estimation algorithms reported in the literature is undertaken. Finally, the recent studies in the existing literature on online SOC estimation using KF family algorithms were thoroughly reviewed.

2.2 Suitable Lithium-ion battery chemistries for EV applications

Over the past decade, the lithium-ion batteries (LIBs) penetration in the EV market is exponentially increasing, where high energy/power density is needed (Hannan, Hoque, et al., 2017b). Based on the positive electrode material chemistry, the existing LIBs can be classified into different categories such as lithium cobalt oxide (LCO), lithium-ion iron phosphate (LFP), lithium-ion nickel manganese cobalt oxide (NMC), lithium nickel cobalt aluminum oxide (NCA) and lithium-titanate (LTO) (Miao et al., 2019). The properties of mentioned LIBs are listed in Table 2.1. Mostly, carbon and lithium titanate are utilized as negative electrode material (Linchao Zhang & Chen, 2011). All types of LIBs are being utilized by EV manufacturers. However, LFP, NMC, and NCA are gaining popularity amongst EV manufacturers due to high voltage and high specific energy density (L. Lu et al., 2013). NCA is widely utilized by Tesla in its current development establishes by Panasonic in the cylindrical form such as Tesla S and Tesla X models (*Exclusive: Panasonic Aims to Boost Energy Density in Tesla Batteries by 20% -*

Executive | Reuters, n.d.). NCM batteries are preferred for high-power applications. NMC batteries are used in EV models such as BMW i3, Nissan Leaf, Fiat 500e, Kia Soul EV, Ford Focus EV. Whilst LFP batteries with higher discharge current rate and superior thermal stability characteristics are used in Chevrolet spark, and BYD e6 (Sanguesa et al., 2021). Due to the low voltage and energy density of LFP batteries, it is more expensive on the scale of a cost/kWh.

To meet the increasing demand for EVs in the market, high levels of academic and industrial research are going on to develop more advanced battery technologies. In this thesis, the commercially available NCA, NMC, and LFP cells for the development of the online state monitoring method. It is worth noting that the algorithms developed in this thesis are also applicable to other battery chemistries, given knowledge of certain battery design limits and algorithm tuning parameters are available at the initialization step.

Table 2.1: Comparison of different Lithium-ion batteries suitable for EV (L. Lu et al., 2013; Miao et al., 2019; Sanguesa et al., 2021)

Specification	LCO/NCA	LFP	NMC	LMO	LTO
Nominal cell voltage (V)	3.6–3.7	3.2	3.65	3.7–3.8	2.3
Specific Power ($W.kg^{-1}$)	1500	150-1500	300-1500	700-1300	3000-5100
Specific Energy ($Wh.kg^{-1}$)	90-200	100-140	100-240	90-120	70
Energy Density ($Wh.l^{-1}$)	400-640	125-250	250-630	245-430	170
Peak currents (C-rate)	Charge:<1C Discharge: 3C	Charge:1C Discharge:> 10C	Charge:1C Discharge:>3C	Charge:1C Discharge:> 10C	Charge:5C Discharge:> 10C
Operating temperatures (°C)	Charge: 0–45 Discharge: -20–60	Charge:0–45 Discharge: -30–60	Charge: 0–45 Discharge: -20–60	Charge: 0–45 Discharge: -40–65	Charge: -20–45 Discharge: -30–60
Cycle Life	< 1,000	1500 +	1000 +	< 1,000	10,000+
Safety	Low	High	Moderate	Moderate	High
Used in EV models	Tesla S, Tesla X	Chevrolet spark BYD e6	BMW i3, Nissan Leaf, Fiat 500e, Kia soul EV, Ford Focus EV	Nissan Leaf (1G), Honda Fit EV	Mitsubishi I

2.3 Definition of different states of the Lithium-ion battery (LIB)

2.3.1 State of Charge (SOC)

SOC can be defined as the ratio of remaining capacity (Q_{rem}) to the actual capacity (Q_n) of the battery as expressed in (2.1) (I. Kim, 2008). Where Q_{rem} is the capacity in Ah refers to the maximum possible limit of charge that can be extracted from the battery at a particular time of instant and Q_n is the maximum possible limit of charge in Ah called actual capacity that can be extracted from the battery in its actual aged state starting from a fully charged state. The rated capacity in Ah (Q_{rated}) is the battery capacity provided by the manufacturer for operation under normal conditions. SOC is an important parameter to measure battery performance. Since it depends on the internal battery chemistry, the direct measurement from electrical signals is impossible. An accurate estimation of SOC is typically needed to avoid detrimental situations during the charging and discharging process.

$$SOC(t) = (Q_{rem}/Q_n) \times 100\% \tag{2.1}$$

Conventionally, the $SOC(t)$ can be calculated by (2.2), where η_c is the coulombic efficiency, $SOC(0)$ is the initial SOC, and $I(t)$ is the battery charging/discharging current. The η_c generally describes as the ratio of the consumed electrons and available electrons during the charging/discharging process. This ratio is assumed to be 0.9 and 1 during the charging and discharging process respectively (Plett, 2004e). The SOC is expressed in percentage as presented in Fig 4, the 100% SOC and 0% SOC implies the fully charged and fully discharged cell condition, respectively.

$$SOC(t) = SOC(0) - \left(\int_0^t \eta_c I(t) d(t)/(Q_n(t) \times 3600)\right) \tag{2.2}$$

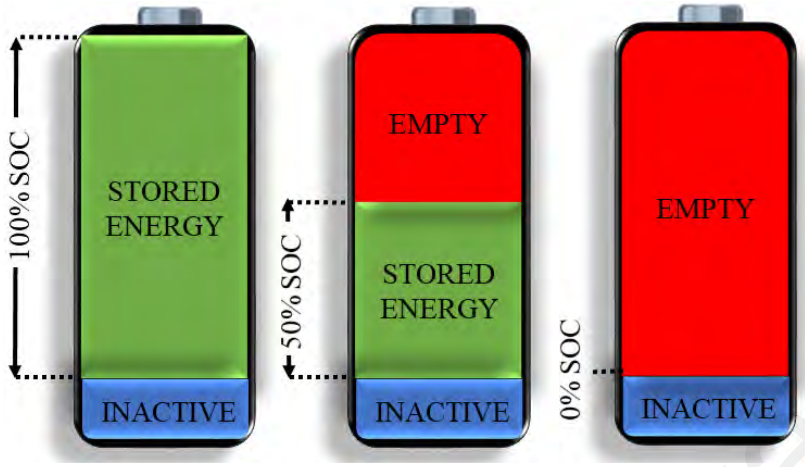

Figure 2.1: LIB stored energy status at different SOC (100%, 50% and 0%)

2.3.2 State of energy (SOE)

SOE is a percentage ratio of the residual energy to the actual energy of the battery as represented by (2.3). The accurate SOE estimation is crucial for the optimal energy management of an EV application and microgrid application (Lin et al., 2017).

$$SOE = Residual\ Energy\ (E_r)/Actual\ Energy(E_n) \tag{2.3}$$

The actual energy of the battery is varying with the change in the operating conditions. Due to this, it becomes mandatory to consider the effect of temperature, current rate, and aging level for the accurate estimation of battery SOE (L. Zheng et al., 2016a). Further, the $SOE(t)$ can be expressed in power integral form as (2.4) (Yongzhi Zhang et al., 2017),

$$SOE(t) = SOE(0) - \left(\int_0^t \eta_e V(t).I(t)d(t)/(E_n(t) \times 3600)\right) \tag{2.4}$$

Where $E_n(t)$ is the actual energy or maximum available energy in Watt-hour (Wh), $V(t)$ is the terminal voltage, $I(t)$ is the charging/discharging current, η_e is the battery energy efficiency and $SOE(0)$ is the initial value of SOE.

Estimation of SOE is useful for the direct determination of the percentage of remaining energy of the battery. In the case of EVs, it is the more accurate parameter to predict the

useful remaining driving range of EVs. Due to the consideration of different parameters such as internal resistance energy loss and battery open circuit voltage (OCV), the SOE of the battery varies nonlinearly with the battery current.

2.3.3 State of power (SOP)

Battery peak power (P_{Peak}) is the maximum power delivered in the time span (T) without violating the set operating parameters limits like the voltage, current, temp, and SOC (Pei et al., 2014). Due to the non-linear dynamic behavior of the LIB, these parameters significantly change throughout the battery life. And the SOP is the ratio of peak power (P_{Peak}) to the nominal power (P_N) (2.5). In other words, it is simply a parameter to quantify the battery maximum power handling capacity during dynamic loading conditions (S. Wang et al., 2012). To maintain the life cycle with the full utilization of the battery power, it is necessary to estimate the SOP of the battery.

$$SOP = |P_{Peak}/P_N|_{t=T} \tag{2.5}$$

For the operation of energy management systems in EVs, SOP estimation is important to control the energy flow from the battery to maintain its safe operating limit. The real-time SOP estimation is requested, to measure and control the acceleration/deceleration and charging/discharging power requirement of the EVs in a certain duration of time (Waag et al., 2014).

2.3.4 State of health (SOH)

The battery SOH is a figure of merit that indicates the battery aging level. Due to complex internal electrochemical dynamics, understanding the battery aging process is very difficult. The aging phenomenon includes capacity fade and power fade of the battery cell. Usually, the capacity fade refers to the loss of active material inside the battery cell whereas the power fade refers to an increase in internal resistance. There are

multiple reasons behind the battery capacity fade and power fade. For example, the aging of the anode and cathode material of battery cells differs from each other significantly. In industry, the battery cell's remaining capacity and internal ohmic resistance are the two indicators utilized for SOH estimation. In the case of EV, the battery cell End of life (EOL) is defined as the time when the battery cell remaining capacity reaches 80% of the capacity at beginning of life (BOL) and the internal resistance cross the threshold limit of 200% of internal resistance at BOL (W. Li et al., 2021a). As the battery cell crosses the EOL threshold limits, it could not be suitable for EV application. Based on capacity fade and power fade, the battery $SOH(t)$ at time instant t can be expressed as (2.6) and (2.7), respectively (Zhengyu Liu et al., 2020). Where, C_t and R_t are the battery cell actual capacity and internal resistance at time instant t. C_{BOL} and R_{BOL} are the battery capacity and resistance value at BOL or fresh battery cell.

$$SOH(t) = (C_t/C_{BOL}) \times 100\% \tag{2.6}$$

$$SOH(t) = (R_t/R_{BOL}) \times 100\% \tag{2.7}$$

2.4 Battery Management System

Owing to the highly nonlinear and dynamic nature of LIBs, an effective BMS is continuously required to operate them in a safe operating area (L. Lu et al., 2013). The battery management system (BMS) is an electronic system that serves as the brain of the battery system. In this section, an overview of BMS key functions is provided. Thereafter, the focus is brought to the online battery modeling and parameter identification and states estimation algorithms, and suitable Kalman filter family algorithms for SOC estimation, which are the main topic of the study in this thesis.

As shown in Figure 2.2, some of the key functions of BMS are data acquisition, energy management system, thermal management system, safety and protection, cell balancing, and state monitoring (K. Liu et al., 2019; Xing et al., 2011).

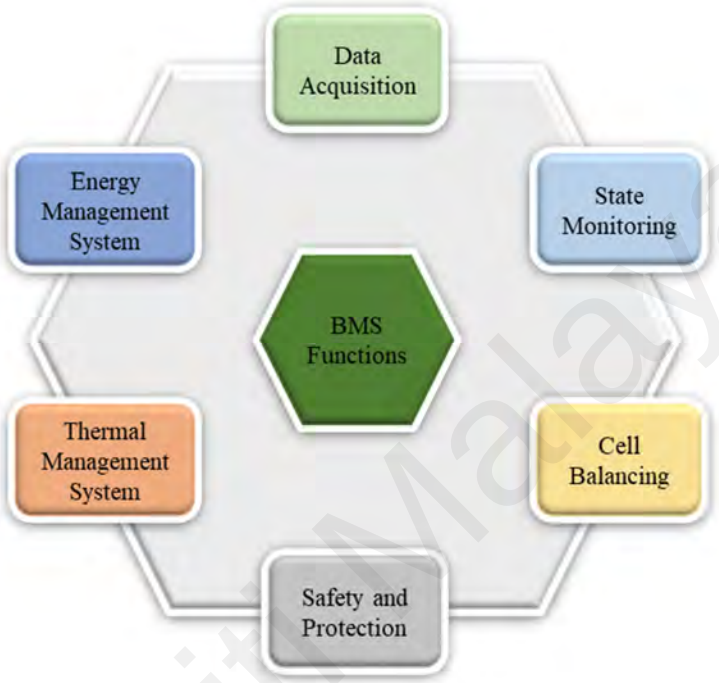

Figure 2.2: Basic functions of the battery management system

2.4.1 Data Acquisition

The data acquisition includes the monitoring and storing of the most relevant battery data for decision-making units of BMS. The most relevant battery data are the measured voltage of every battery-connected battery cells, the current flows in parallel connected modules in the battery pack, and the temperature of each battery cells. The proper sampling frequency of voltage and current measurement is always required to capture the transient response of the battery cells.

2.4.2 Energy Management system

To control the energy flow to fulfill the fast-transient and slow-transient power requirements in the most practical application like EV, the proper energy management

system (EMS) is always needed. The EMS also creates communication between the DC-DC converter, battery charger, propulsion motor, and battery pack. It also helps to control the power flow in the power train of the EV.

2.4.3 Thermal management system

LIBs are very sensitive to temperature. The increase in temperature has two effects on the performance of the LIBs. With the increase in temperature, the LIBs performance improves and work more efficiently. On the other side, it creates the problem of the thermal runway that can reduce their reliability because of probable explosion (Qian Wang et al., 2016). Therefore, to maintain the temperature within the safe operating temperature range, the thermal management system is generally equipped with a battery pack. Depending on the applications, two different types of TMS such as active and passive systems are widely used (Lopez Sanz et al., 2016).

2.4.4 Safety and protection

To protect the battery cells or battery pack from malfunctioning and permanent damage, different sensors are incorporated with BMS. With the help of sensor signals, the battery cells can be protected from overcharge, undercharge, insulation fault, uniformity fault, over-fast temperature rise, and low temperature (L. Lu et al., 2013). When the faults are diagnosed, the sensor signals are transmitted to the vehicle control unit to handle the faults. Under a serious fault condition, the vehicle control unit disconnects the battery pack from the power supply also.

2.4.5 Cell balancing

To fulfill the energy and power demand of the load, a large number of battery cells are connected in the series-parallel configuration in a battery pack. The battery cells connected in the series configuration operate with the amount of current under and discharge conditions. However, due to inconsistency amongst the battery cells, the small

imbalance in voltages of the battery cells is always present. Voltage differences may cause overcharging and deep discharging for a few cells, which leads to cell distortion. Voltage differences also affect the operation, performance, and safety of the entire battery pack. To outperform this, the cell balancing circuit is available in BMS. Generally, two types of cell balancing circuits are used in BMS such as active cell balancing and passive cell balancing that are also known as dissipative and non-dissipative cell balancers, respectively (Das et al., 2020). With the application of effective cell balancing, the energy and power delivery to the battery pack can be controlled.

2.4.6 Battery States monitoring

For the development of robust and efficient BMS, various battery states need to be monitored accurately. However, the battery states cannot be measured directly using electronic sensors. Therefore, the battery states estimation is performed with the help of other directly measurable quantities, such as battery terminal voltage, current, and operating temperature. The states estimation must be quick, reliable, and accurate to ensure the high performance of BMS. Due to dynamic operating conditions and battery aging, the battery characteristics such as battery capacity, and impedance parameters are varied significantly. Therefore, these variations in battery characterizations must be adaptively updated with the battery state estimation to produce an accurate and reliable set of battery state estimates.

The overall structure of the battery state monitoring system is shown in Figure 2.3. Generally, the battery dynamic model is utilized with the battery states estimation algorithms of SOC (Hannan, Lipu, et al., 2017), SOE (X. Li et al., 2021), SOH (Berecibar et al., 2016a), and SOP (Farmann & Sauer, 2016). At every instant, the battery dynamic model parameters are identified by using the online model parameter identification method. Thereafter, the prediction of the OCV is made based on the battery dynamic

model identified parameters, which is then utilized in SOC estimation algorithm. Consequently, this information is processed into estimation algorithm s responsible for SOE, SOH and SOP. Furthermore, the battery's actual capacity and maximum available energy are predicted based on estimated SOC and SOE to develop the comprehensive BMS for EV applications.

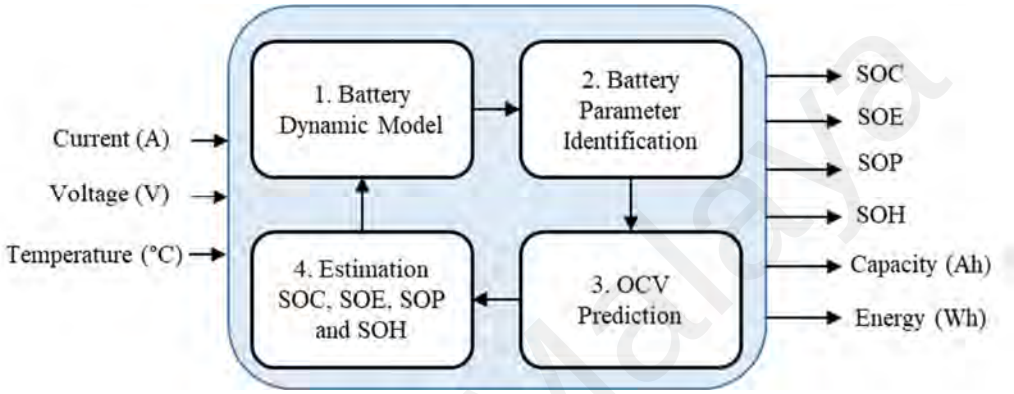

Figure 2.3: Overall structure of battery states monitoring system

2.5 Lithium-ion Battery Modeling methods

Battery model development is the primary step of online SOC estimation. The purpose of the battery model is to replicate the performance of the battery behavior in a simulation environment. LIBs have a complex working phenomenon and incorporate different parameters, such as mass transfer, migration of ions between electrodes, side reactions, and current collector reactions. Thus, battery models with high reliability and accuracy are crucial for model-based parameter estimation. Based on control theory, battery models can be classified as the black model, white model, and gray model (Lai et al., 2018).

2.5.1 Types of Battery Models

The battery model is classified into five categories, namely empirical model (EM) (Plett, 2004e, 2004c, 2004d, 2006a), ECM (Newman & Tiedemann, 1975), EECM (Mousavi G. & Nikdel, 2014), (Mu et al., 2017), ECIM (Stephan Buller et al., 2003;

Westerhoff et al., 2016) and DDM (Hametner & Jakubek, 2013), as depicted in Figure 2.4. EECM is the most suitable for online SOC estimation because of its low complexity and computational requirements and high compatibility for embedded system applications. The EECM model can be classified into three: the Rint model, Randles model, and nRC model.

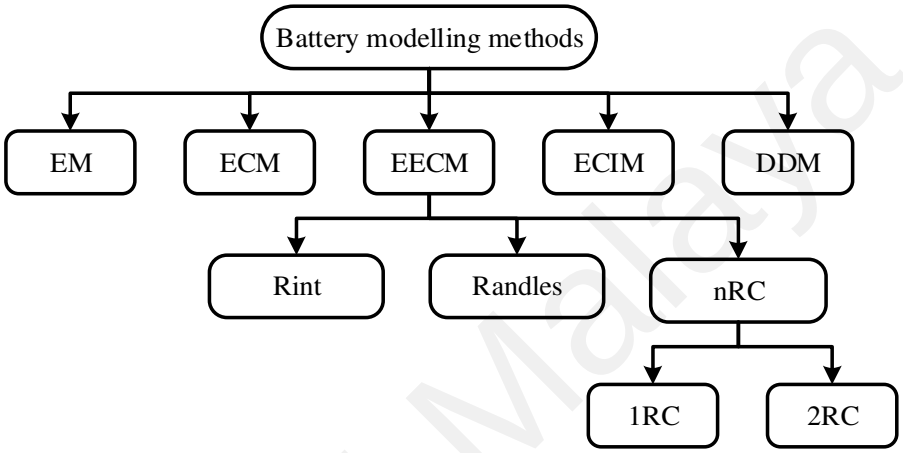

Figure 2.4: Types of LIB modelling methods

2.5.1.1 Empirical model

In EMs, the battery internal electrochemical dynamics is represented by using a mathematical expression and reduced-order polynomial. The mathematical function is utilized to represent the relation between battery terminal voltage with the SOC and battery current. The Shepherd model, Unnewehr universal model, and Nernst model are the main categories of EM (Meng, Luo, et al., 2018). The combined model was proposed in (Plett, 2004d) to improve the accuracy and computational burden of EM. The combined model of LIB is the combination of the three aforementioned models, and it shows better performance compared with the individual model performances (Plett, 2004e, 2004c, 2004d, 2006a).

The terminal voltage ($V_{t,k}$) can be expressed by (2.8) at k^{th} sample time and comprises two parts: the function of SOC_k in which the value of the constants d_0, d_1, d_2, d_3 and d_4

depend on OCV and the function of current (I_k) where I_k and SOC_k are the respective values of current I and SOC at the k^{th} sample time.

$$V_{t,k} = \underbrace{d_0 + \ d_1/SOC_k + d_2 SOC_k + d_3 \ln SOC_k + d_4 \ln(1 - SOC_k)}_{f(SOC_k)} - \underbrace{RI_k}_{f(I_k)} \quad (2.8)$$

The accuracy of the EM can be improved by adding more battery parameters. By contrast, the utilisation of numerous parameters proportionally increases the computational burden. Therefore, this modelling method is not suitable for online SOC estimation.

2.5.1.2 Electrochemical model

The first ECM was developed by Newman and Tiedemann (Newman & Tiedemann, 1975), and it uses microscopic- and macroscopic-level information to describe the electrochemical and physical properties of the battery (Dees et al., 2002; C. Y. Wang et al., 1998). The pseudo-two-dimensional (P2D) model is amongst the most popular ECM models (Jokar et al., 2016a; J. L. Lee et al., 2012b; Smith et al., 2007). It works on the principles of porous electrode theory, concentrated solution theory and kinetic equations (Jokar et al., 2016a). In the past few years, the P2D model has been extensively utilised for LIB modelling. However, the overall computation time and modelling the complexity of this P2D model increase because of the need for numerous nonlinear PDEs to solve the P2D. In the past few years, several models, such as single particle (SP) model (Han et al., 2015a), simplified P2D model (SP2D) (Jokar et al., 2016b) and improved SP model (SP3), (Han et al., 2015b) have been developed to overcome the issues related to the P2D model. In (Wu et al., 2013), the P2D model was coupled with a thermal model for the development of BMS to address thermal runaway and performance degradation caused by dynamic loading (charge/discharge at medium-to-high C-ratings) of the LIB. Application of the full-order model of P2D, SP, SP2D and SP3 can accurately predict the

electrochemical properties of LIB. However, for the solution of PDEs, highly complex and costly software is usually required, which makes P2D model inappropriate for online application. Furthermore, for the identification of real-time parameters (voltage, SOC and electrochemical variables) of ECM with low computation time and complexity, the reduced-order model (ROM) with discrete-time realisation algorithm was used in (J. L. Lee et al., 2012a, 2012c; Smith, 2006). The developed ROM was successfully implemented with BMS, and it could track all electrochemical states with high accuracy (X. Guo et al., 2016). To further improve the performance of ROM, the time-varying ROM was developed with the generally preferred model blending (J. L. Lee et al., 2014). This ROM could track the variables over a wide range of SOC at the cost of reduced SOC estimation accuracy (Bartlett, Marcicki, Onori, Rizzoni, Yang, et al., 2016; Stetzel et al., 2015). Therefore, the use of PDEs in computation remains doubtful for the real-time application in BMS of EV.

2.5.1.3 Electrical equivalent circuit model

To maintain the trade-off between battery model complexity and accuracy, a new modeling approach called EECM has been investigated by researchers (Mousavi G. & Nikdel, 2014; Rzepka et al., 2021) EECM is one of the most promising approaches for online battery parameter/state estimation, especially for EV applications. It uses lumped components such as resistors, capacitors and voltage source, to describe the complete battery dynamic behavior. The EECM approach can be classified into three categories, such as Rint model, Randles model and RC model (Mousavi G. & Nikdel, 2014), as presented in Figure 2.4. For the efficient utilization of EECM for online SOC estimation, an accurate model PIM is always needed.

Based on the operating condition, PIMs suitable for battery EECM can be classified into two categories, online and offline. In the online method, tests are conducted during

the active application mode, whereas in the offline method, ad-hoc tests are conducted on the battery during the standby application mode. The offline method of battery parameter identification is extensively utilized in online SOC estimation. Additionally, it helps reduce the complexity of online SOC estimation. The commonly used offline PIMs are curve fitting (L. Lu et al., 2013), RLS algorithm (Barcellona & Piegari, 2017a; S. Zhang & Zhang, 2021b) multi-swarm particle swarm optimisation (MPSO) (C. Huang et al., 2018) and GA (Q. Yang et al., 2017). However, the accuracy of the model parameters is highly sensitive to battery temperature and charging/discharging rate (Yun Zhang et al., 2017). Thus, the application of an online adaptive algorithm for parameter identification seems more appropriate. For online parameter identification, the weighted RLS (Cheng Zhang, Allafi, Dinh, et al., 2018) is the most appealing method, and it requires only the battery current and voltage for parameter identification.

With the advancement of control theory in the past decade, the different adaptive filters and nonlinear observers like KF and its variants, PF (Yun Zhang et al., 2017), RLS (P. Shen, Ouyang, Lu, et al., 2018), forgetting factor RLS (FFRLS) (Xia et al., 2018), multiple forgetting factors RLS (MFFRLS) (Safwat et al., 2017), UPF (Waag et al., 2014) and H-infinity (Barcellona & Piegari, 2017b; Hongwen He et al., 2012b; Mousavi G. & Nikdel, 2014; Partovibakhsh & Liu, 2012; Tian, Yong, Rusheng Yan, Jindong Tian, Shijie Zhou, 2017), have been investigated for the accurate parameter identification of LIBs.

(a) Rint model

The Rint model is the simplest type of battery equivalent circuit model that was developed from the combined model of LIB. As shown in Figure 2.5, it contains a single-value internal ohmic resistance (R_{st}) and an OCV source (V_{ocv}) (P. Shen, Ouyang, Lu, et al., 2018). The value of both components depends on the SOC, SOH and temperature of

the LIB (Hongwen He et al., 2011b). The hysteresis effect is an important attribute of LIB that cannot be neglected. The relaxed voltage is higher and lower than the true OCV during charging and discharging, respectively, because of the hysteresis effect in the battery. Consequently, two OCVs represent a single value of SOC, and this effect becomes severe at low temperatures. Hysteresis must be considered for accurate SOC estimation. In (Plett, 2004d), the zero-state hysteresis model was combined with the Rint model. The results illustrated that the consistency and performance of the zero-state hysteresis Rint model are better than those of the simple Rint model. Nevertheless, weak battery dynamics make the zero-state hysteresis Rint model unsuitable for LIB modelling under a dynamic load such as EV.

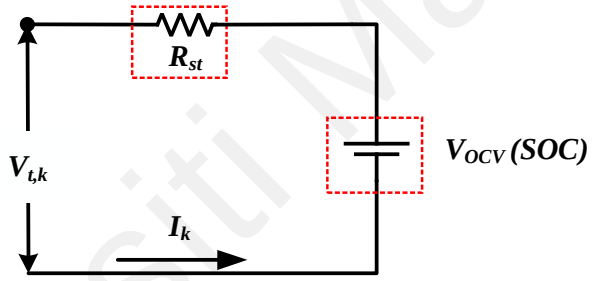

Figure 2.5: Rint battery model (P. Shen, Ouyang, Lu, et al., 2018)

(b) Randle's model

In the Randle's model, the battery is considered a large capacitor and is mostly used in CCM-based SOC estimation. The model was initially used in lead acid battery (Fairweather et al., 2012). In (C. Gould et al., 2012), it was used for LIB application, as presented in Figure 2.6, where C_p is the main capacitor to store the charge, parallel combination C_n and R_n represent the small time-constant electrochemical transitions, R is the internal resistance (a terminal and interconnection resistance) and R_p is a self-discharge resistance. The n number of parallel RC branches can be added to the original model to analyse the more transient response (Nejad et al., 2016a). In (C. R. Gould et al., 2009), the authors validated the Randles model on an ultra PRT vehicle by estimating the

SOC and SOH through real-time state observers such as Utkin and KF. In this thesis, the Rint is employed for SOP estimation of the battery cells due to intes low complexity.

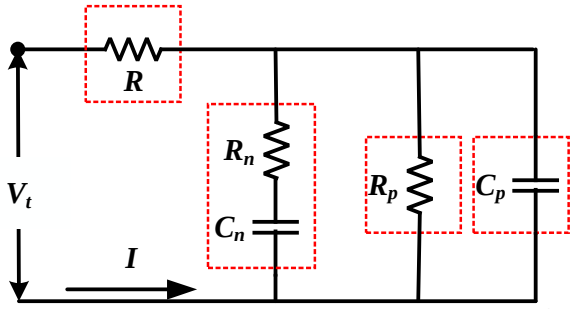

Figure 2.6: Randle's battery model (Nejad et al., 2016b)

(c) nRC model

The nRC Model incorporates a series of internal resistances (R) and n number of parallel RC branches to represent the transient responses of different time constants associated with LIB charge transfer, diffusion and voltage source V_{ocv}. As shown in Figure 2.7, depending on the load requirement and model accuracy, the number of parallel RC branches varies from 1 to n. The 1RC and the 2RC are commonly used RC models for online SOC estimation. In the 1RC model called Thevenin model, a single RC branch is used to describe the battery dynamics and transient response during charging and discharging. To further improve the performance of the 1RC model, in (Plett, 2004b; Xiaoqiang Zhang et al., 2016), the battery model called Partnership for a New Generation of Vehicles (PNGV) was adopted to describe the nonlinear characteristics. As shown in Figure 2.8, in the PNGV model, the capacitance C_b is connected in series with the resistance R to simulate the effect of the change in SOC on OCV, and resistance R_p and capacitance C_p are used to describe the polarisation effects. The model can define the battery voltage at a different SOC during the transient phase. The 2RC model is a highly preferred and accurate LIB model for online SOC estimation. It consists of two RC branches that describe the slow and fast transient response caused by charge transfer and

diffusion of LIB (P. Shen, Ouyang, Lu, et al., 2018). The value of all the parameters, such as U_{oc}, R and time constants (τ_1 and τ_2), are highly influenced by the battery temperature and SOC (S. Yang et al., 2017). In (Ouyang et al., 2014), the extended 2RC model was used to improve the model performance in the low SOC region in which the RC components indicate the solid-phase diffusion. The hysteresis model is usually combined with the 1RC and 2RC model to improve the model accuracy, especially for the EV application (Huria et al., 2014).

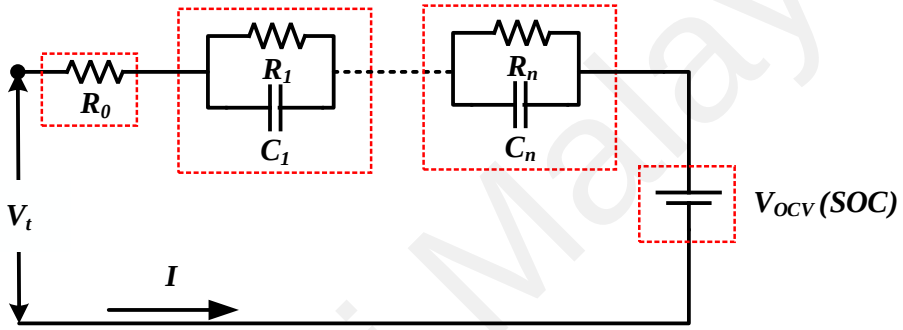

Figure 2.7: nRC battery model (Nejad et al., 2016b)

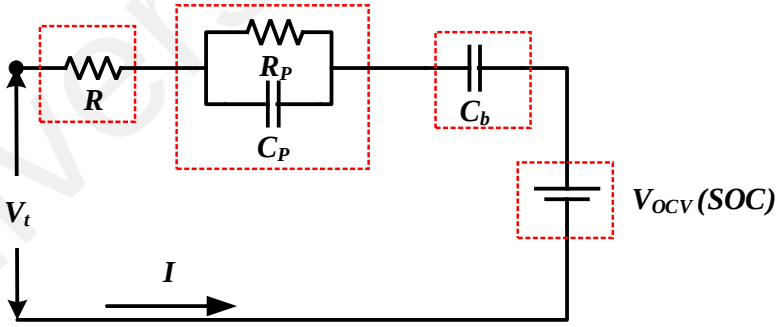

Figure 2.8: PNGV battery model (Pai, 2019)

2.5.1.4 Electrochemical impedance model

In ECIM, the properties of battery electrochemical impedance and electric impedance are composed to overcome the shortcomings of the EECM. The fractional order model based on fractional order calculus (FOC) and electrochemical impedance spectroscopy

(EIS) theory are used to investigate the ECIM (Mu et al., 2017). The FOC is suitable for modelling the battery dynamics. It can also incorporate the mass transport, diffusion dynamics and memory hysteresis effects of LIB into the developed model. EIS is the non-destructive approach used for the development of ECIM of LIB to manifest the internal dynamics at different SOH of the battery (S. Buller et al., 2005). In EIS, the sinusoidal alternating current of different frequencies is applied to the battery, and the voltage response is recorded to develop the complex impedance frequency spectrum that is directly correlated with the SOC, SOH, temperature and amplitude of the applied current (Stephan Buller et al., 2003; Westerhoff et al., 2016). In the ECIM model, the charge transfer between electrolyte, active material and solid electrolytic interference is modelled by a constant phase element (CPE) parallel with a resistor, and the solid-state Li diffusion is captured by the Warburg component (S. Liu et al., 2017). To reduce the complexity of the n-order RC model, the authors in (C. Zou et al., 2018) developed the ROM with fraction element. The performance of the ECIM with one CPE is similar to the fifth-order RC model (Mu et al., 2017). The ECIM developed from the Randles model depicts higher accuracy compared with the commonly used 1RC model under a wide range of uncertainties (B. Wang et al., 2015), (Liao et al., 2012). The modified 2RC model employing two CPEs infer high robustness compared with the 2RC EECM (B. J. Wang et al., 2017). The ECIM method is more advantageous and accurate than ECM and EECM, but this method is not suitable for online parameterisation and SOC estimation in EV application because it requires a long test time (Waag et al., 2013).

2.5.1.5 Data-driven model

Establishing the precise battery model utilising the ECM, EECM and ECIM approaches is difficult due to the complex internal dynamic behaviour of the battery and uncertain external operating conditions. DDM method based on statistical machine learning tools, such as fuzzy logic (Hametner & Jakubek, 2013), neural network (C. Li et

al., 2019; Tong et al., 2016) and support vector machine (Klass et al., 2015a), (Klass et al., 2015b) is another convenient way to estimate online SOC. The need for an accurate plant model and the performance of the controller developed by a data-driven method depend on available signals, such as voltage, current and temperature. The application of highly nonlinear input and output training data pattern in modelling has several potential benefits, such as distributed processing, high computation rate and adaptive capability to solve the complex problems (R Xiong et al., 2018). However, the problems caused by the high involvement of data sets in this modelling method, such as the incorrect data selection, can severely influence SOC estimation (Hossain Lipu et al., 2020). The immense number of data sets required to cover all operating conditions significantly increases overall computational cost.

2.5.2 Suitable battery modelling method for real commercial BMS of EV

To analyse the suitable battery modelling method for real commercial BMS of EV, the available patents filed by different battery manufacturers and BMS companies related to online SOC estimation were reviewed (Baba & Adachi, 2013, 2016; Gelso & Bryngelsson, 2018; JR et al., 2005; KIM et al., 2018; T.-K. Lee, 2015, 2017; LIM & JIN, 2012; Mao & Tang, 2014; Paolo Baruzzi et al., 2013; Plett, 2012, 2003, 2009; Quet, 2014; Tang et al., 2013; Vaidya & Kancharla, 2014; Valdez & Angel, 2016; Won et al., 2006; Zhong et al., 2014). Table 2.2 lists information about the battery modelling method employed in the patents. The table demonstrates that the EECM is the most suitable battery modelling method for online SOC estimation. Moreover, owing to the favorable features of 1RC and 2RC models for online SOC estimation, these two models are mostly utilised in the development of BMS of EV by different companies. In this thesis, the 2RC model is employed for SOC estimation.

Table 2.2: Different battery models employed in the patents filed by battery manufacturers and BMS companies

Ref.	Assignee	Battery Modelling Method	Patent Title
(Plett, 2003)	Compact Power	EM	Method and apparatus for a battery state of charge estimator
(JR et al., 2005)	General Motors	EECM (1RC)	Generalized electrochemical cell state and parameter estimator
(Plett, 2009)	LG Chem	EECM (1RC)	Method and system for joint battery state and parameter estimation
(Plett, 2012)	LG Chem	EECM (1RC)	State and parameter estimation for an electrochemical cell
(LIM & JIN, 2012)	SK Innovation	EECM (1RC)	The method of measuring SOC of a battery in a battery management system and the apparatus thereof
(Paolo Baruzzi et al., 2013)	Qualcomm	EECM (2RC)	Battery fuel gauge
(Tang et al., 2013)	GM Global Technology Operations LLC	EECM (2RC)	Dynamic battery capacity estimation
(Mao & Tang, 2014)	GM Global Technology Operations LLC	EECM (2RC)	Battery State of Charge observer

‘ Table 2.2 continued’

Ref.	Assignee	Battery Modelling Method	Patent Title
(Vaidya & Kancharla, 2014)	KPIT Technologies, KPIT Cummins Info systems	EECM (Rint)	System and method for battery monitoring
(T.-K. Lee, 2015)	Ford Global Technologies LLC	ECM (ROM)	Method and system for estimating battery model parameters to update battery models used for controls
(Valdez & Angel, 2016)	Jaguar Land Rover	EECM (1RC)	Battery condition monitoring
(Quet, 2014)	Nuvera Fuel Cells	EECM (Rint)	Battery State of Charge management method
(Baba & Adachi, 2016)	Calsonic Kansei	EECM (Unspecified)	Battery SOC estimation device
(T.-K. Lee, 2017)	Ford Global Technologies LLC	ECM (ROM)	Method and system for battery state of charge estimation
(KIM et al., 2018)	Samsung Electronics	EECM (1RC)	Method and apparatus for estimating a state of the battery based on the error correction
(Gelso & Bryngelsson, 2018)	Volvo Truck	EECM (2RC)	A method and arrangement for determining the state of charge of a battery pack

2.6 Individual online states estimation method

2.6.1 SOC estimation methods

A precise and reliable online SOC estimation method is needed for the development of elite BMS. In recent years, several online SOC estimation methods have been developed (Figure 2.9). Table 2.3 lists the various attributes of these SOC estimation methods.

2.6.1.1 Coulomb counting method

CCM is one of the simplest methods of SOC estimation. It is used to find a direct relationship between the SOC and the battery charging/discharging current. This method is commonly used in small electronic devices. Despite its simple computation, this method is not suitable for online SOC estimation because of its large error accumulation and the need for an initial SOC value (Caiping Zhang et al., 2016).

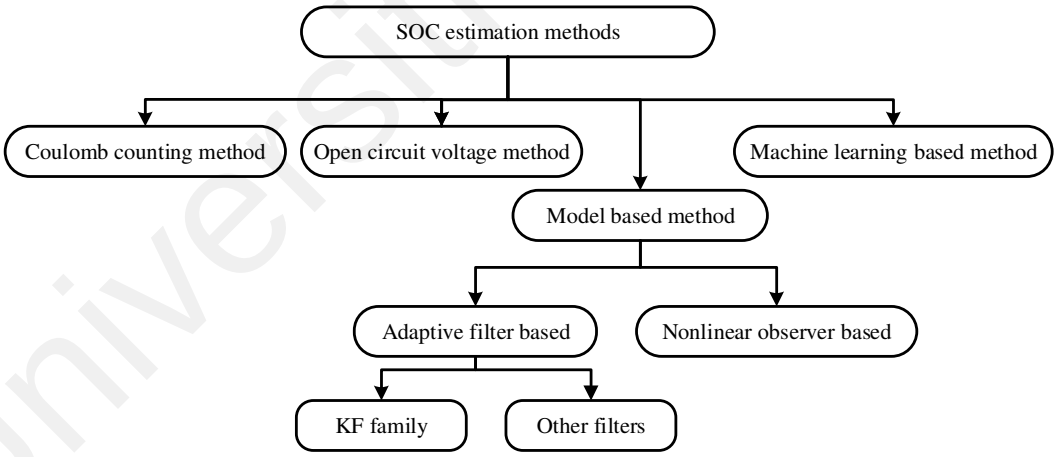

Figure 2.9: Categorisation of SOC estimation methods

2.6.1.2 Open-circuit voltage method

OCVM has high precision and is easily implementable for SOC estimation. In this method, the OCV–SOC relationship is derived from the stepwise measurement of OCV for different values of SOC. Moreover, every LIB has its OCV–SOC curve that changes throughout the battery's life and the associated hysteresis effect, even though

they are of the same material, structure and rating (S. Lee et al., 2008). According to (Cuma & Koroglu, 2015), the OCV–SOC curve changes slightly throughout the battery life and can thus be neglected.

For the same SOC level, the value of OCVs cannot be the same during charging and discharging because of the hysteresis characteristic (Hannan, Lipu, et al., 2017). However, in some LIB chemistries, the hysteresis effect can be ignored (Waag et al., 2014). In previous years, various modified OCVMs have been proposed in the literature to improve accuracy and processing time (Leng et al., 2014; Waag & Sauer, 2013). However, this estimation method remains inappropriate for online SOC estimation owing to its high dependency on OCV values and the necessity of a long period to achieve a satisfactory equilibrium condition (S. Lee et al., 2008). It also requires high precision during the charging/discharging voltage measurement.

2.6.1.3 Model-based method

The main principle of the model-based SOC estimation method is to relate the measured battery signals (voltage, current and temperature) with the battery model. Three types of battery models, namely ECM, EECM and electrochemical impedance model (ECIM), are mainly employed in this method (R Xiong et al., 2018). In the ECM-based approach, parameters related to lithium (Li) concentration on positive and negative electrodes are utilised for SOC estimation (Junfu Li et al., 2016, 2017; Tagade et al., 2016). However, these ECM-based approaches are not reasonable for SOC estimation because of the high participation of unknown variables and nonlinear partial differential equations (PDEs) (Bartlett, Marcicki, Onori, Rizzoni, Yang, et al., 2016). In the case of SOC estimation using ECIM, the relationships between battery impedance and SOC are used. Nevertheless, due to the high sensitivity of battery impedance against operating conditions, this method is not appropriate for online SOC estimation. Conversely, the

merits of the EECM-based approach, such as low complexity and high accuracy, make it favourable for online SOC estimation.

The nonlinear techniques developed by researchers for EECM-based online SOC estimation can be classified into two groups: adaptive filter based and nonlinear observer based. In nonlinear techniques, a voltage-based correction method is used to update the algorithm for accurate SOC estimation, in which the difference between the model voltage and the measurement voltage is used for SOC estimation. According to the mathematical approach, this method can be further classified into two categories, KF based and other adaptive filter based, as shown in Figure 2.9. The performance of the KF-based SOC estimation is highly dependent on the accuracy of the battery model and the measurement covariance information (Hongwen He et al., 2013; Jiahao Li et al., 2013; Meng et al., 2016; Xia, Wang, Tian, et al., 2015). Currently, owing to its high accuracy and self-correcting features, KF family-based SOC estimation is one of the preferred approaches for online SOC estimation (Meng, Ricco, Luo, et al., 2018). Different advance variants of KF family algorithms have been proposed by researchers for SOC estimation. These algorithms are elaborated with the help of suitable examples in Section 5. KF family algorithms can typically attain high accuracy with the assumption of Gaussian distribution system noise during SOC estimation. In previous years, other adaptive filters have been utilised for SOC estimation, including PF (Chin & Gao, 2018; El Mejdoubi et al., 2016; Xia, Wang, Wang, et al., 2015; Yongzhi Zhang et al., 2017), unified particle filter (UPF), modified particle filter (MPF) (B. Li et al., 2018; G. Li et al., 2018; Shao et al., 2014; Y. Wang et al., 2015; Xia et al., 2017), H-infinity (Rivera-Barrera et al., 2017), PSO (Chin & Gao, 2018; Mesbahi et al., 2016) and proportional integral (Meng, Ricco, Acharya, et al., 2018).

2.6.1.4 Machine learning based method

With the advancement of computer technologies, SOC estimation using machine learning is becoming an attractive area for researchers to investigate. SOC estimation based on machine learning can be divided into two phases: data training and learning (Z. Li et al., 2017b). In the data training phase, some experiments are performed in a controlled environment on the LIB to generate a training data set. CCM is used to generate numerous data sets analogous to the relationship between input (voltage, current, temperature, SOH and impedance) and output (SOC). With the assistance of these data sets, SOC estimation is performed during the learning phase. Some machine learning tools, such as artificial neural network (F. Liu et al., 2015; Pu Shi et al., 2005), fuzzy logic (Y. Ma et al., 2018; Salkind et al., 1999; Singh et al., 2006; Zenati et al., 2010), support vector mechanism (Alv et al., 2013; Alvarez Anton et al., 2013; J. N. Hu et al., 2014; Meng et al., 2016; Sheng & Xiao, 2015), support vector regression (Farmann et al., 2015; Shi et al., 2008), extreme learning machine (Cao et al., 2017; G.-B. Huang & Chen, 2008) and genetic algorithm (GA), are used for SOC estimation (L. Chen et al., 2018; J. Lu et al., 2018a; Panday & Bansal, 2016). Real-world dynamic conditions can be considered during the data training phase, and this approach is suitable for all types of chemistry batteries. However, accurate SOC estimation requires enormous hardware (CPU and memory) to handle a large data set.

Table 2.3: Comparison of different SOC estimation methods

Method	Complexity	Computational Burden	Accuracy	Limitations
CCM (Plett, 2004e; Caiping Zhang et al., 2016)	Low	Low	Low	Open-loop method Difficult initial SOC prediction High possibility of error accumulation Battery lifespan affected by the maximum capacity value.
OCVM (Hannan, Lipu, et al., 2017; S. Lee et al., 2008; Roscher & Sauer, 2011)	Medium	Low	Medium	Variable and unique OCV–SOC relationship Accuracy affected by the flat curve of the LIB for the wide range of SOC Estimated SOC value is largely affected by the battery hysteresis Longer rest time is needed for equilibrium
MBM (Meng et al., 2019; Z. Zhang et al., 2021)	Low	Medium	High	High correlation between model parameter and estimated SOC accuracy Time-consuming process
MLM (Z. Li et al., 2017b; F. Liu et al., 2015; Pu Shi et al., 2005)	High	High	High	Numerous trained data are needed for accurate measurement Large memory and advanced CPU are required Not suitable for vehicle application Highly precious fitting tool is always needed

2.6.2 SOE estimation methods

The battery SOC refers to the available capacity (Ah) instead of available energy (Wh) and the information related to battery available energy can calculate by using the battery state of energy (SOE) estimation. The SOE is a more suitable battery state which can be used to offer user-friendly driving. Further, the online SOE estimation is generally required for the optimization and management of the energy flow within EVs. As shown in Figure 2.10, the battery SOE estimation methods can be classified into three categories such as power integral method, model-based method, and machine learning-based method (Chang et al., 2020). Table 2.4 lists the various attributes of these SOE estimation methods.

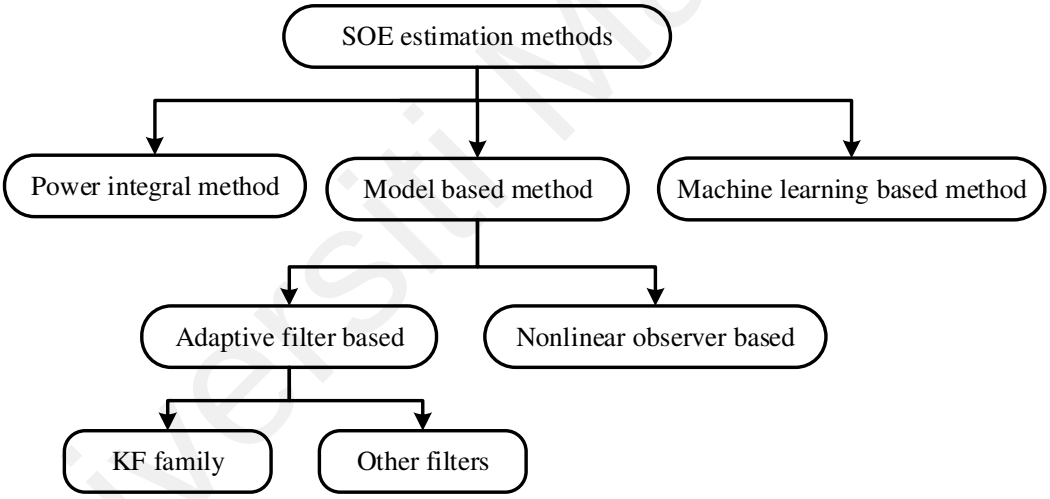

Figure 2.10: Categories of SOE estimation method

2.6.2.1 Power integral method

In the power integral method, the SOE estimation can be performed by using (2.4). Despite its simple implementation, this method is not suitable for online SOE estimation because of its large error accumulation and the need for an initial SOE value. Furthermore, due to change in $E_a(t)$ with battery aging and operating conditions, the

power integral method is not suitable for the SOE estimation under complex and dynamic operating conditions (Y. Wang et al., 2016).

2.6.2.2 Model-based method

Interestingly, the approaches used in SOC estimation can also be employed for SOE estimation as well (Dong, Chen, et al., 2016; Xu Zhang, Wang, Wu, et al., 2018). For instance, a hybrid LIB model-based analytical method was proposed to estimate the battery SOE in (K. Li et al., 2018). The coulomb counting method was utilized for the SOC estimation. It is demonstrated that the SOE estimation error is always less than 4.7 % under dynamic loading conditions. In (Y. Wang et al., 2016), the model-based SOE estimation using extended Kalman filter (EKF) is investigated, but the offline method of the 1RC battery model parameter identification method was used in the study. In (Chang et al., 2020), model-based SOE estimation using an unscented particle filter (UPF) is developed. The recursive least square with forgetting factor (RLSF) algorithm is used for battery modeling and the result demonstrates the SOE estimation error of less than 1.8 %. In (Chang et al., 2020), the method of SOE estimation using the UKF algorithm is developed and the error is less than 1.8 %. However, the performance of the estimation method highly depends on the battery model accuracy due to the non-linear relationship between the SOE and battery terminal voltage. Furthermore, the computational complexity of the SOE estimation method increases significantly as a new state-space model is required.

2.6.2.3 Machine learning-based method

Recently, a few data-driven methods also have been investigated for SOE estimation to further improve the estimation accuracy such as in (X. Liu et al., 2014), the back-propagation neural network-based open-loop SOE estimation was developed and demonstrates good accuracy under dynamic load current and temperature conditions.

However, the performance of this estimation method is very sensitive to measurement errors. The Long Short-Term Memory Neural Network (LSTNM-NN) is utilized for SOE estimation in (L. Ma et al., 2021). However, large data sets were involved in the training of the NN model.

Table 2.4: Comparison of different SOE estimation methods

Method	Complexity	Computational Burden	Accuracy	Limitations
Power integral method (Y. Wang et al., 2016)	Low	Low	Low	Open-loop method Difficult initial SOE prediction High possibility of error accumulation Battery lifespan affected by the available energy determining process
Model-based method (Dong, Chen, et al., 2016; Xu Zhang, Wang, Wu, et al., 2018)	Low	Medium	High	High correlation between model parameter and estimated SOE accuracy Time-consuming process
Machine learning-based method (X. Liu et al., 2014; L. Ma et al., 2021)	High	High	High	Numerous trained data are needed for accurate measurement Large memory and advanced CPU are required Not suitable for vehicle application Highly precious fitting tool is always needed

2.6.3 SOP estimation methods

To operate the battery in its safe operating region, the SOP estimation plays a crucial role along with the SOC and SOH estimation. The SOP is the function of different battery parameters and battery internal/external conditions (Farmann & Sauer, 2016). As the battery internal conditions change with the aging effect, it is hard to estimate the accurate real-time SOP value.

As shown in Figure 2.11, the SOP estimation techniques can be categorized into three groups: characteristic map (CM) method, Model-based method (Waag et al., 2014) (Farmann et al., 2015; Farmann & Sauer, 2016; J. Lu et al., 2018b) and Machine learning-based method. Table 2.5 lists the various attributes of these SOP estimation methods.

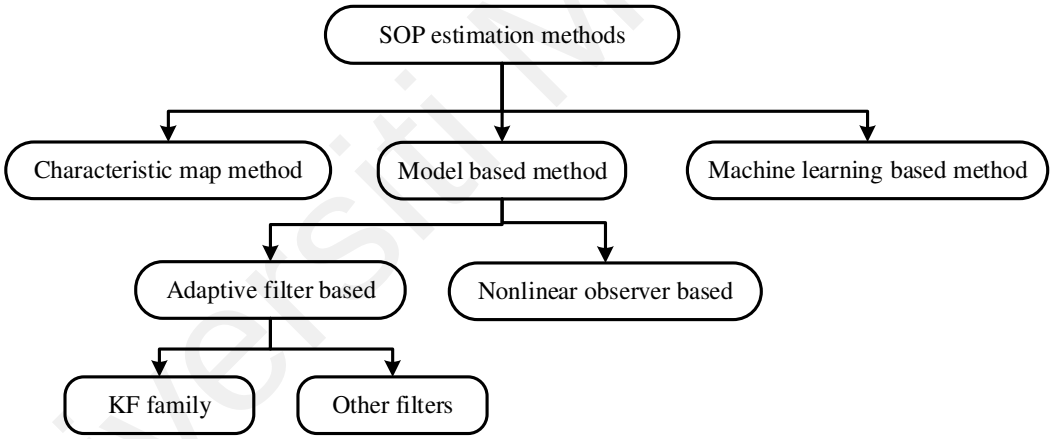

Figure 2.11: Categories of SOP estimation method

2.6.3.1 Characteristics map-based method

In this method, the relation between the available power and the different states (such as SOC, SOH, temperature), and parameters (like power pulse time scale) are used to develop the characteristic map. As shown in Figure 2.11, the data related to CM is generated by the standard laboratory tests such as HPPC (Farmann & Sauer, 2016; Plett, 2004b) and EIS (J. Lu et al., 2018b) test, and the results are stored in the non-volatile memory of BMS. In (Cecile Vacher, 2002), the available power is determined from OCV

and internal resistance for a given SOC from CM data. In the proposed method, the fixed value temperature is used consequently the internal resistance remains constant through the lifetime although the increase in resistance is expected with time. The non-adaptive character of this proposed method is the main drawback, and it would be a cause of error in estimation. Since all the battery states are time-variant so that some adaptive technique is required to employ with this method (Lashway & Mohammed, 2016). With the addition of the adaptability feature, the SOP estimation error improves (Farmann et al., 2015; Farmann & Sauer, 2016). It is a simple method for SOP estimation. Nevertheless, it has some drawbacks like static battery characteristics are considered for estimation, employment of the adaption technique is not suitable for maximal power prediction, large space is required to store the multi-dimensional CMs. Memory problems can be resolved with the approximation of some parameters in the CMs but it will increase the adaptive technique complexity (Farmann et al., 2015).

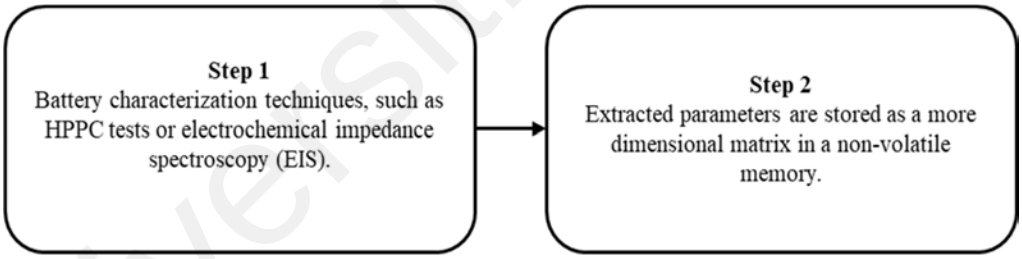

Figure 2.12: Fundamental steps involved in SOP estimation using CM method

2.6.3.2 Model-based method

The model-based SOP estimation method is the most promising approach, and it outperforms all the downsides related top CM method. The accuracy of the estimated SOP depends on the model accuracy. Low complexity and computational effort features of the EECM of LIB make it the most advantageous LIB model for the SOP estimation process of EVs where the high dynamic load is available. Further, the consideration of battery design limits also affects the performance of SOP estimation. For example, the

Rint model was utilized for voltage-based SOP estimation in (Plett, 2004f). However, two battery design limits such as voltage and current are considered that may cause overcharge and discharge issues without SOC limit. In (Dong, Wei, et al., 2016), the SOP estimation using KF is investigated. The power capability of the battery is demonstrated in the results. However, the method uses only one constraint for SOP estimation that could produce over-optimistic results. In (W. Zhang et al., 2015a), the SOP estimation using EKF is investigated. 1RC battery model and two constraints such as current and SOC are considered for SOP estimation. Though, the voltage constraint is missing due to which the overvoltage and under-voltage conditions may occur. To improve the SOP estimation accuracy, the multi-constraints (voltage, current, and SOC) SOP estimation method using the 1RC model is proposed in (Pan et al., 2017). The advantages of multi-constraints SOP estimation over a single constraint are deeply analyzed. The results demonstrated that the consideration of multi-constraint, accuracy, and robustness of the SOP estimation can be significantly improved. For example, in (J. Lu et al., 2018c), Genetic algorithm-based SOP estimation using the 1RC model is proposed. By considering three constraints (SOC, current, and voltage), the results demonstrate high SOP estimation accuracy up to 7.2 % as compared to the traditional Taylor method (T-method). In (L. Yang et al., 2020), a long-term power demand (LTPD) prediction model is employed for SOP estimation. As compared to the traditional method, the proposed method able to reduce error by 85.9%. However, with the application of the 1RC model, the accuracy of SOP estimation improves at cost of higher computational effort. In this thesis, to maintain the trade-off between accuracy and computational complexity, the Rint model is utilized for SOP estimation.

2.6.3.3 Machine learning-based method

In the machine learning-based method, the battery is regarded as a black box where the internal electrochemical dynamics of the battery are not considered. The SOP

estimation is done based on the model developed employing data collected from the experimental study. Generally, in the model development, the battery voltage, current, and operating temperature are considered as input and the SOP is taken as output. For example, in (Fleischer et al., 2013) an adaptive neuro-fuzzy-inference system (ANFIS) is used for SOP estimation. Though, the current limiting factor was not neglected in the study.

Table 2.5: Comparison of different SOP estimation methods

Method	Complexity	Computational Burden	Accuracy	Limitations
Characteristics map-based method (Farmann et al., 2015; Farmann & Sauer, 2016)	Low	Low	Low	Open-loop method Static battery characteristics are considered for estimation large Large size memory is required to store the multi-dimensional CMs
Model based method (Dong, Wei, et al., 2016) (Pan et al., 2017)	Low	Medium	High	Accuracy of estimated SOP depends on the model accuracy Time-consuming process
Machine learning based method (Fleischer et al., 2013)	High	High	High	Numerous trained data are needed for accurate measurement Large memory and advanced CPU are required Highly precious fitting tool is always needed

2.6.4 SOH estimation methods

Like other battery states, the direct monitoring of SOH is not possible due to battery complex internal dynamics. Mostly, the battery internal resistance and available capacity are related to the SOH that denotes the extent of the battery aging. Different SOH estimation methods have been investigated in the literature that can be broadly classified into two categories such as experimental method and model-based method, as presented in Figure 2.13. Table 2.6 lists the various attributes of these SOH estimation methods.

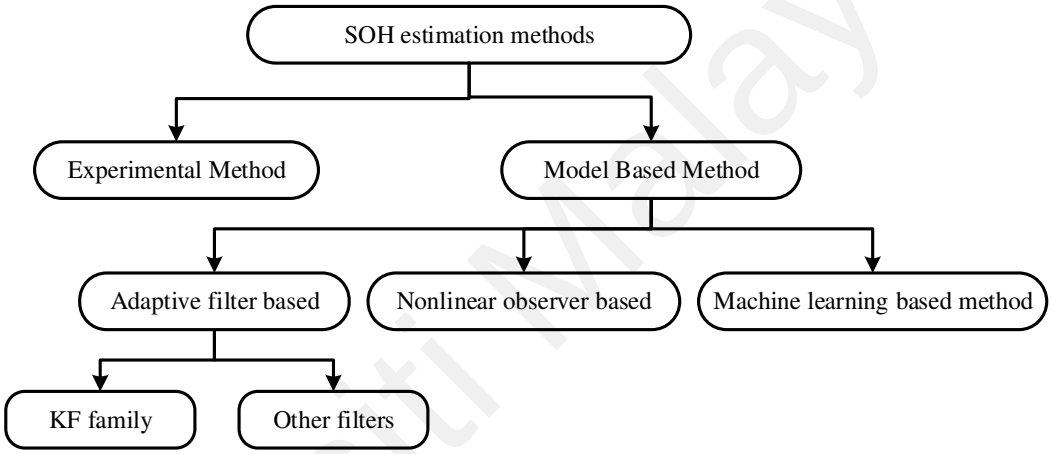

Figure 2.13: Categories of SOH estimation method

2.6.4.1 Experimental Techniques

There are several experimental methods available in the literature for SOH estimation. Mainly, the coulomb counting, electrochemical impedance spectroscopy (EIS), and incremental capacity and differential voltage (IC/DV) analysis are utilized in the experimental SOH estimation method (W. Li et al., 2021a). The major limitation of the experimental method is the requirement of a unique charging profile that is hard to achieve in real-time application. Under the coulomb counting method (J. Yang et al., 2018), the number of Ah are counted during the charging and discharging process. Once the battery reached its cut-off voltage, the total counted Ah is divided by the BOL capacity to estimate the SOH (Berecibar et al., 2016b). The main shortcomings of this method are

(*i*) it generally required large-size memory for storing, (*ii*) the possibility of error accumulation during computation is high and (*iii*) achievement of cut-off voltage required to update the total counted Ah during real-time operation is very difficult. As the battery internal impedance increases with battery aging, the different frequency ranges on the EIS are used for SOH estimation. Different battery parameters can be extracted over the wide frequency range through the Nyquist plot draw from the EIS results. For example, very low-frequency impedance spectra show purely ohmic resistance and at the high frequency, it shows the inductive behavior. The small semicircle presents the solid electrolyte interface (SEI) layer and the larger semicircle shows the charge transfer process and the double-layer capacitance. However, the application of EIS in the real-time application is not feasible because of the amplified noise error even with the use of smoothing filters and the requirement of collection of input data over the wide voltage range. The IC/DV method can estimate the SOH accurately by utilizing the measurement voltage and current. In which, the IC is referred to as the ratio of change in battery capacity to the change in terminal voltage during charging and discharging. In IC/DV analysis, the very low current passes through the cell to get the charge-voltage curves. The DV is stated as the inverse of differential capacity. Under IC/DV method, the shift in the peak and valley points on the IC curve is mainly considered for SOH estimation. The peak and valley positions are highly sensitive to the operating conditions, for example, C-rate, temperature, aging/cycles. Several methods have been proposed by the researchers in the literature. For example, to estimate the SOH from the IC curve, in (Z. Wang et al., 2017), the method based on Gaussian process regression with a multi-island genetic algorithm (GRP-MIGA) was proposed by the authors. Under which, the wavelet filtering was used for the peak value and position extraction, and that was considered as health factors (HFs). Further, the grey correlation analysis was utilized to find the correlation between SOH and HFs. Finally, the performance of the proposed SOH

estimation method was validated by using an accelerated battery life test. In (Riviere et al., 2019), the innovative IC analysis method was proposed by Riviere. et. al., under which the area under the IC curve between the voltages is considered to estimate the SOH. To validate the effectiveness of the proposed method, the different chemistries batteries such as LFP and LMO were tested under dynamic operating conditions and the accuracy of less than 2% and 4% were recorded, respectively. However, with the involvement of differentiation, the impact of noise on the performance of SOH estimation is more even with smoothing filters. Also, the gathering of input data for a wide operating range is difficult in real-time applications. To overcome these issues, model-based methods are developed to work with sensor data directly.

2.6.4.2 Model-based method

The identified battery model parameter values are utilized for SOH estimation in the model-based method. Generally, the model parameters such as capacity and internal ohmic resistance are employed for SOH estimation. For the identification of model parameters different adaptive algorithms, non-linear observers, and machine learning methods have been greatly utilized in the literature. For example, in (Remmlinger et al., 2013), the internal resistance of the linear parameter-varying battery model identified by KF is employed for SOH estimation. The results demonstrate the SOH estimation over a wide range of operating conditions. An EKF is a non-linear version of KF and it is widely utilized for battery model parameter identification. In (Plett, 2004c), the EKF is used for the identification of the capacity and internal resistance of the battery model. The results obtained are very accurate and the implementation of EKF for SOH estimation is lighter. To address the variations in battery model parameters with aging, the SOH estimation using EKF is investigated in (J. Kim & Cho, 2011). It is observed that the diffusion resistance is more sensitive than other battery model parameters and implementable for SOH estimation. In (Xu Zhang, Wang, Liu, et al., 2018), the battery model parameters

were identified by using particle swarm optimization-genetic algorithm and SOC-OCV relationship obtained by particle filter. Lastly, the capacity estimation is performed by the RLS method for SOH estimation. The experimental results indicate high SOH estimation accuracy. In (Tan et al., 2021), to reduce the computational cost and achieve high accuracy, the model parameter identification and SOC estimation are performed at a multi-time scale. Further, based on the data collected from the accelerated degradation test, the relationship between RC parameters and SOH is developed. The obtained is employed for SOH estimation using SVR. In (Zhengyu Liu et al., 2020), the indirect enhanced health indicator (HI) and SVR are utilized for SOH estimation. The differential evolution algorithm is utilized to optimize the hyperparameters of the SVR. In (Gou et al., 2020), a novel ensemble learning method is proposed for SOH estimation. For a fast and efficient learning process, the extreme learning machine (ELM) is used to extract the relationship between the HIs and SOH. The developed method can accurately estimate the SOH with RMSE less than 0.78 % in 1ms under dynamic operating conditions. In (W. Li et al., 2021a), a long-short term memory (LSTM) network is developed to estimate the battery remaining capacity as output per cycle. The raw sensor voltage data from partial constant current charging curves are used for the training. The results demonstrated high accuracy even under 15 % missing data.

Table 2.6: Comparison of different SOH estimation methods

Method	Complexity	Computational Burden	Accuracy	Limitations
Experimental Techniques (W. Li et al., 2021a; J. Yang et al., 2018)	Low	Medium	Low	Open-loop method Not suited for situ estimation
Model-based method (W. Li et al., 2021a; Xu Zhang, Wang, Liu, et al., 2018)	High	High	High	High computational effort Difficult in BMS implementation Time-consuming process

2.6.5 Actual capacity and maximum available energy estimation

As the actual capacity (Q_n) and maximum available energy (E_n) decreases with the battery aging. Two essential parameters can contribute to the accurate SOC and SOE estimation and also indicate the SOH of the battery cell. However, the estimation of Q_n and E_n is difficult due to its dependence on operating conditions and battery aging level. For an accurate SOC and SOE estimation, the correct value of Q_n and E_n are required to update during real-time operation. By using the (2.2) and (2.4), the value Q_n and E_n can be calculated by using expressions (2.9) and (2.10), respectively. Where, t_1 and t_2 are two different time instant.

$$\mathrm{Q_n} = \left(\left(\int_{\mathrm{t}_1}^{\mathrm{t}_2} \mathrm{I(t)d(t)}\right) \times 3600\right) / (SOC(\mathrm{t}_1) - SOC(\mathrm{t}_2)) \tag{2.9}$$

$$\mathrm{E_n} = \left(\left(\int_{\mathrm{t}_1}^{\mathrm{t}_2} I(t).v(t)d(t)\right) \times 3600\right) / (SOE(\mathrm{t}_1) - SOE(\mathrm{t}_2)) \tag{2.10}$$

In the literature, there are three types of methods for the actual capacity estimation namely differential analysis (DA) or incremental capacity analysis (ICA)-based method (J. He et al., 2020), machine learning (ML) based method, and model-based method are investigated. In the DA-based (S. Zhang et al., 2020) and ML-based methods (Fan et al., 2021; W. Li et al., 2021a), large experimental datasets are needed to accurately estimate the battery's actual capacity. In both methods, a long testing time and extensive offline investigation are always required. Also, the accuracy of the estimated capacity depends on the quantity and quality of the training data. Though, the model-based method combines battery model and estimation algorithms. In (Plett, 2011), the capacity estimation is performed by an approximated weighted total least square (AWTLS) algorithm. The AWTLS allows nonproportional noises on both the integrated current and SOC difference to make it implementable in BMS. However, as the sigma-point KF (SPKF) with offline identified model parameters employed for SOC estimation, the SOC

estimation accuracy cannot be guaranteed for a long-time. Therefore, with the employment of the online model parameters identification method, the accuracy of estimated capacity can be improved further. Also, there is a need to reduce the computational cost of the AWTLS method.

Compared to actual capacity estimation, few studies are available in the literature on maximum available energy estimation (Deng et al., 2017). For example, the support vector regression algorithm is used for maximum available energy estimation in (Deng et al., 2017). The Long Short-Term Memory Neural Network (LSTNM-NN) is utilized for SOE estimation (L. Ma et al., 2021). Both the studies demonstrate good SOE estimation accuracy. However, large data sets are involved in the training of the SVR model and NN model. In (S. Zhang & Zhang, 2021a), the model based maximum available energy estimation method is investigated with the help of SOE estimated using AEKF. The effect of operating temperature on estimation accuracy is analyzed. The results demonstrated that the estimated maximum available energy MAE and RMSE lies in the range of 1.5 % to 3.5 %. In (L. Zheng et al., 2016b), the moving window energy-integration and average method is used for the maximum available energy estimation. However, the issue of slow convergence and high initial estimation error exists. In this thesis, the estimation of Q_n and E_n are performed by using the new low cost AWTLS method as proposed in chapter 5.

2.7 Battery states co-estimation method

The accuracy of the individual state estimation method is directly or indirectly influenced by the other states information in a LIB system. In most of the single/individual state estimation methods, the correlation between the states is overlooked due to which it is hard to get high estimation accuracy. In the past few years, to improving the accuracy and robustness of BMS, the battery states co-estimation

methods are gaining popularity. Based on the different states involved in the co-estimation method, the existing co-estimation method can be classified into several categories such as 1) SOC and SOH, 2) SOC and SOE, 3) SOC and SOP, and 4) others.

2.7.1 SOC and SOH

Practically, the SOC and SOH are highly correlated with each and it cannot be ignored to achieve high estimation accuracy. As the SOH varies at a very slow rate over the battery life as compared to SOC and both are coupled with sophisticated electrochemical processes, therefore, it is challenging to estimate both simultaneously. In the last couple of years, different methods for co-estimation SOC and SOH have been investigated by researchers.

For example, in (J. Kim & Cho, 2011), the SOC and SOH estimation have been developed by using the modified EKF (MEKF). The SOC and SOH estimation was performed with the employment of per unit (p.u.) values instead of absolute values. Due to the high sensitivity of diffusion resistance than other model parameters, it was used for SOH estimation. The SOC estimation error was within ±5% of the ampere-hour counting that required to improve further. To achieve high estimation accuracy, the multi-state observer has been proposed in (Y. Zou, Hu, Ma, & Eben Li, 2015). In which the 2^{nd} and 4^{th} order EKF observers were utilized for the SOC and SOH estimation, respectively. However, SOH estimation was performed by an offline method, therefore, it cannot be used for online applications. For online SOC and SOH estimation, a new simple and computationally efficient estimation method has been proposed in (Cacciato et al., 2017). The SOC and SOH are simultaneously online estimated by the simple mathematical formulas used by PI-based observers. Although, the results illustrated that the proposed method was suitable for a wide range of operating conditions however the estimator accuracy depends upon the precision of the sensors utilized for the measurement. To

overcome this issue, the co-estimation of SOC and SOH estimation is performed by using dual fractional-order extended Kalman filter (DFOEKF), in (X. Hu et al., 2018),. The high-fidelity fractional-order ECM parameter is identified by using the Hybrid Genetic Algorithm/Particle Swarm Optimization (HGAPSO) technique to reduce the effect of sensor noise. The results demonstrate the fast convergence and high accuracy with the error within 1% for both SOC and SOH at a high computational cost. In (M. Zeng et al., 2019), a fuzzy control trace-free Kalman filter with 2-RC EECM has been investigated for the co-estimation of SOC and SOH. To simultaneously estimate SOC and internal resistance, two complete fuzzy UKF (F-UKF) algorithms were used. High estimation accuracy of SOC and internal resistance was achieved with the assistance of two different fuzzy controllers. The results claimed good performance of the developed co-estimation method with unknown initial SOC condition with good convergence speed under dynamic operating conditions.

In (Song et al., 2020), a sequential algorithm has been investigated for SOC and SOH estimation. To improve the battery capacity and SOC estimation accuracy, the parameters/states estimation and frequency-scale separation were done by injecting the different frequencies' current signals. Experimental results were demonstrated the high estimation accuracy at low computational cost than the concurrent algorithm where all parameters/states are estimated simultaneously. However, the accuracy of the developed algorithm is not validated at low-aged conditions. To outperform this issue, a low-cost method for co-estimation of SOC and SOH using DEKF has been developed, (Park et al., 2021). To reduce the computational cost, the MAFF-RLS method was employed OCV, capacity, and model parameter identification. Whereas DEKF was used for SOC and SOH estimation. The developed method was a self-adaptive algorithm means there was no need to develop OCV-SOC lookup tables under dynamic operating conditions. The results demonstrated that the developed estimator could maintain high accuracy under varying

degradation processes. To further reduce the computational burden and improve the SOC estimation accuracy, the multi-time scale frame for co-estimation of capacity and SOC is investigated (S. Zhang & Zhang, 2021b). The SOC estimation was done by using the AEKF algorithm with 1-RC model parameters identified by using FFRLS. The capacity estimation was performed by using EKF at the macro time scale. It was claimed that estimated SOC and capacity MAE maintained below 1 % under dynamic operating conditions. However, the high estimation accuracy cannot guarantee under real-time applications as the measurement noise effect was not considered.

2.7.2 SOC and SOE

In recent, simultaneous SOC and SOE estimation plays an important role in EV battery performance advancement. SOC and SOE are useful for the estimation of the remaining capacity and energy of the battery respectively. To optimize the application of EV, it is necessary to estimate both states. In (L. Zheng et al., 2016a), to investigate the SOE and maximum available energy, the $LiMn_2O_4$ cell of 90Ah capacity has been utilized under different aged conditions. Also, the different charge/discharge test was conducted to find the relation between the SOC and SOE. The results demonstrate the linear relation between SOC and SOE under different temperature and aged levels. In this paper, a moving-window energy-integral and average method are employed for the accurate SOE and maximum available energy estimation. However, the estimation accuracy depends on the measurable relationship between SOC and SOE that is used for the SOE estimation.

In (Yongzhi Zhang et al., 2017), the estimator has been developed by the authors by using an adaptive H-infinity filter for combined SOC and SOE estimation in the real-time application. To evaluate the performance based on the ME and convergence rate, two other algorithms are used such as EKF and H-infinity. The results demonstrate the highest convergence rate and lowest ME of SOC and SOE estimation using adaptive H-infinity

filter. However, the use of offline model parameters limits the application in the long run. Furthermore, two different H-infinity filters were employed for battery SOC and SOE estimation that causes high computational cost.

2.7.3 SOC and SOP

On the other hand, for the optimal energy management unit in the EV, concurrent SOC and SOP estimation are also needed. Underestimate and overestimate the SOP value, may lead to overly conservative vehicle energy management and premature battery failure, respectively. With the development of EV technology, several individual offline and online SOP estimation methods have been presented. However, these methods are still not reliable enough. The relation between the battery discharge power is calculated by the HPPC method, SOC, and temperature. In (Rui Xiong, Sun, et al., 2013), the combined SOC and SOP estimation method has been presented to achieve high reliability. In this work, the data-driven method is used for battery parameter estimation. The adaptive EKF is used for the SOC and SOP estimation. To improve the accuracy of the estimation for aged batteries, the same method has been used (F. Sun et al., 2014) with the consideration of battery SOH. Though, this method cannot be well suited for online applications due to the requirement of large data. The effect of SOC and SOH on SOP estimation accuracy has been analyzed and discussed in (J. Lu et al., 2018a). It concluded that the effect of SOC error on SOP estimation is lesser for the aged battery as compared to the healthy battery.

2.7.4 Others

Recently, the researchers are focusing on the development of a co-estimation method for concurrent estimation of three or more battery states to further improve the performance of the BMS. For instance, in (Xu Zhang, Wang, Wu, et al., 2018), the simple SOE and SOP estimation is performed based on the online estimated SOC using UKF at

each macro time. To reduce the complexity of the process, the SOP was determining by terminal voltage, SOC, and design limits. On the other hand, PSO and UKF were utilized for the online battery parameter identification and SOC estimation, respectively. The results demonstrate that the proposed algorithm estimates the SOC with less than 0.08% RMSE. However, the influence of SOH on the SOE and SOP estimation process was not considered in this study.

In (P. Shen, Ouyang, Lu, et al., 2018), the co-estimation method for SOC, SOH, and SOP has been investigated. In this work, the estimated SOC using EKF was used to calculate the SOH and SOP of the battery. The method was validated to be effective in online applications with high accuracy. However, due to the employment of the offline parameter identification method, the performance of this method cannot be consistent with the battery age will increase. As the computational burden of the co-estimation algorithm proportionally increases the cost and size of the controller used in BMS. Thus, there is a need to develop an accurate battery states co-estimation method with a low computational burden that acquires the benefits of correlation between the battery states.

As the accurate SOC estimation is the primary step for the development of battery states co-estimation method. In the proceeding section, the insights of online SOC estimation using the KF algorithm are provided as it is a key focus of the thesis. Furthermore, the features of different KF algorithms suitable for SOC estimation are explained.

2.8 Simplified model-based online SOC estimation using KF algorithm

The basic flow chart of the model-based online SOC estimation method using the KF algorithm is depicted in Figure 2.14. For a better understanding of the readers, the complete SOC estimation process is divided into three subtasks. The first task is to estimate a predetermined SOC using the (Ampere Hour Counting) AHC process (Cuma

& Koroglu, 2015). In which, the initial SOC (Y. Zou, Hu, Ma, & Li, 2015), battery charge /discharge current (Hongwen He et al., 2012a), and battery capacity (Y. Zheng et al., 2018) are mainly required for the calculation of the predicted SOC. In the case of online SOC estimation, the value of the initial SOC can be extracted from the SOC-OCV relationship or the stored memory database. Based on the interpolation method, the OCV for the battery model, corresponding to the predicted SOC, can be calculated from the SOC-OCV relationship (Han et al., 2014; S. Yang et al., 2017; R. Zhang, Xia, Li, et al., 2018b). The second task is to estimate the model voltage by using the selected battery model. Based on the measurement voltage, current, and temperature values, the battery model parameters can be evaluated using several PIMs (Waag et al., 2013; B. J. Wang et al., 2017; Rui Xiong, He, Sun, & Zhao, 2013). The final task is to update the Kalman gain, in which the model voltage and measured voltage are compared with each other, and the voltage error is used to modify the Kalman gain. With the help of updated gain based on the KF family algorithm, the estimated SOC can be generated.

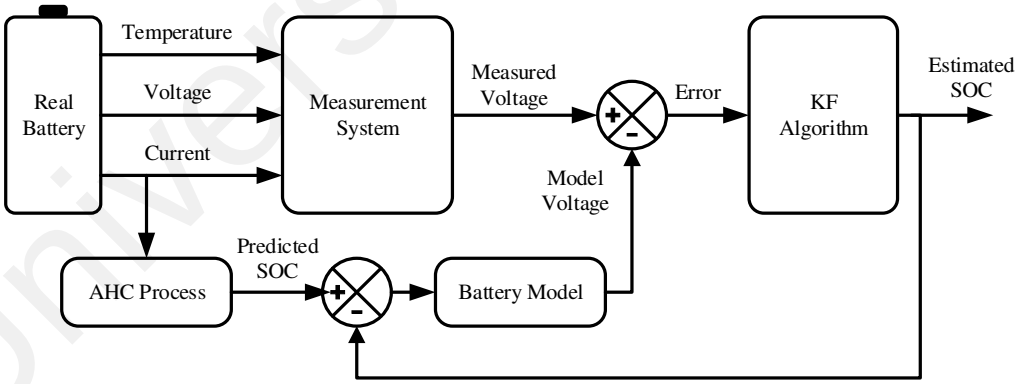

Figure 2.14: Simple flow chart of model-based online SOC estimation method using KF algorithm

2.8.1 General steps to combine battery model with KF algorithm

To combine the battery model with the KF algorithm, the discretized state-space model is utilized. As shown in Figure 2.15, the first step is the discretization of the battery model equations. In the case of ECM, it contains a large number of non-linear PDEs and often

challenging to discretize. For this purpose, different discretization methods have been utilized in the literature, for example, analytical method, integral method approximation, Padè approximation method, finite element method, finite difference method, differential quadrature and Ritz method (Corno et al., 2015; Ying Shi et al., 2011). In (Romero-Becerril & Alvarez-Icaza, 2011), the different discretization methods such as finite difference, finite element, and differential quadrature have been applied to the SP model of Li-ion cell and compared. The best results were obtained by the differential quadrature method in its polynomial version. In (Corno et al., 2015), an efficient electrochemical method-based SOC estimation method has been proposed by the authors. The semi-separable structure-based ECM was utilized in combination with EKF. The finite difference method was employed for the discretization of the battery model. Additionally, the results demonstrated less than 5% estimation error under dynamic loading. On the other hand, in the case of EECM, the bilinear transformation method is mostly employed by the researchers (Rahimi-Eichi et al., 2014; Safwat et al., 2017; Wei et al., 2018; Xia, Wang, Tian, et al., 2015; R. Zhang, Xia, Li, et al., 2018b).

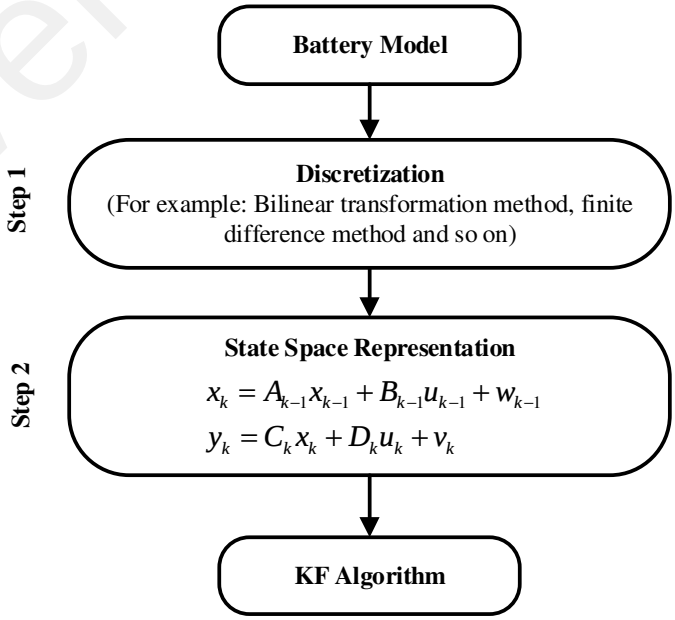

Figure 2.15: General steps to combine battery model with KF algorithm

Hereafter, the second step is to obtain the time domain difference equations from the discretized battery model, and it will be used in the PIM. By using the identified battery model parameters in the time domain difference equations, the state space representation useful for the KF algorithm will be developed. For example, online SOC estimation using 2RC model, the discretized form of state space equations can be represented by (2.8) (P. Shen, Ouyang, Lu, et al., 2018; Wijewardana et al., 2016).

$$\left.\begin{aligned}\begin{bmatrix} V_{1,k+1} \\ V_{2,k+1} \\ SOC_{k+1} \end{bmatrix} &= \begin{bmatrix} e^{-\frac{T_s}{\tau_1}} & 0 & 0 \\ 0 & e^{-\frac{T_s}{\tau_2}} & 0 \\ 0 & 0 & SOC_{k-1} \end{bmatrix} \begin{bmatrix} V_{1,k} \\ V_{2,k} \\ SOC_k \end{bmatrix} + \begin{bmatrix} R_1(1-e^{-\frac{T_s}{\tau_1}}) \\ R_2(1-e^{-\frac{T_s}{\tau_2}}) \\ \frac{\Delta t}{C_{actual}} \end{bmatrix} I_k \\ V_k &= U_{oc}(SOC_k) - V_{1,k} - V_{2,k} - I_k R \end{aligned}\right\} \quad (2.8)$$

2.9 Suitable KF family algorithms for model-based online SOC estimation

The fundamental principle of KF algorithm is that it recursively estimates the current state with the help of the previously estimated state and the current measurement signals. The self-correcting feature of the KF family algorithms makes it suitable for the model-based online SOC estimation for EV application. The complete KF family algorithms can be grouped into two categories based on the linearization process such as linear KF and non-linear KF as presented in Figure 2.16. Simultaneously, the non-linear KF method can be divided into three categories like EKF, SPKF and cubature KF (CKF), further SPKF divided into two parts like central difference KF (CDKF) and UKF. In the current scenario, for concurrent online estimation of battery parameter and SOC, the other two types of KF namely Joint and Dual KF (DKF) have been developed by the researchers.

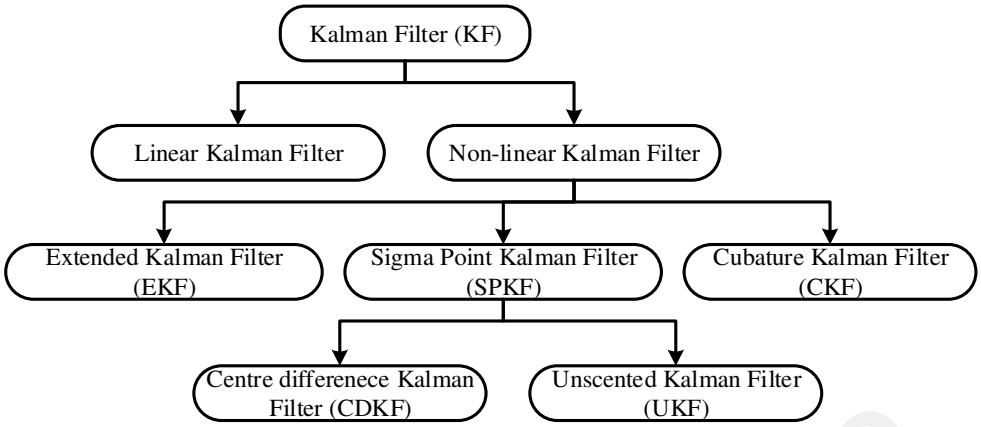

Figure 2.16: Kalman filter family algorithms suitable for online SOC estimation

2.9.1 Linear Kalman Filter (LKF)

The LKF is a well-known mathematical estimation method, and it was introduced in 1960 (S. Grewal & P. Andrews, 2001). It uses discretized mathematical equations of the linear dynamic system in the time domain for computation. It is a recursive estimation technique and provides optimal estimated values of the state with a minimum mean square error whose direct measurement is impossible (Mastali et al., 2013). The main advantage of this method is that it bounds the estimation mean square error. During the estimation process, it utilizes the process and measurement model with the noisy input-output measurements of the system usually described by (2.11) and (2.12) respectively. Where, $x_k \in \mathbb{R}^n$ is the state vector, $u_k \in \mathbb{R}^p$ is the deterministic system input and $y_k \in \mathbb{R}^m$ is the system output at time index k. $A_k \in \mathbb{R}^{n\times n}$, $B_k \in \mathbb{R}^{n\times p}$, $C_k \in \mathbb{R}^{m\times n}$ and $D_k \in \mathbb{R}^{m\times p}$ are system dynamics matrices. $w_k \in \mathbb{R}^n$and $v_k \in \mathbb{R}^m$ are independent white Gaussian process noise and measurement noise matrices with zero mean and known covariance values. P_w and P_v are the covariance matrices of process and measurement noise, respectively.

$$x_k = A_{k-1}x_{k-1} + B_{k-1}u_{k-1} + w_{k-1} \approx \mathrm{f}(x_{k-1}, u_{k-1}, w_{k-1}, k-1) \tag{2.11}$$

$$y_k = C_k x_k + d_k u_k + v_k \approx \mathrm{h}(x_k, u_k, v_k, k) \tag{2.12}$$

Table 2.7: Summary of LKF estimation algorithm (Mastali et al., 2013; Z. Yu et al., 2015)

Definition: Error, $\tilde{x}_k^{\pm} = x_k - \hat{x}_k^{\pm}$ and $\tilde{y}_k^{\pm} = y_k - \hat{y}_k^{\pm}$ Complete observations set, $\mathbb{Y}_k = \{y_0, y_1, y_2, \dots, y_k\}$ Conditional mean, $\hat{x}_k^{+} = E[x_k \mid \mathbb{Y}_k]$ and $\hat{x}_k^{-} = E[x_k \mid \mathbb{Y}_{k-1}]$	
Initialization: For $k = 0$, set	
Step1	State variable, $\hat{x}_0^{+} = E[x_0]$
Step 2	Covariance matrix, $P_{\tilde{x},0}^{+} = E[(x_0 - \hat{x}_0^{+})(x_0 - \hat{x}_0^{+})^T] = E[(\tilde{x}_0)(\tilde{x}_0)^T]$
Computation: for $k = 1,2,3, \dots$ compute	
Step 3	State estimation time update, $\hat{x}_k^{-} = A_{k-1}\hat{x}_{k-1}^{+} + B_{k-1}u_{k-1}$
Step 4	Error covariance time update, $P_{\tilde{x},k}^{-} = A_{k-1}P_{\hat{x},k-1}^{+}A_{k-1}^T + P_w$
Step 5	Output estimate, $\hat{y}_k = C_k\hat{x}_k^{-} + D_k u_k$
Step 6	Kalman gain matrix, $K_k = P_{\tilde{x},k}^{-}C_k^T[C_k P_{\tilde{x},k}^{-} C_k^T + P_v]^{-1}$
Step 7	State estimation measurement update, $\hat{x}_k^{+} = \hat{x}_k^{-} + K_k[y_k - \hat{y}_k]$
Step 8	Error covariance measurement update, $P_{\hat{x},k}^{+} = (I - K_k C_k) P_{\tilde{x},k}^{-}$

Notation: Circumflex (^) indicates the estimated value, Tilde (~) indicates the predicted value, "*T*" indicates the matric transportation. Superscript "+" and "-" indicates posterior and prior value respectively.

Generally, the process model and measurement model contain all the information about the system dynamics and measurement model that provides the idea about the relation between the system outputs, inputs, and states. The complete steps involve in LKF estimation technique are discussed in Table 2.7. The LKF estimation method is used for battery states and parameter estimation. Where the SOC_k and $V_{t,k}$ are considered as x_k and y_k respectively. Generally, in the case of battery $f(\cdot)$ is considered as a linear function while $h(\cdot)$ is a non-linear function due to the non-linear relationship between the U_{oc} and SOC. The LKF assumes that the process and measurement noise are known as independent zero-mean Gaussian noise signals. However, in the case of a practical system, this assumption may not be valid for all the situations. As the battery is a highly non-linear system, in (Z. Yu et al., 2015), a modified LKF is used for SOC estimation. In modified LKF, the local linearization method to map the predictive SOC to the predictive

OCV using a zero axial straight line is added with standard LKF. In the past few years, different types of non-linear KF algorithms have been investigated to achieve higher state estimation accuracy and to tackle the issues related to standard LKF.

2.9.2 Non-linear Kalman Filter

2.9.2.1 Extended Kalman Filter

EKF algorithm is the most preferred method for the battery parameter/state estimation (C. Huang et al., 2018). The EKF algorithm is a non-linear version of the LKF, and it works on the principle of linearization of the non-linear function (Sepasi et al., 2014b). For this purpose, partial derivatives and first-order order Taylor series expansion have been employed. In (Plett, 2004a), the EKF has been used for the battery model parameter identification and state estimation. Usually, the computation of the Jacobian matrix is required during the estimation through the EKF algorithm that conversely effects the accuracy of the estimated SOC (Andre et al., 2013). Furthermore, by the usage of first-order Taylor expansion in the linearization cut off the process in the EKF algorithm, only the first order accuracy is conceivable to achieve. Moreover, the EKF accuracy directly depends on the battery model and the prior knowledge of the system noise variables. If the prior knowledge is not correct, then the estimation process error may lead to divergence (R Xiong et al., 2018). Thus, to enhance the performance of the EKF algorithm, in the previous decades, there are several modifications have been done.

For example, in (Sepasi et al., 2014b), the improved EKF (I-EKF) is proposed for online SOC estimation with the consideration of aging factor to inline adaptively update the battery model parameters. The SOC estimated by I-EKF method of a single cell can be accurately used to present the battery pack SOC of EV. In (Hongwen He et al., 2011b), the SOC estimation has been done with the assistance of robust EKF, and the five different types of RC model are considered to evaluate the performance. The estimation

algorithm sensitivity with different initial values has been examined. The results inferred that SOC estimation using robust EKF could effectively reduce the error resulting from the incorrect initial SOC values. Furthermore, in (Z. Chen et al., 2013), the experimental data have been used to develop the battery model to reduce the effect of measurement and process noise. The outcomes confirmed that the proposed method could effectively eliminate the impact of measurement noise and process noise on the SOC estimation without the utilization of prior knowledge of the initial SOC. However, it has a problem of significant error occurrence with the highly non-linear system due to its approximation of distributed Gaussian random variable and ignorance of higher order terms.

2.9.2.2 Adaptive extended Kalman filter

The assumption of fixed measurement and process noise covariance in EKF estimation reduces the overall performance of estimation (Sepasi et al., 2014a; Z. Zhang et al., 2021). For example, the problem of the biased solution may occur if the initial process and measurement noise covariance matrices are very small. By contrast, if both covariance matrices are very large, then the problem of error divergence usually occurs (Rui Xiong, He, Sun, & Zhao, 2013). The feature of adaptively updating the covariance matrices is added to EKF in the adaptive extended Kalman filter (AEKF) estimation method to overcome error divergence and biased solution. In (Rui Xiong, He, Sun, & Zhao, 2013), the new AEKF algorithm was proposed to estimate the SOC, in which the filter innovation matrix (H_k) based on the innovation sequence (e_i) inside the moving estimation window (M) is added in the estimation steps of the EKF. With the aid of H_k, the measurement ($P_{v,k}$) and process ($P_{w,k}$) covariance matrices are updated iteratively. Divergence is an important factor in the accuracy of EKF, so the divergence judgmental condition was introduced in the AEKF in (Hongwen He et al., 2011) to avoid filter divergence and improve stability.

2.9.2.3 Sigma-point Kalman filter

In the linearisation of EKF, the nonlinear equations expand around the prior mean with the expected covariance scale according to the slope of the function at a particular point. Consequently, many nonlinear terms are dropped from the expansion, which leads to reduced estimation accuracy (Plett, 2006b). Furthermore, the significant error in a true posterior spread may occur if the linearisation of the function is done in the neighbourhood of the prior mean. In (Plett, 2006b), sigma-point Kalman filter (SPKF), an alternative approach for state estimation of nonlinear systems, was proposed to overcome the shortcomings of EKF and AEKF. A second-order Taylor accuracy could be achieved using this method. In addition to a local linearisation, the statistical distribution approach with the utilisation of deterministic sampling points called sigma points ($\mathcal{X}_i$) was utilised for linearisation in SPKF (Liye Wang et al., 2009). The selection of sigma points is typically performed such that the weighted mean and covariance of the posterior random variable must be matched with the prior mean and covariance of the random variables being modelled (Plett, 2006b). Based on the weighing factor, the SPKF algorithm is classified into two categories: unscented Kalman filter (UKF) and central difference Kalman filter (CDFK) (Liye Wang et al., 2009).

(a) Unscented Kalman filter

The statistical method called unscented transformation was introduced in (Dong et al., 2017) to avoid the calculation of the Jacobi matrix for the linearisation of the nonlinear equation used in EKF. In UT, minimal sets of sigma points ($\mathcal{X}_i$) are used to capture the posterior mean and covariance of random variables. During estimation, a set of sigma points is selected at each point such that the filter parameters (mean and covariance) are matched with the prior random value parameters (mean and covariance), as discussed in Table 2.8 (L. Zhao et al., 2013). Estimation utilises the augmented random vector (x^a) to combine the randomness of state, process noise and measurement noise.

Table 2.8: Summary of the UKF estimation algorithm (Plett, 2006b; W. Wang et al., 2018)

Initialisation: For $k = 0$, set	
Step 1	State variable, $\hat{x}_0^+ = E[x_0]$; Covariance matrix, $P_{\tilde{x},0}^+ = E^{[(}{}_{x_0} - \hat{x}_0^+)(x_0 - \hat{x}_0^+)^T] = E^{[(}{}_{\tilde{x}_0})(\tilde{x}_0)^T]$
Step 2	Sigma points at each sample of L dimension state with a λ scaling factor, $\mathcal{X}_{k,i}^{a,+} = \begin{cases} \hat{x}_k^+ ;\ i = 0 \\ \hat{x}_k^{a,+} + \left(\sqrt{(L+\lambda)P_{\tilde{x},k}^+}\right)_i ;\ i = L+1, \dots 2L \\ \hat{x}_k^{a,+} - \left(\sqrt{(L+\lambda)P_{\tilde{x},k}^+}\right)_i ;\ i = 1,2, \dots L \end{cases}$ Mean weight, $w_i^m = \begin{cases} \lambda/(L+\lambda) ; i = 0 \\ \lambda/(2(L+\lambda)) ; i = elsewhere \end{cases}$ Covariance weight, $w_i^c = \begin{cases} \lambda/(L+\lambda) + (1-\alpha^2+\beta); i = 0 \\ \lambda/(2(L+\lambda)) ; i = elsewhere \end{cases}$ where $\lambda = \alpha^{2(}n + k) - n$, $\alpha \in [0,1]$ describes the distance between the sample point and mean point, and it may be different for $w_i^m$and w_i^c. β is equal to 2 for Gaussian random variables.

‘ Table 2.8 continued’

Computation: for k = 1,2,3, … compute	
Step 3	State estimation time update, $\hat{x}_k^- = \sum_{i=0}^{2L} w_i^m \mathcal{X}_{k,i}^{x,-}$ where $\mathcal{X}_{k,i}^{x,-} = f(\mathcal{X}_{k-1,i}^{x,+}, u_{k-1}, \mathcal{X}_{k,i}^{w,+}, k-1)$
Step 4	Error covariance time update, $P_{\tilde{x},k}^- = \sum_{i=0}^{2L} w_i^c (\mathcal{X}_{k,i}^{x,-} - \hat{x}_k^-)(\mathcal{X}_{k,i}^{x,-} - \hat{x}_k^-)^T$
Step 5	Output estimate, $\hat{y}_k = \sum_{i=0}^{2L} w_i^m \mathcal{Y}_{k,i}$ where $\mathcal{Y}_{k,i} = h(\mathcal{X}_{k,i}^{x,-}, u_k, \mathcal{X}_{k,i}^{v,+}, k)$
Step 6	Kalman gain matrix, $K_k = P_{\tilde{x}_k \tilde{y}_k}^- P_{\tilde{y}k}^{-1}$ Where, $P_{\tilde{x}_k \tilde{y}_k}^- = \sum_{i=0}^{p} w_i^c (\mathcal{X}_{k,i}^{x,-} - \hat{x}_k)(\mathcal{Y}_{k,i} - \hat{y}_k), P_{\tilde{y}_k} = \sum_{i=0}^{2L} w_i^c (\mathcal{Y}_{k,i} - \hat{y}_k)(\mathcal{Y}_{k,i} - \hat{y}_k)^T$
Step 7	State estimation measurement update, $\hat{x}_k^+ = \hat{x}_k^- + K_k[y_k - \hat{y}_k]$
Step 8	Error covariance measurement update, $P_{\tilde{x},k}^+ = P_{\tilde{x},k}^- - K_k P_{\tilde{y},k} K_k^T$

The introduction of sigma points in the UKF algorithm is the main difference between the EKF and UKF (Van der Merwe & Wan, 2001). Figure 2.17 shows that the mean covariance of the output sigma points is well matched with the true mean and covariance values. The second-order accuracy can be achieved through the second-order approximation with the predetermined sampling period. In (Shehab El Din, Hussein, & Abdel-Hafez, 2018), to further enhance the accuracy, the measurement noise covariance was estimated by the autocovariance least-squares (ALS) technique. The performance and robustness of UKF and EKF was compared in (C. Huang et al., 2018) to confirm the high accuracy, robustness and convergence rate with the unknown initial SOC of UKF. Several issues were identified with UKF. For example, it is not appropriate for high measurement noise because it may cause divergence. Additionally, it may produce a significant error and slow the convergence if the sampling data go beyond the defined limit because of the effect of external factors. Some advanced variants of UKF have been proposed by researchers in the past few years to address these issues. For example, an improved UKF (I-UKF) was proposed in (W. Wang et al., 2018), in which the noise suppression and invalid value elimination algorithms were combined with the UKF algorithm. For the SOC estimation under the real-time EV dynamic condition, the author (Shehab El Din, Hussein, & Abdel-Hafez, 2018) proposed a new adaptive UFK (AUKF) estimation method that illustrates better performance than EKF and UKF.

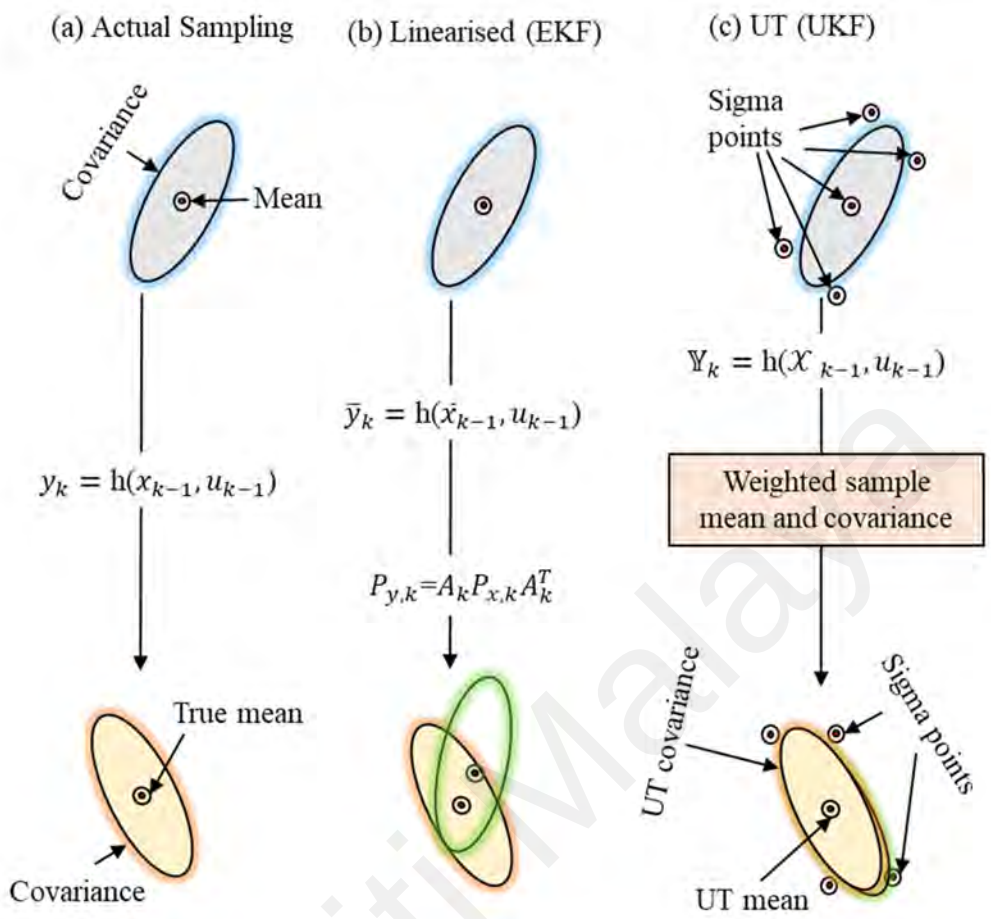

Figure 2.17: Linearisation of nonlinear function in EKF and UKF algorithm
(Van der Merwe & Wan, 2001)

i Adaptive unscented Kalman filter

In AUKF, the parameters of the error covariance matrix are estimated and updated interactively. Through the application of AUKF algorithm, the unsatisfactory impression of uncertain measurement and process noise covariance on estimation accuracy can be reduced. In (Peng et al., 2017), EKF, UKF and AUKF were used for SOC estimation, and the results illustrated that the AUKF has the most minimal root mean square error (RMSE) and mean absolute error (MAE) compared with other under dynamic surroundings. In (W. Zhang et al., 2015b), AUKF was utilised to build the joint SOP and SOE estimator; the estimation error was less than 2% for assumed erroneous initial conditions. The main limitation of the AUKF is that noise statistics are calculated

assuming white noise measurement residuals. However, this condition will not be valid in all conditions, particularly when the filter initialises with incorrect values of noise statistics.

ii Square-root unscented Kalman filter

The calculation of the new sigma point at each time update is the computationally most expensive part in the entire UKF algorithm (Liye Wang et al., 2009) because it requires a square root of state covariance matrix $P \in \mathbb{R}^{L\times L}$. Instead of recursively updating full covariance P utilised in UKF algorithm, the application of the Cholesky factorisation given by $SS^T \in P$ (where S is the lower triangular matrix for covariance P matrix) can significantly reduce the computational effort in SR-UKF (Dai et al., 2012). Firstly, the square-root unscented KF (SR-UKF) algorithm for parameter and state estimation was introduced by Merve et al. in 2001 (Van der Merwe & Wan, 2001), in which the matrix S propagates directly throughout estimation to avoid the re-factorisation of P matrix at each step. Three linear algebra techniques, such as QR decomposition (qr), Cholesky factor updating (cholupdate) and efficient least squares, are used for square-root covariance update and propagation (Van der Merwe & Wan, 2001). The SR-UKF algorithm is a logical replacement of EKF in state and parameter estimation in LIB applications.

iii Adaptive square-root unscented Kalman filter

In (Batteries, 2017), the ASR-UKF was proposed for SOC estimation; it combines the principle of SR-UKF and AUKF. The improved Sage–Husa estimation method was employed for adaptively updating the covariance matrices. The non-negative qualitative and symmetry character of covariance matrices ensure that the produced estimation results will not diverge. The ASR-UKF-based SOC estimation performance was

compared with the EKF and UKF, and the outcomes inferred that the ASR-UKF has the highest robustness and convergence during SOC estimation under inaccurate measurement noise conditions. This estimation method is more suitable for EV applications where the battery is operated under high stress and high temperature.

iv Square-root spherical-unscented Kalman filter

In (Aung et al., 2015), a square-root spherical-unscented Kalman filter (SRS-UKF) method was proposed for SOC estimation which uses a Jacobian-free linearisation approach with UKF for a nonlinear system. The computational complexity and cost of the UKF algorithm are proportional to the number of sigma points. When the single weight function (W_i) and spherical transformation in SRS-UKF are employed, the requirement of numerous sigma points and high computational cost are significantly reduced. The application of SRS-UKF method reduces the number of multiplications performed during estimation by ~32% compared with regular UKF.

(b) Central difference Kalman filter

In CDFK, Stirling's formula is used for the approximation of derivatives, and a set of sigma points is used to reduce the computational burden by eliminating the Jacobian matrix. The function used to determine the value of the set of sigma points is chosen, such that the weighted mean and covariance can be matched with the mean and covariance of the prior modelled random variables. Unlike the UKF, this algorithm uses only a single tuning parameter h, which makes it more straightforward. The value of h may be any positive number, for example, in the case of Gaussian random variables, h is set to $\sqrt{3}$. Similar to SPKF, the augmented variable x^a defines the combined randomness of state, process noise, and measurement noise. Except for the sigma point weighing, the CDKF and UKF illustrate nearly the same accuracy during SOC estimation (Plett, 2006b). In (Sangwan et al., 2017), CDFK was used for the SOC estimation, and the results were

compared with those of EKF; CDKF had lower RMSE than EKF under identical testing conditions. In (HongWen He et al., 2015), the SOE estimator employed CDFK algorithm, and the proposed SOE estimator was reliable and highly accurate (maximum error of less than 1% for erroneous initial SOE) for EV application.

2.9.2.4 Cubature Kalman filter

EKF and SPKF suffer from divergence and dimensionality. To address these issues, the cubature Kalman filter (CKF) was proposed by Arasaratnam et al. in 2010 (Tanachutiwat et al., 2010), in which the third-degree spherical radial cubature rule is applied for the numerical computation of the Gaussian weighted noise signals. The cubature rule transforms the variables from Cartesian to radial. Interestingly, the unique feature of CKF is that it uses equally weighted, uniformly distributed even number ($2n$; n is the state vector dimension) cubature points ($\mathcal{C}_i$) on the zero origin ellipsoid centre to calculate the state mean and covariance (Pathuri Bhuvana et al., 2013) (Xia, Wang, Tian, et al., 2015). In UKF, the odd number ($2n+1$) of sigma points ($\mathcal{X}_i$) is distributed on a non-zero centre point ellipsoid. In (Pathuri Bhuvana et al., 2013), the CKF algorithm was used for SOC estimation, and its performance was compared with the EKF and UKF algorithms. The results demonstrated that the CKF had the highest accuracy with more computation time than EKF. To enhance the performance of CKF, a new adaptive CKF (ACKF) algorithm was proposed for SOC estimation in (Xia, Wang, Tian, et al., 2015), in which the performance of the proposed ACKF was compared with that CKF and EKF. The outcomes illustrated that the ACKF has the highest accuracy with the least convergence rate with high robustness against measurement error, though the computation time of ACKF exceeded that of CKF and EKF. The authors in (Z. Zeng et al., 2018) explained that the estimated SOC value using ACKF algorithm converges more rapidly than CKF and UKF with different initial SOC error conditions.

(a) Strong tracking-cubature Kalman filter

In (Xia, Wang, Wang, et al., 2015), the attributes of CKF and STF algorithms were combined and a new advance algorithm called strong tracking-cubature Kalman filter (ST-CKF) was proposed for the online SOC estimation. With the addition of STF algorithm with CKF algorithm, the filter gain matrix can be updated online by introducing fading factor (λ_k) in the state estimation covariance matrix. In [43], the performance of the SOC estimation utilising ST-CKF was compared with the EKF and CKF algorithms. The results illustrated that the complexity of the ST-CKF is higher than those of the CKF and EKF because it is more robust to measurement noise. Additionally, the ST-CKF claims the lowest SOC estimation error under observable initial SOC conditions compared with the EKF and CKF algorithms.

Table 2.9 presents a detailed comparison of the above specified different KF family algorithms based on previous studies. The distinctive highlights of the different KF family algorithms utilised in online SOC estimation, such as MAE, complexity and associated mathematical formulas, are briefly discussed. The associated key issues with KF family algorithms suitable for online SOC estimation are listed in Table 2.10.

Table 2.9: Highlights of different KF family algorithms utilised in model-based online SOC estimation

Algorithm	Complexity	Gain matrix (K_k)	Other associated important formulas
LKF (Mastali et al., 2013; Rahmoun et al., 2012; Topan et al., 2016), (Luo et al., 2015)	High	$P_{\hat{x},k}^{-} C_k^T [C_k P_{\hat{x},k}^{-} C_k^T + P_v]^{-1}$	Error covariance time update, $P_{\hat{x},k}^{-} = A_{k-1} P_{\hat{x},k-1}^{+} A_{k-1}^T + P_w$ Error covariance measurement update, $P_{\hat{x},k}^{+} = (I - K_k C_k) P_{\hat{x},k}^{-}$
EKF (Plett, 2004a),(Mastali et al., 2013), (C. Huang et al., 2018)	Medium	$P_{\hat{x},k}^{-} \hat{C}_k^T [\hat{C}_k P_{\hat{x},k}^{-} \hat{C}_k^T + \hat{D}_k P_v \hat{D}_k^T]^{-1}$	Partial derivatives of A_k and C_k, $\hat{A}_k = \left.\frac{\partial f(x_k, u_k)}{\partial x_k}\right\|_{x_k = \hat{x}_k^{+}}$, $\hat{C}_k = \left.\frac{\partial h(x_k, u_k)}{\partial x_k}\right\|_{x_k = \hat{x}_k^{-}}$
AEKF (Hongwen He et al., 2011), (Rui Xiong, He, Sun, & Zhao, 2013), (Y. Shen, 2018; Y. Zhao et al., 2018), (Rui Xiong, He, Sun, & Zhao, 2013)	High	$P_{\hat{x},k}^{-} \hat{C}_k^T [\hat{C}_k P_{\hat{x},k}^{-} \hat{C}_k^T + \hat{D}_k P_v \hat{D}_k^T]^{-1}$	Innovation covariance matrix, $H_k = \frac{1}{M} \sum_{i=k-M+1}^{k} e_i e_i^T$ Updated process covariance matrix, $P_{v,k} = K_k H_k K_k$ Updated measurement covariance matrix, $P_{w,k} = H_k - \hat{C}_k P_{\hat{x},k}^{-} \hat{C}_k^T$

‘ Table 2.9 continued’

Algorithm	Complexity	Gain matrix (K_k)	Other associated important formulas
UKF (Shehab El Din, Hussein, & Abdel-Hafez, 2018), (C. Huang et al., 2018), (Dai et al., 2012; Hongwen He et al., 2013; L. Zhao et al., 2013)	Low	$P_{\tilde{x}_k\tilde{y}_k}P_{\tilde{y}k}^{-1}$	Sigma points, $\mathcal{X}_i = \begin{cases} \hat{x}_k\,;\, i=0 \\ \hat{x}_k + \left(\sqrt{(L+\lambda)P_{x,k}}\right)_i\,;\, i=L+1,\dots 2L \\ \hat{x}_k - \left(\sqrt{(L+\lambda)P_{x,k}}\right)_i\,;\, i=1,2,\dots L \end{cases}$ Mean weight, $w_i^m = \begin{cases} \lambda/(L+\lambda)\,;\, i=0 \\ \lambda/(2(L+\lambda))\,;\, i=elsewhere \end{cases}$ Covariance weight, $w_i^c = \begin{cases} \lambda/(L+\lambda)+(1-\alpha^2+\beta);\, i=0 \\ \lambda/(2(L+\lambda))\,;\, i=elsewhere \end{cases}$
AUKF (Li Zhang et al., 2017; W. Zhang et al., 2015b)	High	$P_{\tilde{x}_k\tilde{y}_k}P_{\tilde{y}k}^{-1}$	Innovation covariance matrix, $H_k = \frac{1}{M}\sum_{i=k-M+1}^{k} e_i e_i^T$ Updated process covariance matrix, $P_{v,k} = K_k H_k K_k$ Updated measurement covariance matrix, $P_{w,k} = H_k - \hat{C}_k P_{\hat{x},k}^- \hat{C}_k^T$

‘ Table 2.9 continued’

Algorithm	Complexity	Gain matrix (K_k)	Other associated important formulas
SR-UKF (Van der Merwe & Wan, 2001),(Liye Wang et al., 2009)	High	$(P_{\tilde{x}_k\tilde{y}_k}^{-}/S_{\tilde{y}k}^{-T})S_{\tilde{y}k}^{-}$	At k=o, $\hat{x}_0^+ = E^{(}x_0^{+)},\ S_{x,0} = chol\{E^{[(}x_0 - \hat{x}_0^{+})^{(}x_0 - \hat{x}_0^{+})^{T]}\}$ Sigma points at each time step,$\mathcal{X}_i =$ $\begin{cases} \hat{x}_k\ ;\ i = 0 \\ \hat{x}_k + (\sqrt{(L+\lambda)S_{x,k}})_i ; i = 1,2,\dots L \\ \hat{x}_k - (\sqrt{(L-\lambda)S_{x,k}})_i ; i = L+1,\dots 2L \end{cases}$
ASR-UKF (Batteries, 2017), (Van der Merwe & Wan, 2001)	Medium	$(P_{\tilde{x}_k\tilde{y}_k}^{-}/S_{\tilde{y}k}^{-T})S_{\tilde{y}k}^{-}$	Updated measurement covariance matrix, $\begin{cases} \sqrt{P_v^{**}} = cholupdate\{\sqrt{1-d_k}\sqrt{P_{v,k-1}}, \lvert y_k \rvert, d_k\} \\ \sqrt{P_v^{*}} = cholupdate\{\sqrt{P_v^{**}}\mathbb{Y}_{0:2L,k}^{-} - \hat{y}_k^{-} - d_k w_i^c\} \\ \sqrt{P_{v,k}} = diag\left\{\sqrt{P_v^{*}}\sqrt{P_v^{*}}^{T}\right\} \end{cases}$ Updated process covariance matrix, $\begin{cases} \sqrt{P_w^{**}} = cholupdate^{\{}\sqrt{P_{w,k-1}}, \lvert \hat{x}_k - \hat{x}_k^{-} \rvert, d_k\} \\ \sqrt{P_w^{*}} = cholupdate\left\{\sqrt{P_w^{**}}\mathbb{Y}_{0:2L,k}^{-} - \hat{y}_k^{-}, k_k S_{y,k}, -d_k\right\} \\ \sqrt{P_{w,k}} = diag\left\{\sqrt{P_w^{*}}\sqrt{P_w^{*}}^{T}\right\} \end{cases}$ where $d_k = {}^{(}1-b^{)}/{}^{(}1-b^{k+1)},$

‘ Table 2.9 continued’

Algorithm	Complexity	Gain matrix (K_k)	Other associated important formulas
SRS-UKF (Aung et al., 2015; Xiaojun Tang et al., 2008)	Low	$(P^{-}_{\tilde{x}_k\tilde{y}_k}/{S^{-}_{\tilde{y}k}}^{T})S^{-}_{\tilde{y}k}$	Initial weight function,$W_0;\ 0 < W_0 < 1$ Rest weight, $W_i = (1 - W_0)/(L + 1)$
CDFK (Plett, 2006b; Sangwan et al., 2017), (HongWen He et al., 2015), (Liye Wang et al., 2009), (Plett, 2006c)	Medium	$P^{-}_{\tilde{x}_k\tilde{y}_k}P^{-1}_{\tilde{y}k}$	Sigma points, $\mathcal{X}_i = \begin{cases} \hat{x}_k\ ;\ i = 0 \\ \hat{x}_k + \left(\sqrt{h^2 P_{\tilde{x},k}}\right)_i ; i = 1,2,\dots L \\ \hat{x}_k - \left(\sqrt{h^2 P_{\tilde{x},k}}\right)_i ; i = L+1,\dots 2L \end{cases}$ $w_i^m = w_i^c) = \begin{cases} (h^2 - L)/h^2 ; i = 0 \\ 1/2h^2 ; i = elsewhere \end{cases}$
CKF (Tian, Yong, Rusheng Yan, Jindong Tian, Shijie Zhou, 2017), (Xia, Wang, Tian, et al., 2015)	Low	$P^{-}_{\tilde{x}_k\tilde{y}_k}P^{-1}_{\tilde{y}k}$	Cubature points, $\mathcal{C}_{i,k-1}$=$S_{k-1}\xi_i + x_{k-1}$; i=1, 2…,2n where ξ_i is the i-th cubature point and $P_{k-1} = S_{k-1}S_{k-1}^T$
ST-CKF (Xia, Wang, Wang, et al., 2015)	High	$P^{-}_{\tilde{x}_k\tilde{y}_k}P^{-1}_{\tilde{y}k}$	New state covariance ($P_{x,k+1}$) after the introduction of λ_{k+1} in the old state covariance, $P^{+}_{\hat{x}',k+1} = \lambda_{k+1}P^{+}_{\hat{x},k+1} + P_{w,k}$
Note: Complexity: High = >L^3, Medium = L^3, Low = < L^3, where L is the dimension of the augmented state matrix			

Table 2.10: Associated key issues with different KF family algorithms

Algorithms	References	Associated key issues
LKF	(Mastali et al., 2013; Rahmoun et al., 2012; Topan et al., 2016), (Luo et al., 2015)	Assumes independent zero-mean Gaussian noise signals Not suitable for nonlinear system application
EKF	(Plett, 2004a),(Mastali et al., 2013), (C. Huang et al., 2018)	Frequent error occurrence for highly nonlinear system caused by the ignorance of the higher-order terms Accuracy directly influenced by the prior knowledge of the system noise Requirement of Jacobian matrix computation for linearisation
AEKF	(Hongwen He et al., 2011), (Rui Xiong, He, Sun, & Zhao, 2013), (Y. Shen, 2018; Y. Zhao et al., 2018), (Rui Xiong, He, Sun, & Zhao, 2013)	Requirement of Jacobian matrix computation for linearisation Utilises first-order Taylor series expansion that conversely effects estimation accuracy
UKF	(Shehab El Din, Hussein, & Abdel-Hafez, 2018), (C. Huang et al., 2018), (Dai et al., 2012; Hongwen He et al., 2013; L. Zhao et al., 2013)	Not suitable for the application with high measurement noise signals Convergence rate depends on maximum sampling data limit Problem of dimensionality
AUKF	(W. Zhang et al., 2015b), (Li Zhang et al., 2017)	Assumes white noise measurement residuals Initial wrong initialisation noise statistics severely affect filter performance
SR-UKF	(Van der Merwe & Wan, 2001),(Liye Wang et al., 2009)	Numerous sigma points are generally required during estimation High computational cost Utilisation of fixed values of covariance matrices affects filter performance

‘ Table 2.10 continued’

Algorithms	References	Associated key issues
ASR-UKF	(Batteries, 2017), (Van der Merwe & Wan, 2001)	Numerous sigma points are generally required during estimation High computational cost
SRS-UKF	(Aung et al., 2015; Xiaojun Tang et al., 2008)	Numerous sigma points are generally required during estimation
CDKF	(Plett, 2006b; Sangwan et al., 2017), (HongWen He et al., 2015), (Liye Wang et al., 2009), (Plett, 2006c)	High complexity Selection of sigma points is more critical
CKF	(Tian, Yong, Rusheng Yan, Jindong Tian, Shijie Zhou, 2017), (Xia, Wang, Tian, et al., 2015)	High computation time and convergence rate
SR-CKF	(Xia, Wang, Wang, et al., 2015)	High complexity

2.10 Joint and dual Kalman filter

The battery model parameters and SOC–OCV relation are time varying in nature and depend on operating conditions. Offline parameter estimation techniques are commonly utilised in battery state estimation by researchers. However, to improve the state estimation accuracy, the battery parameters must be updated alongside estimation in the task time frame. In (Plett, 2006c), two types of estimation approaches, namely joint KF estimation approach and dual KF estimation approach, were introduced. The concurrent estimation of battery state and parameter using a single member of the KF family algorithm became possible through the estimation of the augmented vector ($\mathbb{X}$) values in joint KF estimation approach [as expressed in (6)]. In this approach, the state and parameter comprise fast and slow dynamics of the system. The complete system dynamics can be described by (2.13) and (2.14). The basic structure of the joint KF estimation approach depicted in Figure 2.18 reveals that a single KF is sufficient for simultaneous online state and parameter estimation. The figure likewise demonstrates how the information flows from one step to another during estimation. Different KF algorithms, such as AKF (Dai et al., 2009; Gao et al., 2016), SPKF (Plett, 2006c) and SR–SPKF (Plett, 2006c), were utilised for online SOC and battery parameter estimation; all KF family algorithms claim high accuracy. However, owing to the incorporation of the large size of the augmented vector ($\mathbb{X}$), the overall computational complexity of the joint KF-based SOC estimation significantly increases. Additionally, the time scale mismatch of state and parameter vector builds up the problem of poor numeric conditioning.

$$\mathbb{X} = \begin{bmatrix} x_k \\ \theta_k \end{bmatrix} = \begin{bmatrix} f(x_{k-1}, u_{k-1}, \theta_{k-1}) \\ \theta_{k-1} \end{bmatrix} + \begin{bmatrix} w_{k-1} \\ r_{k-1} \end{bmatrix} \tag{2.13}$$

$$y_k = g(x_k, u_k, \theta_k) + v_k \tag{2.14}$$

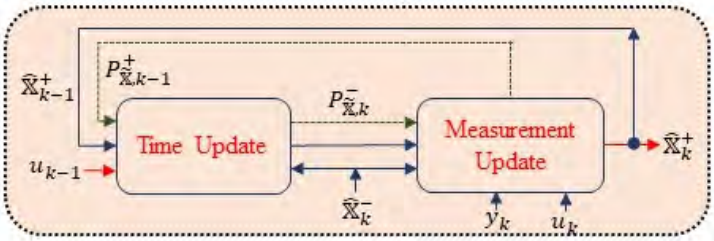

Figure 2.18: Joint KF estimation approach

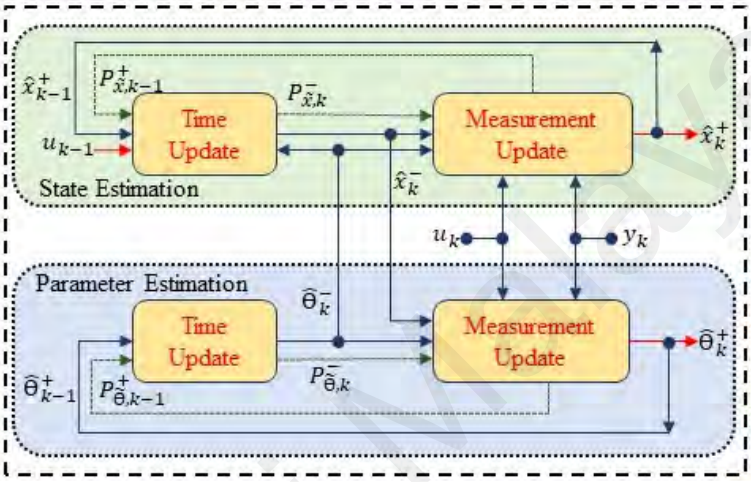

Figure 2.19: Dual KF estimation (Campestrini et al., 2016)

The issues of large size augmented vector and poor numerical conditioning identified with joint KF estimation can be resolved by using the dual KF estimation approach (Campestrini et al., 2016). In dual KF estimation, two separate KFs are utilised, one for state estimation and one for parameter estimation. The path of data flow from one KF to another KF is represented in Figure 2.19. The dynamic mathematical model represented by (2.15) and (2.16) explicitly includes the parameter vector θ_k (Plett, 2006c).

$$x_k = f(x_{k-1}, u_{k-1}, w_{k-1}\theta_{k-1}, k-1) \tag{2.15}$$

$$y_k = h(x_k, u_k, v_k, \theta_k, k) \tag{2.16}$$

In (Mastali et al., 2013), the dual KF was used for the LIB; dual KF could track SOC under a dynamic environment, such as EV with an error less than 4%. In (Plett, 2006c),

the dual SPKF and dual SR-SPKF were used for SOC estimation, and the results were compared with those of individual SPRK and SR-SPFK estimation. The members of the KF family, such as EKF (Dragicevic et al., 2013), SP-UKF (Erlangga et al., 2018), UKF (Y. Liu et al., 2012) and AUKF (H. Guo et al., 2017), were concurrently utilised in dual KF-based states and parameter estimation. All dual KFs demonstrate higher accuracy compared with individual KF state or battery parameter estimation approaches. In (Y. Zou, Hu, Ma, & Li, 2015), dual EKF was used for the combined SOC/SOH estimation. The two distinct EKFs with different time scales were used for online SOC estimation and offline SOH (capacity and internal ohmic resistance) estimation. The proposed method could estimate online SOC and SOH without heavy computational burden, divergence events and instability. In (Andre et al., 2013), dual KF was utilised for SOC and resistance estimation; it demonstrated high accuracy (less than 1% error) in SOC and resistance estimation even in the presence of 20% error in initial capacity. In (Mastali et al., 2013), dual EKF was used for SOC estimation of two commercial LIBs with different structures; the effect of battery structure on battery parameter was analysed using zero-hysteresis Rint model. The results of the study illustrated that the parameter estimated by the filter depends on the battery model. However, the main drawback of the dual KF estimation approach is the high chance of information loss during estimation, which may lead to poor SOC estimation accuracy.

2.11 Challenging steps in the implementation of KF family algorithms

Some important steps involve determining the performance of the overall SOC estimation, such as (i) selection of battery model and its PIMs, (ii) selection initial SOC and filter tuning, (iii) selection of operating conditions and (iv) consideration of different error accumulation.

2.11.1 Selection of battery model and its estimated parameter accuracy

Different battery models maintain their characteristics under varying environmental conditions, such as adaptability and precision. However, due to the complicated electrochemical behaviour under dynamic environmental circumstances, model selection for the appropriate implementation of the SOC estimation method becomes a difficult step. The complexity of the model is also an important factor that depends primarily on the number of model parameters to be identified. The model usually needs advanced hardware integrated into BMS with robust computational strategy and large memory storage room. The selection of the model relies on the dynamics of the present load profile. Importantly, the more complicated or higher-order model is required to capture extremely fluctuating load. The battery model's accuracy is typically assessed in terms of its terminal voltage error. Therefore, the accuracy can be improved by applying the appropriate PIM. The literature was analysed to compare the average RMSE of various models obtained under DST and FUDS test circumstances (Figure 2.20). The Rint model shows the highest voltage error under specified test conditions owing to the absence of transient states to capture electrochemical dynamics. By contrast, the 2RC model shows excellent modelling capability. In addition, Randles model shows significant error owing to the battery model's transient states. The researchers preferred the 2RC model with offline parameters for online model-based SOC estimation because it decreases the complexity of the online SOC estimation algorithm.

In (Qianqian Wang et al., 2017), the performance of three distinct models (PNGV, 1RC and 2RC) under distinct environmental circumstances (CCD test, DST test and HPPC test) was assessed. For all battery models, the offline PIM and the SOC estimation EKF were used. The standardised RMSE of the simulated voltage model was compared with the estimated SOC. The results showed a linear and strong correlation between the LIB model accuracy and model-based SOC estimation error (Figure 2.21). For the choice

of SOC estimation algorithm, the trade-off between model complexity and precision is more critical.

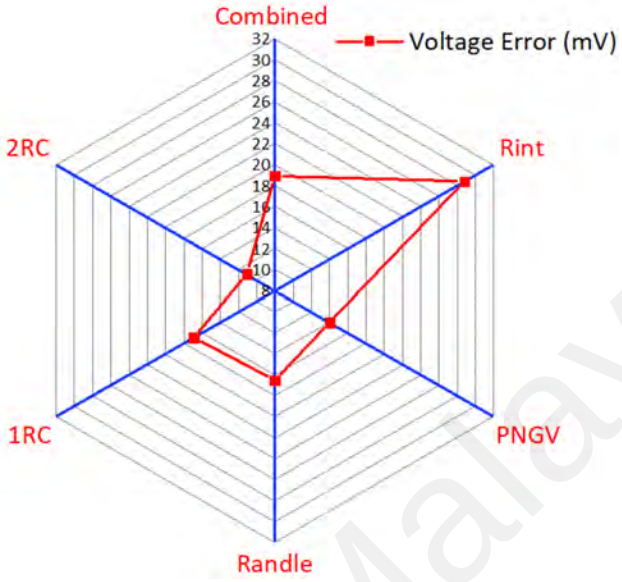

(a)

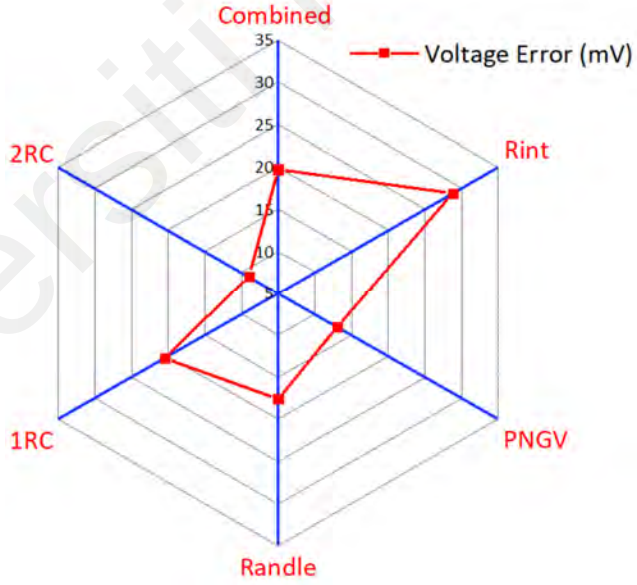

(b)

Figure 2.20: Voltage RMSE of models under test condition (a) DST and (b) FUDS (Andre et al., 2013; Bartlett, Marcicki, Onori, Rizzoni, Xiao Guang Yang, et al., 2016; Z. Chen et al., 2013; I. Kim, 2008; Qianqian Wang et al., 2017; Rui Xiong, He, Sun, & Zhao, 2013; Z. Yu et al., 2015; Y. Zou, Hu, Ma, & Eben Li, 2015)

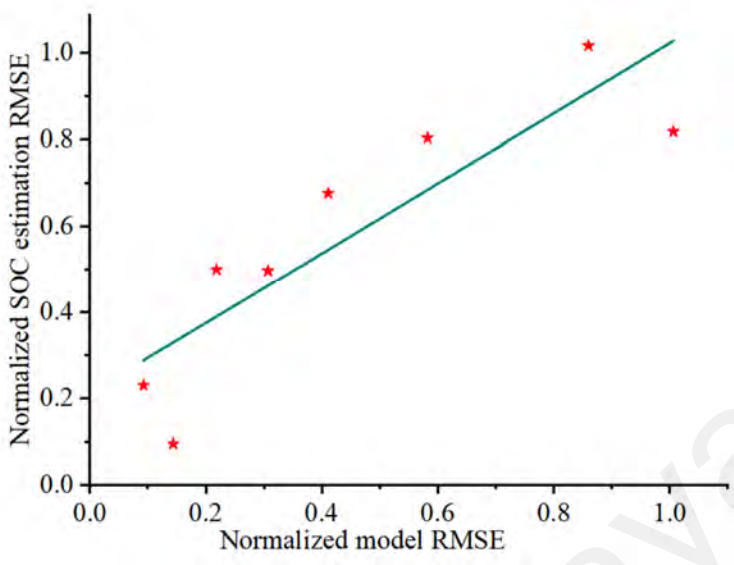

Figure 2.21: Correlation between the normalised RMSE of the model and SOC estimation (Qianqian Wang et al., 2017)

2.11.2 Selection initial SOC and filter tuning

The inner dynamics of the battery varies depending on the true SOC value. The accuracy of the battery SOC estimation is high when its true SOC is set at 50% because the electrochemical responses within the battery are insufficient and unstable at 100% or 0% SOC (D. Li et al., 2015). The convergence rate typically relies on the difference between the initial SOC and the true SOC during estimation, particularly in the case of unknown initial SOC. The convergence rate usually decreases as the true SOC error increases (Hongwen He et al., 2013). For example, in (C. Huang et al., 2018), the authors conducted experiments under various initial SOC error conditions to evaluate the robustness of EKF and UKF algorithms. The findings showed that the SOC estimation error value and divergence rate are directly affected by the initial SOC error level. RMSE's value ranged from 0.7 to 6.72 for the initial SOC error range of 10%–90%. Issues linked to the initial SOC mistake can be fixed to some extent by using modified KF algorithms in the model-based Internet SOC estimation method. For example, for the SOC estimation of the EV battery, the EKF algorithm was used in (Z. Chen et al., 2013). The findings showed that the accurate estimation of SOC is feasible using EKF without

the previous understanding of the initial SOC and automatically converges to a true value within two minutes. The process and measurement noise were efficiently removed. Table 2.11 describes the relative performance evaluation of various KF family algorithms used in the literature for model-based SOC estimation under observed/unobserved initial SOC circumstances. It also includes examples of the change in relative convergence rate of estimation algorithms under various initial conditions of SOC. For observable initial SOC situation, the value of MAE is almost continuous. However, in some instances of an unknown initial SOC error situation in the literature, a significant practically unacceptable variation in MAE values is registered.

In addition, when using KF family algorithms, selecting the initial noise covariance matrix component called KF tuning assumes an important task in defining estimation and accuracy. The four distinct KF algorithms were separately tuned in (Campestrini et al., 2016) to explore the accuracy of the SOC estimation. The findings inferred that each KF algorithm requires a distinctive set of KF tuning parameters to optimise KF performance. Three key parameter values, P_w, P_v and P_x, are typically needed for ideal filter tuning. However, finding the precise value of these parameters is a difficult task. The influence of the initially set diagonal element values of P_w, P_v and P_x on filter performance is briefly discussed in Table 2.12.

Table 2.11: Summary of KF-based estimation techniques and battery modelling method under different initial conditions utilised in the literature

Ref.	Estimation technique			Model	PIM	Test condition	Initial SOC error (%)	MAE (%)		
	I	II	III					I	II	III
(Z. Yu et al., 2015)	CC	LKF	–	2RC	Offline	DST	0	High	Low (< 5)	–
(Mastali et al., 2013)	CC	EKF	–	Rint	Online	DST	0	High	Low (< 4)	–
(J. Kim & Cho, 2011)	CC	EKF	–	1RC	Offline	DST	0	High	Low (< 5)	–
(Z. Chen et al., 2013)	CC	EKF	–	2RC	Offline	FUDS	100	6	3	–
(Sepasi et al., 2014b)	EKF	I-EKF	–	2RC	Online	NEDS	0	High	Low (1.1)	–
(Hongwen He et al., 2012b)	CC	AEKF		1RC	Offline	UDDS	0	High	Low (< 4.1)	–
(Y. Shen, 2018)	Other (ISA)	Other (MSA)	AEKF	2RC	Offline	UDDS	0	6.25	2.29	2.07

‘ Table 2.11 continued’

Ref.	Estimation technique			Model	PIM	Test condition	Initial SOC error (%)	MAE (%)		
	I	II	III					I	II	III
(Y. Zhao et al., 2018)	EKF	AEKF	–	1RC	Offline	UDDS	20	< 2	< 2	–
(Hongwen He et al., 2013)	EKF	UKF	–	1RC	Online	BJDC	90	4.42	1.16	–
(C. Huang et al., 2018)	EKF	UKF	–	Combined	Offline	FUDS	50	0.98	0.8	–
	EKF	UKF	–	1RC	Online	FUDS	50	1.63	1.20	–
(Partovibakhsh & Liu, 2012)	EKF	UKF	–	PNGV	Online	DST	0	< 2.1	< 1.05	–
(Jiahao Li et al., 2013)	EKF	UKF	–	2RC	Online	DST	20	< 6.2	< 4.3	–
(Seo et al., 2012)	EKF	UKF	–	1RC	Offline	DST	0	< 2.0	< 2.0	–
(W. Wang et al., 2018)	UKF	I-UKF	–	PNGV	Offline	DST	0	6.0	1.5	–

‘ Table 2.11 continued’

Ref.	Estimation technique			Model	PIM	Test condition	Initial SOC error (%)	MAE (%)		
	I	II	III					I	II	III
(Peng et al., 2017)	EKF	UKF	AUKF	2RC	Offline	DST	30	2.92	2.14	1.49
(Shehab El Din, Hussein, & Abdel-Hafez, 2018)	EKF	UKF	ALS-UKF	1RC	Offline	DST	0	2.50	1.50	0.70
(Sangwan et al., 2017)	EKF	CDKF	–	1RC	Offline	DST	0	High	Low	–
(Meng, Ricco, Luo, et al., 2018)	EKF	UKF	CDKF	2RC	Offline	FUDS	0	1.21	1.05	0.96
(Pathuri Bhuvana et al., 2013)	EKF	UKF	CKF	2RC	Offline	DST	0	4.48	4.02	3.31
(Xia, Wang, Tian, et al., 2015)	EKF	CKF	ACKF	2RC	Offline	DST	40	2.3	2.4	2.1

Table 2.12: Summary effect of diagonal elements values of P_w, P_v, and P_x (Campestrini et al., 2016; S. Yang et al., 2017; Z. Yu et al., 2015)

Parameter	Refers	Set value	Consequences
Diagonal elements of P_w	Model uncertainty	Zero	Indicates model is perfect States are completely uncorrelated
		Very large	Increase in estimation error High uncertainty in the filter states
Diagonal elements of P_x	Convergence pattern	Zero	Indicates accurate initial conditions Slows down the adaption of wrong initial conditions
		Very large	Fast correction of initial conditions Unstable behaviour
Diagonal elements of P_v	Measurement uncertainty	Small	Indicates high accuracy measurement sensors Completely ignore the model in state calculation
		Very large	Lower Kalman gain Estimation follows the model without correction by ignoring the measurement

During estimation, the noise covariance matrices with a restricted understanding of model inaccuracies and system disturbances are difficult to initialise correctly. To maximise estimation accuracy, the choice of noise covariance components should be produced under the account of initial SOC because of high model uncertainty in low SOC region (S. Yang et al., 2017). The stability of the KF algorithm is usually readily diverged because of battery model error and noise statistics (Z. Yu et al., 2015). However, it can be enhanced by adding an optimisation method along with various KF family algorithms. For example, in (Shehab El Din, Hussein, Abdel-Hafez, et al., 2018), for accurate SOC estimation, the ALS optimisation technique was added to find the optimal value of P_v elements with the EKF and UKF algorithms. The performance of UKF + ALS under the incorrect initialisation was better than those of EKF + ALS, UKF and EKF without a substantial increase in computational complexity.

2.12 Selection of operating conditions

The accuracy of the model-based online SOC estimation is greatly influenced by the variation of battery model parameters and the OCV–SOC relationship caused by the temperature, current rate and SOC range (C. Huang et al., 2018; S. Yang et al., 2017; Yun Zhang et al., 2018). Therefore, a suitable operating condition must be selected.

For example, in (Yun Zhang et al., 2018), the authors conducted few tests on the LFP 18650 battery at different temperatures (−20 °C, −10 °C, 0 °C, 10 °C and 20 °C) and current rates (0.5C, 1C and 1.5C). In this study, the variation of the 1RC battery model parameters induced by the various operating conditions was evaluated thoroughly. The results showed that the value of internal resistance R is approximately independent of the operating SOC range. The values of model parameters R, R_1 and C_1 are highly sensitive to temperature but less sensitive to current rate and SOC range. The average OCV–SOC relationship stays compatible with the various operating conditions.

To analyse the effect of temperature and SOC range on the OCV–SOC relationship, the OCV–SOC relationship at different temperatures was developed by researchers in (S. Yang et al., 2017). The results illustrated that owing to the high Li concentration on the electrode, the difference in OCV under the low SOC region (< 10% SOC) is considerably large. Therefore, in the low SOC range (0%–10%), the deviation in OCV can lead to significant SOC error. In the 30%–40% SOC region, the deviation in OCV of approximately 4 mV/1% SOC was registered at a temperature of 25 °C.

In addition, knowledge of the accurate discharge capacity is always needed in the AHC of the model-based SOC estimation. According to (R. Zhang, Xia, Li, et al., 2018a), such discharge capacity usually varies with the change in operating conditions. For instance, the 90 Ah $LiFePO_4$ was used in (Junfu Li et al., 2016) to analyse the effect of temperature on battery discharge capacity. The results demonstrated that the battery discharge capacity decreases with a change in temperature. However, in case of a rapid change in temperature during high current rate, the rate of change of battery capacity will be less (S. Yang et al., 2017). Owing to the slow Li diffusion process, the impact of temperature on the battery sets aside a prolonged effort to show up. Therefore, estimating the battery discharge capacity at ambient temperature (25 °C) is more appropriate (S. Yang et al., 2017).

In the case of EVs, the variation in operating conditions, such as temperature and current rate, is relatively large, so the model parameter variation will be more important. Therefore, the model parameters must be updated online during estimation for accurate SOC estimation. Research efforts on online updating of the model parameters are divided into two groups of methods: KF based, and regression based (RLS, variants of RLS). In Section 2.10, the family of KF algorithm was used to simultaneously estimate battery parameters and states, such as joint and dual KF. Table 2.13 lists the different regression-

based methods proposed by researchers in recent years (P. Shen, Ouyang, Lu, et al., 2018; Qianqian Wang et al., 2018; Q. Yu et al., 2017).

Table 2.13: Online model parameter and SOC estimation methods of LiBs

Ref.	Algorithms	Model	RMSE (%)
(Dai et al., 2009)	Dual AKF	2RC	< 3.0
(J. Kim & Cho, 2011)	Dual EKF	1RC	< 5.0
(Z. He et al., 2012)	Joint SPKF	Rint	Undefined
(Andre et al., 2013)	KF+UKF	2RC	< 1.0
(T. Kim et al., 2015)	Dual EKF	1RC	0.22
(X. Guo et al., 2016)	FFLS + AUKF	2RC	1.6
(Xu Zhang et al., 2016)	EKF + UKF	1RC	0.30
(Safwat et al., 2017)	MFFRLS + EKF	2RC	4.48
	MFFRLS + UKF		4.02
	MFFRLS + CKF		3.31
(Xia et al., 2018)	FFRLS + EKF	1RC	1.10
	FFRLS + UKF		1.40
(P. Shen, Ouyang, Lu, et al., 2018)	RLS + EKF	2RC	1.10
(Wassiliadis et al., 2018)	Dual EKF	2RC	0.50
(X. Hu et al., 2018)	Dual EKF	2RC	1.0
(Qianqian Wang et al., 2018)	Dual UKF	2RC	0.34

2.13 Consideration of different error accumulation

During the implementation of the KF algorithm for model-based SOC estimation, the errors induced by multiple sources and their effect on estimation must be considered. The different error accumulation in estimation directly influences the accuracy and the convergence rate. Six types of errors can be induced during two sub-processes, such as AHC and voltage-based correction of complete estimation (Figure 2.22). The errors produced in AHC may be caused by capacity error (CE), initial SOC error (ISE) and current measurement error (CME). The errors produced in the voltage-based correction may be caused by the model prediction error (MPE), voltage measurement error (VME) and CME.

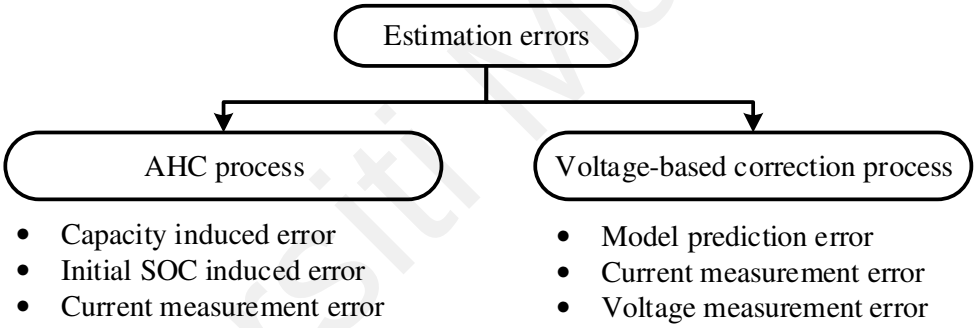

Figure 2.22: Different errors in the model-based SOC estimation

2.13.1 Initial SOC error

Initial SOC error (ISE) is the difference between real SOC and estimated SOC. For the initialisation of estimation, ISE is needed to provide the initial SOC in the first iteration. The value of the initial SOC can be taken from the look-up table or the latest stored value of SOC. The value of ISE is reduced and approximately eliminated with the next several iterations because of the recursive update of KF gain during estimation (Y. Zheng et al., 2018). ISE always converges at a fast rate towards zero with a large KF gain (P. Shen, Ouyang, Han, et al., 2018).

2.13.2 Capacity error

The decrease in aged battery capacity is responsible for the induction of CE and it can be reduced by updating the battery capacity during estimation. With the application of KF family algorithm for SOC estimation, the effect of CE during dynamic loading can be reduced (Y. Zheng et al., 2018). In the case of a highly accurate battery model, the value of SOC error caused by the CE can be small with a large KF gain (P. Shen, Ouyang, Han, et al., 2018).

2.13.3 Current measurement error

The measured current is fed to AHC and voltage-based correction, resulting in CME availability in both. CME is mainly caused by the low precision of current sensors, bias error and noise generated during current measurement. The influence of current noise is minimal on SOC errors owing to the effect of integration in AHC. The CME generated in AHC is usually unidirectional and may increase in the first several iterations (Y. Zheng et al., 2018). However, the CME generated in voltage-based correction is opposite in sign to the CME generated in AHC (P. Shen, Ouyang, Han, et al., 2018). Hence, for the CME generated by AHC, the KF gain increases and, finally, the complete elimination of the increasing trend of error could be possible with the several next iterations (P. Shen, Ouyang, Han, et al., 2018). The appropriate value of KF gain is significant for accurate SOC estimation. For low KF gain, CME in AHC increases. The high KF gain produces more CME in correction (Y. Zheng et al., 2018).

2.13.4 Voltage measurement error

Similar to current measurement, bias error and noise may occur during voltage measurement. The value of noise depends on the environment, such as earthing and electromagnetic interference, and it is difficult to estimate. Nevertheless, the KF family algorithm can efficiently suppress noise (P. Shen, Ouyang, Han, et al., 2018). Bias error

is caused by the change in measured voltage from real voltage. To compensate for this bias error, the battery model state variables produce voltage deviation (Y. Zheng et al., 2018). For example, in the case of 2RC model, SOC_k, $V_{1,k,}$ and $V_{2,k}$ produce the voltage deviation to compensate for voltage bias error. The value of covariance matrix P_w elements is responsible for the magnitude of change in the state variables (Y. Zheng et al., 2018).

2.13.5 Model prediction error

Model prediction error (MPE) refers to the difference between model voltage and real voltage. It has a major contribution to the error of SOC estimation. Same as VME, it can be divided into two parts, namely bias error and noise. MPE and VME influence SOC estimation in the same fashion as well. The model voltage noise has no adverse effect on SOC estimation and its accuracy (Peng et al., 2017; Y. Zheng et al., 2018). The high dependency of MPE on the OCV–SOC relationship is the most challenging issue for the model-based SOC estimation using the KF algorithm in any working environment (P. Shen, Ouyang, Han, et al., 2018).

Finally, the selection of hardware technology and software technology plays a vital role in SOC estimation. To reduce the effect of the accumulation of different errors, SOC estimation should include high-precision sensors, a good capacity estimation algorithm, and a highly accurate battery modelling method.

2.14 Commonly used performance evaluation matrices

In the existing studies, different types of evaluation matrices are commonly utilized for the performance evaluation of the state estimation algorithms such as estimation errors, convergence time, computational cost and computational complexity.

The estimation error can define as the difference between the measured value and the estimated value. The measured values are acquired from the experiments conducted in operating conditions demarcated according to the different tests, such as constant current discharge (CCD) (Petzl & Danzer, 2013; Tagade et al., 2016), PCPD (D. Li et al., 2015; Weigert et al., 2011), DST [57], HPPC (Hongwen He et al., 2011a; Tagade et al., 2016; Qianqian Wang et al., 2017), FUDS (Sangwan et al., 2017), UDDS (Rui Xiong, He, Sun, Liu, et al., 2013; J. Yang et al., 2018) and BJDC (Hongwen He et al., 2013). For example, the model terminal voltage error values are computed to analyse the accuracy of the identified battery model parameters using an estimation algorithm. The estimated SOC error values are evaluated to analyse the accuracy of SOC estimation. To evaluate the accuracy of the estimation algorithm, different estimation errors such as maximum absolute error (MaxAE) (HongWen He et al., 2015), mean absolute error (MAE) (W. Li et al., 2021b), and root mean square error (RMSE) (S. Zhang & Zhang, 2021b) are utilized by the researchers.

The convergence time of the estimation algorithm is evaluated to analyse the robustness of the estimation algorithm (Zhu et al., 2020). It can be defined as the range from the initialization to the time when the absolute estimation error is less than threshold value. Generally, the estimation error ranges from 2-5 % is considered as threshold value.

The computational cost and complexity are two important matrices are generally utilized to analyse the computational time and memory requirement of the estimation algorithm. In the past literature, the mean execution time (MET) (Hossain Lipu et al., 2021)and worst-case big O notation (Lucu et al., 2018) are utilized for the evaluation of computational cost and complexity, respectively. The value of MET varies with the programming efficiency of the algorithm and the hardware specification. Practically, it is difficult to compare the MET of the algorithm with the other studies, as they were

implemented with different hardware and by different researchers. On the other hand, the worst-case big O notion provides an idea about the computational complexity of the algorithm. Due to the limited memory size and computational power of the microcontroller used in BMS, it is essential to have an idea about the computational complexity in terms of the big O notation of the estimation algorithm.

Based on the literature, the above-mentioned evaluation matrices are considered for the performance of the proposed algorithm in this thesis. A detailed explanation about considered evaluation matrices is given in Section 3.3.

2.15 Summary

In this chapter, a state-of-the-art review on battery modeling and battery states estimation methods have been conducted. The properties of five categories of battery modelling methods such as EM, ECM, EECM, ECIM, and DDM are analyzed. The overall battery states estimation methods are classified into two broad categories namely individual states estimation method and combined states estimation or states co-estimation methods. In individual state estimation methods, the different estimation methods utilized for SOC, SOE, SOP, and SOH are discussed. The four commonly used types of SOC estimation methods such as CCM, OCVM, MBM, and MLM are reviewed. This study showed that the MBM for online SOC estimation with battery EECM is more appropriate for EV applications because of its possible benefits, including the capability to deal with unknown noise signals, low complexity, and high accuracy over other modeling methods. Similarly, the different estimation methods for SOE, SOP, and SOH are also discussed. Further, the existing methods for battery actual capacity and maximum available energy estimation are reviewed. Due to the existing high correlation amongst the different battery states and improve the functioning of BMS, it is crucial to develop the states co-estimation method for the estimation of the different battery states in real-

time application. The different existing co-estimation methods for SOC, SOE, SOP, and SOH estimation have been discussed. Presently, to effectively utilize the correlation between the battery states and for the development of computationally efficient BMS, the states co-estimation method is preferred by the researcher for different states estimation.

Finally, the most recent studies in the existing literature on online SOC estimation using KF family algorithms were thoroughly reviewed. The results showed that the merits of self-correction and low computational burden make KF family algorithms suitable for model-based online SOC estimation. The estimation procedure and related issues of the KF family algorithms are discussed and compared. The challenging steps in the implementation of KF family algorithms for model-based online SOC estimation were analyzed in-depth and discussed. As the battery model parameter identification is always a crucial task in model-based SOC estimation. For accurate SOC estimation in EV, the dual KF is preferred for online estimation of battery model parameters and SOC simultaneously.

CHAPTER 3: RESEARCH METHODOLOGY

3.1 Introduction

This chapter describes the experimental setting used to validate the proposed estimation methods in this thesis. The data sets developed from the testing of the battery cells are utilized for validation purposes. For the validation of the proposed estimation methods, the load current profiles are derived based on the requirement of EV batteries under some prescribed dynamic profile and drive cycles. Different experimental settings are done for three battery cells of different chemistries based on the information given in the respective manufacturer datasheet.

The sections of the chapter are arranged in this sequence. In Section 3.1, the introduction of the chapter is provided. In Section 3.2, the research methodology used in this study is presented. In Section 3.3, detailed experimental settings for dataset development are discussed. The specifications of considered battery cells are provided. Also, the conducted battery cell tests are explained. In Section 3.4, The different evaluation metrics considered for performance evaluation of the proposed battery states co-estimation methods are described.

3.2 Methodology

To achieve the thesis objectives as discussed in Section 1.3, the considered research methodology in this study divided into four phases (Figure 3.1).

In Phase 1, a state-of-the-art review on battery modeling and battery states estimation methods have been conducted. The battery states estimation methods are classified into two broad categories namely individual states estimation method and combined states estimation methods. In individual state estimation methods, the different estimation methods utilized for SOC, SOE, SOP, and SOH are discussed. This study showed that the MBM for online SOC estimation with battery EECM is more appropriate for EV

applications because of its possible benefits, including the capability to deal with unknown noise signals, low complexity, and high accuracy over other modeling methods. The most recent studies in the existing literature on online SOC estimation using KF family algorithms were thoroughly reviewed. The results showed that the merits of self-correction and low computational burden make KF family algorithms suitable for model-based online SOC estimation. As the battery model parameter identification is always a crucial task in model-based SOC estimation. For accurate SOC estimation in EV, the dual KF is preferred for online estimation of battery model parameters and SOC simultaneously. Furthermore, the different estimation methods for SOE, SOP, and SOH are also discussed. The existing methods for battery actual capacity and maximum available energy estimation are reviewed. Due to the existing high correlation amongst the different battery states and improve the functioning of BMS, it is crucial to develop the states co-estimation method for the estimation of the different battery states in real-time application. The different existing battery states co-estimation methods for SOC, SOE, SOP, and SOH estimation have been discussed. Presently, to effectively utilize the correlation between the battery states and for the development of computationally efficient BMS, the co-estimation method is preferred by the researcher for battery states estimation.

In Phase 2, the different battery cell testing methods utilized for the development of useful datasets are performed on the considered battery cells of different chemistries such NCA, NMC, and LFP. Different dynamic load current profiles corresponding to DST, US06 drive cycle, and HPPC test are considered for testing of considered battery cells. The developed datasets will be utilized for the validation of the proposed estimation methods.

In Phase 3, to simultaneously estimate the battery model parameters and SOC at high accuracy and low computational cost, a proposed DFFAEKF algorithm is developed. In which, the benefits of the forgetting factor (high variations in the filter coefficients) together with the features of the DKF algorithm are utilized. Later, the co-estimation method for battery SOC and SOE estimation using the DFFAEKF algorithm is developed. In which, a proposed DFFAEKF was utilized for SOC estimation and experimental quantitative relation between SOC and SOE for SOE estimation to make it highly accurate and computational less expensive. The proposed method is capable to estimate the battery SOC and SOE with high accuracy and, strong robustness to the battery model parameter inaccuracy and measurement noise uncertainties. Further, to effectively utilize the correlation between different battery states and to reduce the computational burden of the overall co-estimation method, a unified frame of battery states co-estimation method for battery SOC, SOE, SOP, actual capacity, and maximum available estimation is developed. The robust and less computational burden methods are considered for the battery states (SOC, SOE, SOP) estimation. A proposed co-estimation method for SOC and SOE estimation using the DFFAEKF is utilized to estimate the SOC and SOE. By utilizing the identified Rint battery model parameters using the FFRLS algorithm and the estimated SOC, the battery model-based SOP estimation algorithm is implemented. Moreover, the actual capacity and maximum available energy estimation are performed by using a new SW-AWTLS algorithm. The SW-AWTLS algorithm can converge to true value at a fast rate with a low computational burden as compared to the AWTLS algorithm due to the sliding window. All the proposed methods are implemented in MATLAB environment for the evaluation purpose.

In Phase 4, the performance of the proposed methods are validated and evaluated based on the various extensive simulation conducted in MATLAB environment. The data collected with the testing of different chemistry cells under different dynamic operating

conditions in Phase 2 and the different evaluation metrices are used to ensure the effectiveness of the proposed methods. The results of the proposed battery states co-estimation methods are presented in Chapter 6.

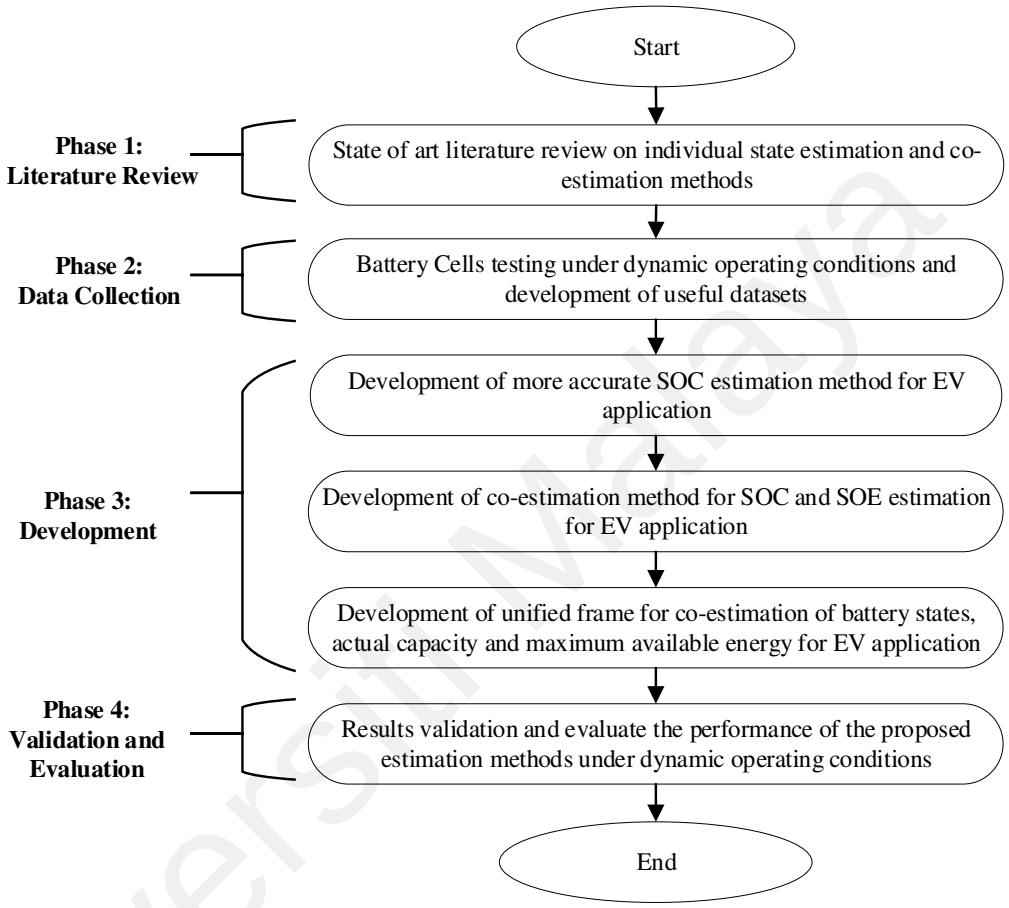

Figure 3.1: Flow chart of research methodology

3.3 Experimental settings

The experimental setup involved in acquiring the experimental useful data is shown in Figure 3.2. It contains the battery testing system (Neware BTS4000), programmable temperature chamber (ESPEC SU-241), host computer, and battery cells. The battery testing system is used to charge and discharge the battery cell according to the load profiles. Then, the data is recorded and send to the host computer. The maximum operating current and voltage range of BTS 4000 are 10 A and 5V, respectively. The BTS 4000 has the accuracy and stability of ± 0.05 % of FS. It can record the data at a frequency

of 10 Hz. The temperature chamber ESPEC SU-241is used to maintain the desired temperature settings. The operating temperature range of ESPEC SU-241is - 40°C to 150°C. Where the balance temperature control system is used to control the operating temperature inside the chamber.

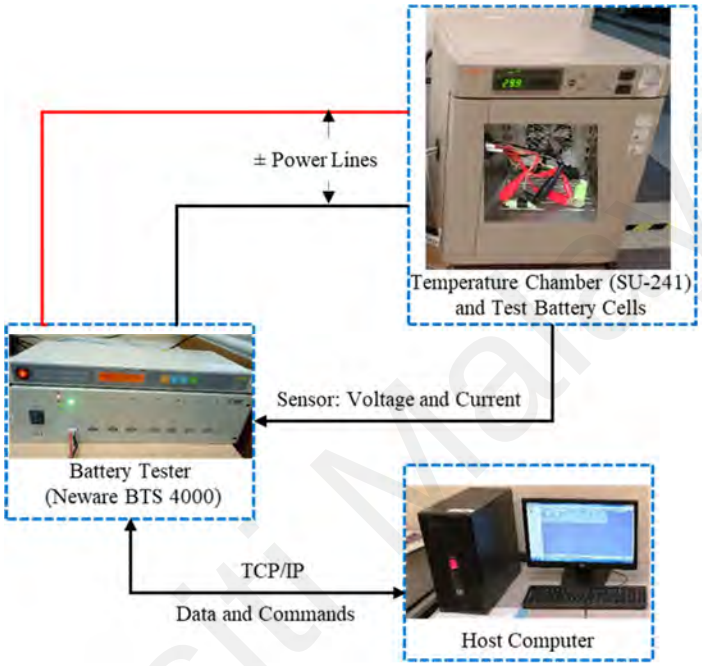

Figure 3.2: Experimental Test Bench

3.3.1 Considered battery cells specification

As listed in Table 3.1, the three battery cells of different chemistries are considered for the validation of the proposed algorithms. The Lithium nickel cobalt aluminum oxide battery cell NCR 18650B manufactured by Panasonic is considered as Cell 2, as presented in Figure 3.3 (a). It has a nominal capacity of 3.4 Ah and a nominal voltage of 3.6 V. The Lithium nickel manganese cobalt oxide battery cell US18650VTC6 manufactured by Sony is considered as Cell 3, as presented in Figure 3.3 (b). It has a nominal capacity of 3.0 Ah and a nominal voltage of 3.7 V. The high-performance nanophosphate lithium iron phosphate battery cell ANR26650M1-B manufactured by A123 is considered as Cell

1, as presented in Figure 3.3 (c). It has a nominal capacity of 2.6 Ah and a nominal voltage of 3.6 V with high power and energy density.

The details specification of the Cell 1, Cell 2 and Cell 3 is given in appendix A.

(a)

(b)

(c)

Figure 3.3: Considered battery cells: (a) Cell 1, (b) Cell 2, and (c) Cell 3

Table 3.1: Considered different chemistry test battery cells

Battery Cells	Part Name	Chemistry	Nominal Capacity (Ah)	Nominal Voltage (V)
Cell 1	NCR18650B	NCA	3.4	3.6
Cell 2	VTC6 18650	NMC	3.0	3.7
Cell 3	ANR26650M1-B	LFP	2.6	3.3

3.3.2 Battery Cell Testing Methods

Different tests are conducted on the battery cells, to develop useful datasets for the validation of the proposed methods. The name of the different conducted tests, associated test settings, and the purpose/results of the test considered in this study are shown in Figure 3.4.

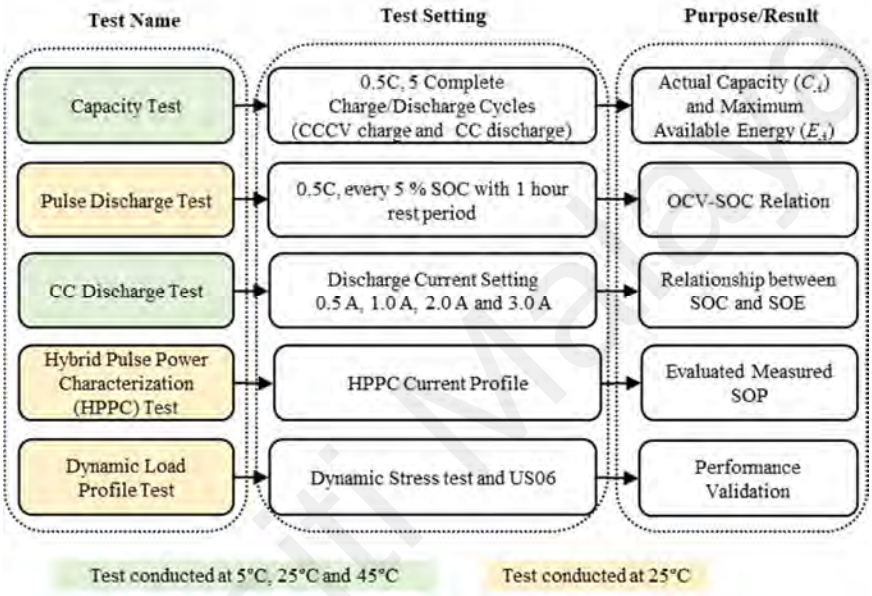

Figure 3.4: Details of battery cells tests considered in the thesis

3.3.2.1 Capacity test

The capacity test is conducted to obtain the experimental actual capacity, which contains constant current- constant voltage (CC-CV) charge and CC discharge. With the help of obtained test results, the experimental maximum available energy values are also evaluated. Firstly, the battery cells are placed inside the battery chamber and soaked at the set temperature for 5 hours. The battery cells are charged using the CC-CV charging method to the test cells' upper cut-off voltage. Three different discharge C-rates (e.g. 0.5 C, 1.0 C, and 1.5 C) are considered for discharge the battery cell to lower cut-off voltage. The procedure is repeated at three distinct temperature values such as 5°C, 25°C, and 45°C. The values of the obtained actual capacity and maximum available energy under

different operating conditions are presented in Figure 3.5. The obtained experimental actual capacity and maximum available energy for Cell1, Cell 2, and Cell 3 under three different operating temperatures are demonstrated in Figures 3.5 (a), 3.5 (b), and 3.5 (c), respectively.

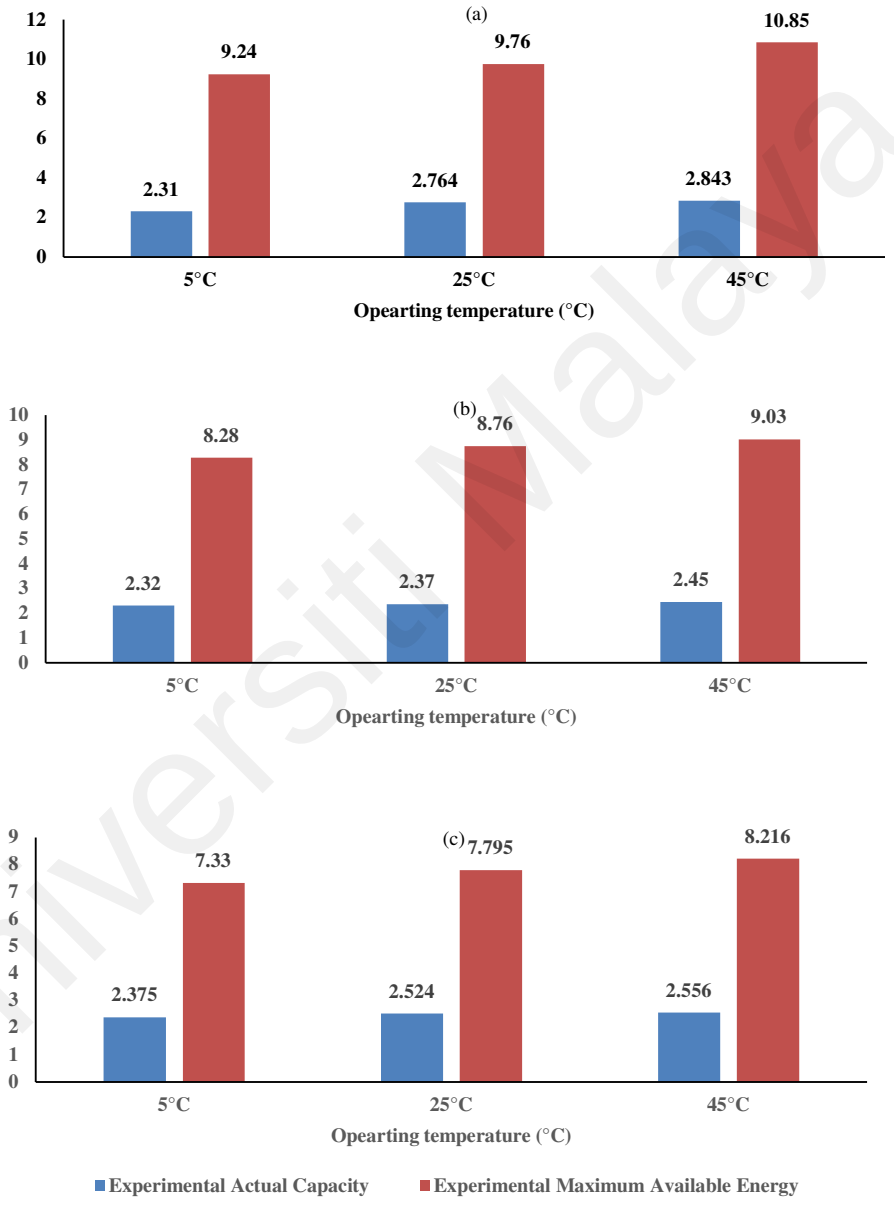

Figure 3.5: Obtained experimental actual capacity and maximum available energy of fresh battery cells at different operating temperature: (a) Cell 1, (b) Cell 2, (c) Cell 3

3.3.2.2 Pulse discharge test

The pulse discharge test is performed to evaluate the relationship between OCV and SOC. Firstly, the test battery cells are charged by using the CC-CV charge current profile. The test battery cells are considered to be fully charged to 100 % SOC at the end of the CC-CV charge. The test battery cells are kept at rest condition for 1-hour rest to measure the OCV at 100 % SOC. Hereafter, the test battery cells are discharged using CC discharge at a 1 C rate for every 10 % SOC with 1 hour rest period to determine the relationship between the OCV and SOC. The obtained OCV-SOC relationship for the test battery cells at 25°C is presented in Figure 3.6.

The polynomial fitted equation is used to define the relationship between SOC and OCV and expressed by a function that contains SOC:

$$OCV = \sum_{i=0}^{n} k_n SOC^n : \mathrm{i} = 1,2, \dots n \tag{3.1}$$

Where, k_i $(i = 0, 1, 2, \dots, n)$ are the coefficients of the ´n´ order polynomial equation and can be determined by using the robust linear least-squares fitting method as shown in Fig 3.3. The centering and scaling approach were employed to normalize the experimental values. To obtain a better fit or high R-square value, the order of the polynomial is set to 7 for all the test battery cells. The obtained polynomial coefficients value of the fitted curve of OCV-SOC relationship for test battery cells are listed in Table 3.2.

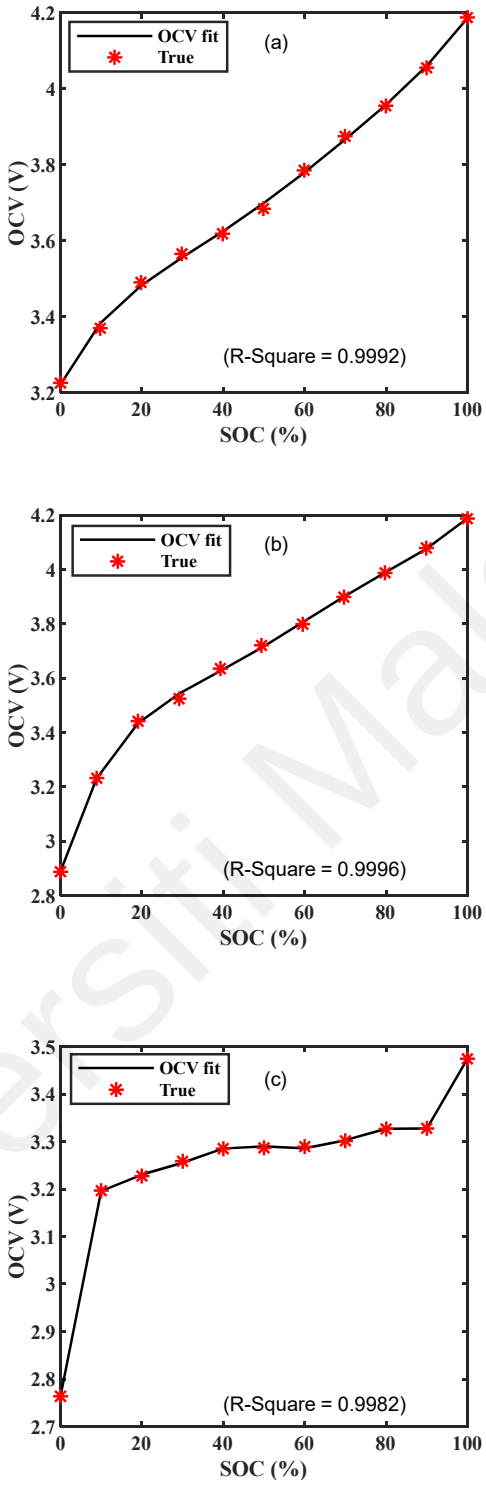

Figure 3.6: Average OCV and SOC curve of test battery cells at 25°C:

(a) Cell 1, (b) Cell 2, and (c) Cell 3

Table 3.2: Obtained coefficient values of fitted OCV-SOC curve of test battery cells

Battery Cells	Coefficients									RMSE
	k_1	k_7	k_6	k_5	k_4	k_3	k_2	k_1	k_0	
Cell 1	0.0079	-0.0388	0.0053	0.1433	-0.0601	0.128	0.090	0.287	3.692	0.0079
Cell 2	0.0158	0.080	-0.076	-0.219	-0.151	0.183	-0.0722	0.233	3.767	0.0158
Cell 3	0.0054	0.079	-0.057	-0.24	0.118	0.229	-0.072	-0.017	3.291	0.0054

3.3.2.3 Constant current (CC) discharge test

The CC discharge test is performed to obtain the experimental relation between SOC and SOE. Firstly, the test battery cells are fully charge using CC-CV charging profile. Hereafter, the test battery cells are discharged using CC discharge at 0.5 C, 1.0 C, and 1.5 C under set temperature. The CC discharge test is repeated at three distinct temperature values such as 5°C, 25°C, and 45°C. Further, the experimental relations between SOC and SOE are evaluated under different operating conditions. According to the results, as shown in Figure 3.7, the relationship between SOE and SOC for all considered battery cells is expressed by the quadratic function as expressed by (3.2). Where a, b, and c are the function coefficients. The robust linear least square method is used to determine the value of the coefficients in (3.2) and the obtained values are listed in Table 3.3. The high value of R-Square indicates that the fitting function precisely matches the average experimental relationship between battery SOE and SOC. The coefficient of determination R-Square is 1 for all the test battery cells. The value of RMSEs is 0.1493, 0.008, and 0.01232 of the fitted curves for Cell 1, Cell 2, and Cell 3, respectively.

$$SOE = a \times SOC^2 + b \times \mathrm{SOC} + c \tag{3.2}$$

Table 3.3: Obtained coefficient values of the fitted curve of average SOC and SOE relation of test battery cells

Battery Cells	Coefficient Values			RMSE
	a	b	c	
Cell 1	-1.228	29.17	53.8	0.1493
Cell 2	-1.01	29.19	53.58	0.008158
Cell 3	-0.2319	29.78	52.35	0.01232

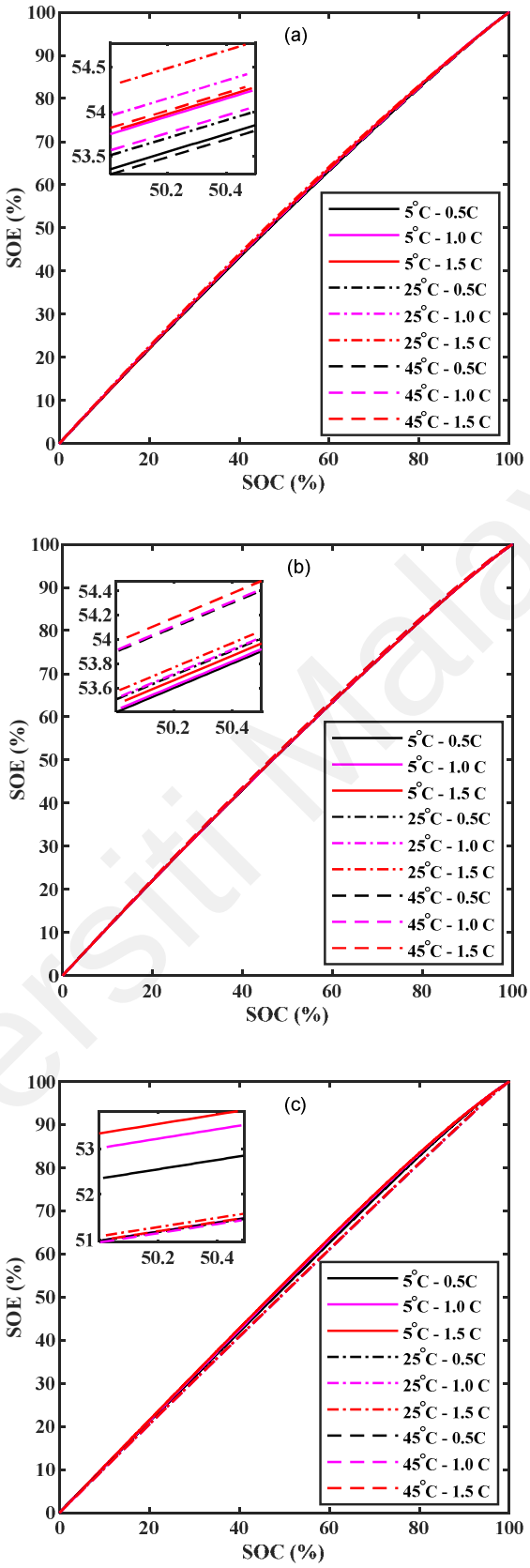

Figure 3.7: Experimental SOC and SOE relationship of test battery cells: (a) Cell 1, (b) Cell 2, and (c) Cell 3

3.3.2.4 Hybrid pulse power characterization (HPPC) test

The high-power charging and discharging of the battery cell can accelerate the degradation process. To protect the cell from degradation, the maximum power limits are computed for the next ΔT seconds. Generally, the HPPC test is conducted on the battery cell to estimate the battery cell power. The load current profile presented in Figure 3.8 is used to perform the HPPC test on the battery cell. Under which, a current pulse of 1.5 C rate is injected for 10s followed by the rest of 40s at every 10 % SOC as shown in Figure 3.9. A fully charged battery cell is discharged at a pulse of 0.5C for 10 % SOC. The rest of 1 hour is given after the discharge of every 10 % SOC. The rest of the 40s is given between the current pulse. The first and second pulse refers to discharge and charge, respectively. The magnified HPPC load current and voltage profile is shown in Figure 3.9.

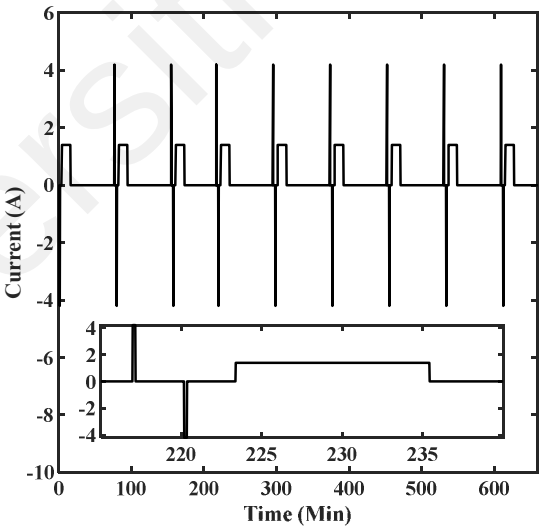

Figure 3.8: Load current profile for HPPC test

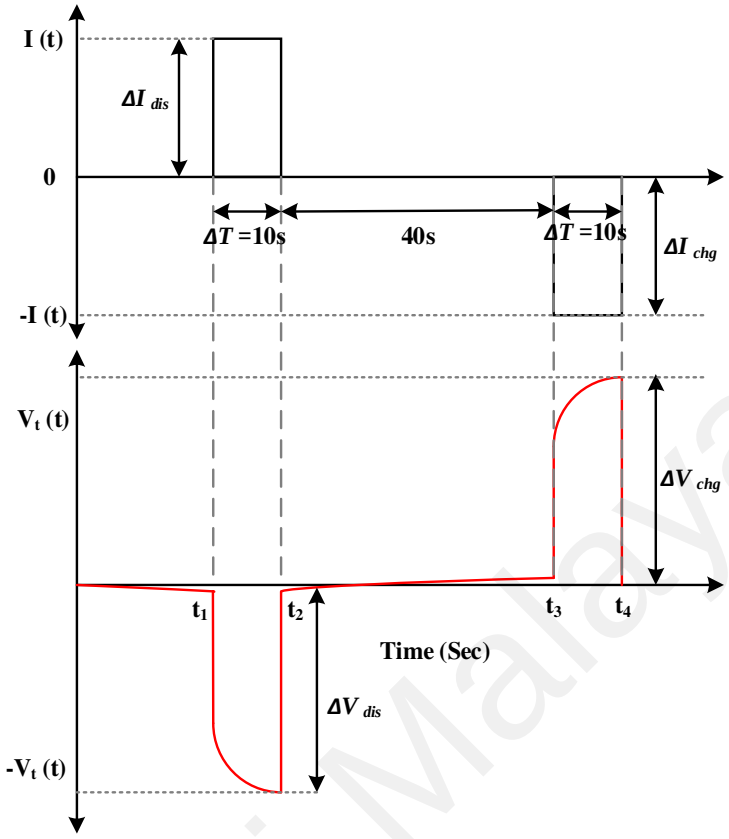

Figure 3.9: Magnified load current and terminal voltage profile for HPPC test

By using the load current and voltage profile shown in Figure 3.9 and the Rint battery model as shown in Figure 3.10, the steps involved in charge and discharge power limits based on voltage are described below.

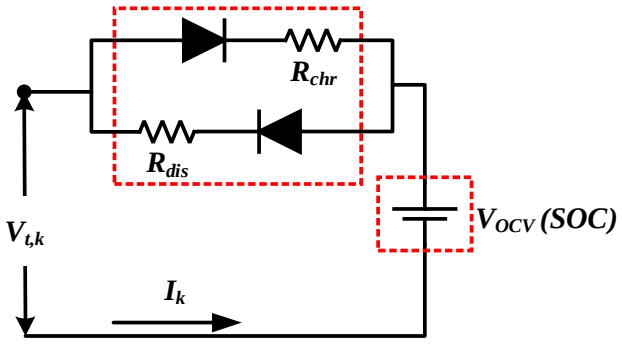

Figure 3.10: Battery Rint Model with different charge and discharge resistance
(Nabi Akpolat et al., 2020)

Firstly, by using the HPPC test results, the discharge resistance (R_{dis}^{HPPC}) and charge resistance (R_{chg}^{HPPC}) can be calculated by using:

$$R_{dis}^{HPPC} = \left|\frac{\Delta V_{dis}}{\Delta I_{dis}}\right| = \left|\frac{V_t(t_2)-V_t(t_1)}{I(t_2)-I(t_1)}\right| \tag{3.3}$$

$$R_{chg}^{HPPC} = \left|\frac{\Delta V_{chg}}{\Delta I_{chg}}\right| = \left|\frac{V_t(t_4)-V_t(t_3)}{I(t_4)-I(t_3)}\right| \tag{3.4}$$

At k^{th} time instant, the terminal voltage of the battery cell ($V_{T,k}$) and the battery cell current (i_k) are computed as:

$$V_{T,k} = V_{OCV,k} - i_k R_{st} \tag{3.5}$$

$$i_k = \frac{V_{OCV,k}-V_{T,k}}{R_{st}} \tag{3.6}$$

To compute the battery discharge power, the value of $R_{st} = R_{dis}^{HPPC}$ and $V_{T,k} = V_{min}$, Then,

$$P_{dis,k} = V_{T,k} i_k = V_{min}\left(\frac{V_{OCV,k}-V_{min}}{R_{dis}^{HPPC}}\right) \tag{3.7}$$

Similarly, to compute battery charge power, the value of $R_{st} = R_{chg}^{HPPC}$ and $V_{T,k} = V_{max}$, Then,

$$P_{chg,k} = V_{T,k} i_k = V_{max}\left(\frac{V_{max}-V_{OCV,k}}{R_{chg}^{HPPC}}\right) \tag{3.8}$$

Where, V_{max} and V_{min} are the upper cut-off voltage and a low cut-off voltage of the battery cell, respectively. In the study, the computed $P_{dis,k}$ and $P_{chg,k}$ are considered as the true values discharge SOP and charge SOP, respectively.

3.3.2.5 Dynamic load profile test

To validate the performance of the proposed methods in dynamic operating conditions under the variable power discharge regimes, two types of dynamic profiles namely dynamic stress test (DST) profile and the US06 drive cycle profile are used in this study. The DST profile is an improved version of the simplified Federal Urban Driving Schedule (SFUDS) and is used for drive cycle testing of USABC batteries. The US06 is a Supplemental Federal Test Procedure (SFTP) developed by the US Environmental Protection Agency (EPA) for an aggressive driving study. Due to the rapid speed fluctuations of US06, the robustness analysis of the proposed algorithm can be done. The dynamic load current profile of DST and US06 is presented in Figure 3.11 and Figure 3.12, respectively. The positive and negative current values represent discharging and charging, respectively.

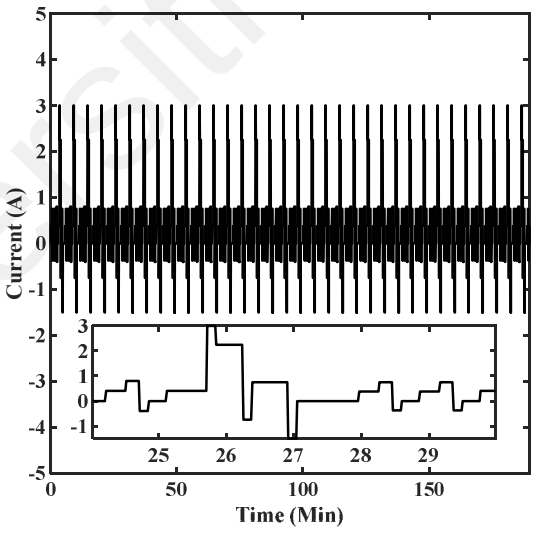

Figure 3.11: Load current profile for a dynamic stress test (DST)

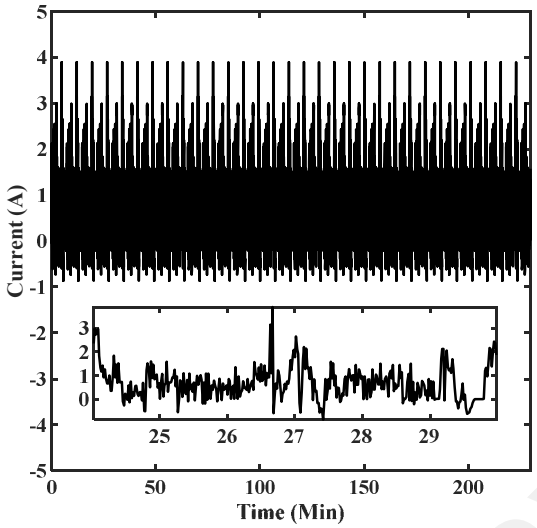

Figure 3.12: Load current profile for US06 drive cycle test

3.4 Evaluation Metrics

Consideration of appropriate evaluation matrices are very important for the validation of the proposed methods. In the study, four different types of evaluation metrics are considered for the evaluation of the proposed algorithm such as estimation errors, computational complexity, convergence speed, and computational burden.

3.4.1 Estimation Errors

To compare the estimation results, three different errors such as maximum absolute error (MaxAE), mean absolute error (MAE) and root mean square error (RMSE) are considered. The RMSE always a decent choice as an evaluation matric as it gives more weight to large errors. The value of estimation MAE, MaxAE, and RMSE can be evaluated by using (3.9), (3.10), and (3.11), respectively.

$$\text{MaxAE} = \max[|(Estimated)_k - (Measured)_k|] \tag{3.9}$$

$$\text{MAE} = \frac{1}{N}\sum_{k=1}^{N}(|(Estimated)_k - (Measured)_k|) \tag{3.10}$$

$$\text{RMSE} = \sqrt{\frac{1}{N}\sum_{k=1}^{N}((Estimated)_k - (Measured)_k)} \quad (3.11)$$

The accuracy of the identified battery model parameters is computed with the help of battery terminal voltage errors. The terminal voltage absolute error (AE) is evaluated by comparing the estimated battery model terminal voltage with the measured battery terminal voltage.

Similarly, the accuracy of the estimated battery states e.g., SOC and SOE are computed with the assistance of estimation errors. The estimated state absolution error is evaluated by comparing the estimated battery states with the measured battery states.

3.4.2 Computational complexity

The worst-case big O notation complexity $O(.)$ is widely used for the evaluation of the time complexity of the algorithm. The time complexity of the algorithm is commonly evaluated by the number of elementary mathematical operations performed. The big O complexity of the KF algorithm depends on the implicated matrices and vector dimensions and different operations. The fundamental algorithmic complexity associated with the simple matrices and vectors operation complexity is listed in Table 3.5. Generally, in the KF algorithm, the state vector size is n, measurement vector size is m, and command vector size is p involved. Based on the complexity fundamental given in table 3.5, the value of worst-case big O notation complexity $O(.)$ of the proposed algorithm is computed.

Furthermore, the running time $T(.)$ of the proposed algorithm is evaluated. The $T(.)$ depends on the number of executed operations in an algorithm. The high value of operations, the longer $T(.)$ of the algorithm.

Table 3.4: Matrix operation complexity fundamental (Valade et al., 2017)

Operation	O (.)
Matrix multiplication	$2 \times n \times m \times p$
Addition of two vectors of size n	n
Addition of two matrices of size (n, m)	$n \times m$
Transposition of a matrix	0
Inversion of a matrix	$4 \times n^3$
Mean vector of a matrix	$n \times m$
Mean value of a vector	n

3.4.3 Computational cost

Usually, the mean execution time (MET) is utilized to compare the computational cost of SOC estimation algorithms (Lucu et al., 2018). The final value of MET for a dynamic profile is calculated by using (3.12). Where $MET_{Cell\,i}$ is the mean execution time of the i^{th} battery cell. To evaluate the value of $MET_{Cell\,i}$ of an i^{th} battery cell, the algorithms are executed for 10 times under the same dynamic profile (Meng et al., 2016).

$$MET = \frac{1}{N}\sum_{i=1}^{N} MET_{Cell\,i} : i = 1, 2, \ldots N \tag{3.12}$$

3.4.4 Convergence speed

Apart from the accuracy, the evaluation of the convergence speed is also an important factor in the performance analysis. The convergence speed can be defined as the time taken by the estimation value reaches the threshold value. In this study, the convergence threshold is set to a 5 % estimation error value. The convergence speed also helps to evaluate the robustness of the proposed algorithm under erroneous initial conditions. The

high value of convergence speed means the high robustness of the proposed algorithm. The convergence speed also represents convergence time.

3.5 Summary

The different phases of research methodology to achieve the research objectives are discussed in this chapter. The experimental settings involved in the battery testing are described. The different battery cell testing methods utilized for the development of useful datasets are explained. The developed datasets will be utilized for the validation of the proposed battery states co-estimation methods. The different evaluation matrices such as estimation errors, computational complexity, convergence speed, and computational burden are briefly discussed in this chapter.

CHAPTER 4: CO-ESTIMATION METHOD FOR SOC AND SOE ESTIMATION USING DUAL FORGETTING FACTOR-BASED ADAPTIVE EXTENDED KALMAN FILTER

4.1 Introduction

As discussed in chapter 2, in model-based SOC estimation using EKF, the estimation accuracy directly depends on the accuracy of identified battery model parameters and the prior knowledge of the system noise variables. With the incorrect prior knowledge of system noise variables, the SOC estimation process error may prompt divergence. Also, the SOC estimation accuracy would not be guaranteed with the application of the offline battery model parameters identification method. Thus, it is always required to adaptively update the covariance matrix elements and the model parameters with the battery SOC estimation at a reduced computational burden. Also, in recent years, researchers are focusing on developing the combined SOC and SOE techniques that can be easily implementable into low-cost BMS chips. For instance, the adaptive H-infinity filters were used for the combined SOC and SOE estimation by using the offline identified model parameters in (Yongzhi Zhang et al., 2017). The results demonstrate a high estimation accuracy of SOC as well as SOE under different erroneous conditions. However, the use of offline model parameters limits the application in the long run. Furthermore, two different H-infinity filters were employed for battery SOC and SOE estimation that causes high computational cost. To reduce the computational cost of the model-based SOE estimation method, in (L. Zheng et al., 2016a), the simple SOE estimation based on the quantitative relationship between SOE and SOC was developed. In this study, the $LiMn_2O_4$ battery cells were considered. The results were analyzed under various operating conditions and the proposed method shows the SOE estimation maximum mean absolute error is 3.4 % under the dynamic stress test (DST) profile. The Luenberger observer was used for battery SOC estimation along with the offline identified battery

model parameters. The SOC estimation error was less than 2 %. However, the estimation accuracy of the Luenberger observer cannot be guaranteed due to the high sensitivity of the observer to battery model parameter variations. Therefore, there is a need to employ a highly accurate SOC estimation algorithm to simultaneously update the battery SOC and the model parameters and to improve the overall accuracy of the combined SOC and SOE estimation. Furthermore, it is also required to validate the concept of the quantitative relationship between battery SOE and SOC for other chemistry battery cells.

In this chapter, a dual forgetting factor-based adaptive extended Kalman filter (DFFAEKF) algorithm is proposed for SOC estimation. Where the forgetting factor feature is used to reduce the computational burden of the proposed algorithm. Also, the proposed DFFAEKF algorithm helps to resolve the issue of battery model parameter divergence from the true value present in the DEKF algorithm to achieve high estimation accuracy under realistic dynamic loading conditions. Thereafter, using the proposed DFFAEKF algorithm, an accurate and low computational burden co-estimation method for SOC and SOE estimation is developed for EV applications. In the proposed co-estimation method, the experimental correlation between SOC and SOE is utilized for SOE estimation. The concept of the proposed co-estimation method for SOC and SOE estimation and mathematics behind the implementation are also discussed. In addition, the experimental setting and battery test involved in the validation of the proposed method under dynamic operating conditions are explained.

The sections of the chapter are arranged in this sequence. In Section 4.1, the introduction of the chapter is provided. In Section 4.2, the mathematical analysis of the proposed DFFAEKF algorithm and its implementation for the SOC estimation method are discussed. Section 4.3 explains the proposed co-estimation method for battery SOC and SOE for EV applications. The experimental setting and test conducted on the

considered battery cells are briefly discussed in Section 4.4. Finally, the summary of the chapter is presented in Section 4.5.

4.2 Proposed dual forgetting factor-based adaptive extended Kalman filter (DFFAEKF) for SOC estimation

A new dual forgetting factor-based adaptive extended Kalman filter (DFFAEKF) for SOC estimation is proposed in this chapter. In which, the benefits of the forgetting factor (high variations in the filter coefficients) together with the features of the DKF algorithm are utilized. The proposed algorithm has the feature of concurrently updating the battery model parameters with the SOC estimation at high accuracy under different dynamic conditions with the same order big O notation complexity as DEKF.

4.2.1 Lithium-ion battery modeling

Due to the low complexity of the ECM of LIB, it is commonly utilized for model-based SOC estimation. Especially, the 2RC battery model is commonly used for SOC estimation, as shown in Figure 4.1. It contains a series of internal resistance (R_0), two parallel-connected resistor and capacitor branches (R_1C_1 and R_2C_2), a voltage source equivalent to an open circuit (OCV) of the battery cell. R_1 and R_2 are the dynamic resistance and C_1 and C_2 are the corresponding dynamic capacitances. V_t is the battery terminal voltage. In this study, the polarity of discharging and charging battery current (I) is assumed to be positive and negative, respectively. The values of battery model elements are highly dependent on the battery SOC, charge/discharge C-rate, state of health, and operating condition.

The battery state-space equations developed by using Kirchhoff's voltage law can be written as:

$$\begin{cases} \dot{V}_1 = -\frac{V_1}{R_1 C_1} - \frac{1}{C_1} I \\ \dot{V}_2 = -\frac{V_2}{R_2 C_2} - \frac{1}{C_2} I \\ V_t = OCV - V_1 - V_2 - IR_0 \end{cases} \tag{4.1}$$

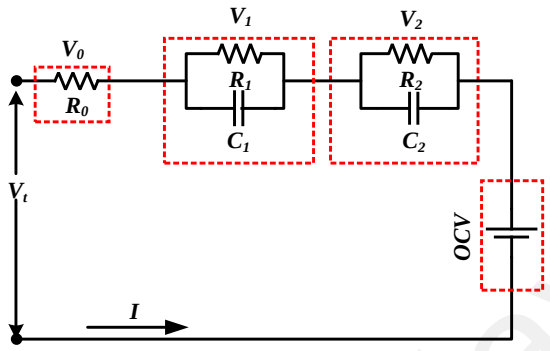

Figure 4.1: The second RC model for Lithium-ion battery

4.2.2 Forgetting Factor-Based Adaptive Extended Kalman Filter (FFAEKF)

Generally, the non-linear system is described by using discrete-time state space and measurement equation as given below:

$$\begin{cases} X_k = A_{k-1} X_{k-1} + B_{k-1} u_{k-1} + w_{k-1} \\ Y_k = C_k X_k + D_k u_k + v_k \\ w_k \approx N(0, P_{w,k}) \\ v_k \approx N(0, P_{v,k}) \end{cases} \tag{4.2}$$

Where matrices A_k, B_k, C_k and D_k are dependent on system dynamics. X_k is the system state and Y_k is the output vector. w_k and v_k are the zero mean small white noise signals with covariance $P_{v,k}$ and $P_{w,k}$ respectively. k denotes the time step for the system vectors.

In the AEKF estimation method used in non-linear systems, the additional feature of adaptively updating the noise covariance matrices is utilized to overcome the error divergence and biased solution in AEKF. There are four adaptive filtering approaches generally used in AEKF such as the Bayesian estimation approach, the maximum likelihood estimation method, the correction technique, and the covariance matching technique (Rui Xiong, He, Sun, & Zhao, 2013). A covariance matching technique is a

simple approach and the idea behind it is to match the residuals consistent with the theoretical covariance. Generally, the noise covariance matrix is updated by using the moving window method (Zhentong Liu & He, 2015), and the forgetting factor method was introduced in (Akhlaghi et al., 2018; X. Li et al., 2019) to simplify the moving window method.

The detailed steps of the forgetting factor-based AEKF (FFAEKF) can be summarized as follows:

Step 1: Initialization

Initialize the mean and covariance at step $k = 0$,

$$\begin{cases} \hat{x}_0^+ = E(x_0) \\ P_{\tilde{x},0}^+ = E[(x_0 - \hat{x}_0^+)(x_0 - \hat{x}_0^+)^T] \end{cases} \tag{4.3}$$

Where $\hat{x}_0^+$ and $P_{\tilde{x},0}^+$ are the estimated initial state and error covariance matrix. And superscript "+" represents the posterior values. Circumflex (^) and tilde (~) represent the estimated and predicted value. 'T' indicates matrix transportation.

Step 2: Time Update or Prediction

Obtain the prior state and its covariance matrix from the projection of step k-1 to step k.

Predicted state estimation,

$$\hat{x}_k^- = \hat{A}_{k-1}\hat{x}_{k-1}^+ + \hat{B}_{k-1}u_{k-1} \tag{4.4}$$

Priori Covariance matrix,

$$P_{\tilde{x},k}^- = \hat{A}_{k-1}P_{\hat{x},k-1}^+\hat{A}_{k-1}^T + P_{w,k-1} \tag{4.5}$$

where $\hat{A}_k = \frac{\partial F(x_k,\theta_k,I_k)}{\partial x_k}\Big|_{x_k=\hat{x}_k^-}$, $\hat{B}_{k-1} = \frac{\partial F(x_k,\theta_k,I_k)}{\partial w_k}\Big|_{w_k=\tilde{w}_k}$ and $P_{w,k}$ is the covariance of the process noise w_k.

Step 3: Measurement Update or Correction

Obtain The improved posterior estimation by utilizing the difference between the actual measurement and predicted measurement calculated from the prior estimation,

Innovation,

$$r_k = y_k - \hat{C}_k^x P_{\tilde{x},k}^- - D_k^x u_k \tag{4.6}$$

Kalman gain matrix,

$$L_k = P_{\tilde{x},k}^- \hat{C}_k^{x^T} [\hat{C}_k^x P_{\tilde{x},k}^- \hat{C}_k^{x^T} + D_k^x P_{v,k}^- D_k^{x^T}]^{-1} \tag{4.7}$$

Posteriori state estimation,

$$\hat{x}_k^+ = \hat{x}_k^- + L_k[y_k - \hat{y}_k\,] \tag{4.8}$$

Posteriori covariance matrix,

$$P_{\hat{x},k}^+ = P_{\tilde{x},k}^- - L_k\, P_{\tilde{y},k} {L_k}^T \tag{4.9}$$

Residual,

$$e_k = y_k - \hat{C}_k^x P_{\hat{x},k}^+ - D_k^x u_k \tag{4.10}$$

Where $\hat{C}_k^x = \frac{\partial F(x_k,\theta_k,I_k)}{\partial x_k}\Big|_{x_k=\hat{x}_k^+}$, $D_k^x = \frac{\partial F(x_k,\theta_k,I_k)}{\partial v_k}\Big|_{v_k=v_k}$ and $P_{v,k}$ is the covariance of the measurement noise v_k.

In the FFAEKF, the forgetting factor 'a' is used to adaptively update the noise covariance matrix. Generally, the value of a can vary from 0 to 1. The application of the forgetting factor is to put more weightage on the current values in the update of the noise

covariance matrix and the updated covariance matrices can be expressed as below (Akhlaghi et al., 2018):

Updated process noise covariance matrix,

$$P_{w,k} = aP_{w,k-1} + (1-a)\left(L_k r_k {r_k}^T {L_k}^T\right) \tag{4.11}$$

Updated measurement noise covariance matrix,

$$P_{v,k} = aP_{v,k-1} + (1-a)\left(e_k {e_k}^T + \hat{C}_k^x P_{\tilde{x},k}^- \hat{C}_k^{x\,T}\right) \tag{4.12}$$

4.2.3 Proposed SOC estimation using DFFAEKF

To estimate both battery state and parameters during the EV running condition, a new DFFAEKF is proposed in this paper. This proposed method will help to jointly update the battery model parameters, SOC as well as the unknown noise covariance matrices.

The state-space equations for the battery SOC and model parameters estimation can be written as

SOC estimation,

$$\begin{cases} X_k = [SOC_k \quad V_{1,k} \quad V_{2,k}]^T \\ x_{k+1} = F(x_k, \theta_k, I_k) + w_k^x \\ y_k = G(x_k, \theta_k, I_k) + v_k^x \end{cases} \tag{4.13}$$

$F(.)$ and $G(.)$ are the nonlinear functions of a state vector X_k, and input battery current I_k, and the battery model parameter vector θ_k . Further, it can be expressed as given below:

$$F(.) = \begin{bmatrix} 1 & 0 & 0 \\ 0 & 1/e^{\frac{-\mathrm{T_S}}{\tau_1}} & 0 \\ 0 & 0 & 1/e^{\frac{-\mathrm{T_S}}{\tau_2}} \end{bmatrix} \begin{bmatrix} SOC_k \\ V_{1,k} \\ V_{2,k} \end{bmatrix} + \begin{bmatrix} -\eta_c \mathrm{T_S}/C_A & 0 & 0 \\ 0 & R_1(1-e^{\frac{-\mathrm{T_S}}{\tau_1}}) & 0 \\ 0 & 0 & R_2(1-e^{\frac{-\mathrm{T_S}}{\tau_2}}) \end{bmatrix} I_k \tag{4.14}$$

$$G(.) = OCV(SOC_k) - V_{1,k} - V_{2,k} - I_k R_0 \tag{4.15}$$

where, T_s is the sampling time interval.

The Jacobian matrix of state can be written as:

$$\hat{A}_k = \frac{\partial F(.)}{\partial x_k}\Big|_{x_k=\hat{x}_k^-} = \begin{bmatrix} 1 & 0 & 0 \\ 0 & e^{\frac{-T_s}{\tau_1}} & 0 \\ 0 & 0 & e^{\frac{-T_s}{\tau_2}} \end{bmatrix} \tag{4.16}$$

$$\hat{C}_k^x = \frac{\partial G(.)}{\partial x_k}\Big|_{x_k=\hat{x}_k^-} = [\partial OCV/\partial SOC_k \quad -1 \quad -1] \tag{4.17}$$

Model parameter estimation,

$$\begin{cases} \theta_k = [R_{0,k} \quad R_{1,k} \quad \tau_{1,k} \quad R_{2,k} \quad \tau_{2,k}]^T \\ \theta_{k+1} = \theta_k + w_k^\theta \\ d_k = G(x_k, \theta_k, I_k) + v_k^\theta \end{cases} \tag{4.18}$$

where $V_{t,k}$ is the battery terminal voltage at step k. w_k^x and w_k^θ represent the zero mean independent white Gaussian process noise of the state and parameter respectively and their respective covariance matrices are $P_{w,k}^x$ and $P_{w,k}^\theta$. Then, v_k^x is the measurement noise random input signal with zero mean and covariance $P_{v,k}^x$.

The Jacobian matrix of time-varying battery model parameters can be written as:

$$\hat{C}_k^\theta = \frac{\partial G(.)}{\partial \theta_k}\Big|_{\theta_k=\hat{\theta}_k^-} = \frac{\partial G(.)}{\partial \hat{\theta}_k^-} + \frac{\partial G(.)}{\partial \hat{x}_k^-} \cdot \frac{\partial \hat{x}_k^-}{\partial \hat{\theta}_k^-} \tag{4.19}$$

The overall steps-wise implementation of the proposed DFFAEKF algorithm for joint estimation of the battery SOC and model parameters in the real-time condition are summarized in Figure 4.2. In this paper, a= 0.98 is chosen to update the process and measurement noise covariance matrices of the battery state and model parameter.

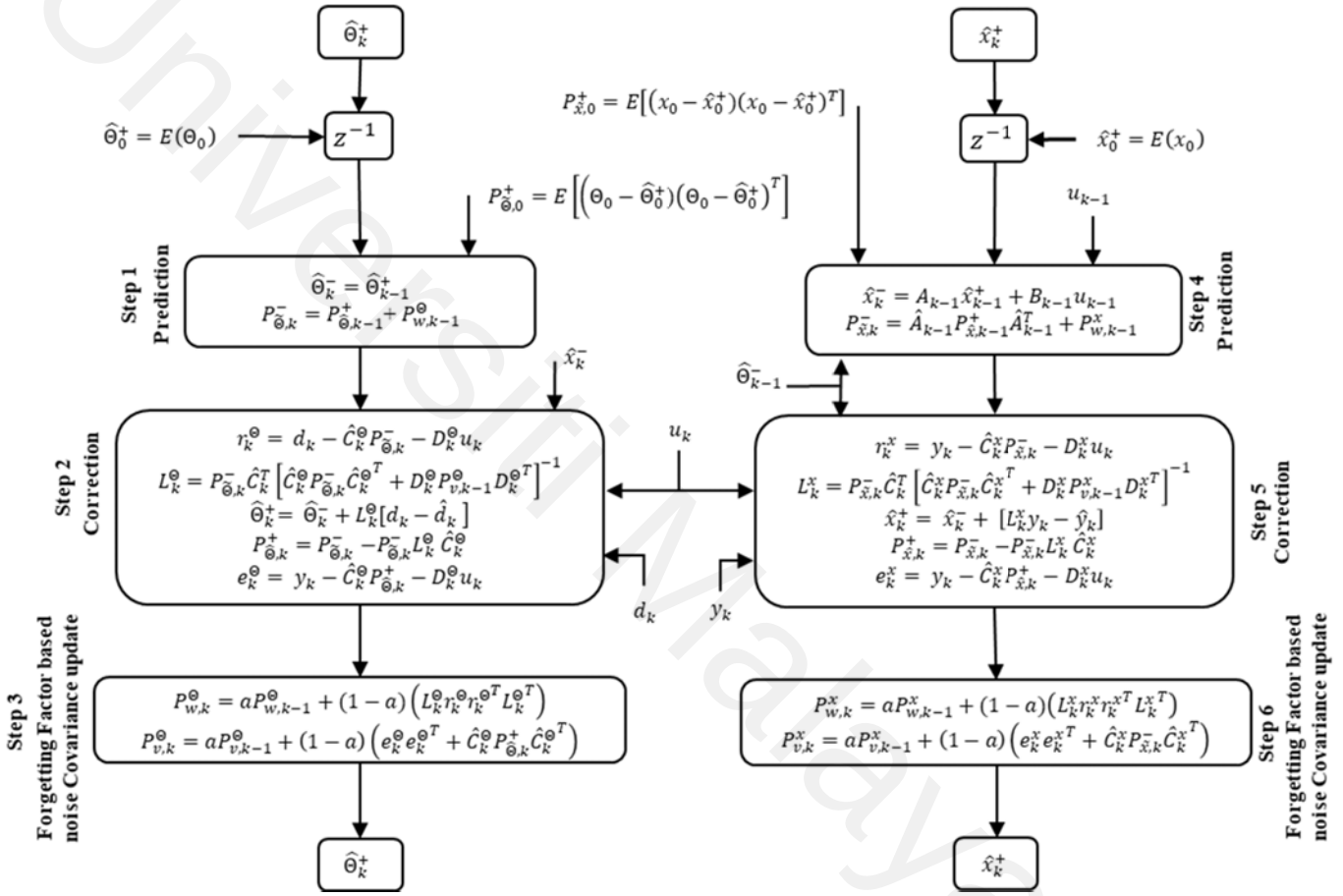

Figure 4.2: Sketch of step by step description of the proposed DFFAEKF

4.3 Proposed co-estimation method for SOC and SOE estimation for EV application

As reported in (W. Zhang et al., 2015b), the battery SOC and SOE are positively correlated with each other, under dynamic operating conditions. To justify the above statement, the different operating conditions (e.g. temperature, C-rate, aging) were considered during the experiments conducted on $LiMn_2O_4$ battery cells in (L. Zheng et al., 2016a). The experiments concluded that the relationship between SOE and SOC remains the same even under a significant change in the operating condition. Furthermore, it almost overlaps with each other in most of the conditions. Instead of using an additional filter or observer for battery SOE estimation, the concept of SOE estimation introduced in (L. Zheng et al., 2016a) in combination with the proposed DFFAEKF based SOC estimation method is utilized to develop a simple and more accurate SOE estimation method. Under this, the quantitative relationship between battery SOC and SOE obtained from the experimental data sets is employed. The battery test involved in the development of the experimental relationship between SOC and SOE is discussed in Section 3.3. The SOC estimation results acquired from the DFFAEKF are utilized for the SOE estimation to improve the estimation results accuracy. The developed MATLB code for co-estimation method for SOC and SOE using DEKF and DFFAEKF is attached in appendix B.

The flow chart of co-estimation for SOC and SOE estimation using the DFFAEKF algorithm is represented in Figure 4.3.

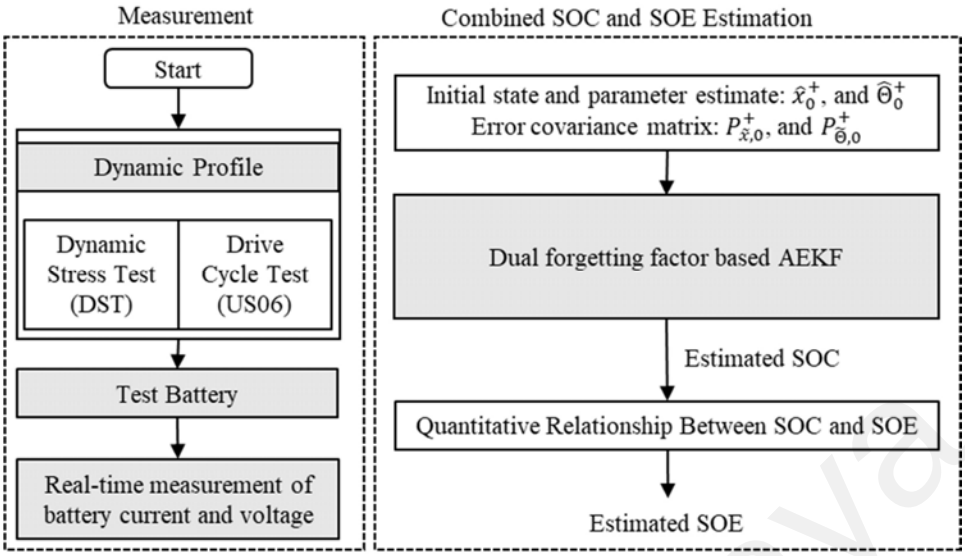

Figure 4.3: Flowchart of co-estimation method for SOC and SOE estimation using DFFAEKF algorithm

4.4 Considered battery Cell tests schedule

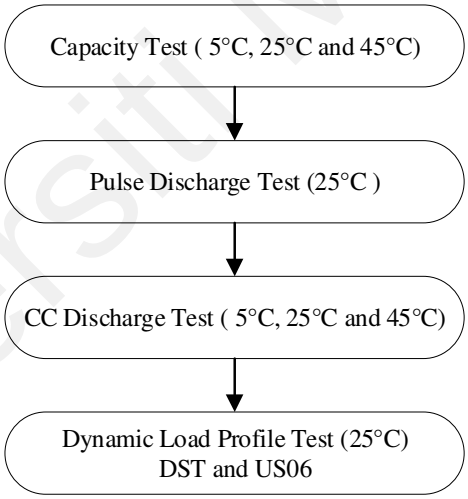

Figure 4.4: Sequence of conducted tests for validation for co-estimation method for SOC and SOE estimation

The sequence of conducted different tests on considered battery cells is presented in Figure 4.4. The test schedule combined four different tests such as capacity test, pulse discharge test, CC discharge test, and dynamic load profile test for the proposed method performance evaluation and validation. The experimental setting required to conduct the tests is discussed in Section 3.2. All the tests are conducted on considered three battery cells of different chemistries as discussed in Section 3.1.1. Different performance indices

such as estimation error, convergence speed, and computational complexity are considered for performance evaluation.

4.5 Summary

In this chapter, the proposed co-estimation method for SOC and SOE estimation using the DFFAEKF algorithm is described. The proposed method is capable to estimate the battery SOC and SOE with high accuracy and, strong robustness to the battery model parameter inaccuracy and measurement noise uncertainties. In which, a proposed DFFAEKF was utilized for SOC estimation and experimental quantitative relation between SOC and SOE for SOE estimation to make it highly accurate and computational less expensive. The implementation of the DFFAEKF algorithm for SOC estimation using the battery 2RC model is also discussed. The sequence of conducted tests for the performance evaluation of the proposed co-estimation method for SOC and SOE estimation is presented.

CHAPTER 5: UNIFIED FRAME OF BATTERY STATES CO-ESTIMATION METHOD FOR SOC, SOE, SOP, ACTUAL CAPACITY, AND MAXIMUM AVAILABLE ENERGY

5.1 Introduction

In chapter 4, the co-estimation for battery SOC and SOE estimation using DFFAEKF for EV application was proposed. However, this method was utilized for battery SOE and SOC estimation only. As the actual capacity and maximum available energy decreases with the battery aging. For an accurate SOC and SOE estimation, the correct value of actual capacity and maximum available energy is also required to update during real-time operation. For the development of efficient BMS for EV, the battery SOP, actual capacity, and maximum available energy are also needed to estimate at low computational burden.

In recent years, the co-estimation method to estimate two or more battery states is gaining popularity due to the existing high correlation between the different states. For instance, in (Xu Zhang, Wang, Wu, et al., 2018), the SOE and SOP estimation using a multi-time-scale filter was introduced where the PSO-UKF was used for SOE estimation. However, the PSO was used for parameter identification of the 1-RC battery model that is not a suitable online application. In (X. Li et al., 2019), the co-estimation method for battery capacity and SOC was introduced. The neural network and AEKF were utilized for capacity and SOC estimation. However, in capacity estimation, a large of amount experimental datasets were involved in the neural network training. In (Yongzhi Zhang et al., 2017), the combined SOC and SOE estimation was performed using the H-infinity algorithm. Two separate filters for SOC and SOE estimation were used that significantly increases the computational burden. In (L. Ma et al., 2021), LSTNM-NN based combined SOC and SOE estimation method was investigated. The performance of the LSTNM-NN is compared with the SVR, random forest (RF), and simple recurrent neural network (Simple RNN). The LSTNM-NN demonstrated high accuracy and robustness at cost of a

high computational load. In (X. Hu et al., 2018), the co-estimation method for SOC and SOH-based fractional-order calculus was proposed. However, the electrochemical impedance spectroscopy (EIS) results were utilized for battery modeling that makes it difficult to implement for real-time application. In (P. Shen, Ouyang, Lu, et al., 2018), the model-based co-estimation method for SOC, SOH, and SOP was proposed. However, the offline identified battery model parameters using the Genetic algorithm used for SOC estimation. As the computational burden of the co-estimation algorithm proportionally increases the cost and size of the controller used in BMS. Thus, there is a need to develop an accurate unified frame of co-estimation method with a low computational burden that acquires the benefits of correlation between the battery states.

In this chapter, an accurate unified frame of battery states co-estimation method is proposed for the estimation of SOC, SOE, SOP, actual capacity, and maximum available energy. The correlation between different battery states is effectively utilized to reduce the computational burden. For the battery states (SOC, SOE, SOP) estimation, robust and less computational burden methods are considered. The co-estimation method for SOC and SOE using DFFAEKF proposed in chapter 4, is utilized for SOC and SOE estimation. The Rint model parameters identified by using the FFRLS algorithm and estimated SOC are utilized for SOP estimation. A sliding widow-approximate weighted total least square (SW-AWTLS) method is proposed for battery actual capacity and maximum available energy estimation. In addition, the experimental setting and battery test involved in the validation of the proposed method under dynamic operating conditions are explained.

The sections of the chapter are arranged in this sequence. In Section 5.1, the introduction of the chapter is provided. In Section 5.2, the mathematical analysis of the proposed unified frame of the battery states co-estimation method is discussed. Algorithms utilized for battery SOP, actual capacity, and maximum available energy

estimation are presented. The experimental setting and test conducted on the considered battery cells are briefly discussed in Section 5.3. Finally, the summary of the chapter is presented in Section 5.4.

5.2 The proposed unified frame of the battery states co-estimation method

As presented in Figure 5.1, the unified frame of battery states co-estimation method for the SOC, SOE, SOP, actual capacity, and maximum available energy estimation is proposed in this study. The main steps involved in the proposed unified frame battery states co-estimation method can be elaborated into four steps as follows: 1) A SOC and SOE estimation is performed by using the DFFAEKF algorithm and quantitative relation between SOC and SOE. 2) The Rint model parameters are identified by using the FFRLS algorithm and estimated SOC utilized for SOP estimation. 3) A new SW-AWTLS algorithm is employed for actual capacity and maximum available energy estimation.

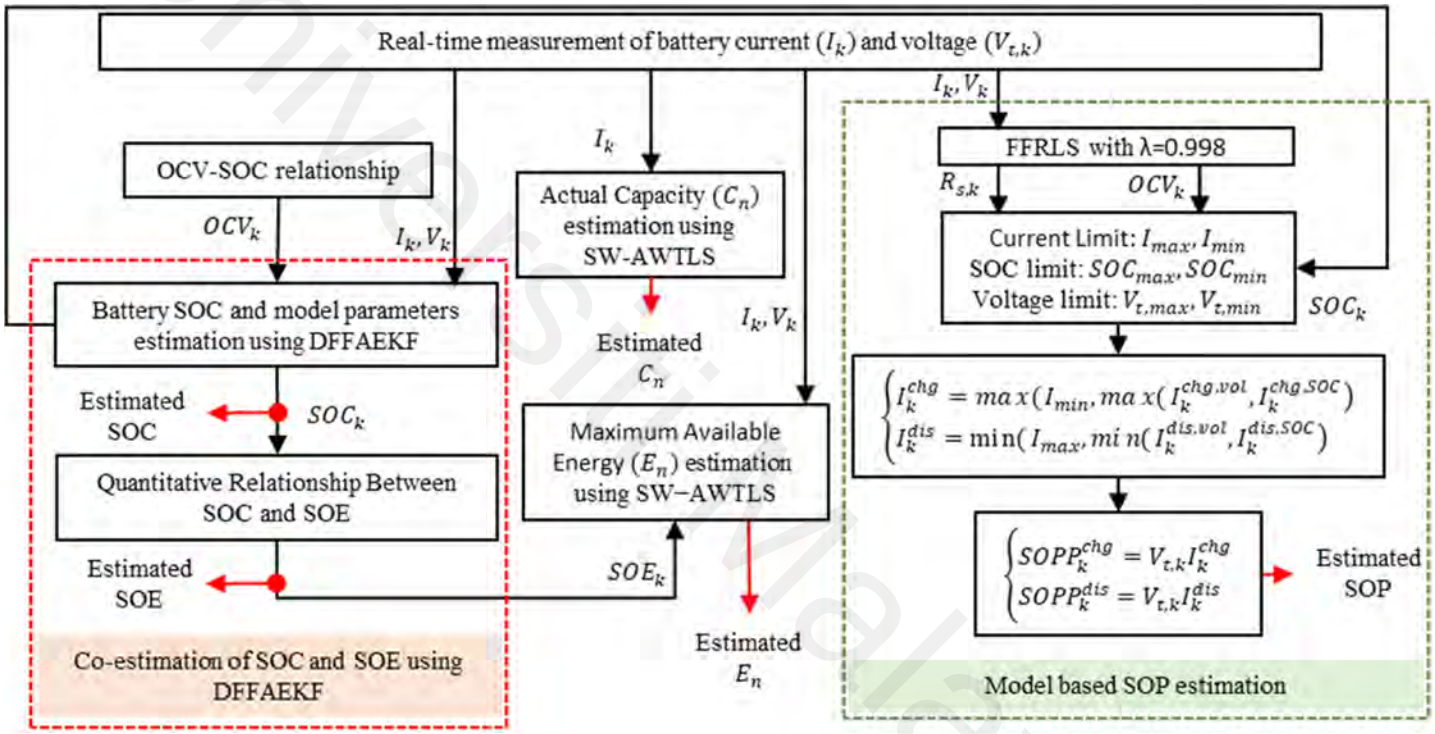

Figure 5.1: Proposed unified frame of battery states co-estimation method for SOC, SOE, SOP, actual capacity, and maximum available energy

5.2.1 SOC and SOE estimation

The proposed co-estimation method for SOC and SOE estimation is utilized for the SOC and SOE estimation. For a detailed explanation, please refer to chapter 4.

5.2.2 Model-based SOP estimation using FFRLS

To protect the battery from over-charging and deep-discharge conditions, it is required to estimate the battery charge/discharge SOP. In this study, the Rint model is utilized to estimate the SOP at a low cost. The Rint model combines a series internal resistance (R_{st}) and the open-circuit voltage source (V_{OCV}) as shown in Figure 5.2. By using Kirchhoff's voltage law, the terminal voltage (U_t) can be described as:

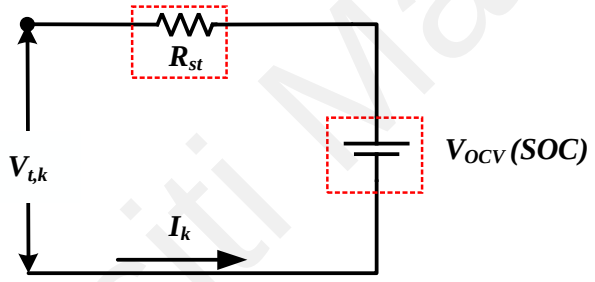

Figure 5.2: Battery Rint Model for SOP estimation

$$V_t = U_{OCV} - IR_{st} \tag{5.1}$$

To identify the Rint model battery parameters, the widely used FFRLS algorithm is considered in this study. The fundamental steps involved in FFRLS can be expressed as below:

$$\begin{cases} \hat{\theta}(k) = \hat{\theta}(k-1) + \mathrm{K}(k)[\mathrm{y}(k) - \hat{\phi}^T(k)\hat{\theta}(k-1)] \\ \mathrm{K}(k) = \big(\mathrm{P}(k-1)\theta(k)\big)/(\lambda + \phi^T(k)\,\mathrm{P}(k-1)\phi(k)) \\ P(k) = [\big(I - \mathrm{K}(k)\phi^T(k)\big)\mathrm{P}(k-1)]/\lambda \end{cases} \tag{5.2}$$

Where,

$$\begin{cases} \mathrm{y}(k) = U_{t,k} \\ \theta(k) = [U_{OCV} \quad R_{st}]^T \\ \phi(k) = [1 \quad -i_k]^T \end{cases} \tag{5.3}$$

With the consideration of battery design limits and identified Rint model parameters, the battery charging/discharging SOP is evaluated. Firstly, the peak current limited by using the battery terminal voltage limits ($V_{t,max}$ and $V_{t,min}$) (Xu Zhang, Wang, Wu, et al., 2018) are calculated by (5.4). The steps involved in Rint model parameter identification using FFRLS are discussed in Table 5.1.

Table 5.1: Rint model parameters identification using FFRLS (X. Chen et al., 2016)

Step 1: Initialization, for $k = 0$, set

$$\phi(0), \theta_r(0), \mathrm{K}(0), \mathrm{P}(0), \lambda$$

Computation : for k = 1,2,3, …

Step 2: Measurement (ϕ) vector and model parameter vector (θ_r)

$$\begin{cases} \theta_r(k) = [U_{OCV} \quad R_{st}]^T \\ \phi(k) = [1 \quad -i_k]^T \end{cases}$$

Step 3: Gain (K)and Error covariance (P) update

$$\begin{cases} \mathrm{K}(k) = \big(\mathrm{P}(k-1)\theta_r(k)\big)/(\lambda + \phi^T(k)\,\mathrm{P}(k-1)\phi(k)) \\ P(k) = [\big(I - \mathrm{K}(k)\phi^T(k)\big)\mathrm{P}(k-1)]/\lambda \end{cases}$$

Step 4: Model parameter update

$$\widehat{\theta_r}(k) = \widehat{\theta_r}(k-1) + \mathrm{K}(k)\big[\mathrm{y}(k) - \hat{\phi}^T(k)\widehat{\theta_r}(k-1)\big]$$

Taking the SOC limits (SOC_{max} and SOC_{min}) into consideration, the peak charge/discharge current is evaluated by using (5.5). Where $3\sigma_{SOC,k}$ confidence interval

is considered on the estimated SOC using DFFAEKF to obtain the more accurate peak power of the battery.

Based on (5.4) and (5.5), the peak charge /discharge current is determined by (5.6). Where the I_{chrg} and I_{dis} are the design limit of peak charge and discharge current of the battery cell, respectively. Finally, the SOP charge (SOP_k^{chg}) and SOP discharge (SOP_k^{dis}) of the battery cell at time instant *k* are calculated by (5.7).

$$\begin{cases} I_k^{chg,vol} = \frac{U_{OCV_{k+1}} - V_{t,max}}{R_{st,k}} \\ I_k^{dis,vol} = \frac{U_{OCV_{k+1}} - V_{t,min}}{R_{st,k}} \end{cases} \tag{5.4}$$

$$\begin{cases} I_k^{chg,SOC} = \frac{(SOC_k + 3\sigma_{SOC,k}) - SOC_{min}}{\eta_c T_s / C_k} \\ I_k^{dis,SOC} = \frac{(SOC_k - 3\sigma_{SOC,k}) - SOC_{max}}{\eta_c T_s / C_k} \end{cases} \tag{5.5}$$

$$\begin{cases} I_k^{chg} = max\,(I_{chrg}, max\,(I_k^{chg,vol}, I_k^{chg,SOC}) \\ I_k^{dis} = min\,(I_{dis}, min\,(I_k^{dis,vol}, I_k^{dis,SOC}) \end{cases} \tag{5.6}$$

$$\begin{cases} SOP_k^{chg} = V_{t,k} I_k^{chg} \\ SOP_k^{dis} = V_{t,k} I_k^{dis} \end{cases} \tag{5.7}$$

5.2.3 Actual capacity and maximum available energy estimation

To estimate the actual capacity of the battery cell, equation (2.9) can be arranged as below:

$$\underbrace{\int_{t_1}^{t_2} \eta_c I(\tau) d\tau}_{r} = Q_n \underbrace{(SOC(t_2) - SOC(t_1))}_{s} \tag{5.8}$$

where the linear relation $r = Qs$ is presented and the cell capacity can be estimated by using integrated current values (*r*) and the difference between the SOC values. Generally, some noise always available in the measurement signal and the estimated SOC. Thus, it

is required to consider the noises during the capacity estimation. In the standard LS method, the noise in the independent variable (r) is not considered (e.g., $r - \Delta r = Qs$). As the estimated SOC values generally imperfect, so that it would be required to consider the noise on x variable also (e.g., $(r - \Delta r) = Q(s - \Delta s)$. It is assumed that Δr and Δs are the zero-mean Gaussian random variables with the known variances $\sigma_{r_i}^2$ and $\sigma_{s_i}^2$, respectively. To address this issue an approximate weighted total least square (AWTLS) method was proposed in (Plett, 2011).

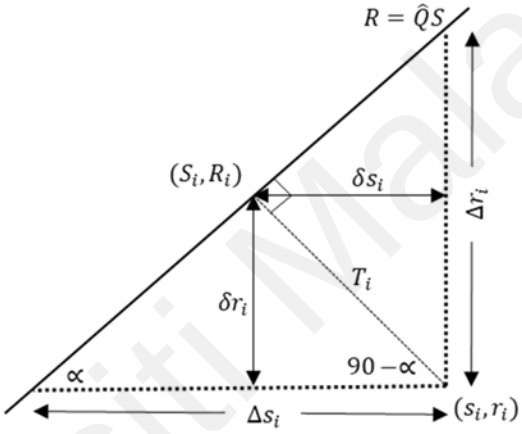

Figure 5.3: Geometrical structure of AWTLS algorithm (Plett, 2011)

The fundamental concept of AWTLS can be explained with the help of Figure 5.3. It shows the relationship between the data points (s_i, r_i) and its optimized map (S_i, R_i) on the line $R_i = \hat{Q}S_i$ with angle $\propto = tan^{-1}\hat{Q}$. The x-distance and y-distance between the data point (s_i, r_i) with the line is Δr and Δs, respectively. The shortest distance between data point (s_i, r_i) and a line is presented by T_i. Further, x- and y- components of the perpendicular distance between the data point (s_i, r_i) and the line is δs_i and δr_i, respectively. By using these variances, the cost function of AWTLS can be written as:

$$\chi_{Q_n}^2 = \sum_{i=1}^{n} \frac{\delta_{s_i}^2}{\sigma_{s_i}^2} - \frac{\delta_{r_i}^2}{\sigma_{r_i}^2} \tag{5.9}$$

As $\Delta r_i = r_i - \hat{Q}_n s_i$, we can write the cost function as:

$$\chi^2_{Q_n} = \sum_{i=1}^{n} \frac{(r_i - \hat{Q}_n s_i)^2}{\left(1-\hat{Q}_n^2\right)^2} \left(\frac{\hat{Q}_n^2}{\sigma_{s_i}^2} + \frac{1}{\sigma_{r_i}^2}\right) \quad (5.10)$$

The Jacobian of the AWTLS cost function,

$$\frac{\partial \chi^2_{Q_n}}{\partial \hat{Q}_n} = \frac{2}{(\hat{Q}_n^2+1)^3}(c_5\hat{Q}_n^4 + (2c_4 - c_1 - c_6)\hat{Q}_n^3 + (3c_2 - 3c_5)\hat{Q}_n^2 + (c_1 - 2c_3 + c_6)\hat{Q}_n - c_2) \quad (5.11)$$

where, $c_{1,n} = c_{1,n-1} + s_n^2/\sigma_{r_n}^2$, $c_{2,n} = c_{2,n-1} + s_n r_n/\sigma_{r_n}^2$, $c_{3,n} = c_{3,n-1} + r_n/\sigma_{r_n}^2$, $c_{4,n} = c_{4,n-1} + s_n^2/\sigma_{s_n}^2$, $c_{5,n} = c_{5,n-1} + s_n r_n/\sigma_{s_n}^2$ and $c_{6,n} = c_{6,n-1} + r_n/\sigma_{s_n}^2$. At the initialization $(n = 0)$, the value $r_0 = Q_{nom}$ and $s_0 = 1$. Therefore, $c_{1,0} = 1/\sigma_{r_0}^2$, $c_{2,n} = Q_{nom}/\sigma_{r_0}^2$, $c_{3,0} = {Q_{nom}}^2/\sigma_{r_0}^2$, $c_{4,0} = 1/\sigma_{s_0}^2$, $c_{5,0} = Q_{nom}/\sigma_{s_0}^2$ and $c_{6,0} = {Q_{nom}}^2/\sigma_{s_0}^2$.

Equation (5.11) is set to zero to obtain the optimal positive candidate solution for $\hat{Q}_n$ that can give the lowest computed value of the cost function, as expressed below:

$$c_5\hat{Q}_n^4 + (2c_4 - c_1 - c_6)\hat{Q}_n^3 + (3c_2 - 3c_5)\hat{Q}_n^2 + (c_1 - 2c_3 + c_6)\hat{Q}_n - c_2 = 0 \quad (5.12)$$

To calculate the error bounds on the estimated capacity the Hessian is computed as expressed below:

$$\frac{\partial \chi^2_{Q_n}}{\partial \hat{Q}_n^2} = \frac{2}{(\hat{Q}_n^2+1)^4}(-2c_5\hat{Q}_n^5 + (3c_1 - 6c_4 + 3c_6)\hat{Q}_n^4 + (-12c_2 + 16c_5)\hat{Q}_n^3 + (-8c_1 + 10c_3 + 6c_4 - 8c_6)\hat{Q}_n^2 + (-12c_2 - 16c_5)\hat{Q}_n - (c_1 - 2c_3 + c_6)) \quad (5.13)$$

Using (5.11) and (5.13), the estimated value of $\hat{Q}_{n,k}$ using AWTLS at k^{th} time instant can be expressed as:

$$\hat{Q}_{n,k} = \hat{Q}_{n,k-1} - \frac{\partial \chi^2_{Q_n}}{\partial \hat{Q}_n} \Big/ \frac{\partial \chi^2_{Q_n}}{\partial \hat{Q}_n^2} \quad (5.14)$$

Besides, to reduce the computation burden, the sliding window (SW) method is associated with the AWTLS algorithm in SW-AWTLS. Under which, SW of specific length is slides over the dataset. The battery actual capacity estimation is performed at every macro time scale L. The steps involved in the SW-AWTLS algorithm are listed in Table 5.2.

Table 5.2: Proposed SW-AWTLS algorithm

For $k = 0$,

M_1, M_2 and $L = M_2 - M_1$

Where, M_1 and M_2 are the starting and end time instant of the sliding window, respectively. L is the length of the window.

For $k = 1$ to end,

If $k > M_2$,

$s = SOC(M_1) - SOC(M_2)$

For $i = (M_1 + 1)$ to M_2,

$r = I(M_1) + I(i)$

end

$Q_{n,k}$ is estimated by using AWTLS

else

$Q_{n,k} = Q_{n,k}$ (No update)

end

Like capacity estimation using AWTLS, the maximum available energy ($\hat{E}_{n,k}$) estimation can be performed by using the AWTLS algorithm. To implement the AWTLS, the (2.10) can be rewritten in form as expressed below:

$$\int_{t_1}^{t_2} V_t(t)I(t)\,dt = E_n(SOE(t_1) - SOE(t_2)) \tag{5.15}$$

The estimated $\hat{E}_{n,k}$ using AWTLS can be expressed as:

$$\hat{E}_{n,k} = E_{n,k-1} - \frac{\partial \chi^2_{E_n}}{\partial \hat{E}_n} \Big/ \frac{\partial \chi^2_{E_n}}{\partial \hat{E}_n^2} \tag{5.16}$$

To reduce the computational burden, the SW-AWTLS is utilized for the estimation of $\hat{E}_{n,k}$. The developed MATLAB code for developed of unified frame of battery states co-estimation is attached in appendix B.

5.3 Experimental setting and tests schedule

The sequence of conducted different tests on considered battery cells is presented in Figure 5.4. The test schedule combined four different tests such as capacity test, pulse discharge test, CC discharge test, and dynamic load profile test for the performance evaluation and validation of the proposed unified frame of battery states co-estimation method. All the tests were conducted repeatedly at 25 °C for all the considered batter cells. The experimental setting required to conduct the tests are discussed in Section 3.2.

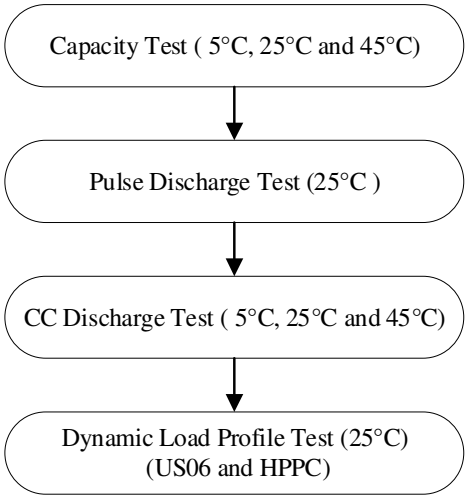

Figure 5.4: Sequence of conducted tests for validation of proposed unified frame of battery states co-estimation method

5.4 Summary

In this chapter, the proposed unified frame of battery states co-estimation method for the estimation of SOC, SOE, SOP, actual capacity, and maximum available estimation is described. The correlation between different battery states is effectively utilized to reduce the computational burden of the developed battery states co-estimation method. For the battery states (SOC, SOE, SOP) estimation, robust and less computational burden methods are discussed. The sequence of conducted tests for the performance evaluation of the proposed unified frame of battery states co-estimation method is presented.

CHAPTER 6: RESULT AND DISCUSSION

6.1 Introduction

In chapter 4, the proposed co-estimation method for battery SOC and SOE estimation using the DFFAEKF algorithm was presented. The proposed unified frame of co-estimation method for battery states (SOC, SOE, SOP), actual capacity, and maximum available energy were discussed in chapter 5. In this chapter, the results obtained from the proposed battery states co-estimation methods in chapter 4 and chapter 5 under dynamic loading conditions are presented. As discussed in chapter 3, the data sets developed for three different chemistry cells tested under different battery test conditions are utilized for the performance evaluation of the proposed methods.

The sections of the chapter are arranged in this sequence. In Section 6.1, the introduction of the chapter is provided. In Section 6.2, the results of the proposed co-estimation method for SOC and SOE estimation using DFFAEKF are presented. This section includes the identified battery 2RC model parameters using DFFAEKF and DEKF. The accuracy and the robustness of the proposed co-estimation method for SOC and SOE estimation under-considered dynamic operating conditions are analyzed. In Section 6.3, the results of the proposed unified frame of battery states co-estimation method for battery states (SOC, SOE, SOP), actual capacity, and maximum available energy are explained. The results analysis of the proposed unified frame of battery states co-estimation method under-considered dynamic operating conditions are also included in this section. Finally, the summary of the chapter is presented in Section 6.4.

6.2 Results of proposed co-estimation method for SOC and SOE estimation using DFFAEKF

6.2.1 Considered Measurement Noise Uncertainty

In the real-time operation of EV, the measured battery terminal voltage and current which utilized for the SOC estimation always contained some noise signals. Due to the presence of the excess measurement noise signal, the estimation accuracy of the algorithm will be affected significantly. In the thesis, to validate the robustness of the proposed DFFAEKF algorithm, the Gaussian white noise signal with zero mean and 0.5 variance is considered as the measurement noise signal, as shown in Figure 6.1. The same measurement noise signal is considered for both battery terminal voltage and current, in the proposed co-estimation method for SOC and SOE.

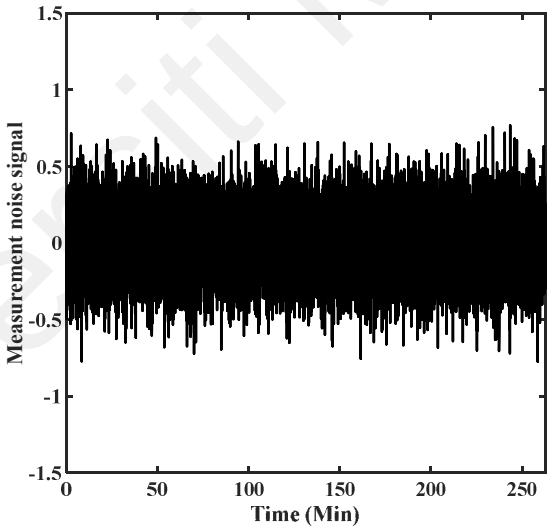

Figure 6.1: Measurement Noise Signal

6.2.2 Battery cell model parameterization results

To evaluate the accuracy of the identified battery model parameters of all the considered battery cells, the estimated terminal voltage results obtained from DFFAEKF and DEKF are compared under the dynamic profile tests (DST profile and US06 profile) at 25°C. The initial value of SOC is set to the correct value (100 %). The initial value of

battery model parameters is evaluated by using the forgetting factor-based recursive least square (FFRLS) method to reduce the convergence time of the estimated model parameters toward true values. The value of the forgetting factor is set to 0.99. The steps involved in the FFRLS method are described in (X. Sun et al., 2019). The developed MATLAB code for FFRLS is attached in appendix B. Under the DST profile, the identified battery model parameters (R_0, R_1, C_1, R_2, and C_2) for Cell 1, Cell 2, and Cell 3 are plotted in Figures 6.2 to 6.4, respectively. For all the considered cells under both DST and US06 profiles, due to the application of the forgetting factor in DFFAEKF, the high variation in the estimated model parameters is presented as compared to DEKF.

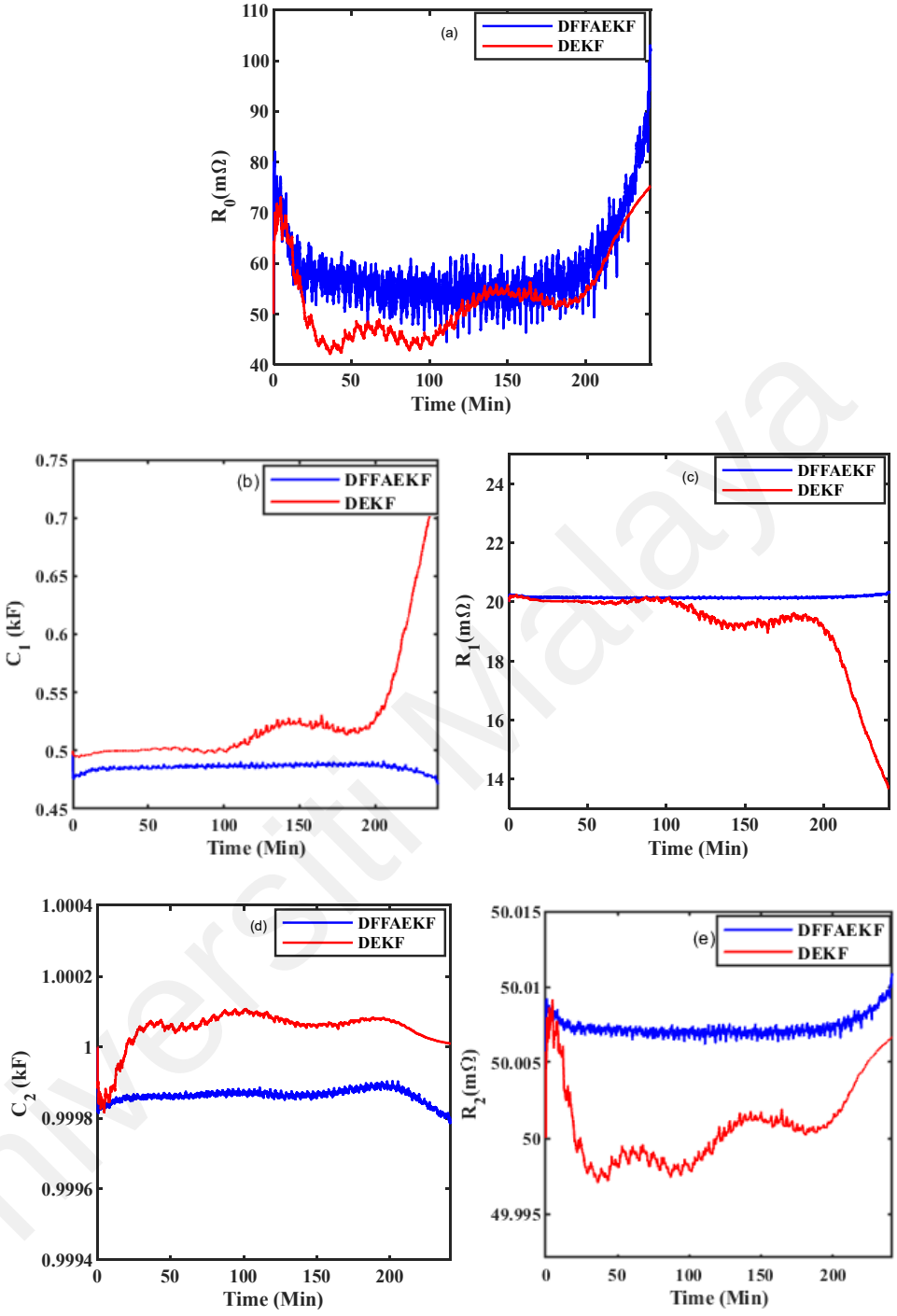

Figure 6.2: Identified battery model parameters using DFFAEKF and DEKF of Cell 1 under DST profile: (a) R_0, (b) C_1, (c) R_1, (d) C_2, (e) R_2

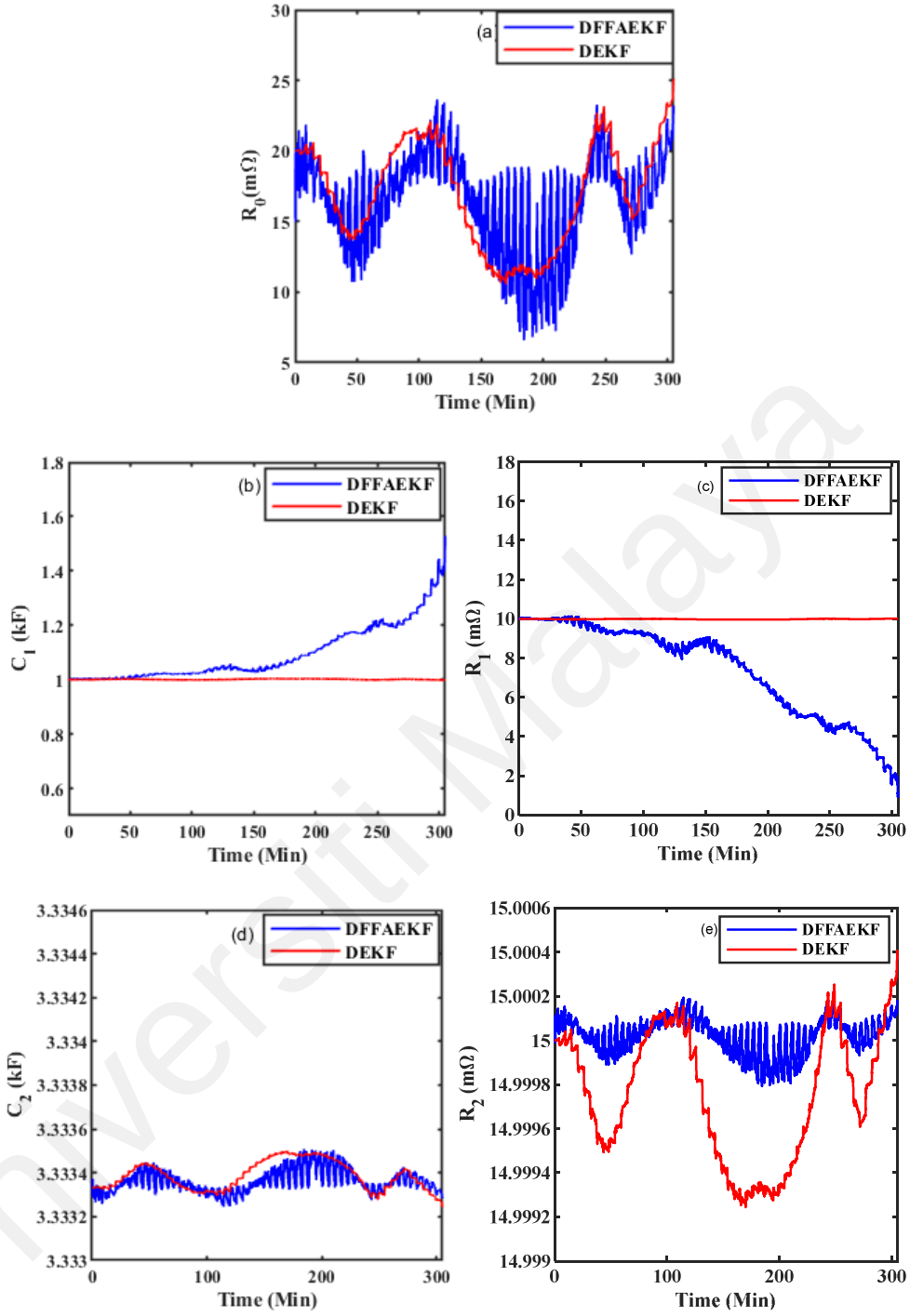

Figure 6.3: Identified battery model parameters using DFFAEKF and DEKF of Cell 2 under DST profile: (a) R_0, (b) C_1, (c) R_1, (d) C_2, (e) R_2

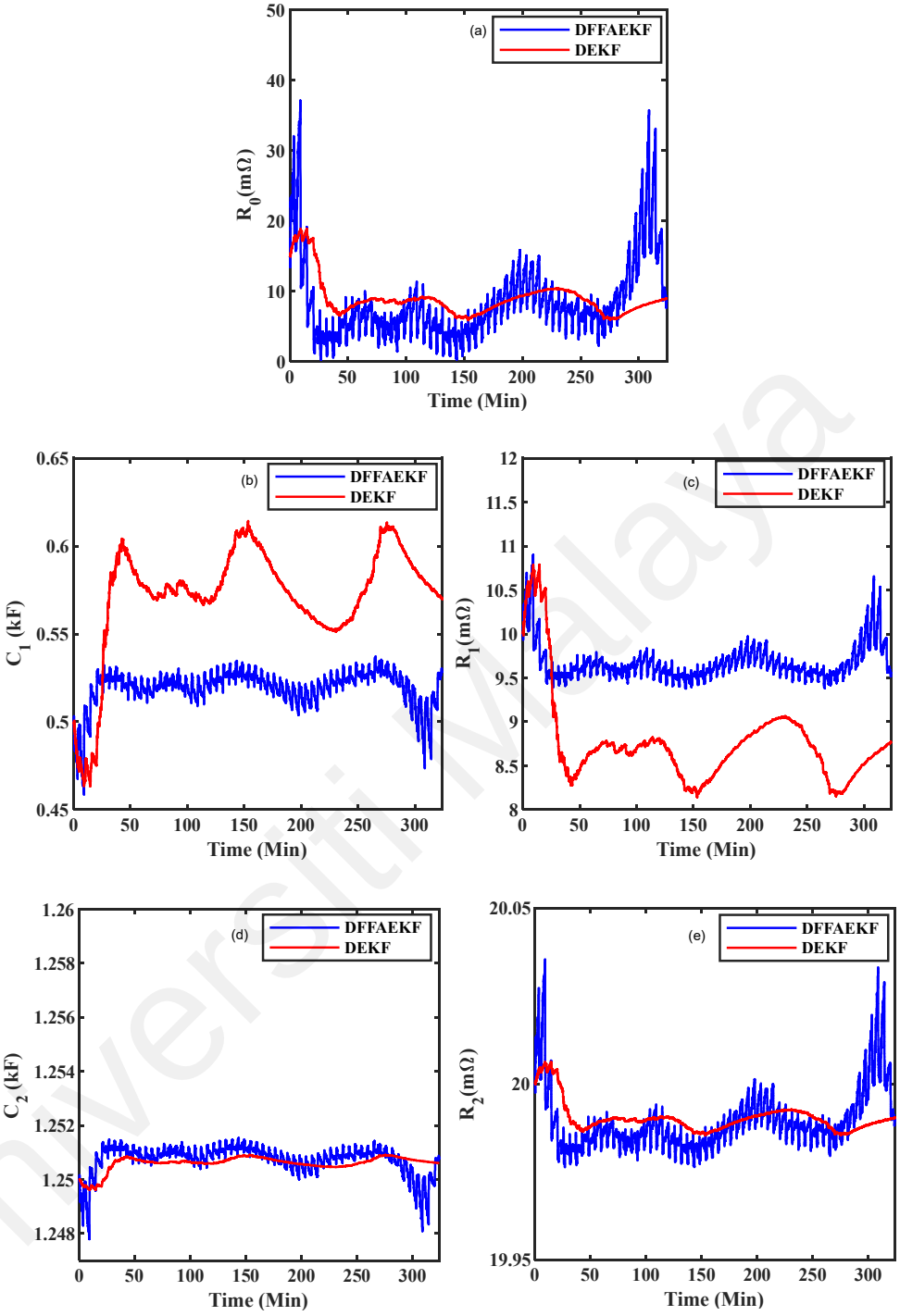

Figure 6.4: Identified battery model parameters using DFFAEKF and DEKF of Cell 3 under DST profile:(a) R_0, (b) C_1, (c) R_1, (d) C_2, (e) R_2

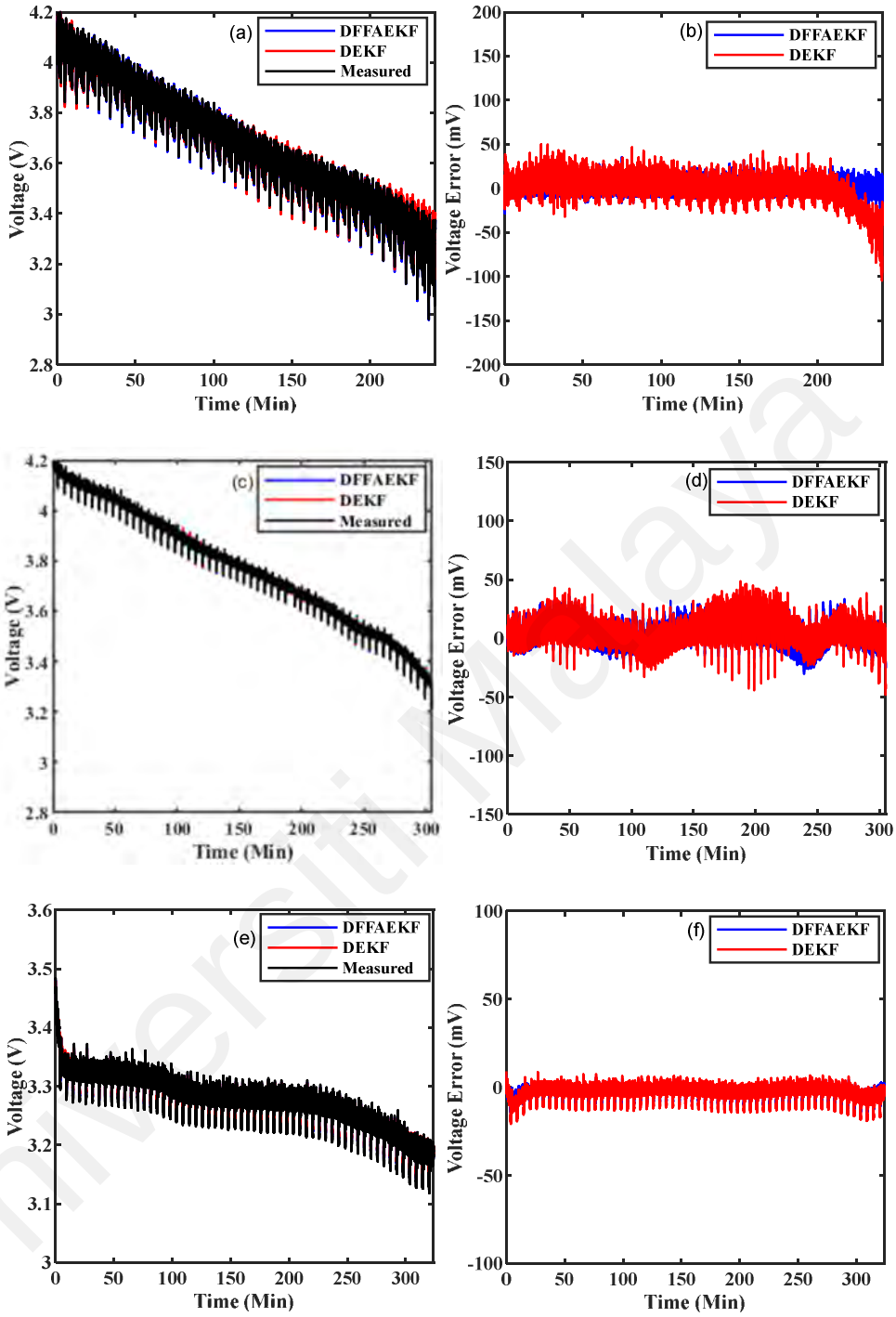

Figure 6.5: Terminal voltage estimation results with correct initial SOC value under DST profile: (a) estimated voltage of Cell 1 (b) voltage error of Cell 1 (c) estimated voltage of Cell 2 (d) voltage error of Cell 2 (e) estimated voltage of Cell 3 (f) voltage error of Cell 3

Terminal voltage estimation results for all the considered battery cells under the DST profile are shown in Figure 6.5. For Cell 1, the measured voltage and estimated voltage from DFFAEKF and DEKF are shown in Figure 6.5 (a), and Figure 6.5 (b) shows their estimation errors. But the estimation error of DEKF is higher than the DFFEKF. The estimation error of DFFAEKF is within ±35 mV. For Cell 2, the measured voltage and estimated voltage from DFFAEKF and DEKF are shown in Figure 6.5 (c), and Figure 6.5 (d) shows their estimation errors. But the estimation error of DEKF is higher than the DFFEKF. The estimation error of DFFAEKF is within ±45 mV. For Cell 3, the measured voltage and estimated voltage from DFFAEKF and DEKF are shown in Figure 6.5 (e), and Figure 6.5 (f) shows their estimation errors. But the estimation error of DEKF is higher than the DFFEKF. The estimation error of DFFAEKF is within ±20 mV. For the DST profile, the RMSE of the recorded terminal voltage of Cell 1, Cell 2, and Cell 3 using DFFAEKF are 6.91 mV, 8.95 mV, and 0.36 mV respectively. Besides, the recorded terminal voltage MaxAE of Cell 1, Cell 2, and Cell 3 using DFFAEKF are 32.66 mV, 43.46 mV, and 15.0 mV respectively as listed in Table 6.1.

Under the US06 profile, the identified battery model parameters (R_0, R_1, C_1, R_2, and C_2) for Cell 1, Cell 2, and Cell 3 are plotted in Figures 6.6 to 6.8, respectively. For all the considered cells under both DST and US06 profiles, due to the application of the forgetting factor in DFFAEKF, the high variation in the estimated model parameters is presented as compared to DEKF.

The model terminal voltage estimation results for all the considered battery cells under the US06 profile are shown in Figure 6.9.

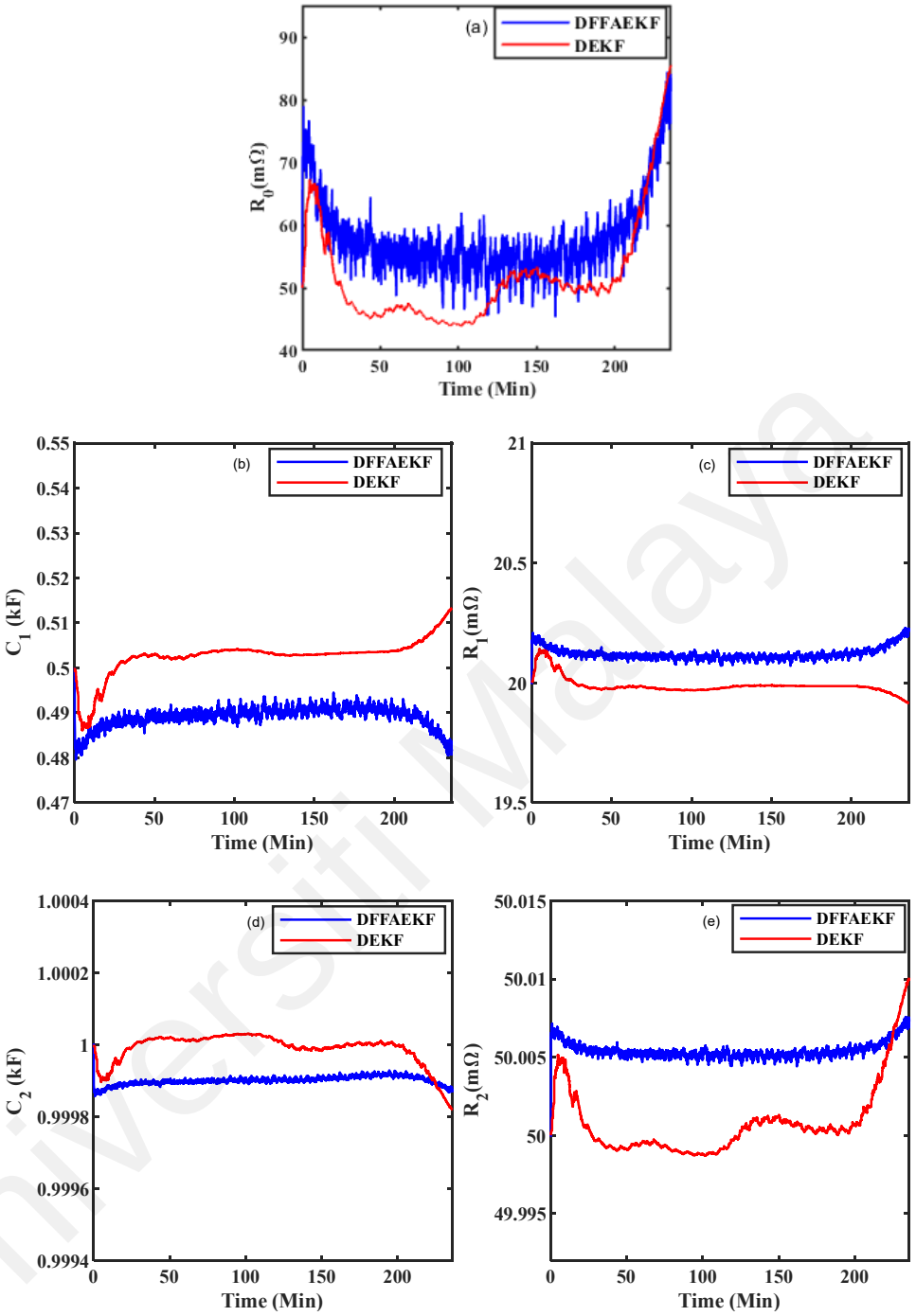

Figure 6.6: Identified battery model parameters using DFFAEKF and DEKF of Cell 1 under US06 profile: (a) R_0, (b) C_1, (c) R_1, (d) C_2, (e) R_2

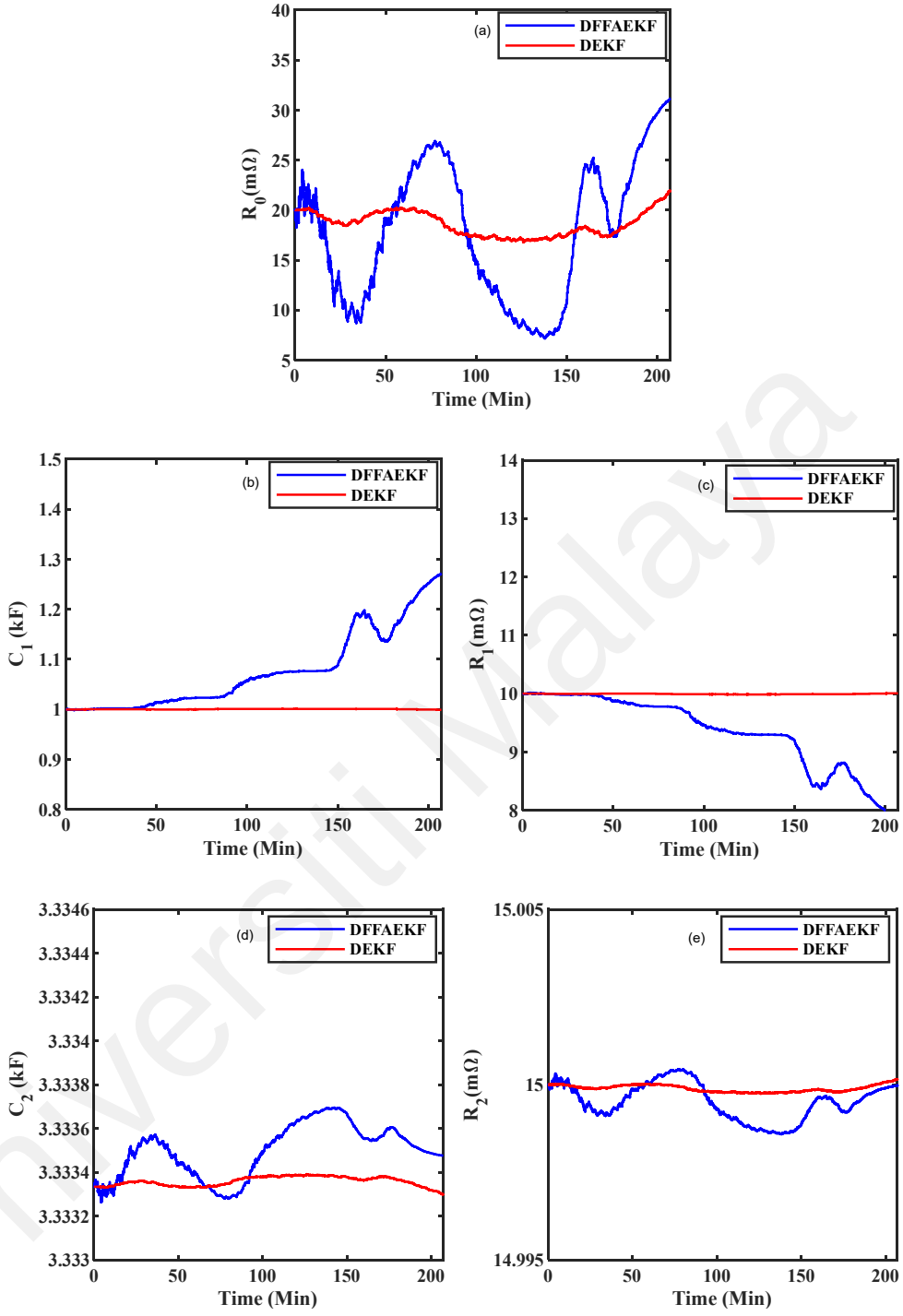

Figure 6.7: Identified battery model parameters using DFFAEKF and DEKF of Cell 2 under US06 profile: (a) R_0, (b) C_1, (c) R_1, (d) C_2, (e) R_2

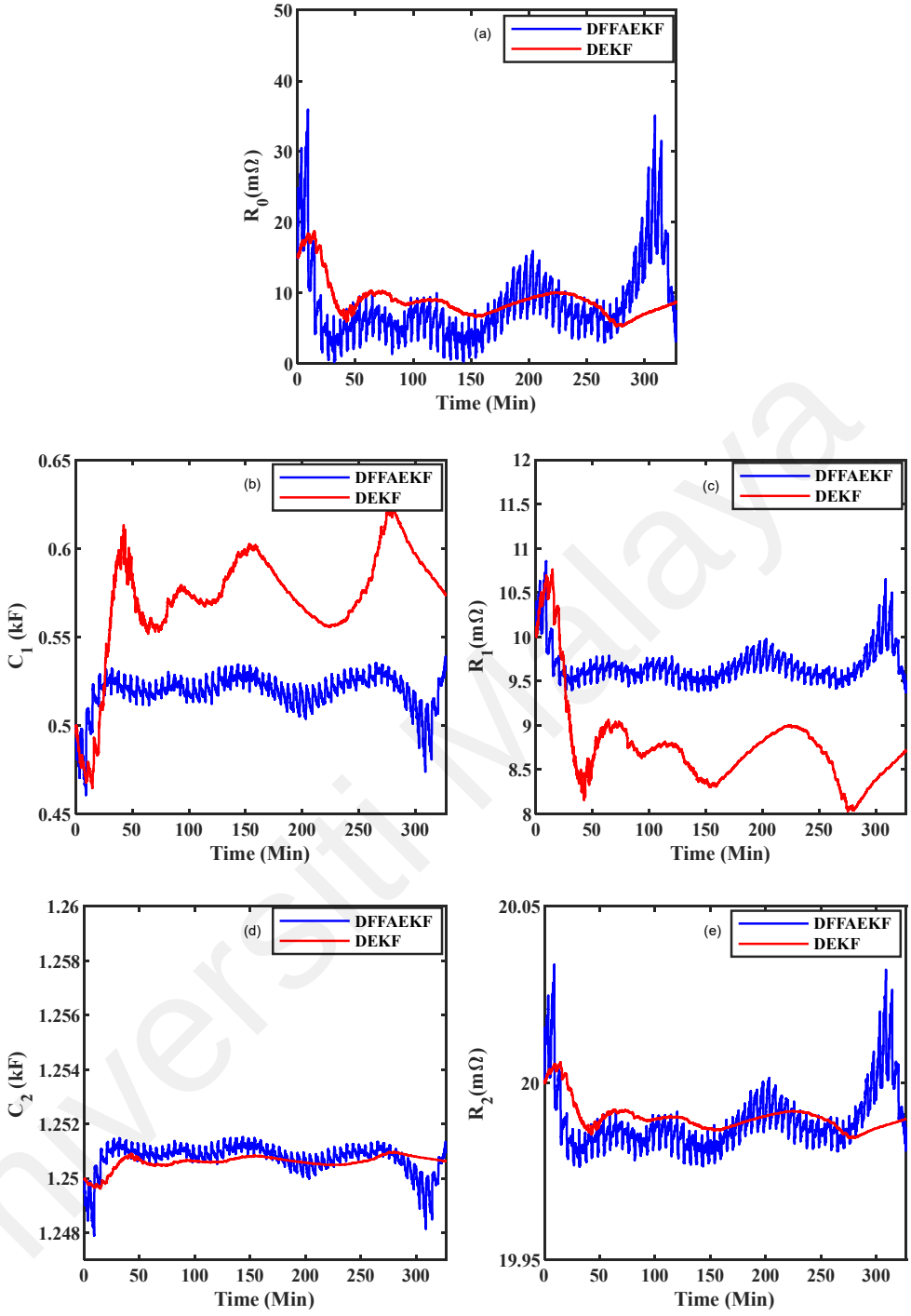

Figure 6.8: Identified battery model parameters using DFFAEKF and DEKF of Cell 3 under US06 profile:(a) R_0, (b) C_1, (c) R_1, (d) C_2, (e) R_2

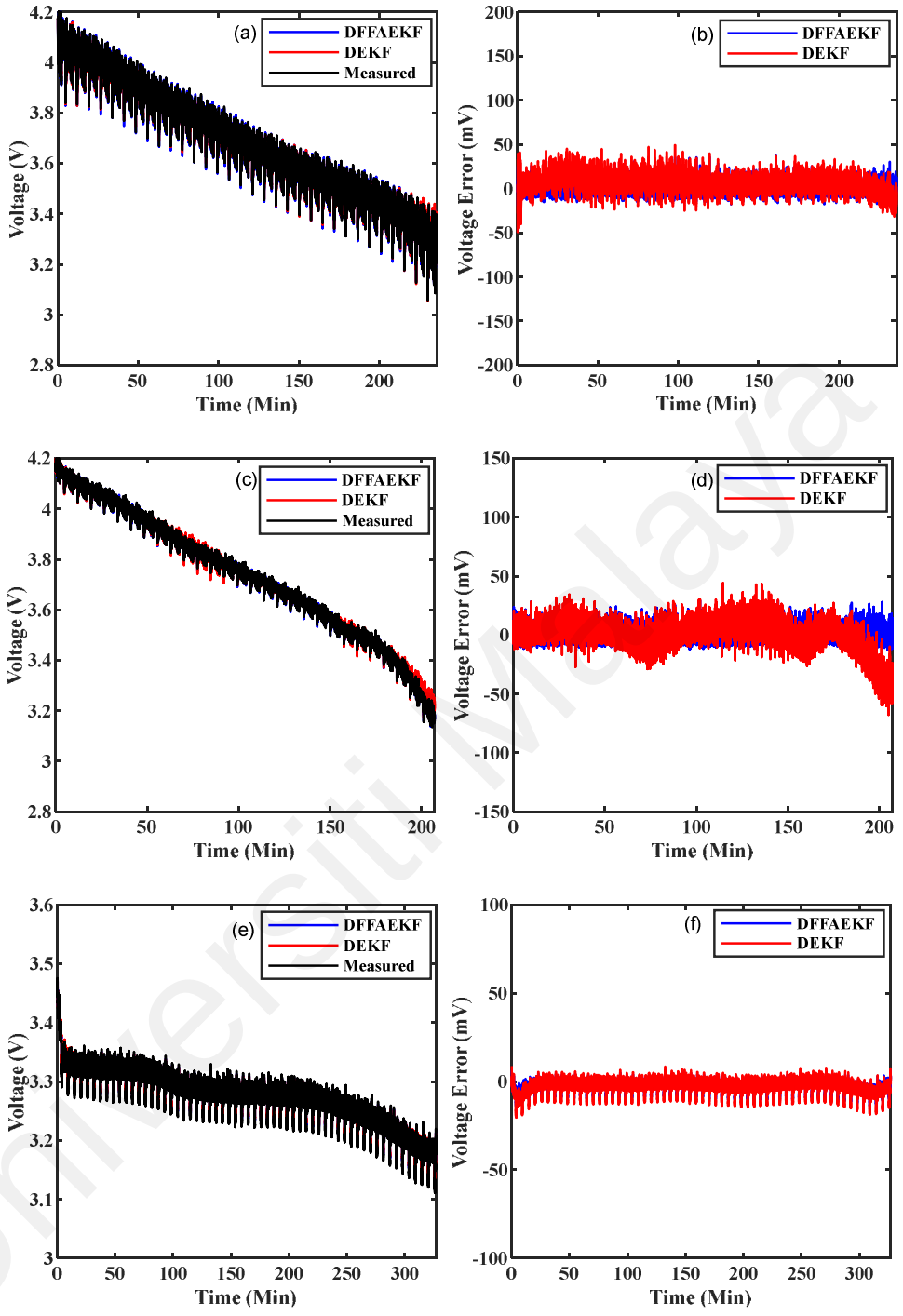

Figure 6.9: Terminal voltage estimation results with correct initial SOC value under US06 profile: (a) estimated voltage of Cell 1 (b) voltage error of Cell 1 (c) estimated voltage of Cell 2 (d) voltage error of Cell 2 (e) estimated voltage of Cell 3 (f) voltage error of Cell

Table 6.1: Results of voltage estimation with correct initial SOC condition

Dynamic Profile	Battery Cells	Voltage RMSE (mV)		Voltage MaxAE (mV)	
		DFFAEKF	DEKF	DFFAEKF	DEKF
DST	Cell 1	6.91	15.07	32.66	104.96
	Cell 2	8.95	10.46	43.46	48.66
	Cell 3	0.36	0.49	15.0	20.8
US06	Cell 1	6.33	13.47	32.90	67.93
	Cell 2	8.34	16.87	41.5	77.90
	Cell 3	0.37	0.50	15.1	20.5

For Cell 1, the measured voltage and estimated voltage from DFFAEKF and DEKF are shown in Figure 6.9 (a), and Figure 6.9 (b) shows their estimation errors. But the estimation error of DEKF is higher than the DFFEKF. The estimation error of DFFAEKF is within ±33 mV. For Cell 2, the measured voltage and estimated voltage from DFFAEKF and DEKF are shown in Figure 6.9 (c), and Figure 6.9 (d) shows their estimation errors. But the estimation error of DEKF is higher than the DFFEKF. The estimation error of DFFAEKF is within ±42 mV. For Cell 3, the measured voltage and estimated voltage from DFFAEKF and DEKF are shown in Figure 6.9 (e), and Figure 6.9 (f) shows their estimation errors. But the estimation error of DEKF is higher than the DFFEKF. The estimation error of DFFAEKF is within ±16 mV. Further, for the US06 profile, the RMSE of the recorded terminal voltage of Cell 1, Cell 2, and Cell 3 using DFFAEKF are 6.33 mV, 8.34 mV, and 0.37 mV respectively. Besides, the recorded terminal voltage MaxAE of Cell 1, Cell 2, and Cell 3 using DFFAEKF is 32.9 mV, 41.5 mV, and 15.1 mV respectively. As listed in Table 6.1, it is evident that during both the dynamic profile tests, the terminal voltage predicted by using DFFAEKF is well-matched

with high accuracy as compared with voltage predicted by using DEKF for all the considered battery cells.

Table 6.2: Results of voltage estimation with incorrect initial SOC (80 %) value

Dynamic Profile	Battery Cells	Voltage RMSE (mV)		Voltage MaxAE (mV)	
		DFFAEKF	DEKF	DFFAEKF	DEKF
DST	Cell 1	10.95	15.81	209.98	218.24
	Cell 2	11.50	13.59	19.044	197.76
	Cell 3	0.49	0.51	49.87	50.55
US06	Cell 1	7.66	11.61	215.73	217.40
	Cell 2	8.90	15.64	201.20	206.90
	Cell 3	0.48	0.51	50.19	51.37

To evaluate the robustness of the proposed DFFAEKF, the initial SOC is set to an incorrect value (80 %). For the DST profile, the RMSE of the recorded terminal voltage of Cell 1, Cell 2, and Cell 3 using DFFAEKF are 10.95 mV, 11.50 mV, and 0.49 mV respectively. Besides, the recorded terminal voltage MaxAE of the Cell 1, Cell 2, and Cell 3 using DFFAEKF are 209.24 mV, 197.76 mV, and 50.55 mV respectively as listed in Table 6.2. Further, for the US06 profile, the RMSE of the recorded terminal voltage of Cell 1, Cell 2, and Cell 3 using DFFAEKF are 7.66 mV, 8.90 mV, and 0.48 mV respectively. Besides, the recorded terminal voltage MaxAE of the Cell 1, Cell 2, and Cell 3 using DFFAEKF are 215.73 mV, 201.20 mV, and 50.19 mV respectively, as listed in Table 6.2. In both cases, voltage errors in the DFFAEKF are significantly lesser than the voltage errors in the DEKF method.

6.2.3 SOC and SOE estimation results

To evaluate the performance of the proposed co-estimation method for SOC and SOE using DFFAEKF, the combined SOC, and SOE estimation by using the DEKF is considered as a benchmark. The estimated SOC and SOE results for all the considered battery cells from DFFAEKF and DEKF under the DST profile at 25°C are compared in Figure 6.10. Similarly, for the US06 profile at 25°C, estimated SOC and SOE results for all the considered battery cells from DFFAEKF and DEKF are compared in Figure 6.11. Further, to evaluate the performance of the proposed co-estimation method for SOC and SOE, two different initial SOC conditions are considered such as (i) correct initial SOC condition and (ii) incorrect SOC condition.

6.2.3.1 With correct initial SOC condition

For the DST profile at 25°C, the estimated SOC and SOE results for all the considered battery cells with the correct initial SOC are depicted in Figure 6.10. Figure 6.10 (a) shows the estimated SOC and measured SOC for Cell 1 from both DFFAEKF and DEKF. It also shows the SOC error for Cell 1 from both DFFAEKF and DEKF. Figure 6.10 (b) shows the estimated SOE and measured SOE for Cell 1 from both DFFAEKF and DEKF. Also shows the SOE error for Cell 1 from both DFFAEKF and DEKF. Figures 6.10 (a) and 6.10 (b) indicate that the estimated SOC and SOE from DEKF is less accurate and diverging as compared to DFFAEKF. The value of recorded RMSE of estimated SOC and SOE for Cell 1 with DFFAEKF is less than 0.35 % as listed in Table 6.3 and Table 6.4. For Cell 2, Figure 6.10 (c) shows the estimated SOC and measured SOC from both DFFAEKF and DEKF. It also shows the SOC error for Cell 2 from both DFFAEKF and DEKF. Figure 6.10 (d) shows the estimated SOE and measured SOE from both DFFAEKF and DEKF. It also shows the SOE error for Cell 2 from both DFFAEKF and DEKF. Figures 6.10 (c) and 6.10 (d) indicate that the estimated SOC and SOE from DEKF is less accurate as compared to DFFAEKF. The value of recorded RMSE of

estimated SOC and SOE for Cell 2 with DFFAEKF is less than 0.50 % as listed in Table 6.3 and Table 6.4. Similarly, for Cell 3, Figure 6.10 (e) shows the estimated SOC and measured SOC from both DFFAEKF and DEKF. It also shows the SOC error for Cell 3 from both DFFAEKF and DEKF. Figure 6.10 (f) shows the estimated SOE from both DFFAEKF and DEKF and measured SOE. Also indicates the SOE error for Cell 3 from both DFFAEKF and DEKF. Figures 6.10 (e) and 6.10 (f) indicate that the estimated SOC and SOE from DEKF is less accurate and diverging as compared to DFFAEKF. The value of recorded RMSE of estimated SOC and SOE for Cell 2 with DFFAEKF is less than 0.57 % as listed in Table 6.3 and Table 6.4. Further, for all the considered battery cells, the values MaxAE of estimated SOC from DFFAEKF is very low (less than 1.1 %) in comparison to DEKF as listed in Table 6.3.

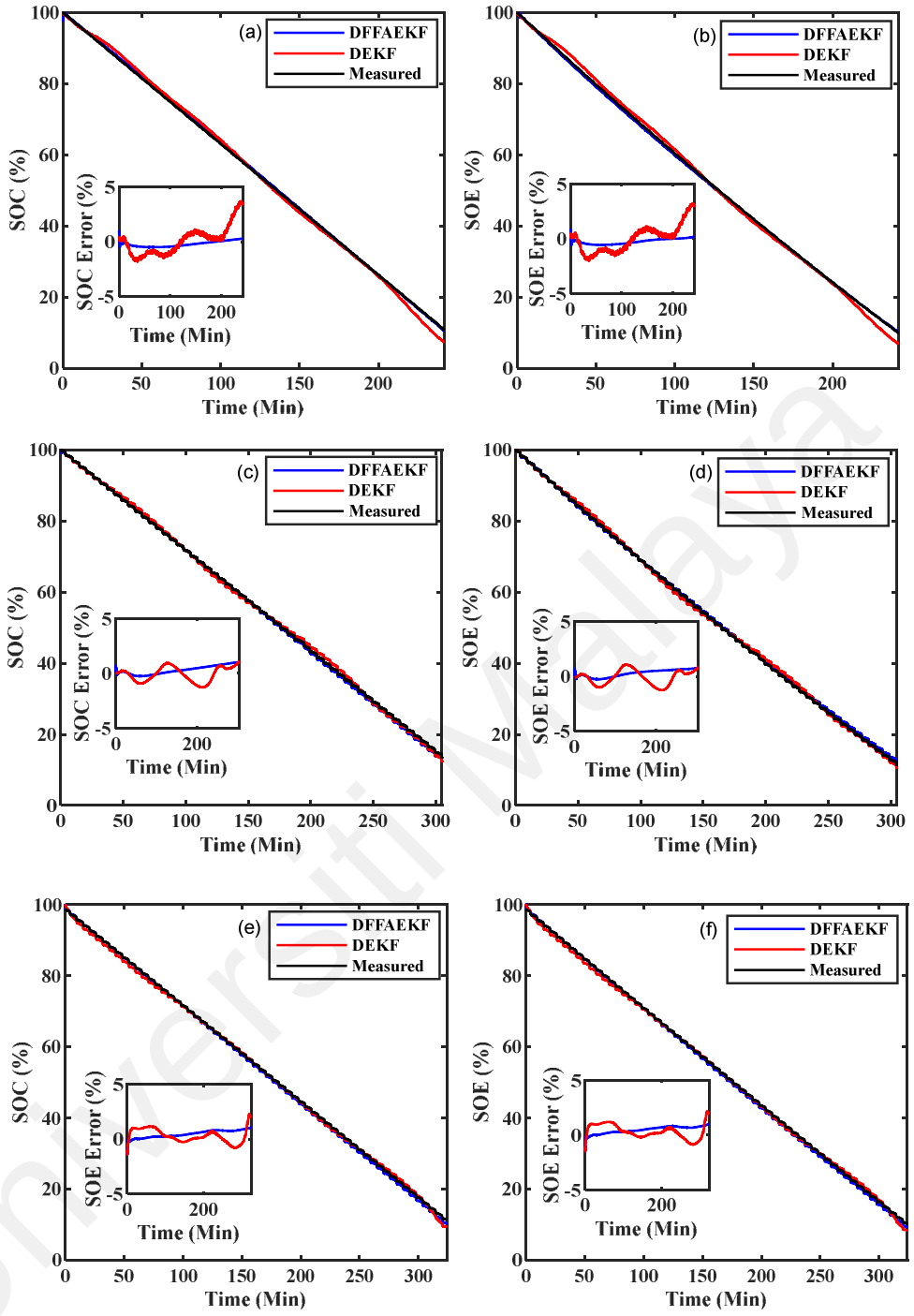

Figure 6.10: SOC and SOE estimation results with correct initial SOC value under DST profile: (a) estimated SOC of Cell 1 (b) estimated SOE of Cell 1 (c) estimated SOC of Cell 2 (d) estimated SOE of Cell 2 (e) estimated SOC Cell 3 (f) estimated SOE of Cell 3

Table 6.3: Results of SOC estimation under DST and US06 profile with correct initial SOC condition

Dynamic Profile	Battery Cells	SOC RMSE (%)		SOC MaxAE (%)	
		DFFAEKF	DEKF	DFFAEKF	DEKF
DST	Cell 1	0.34	1.29	0.26	3.45
	Cell 2	0.49	0.67	1.04	1.26
	Cell 3	0.57	0.71	1.03	2.08
US06	Cell 1	0.28	1.24	0.25	3.07
	Cell 2	0.32	1.26	0.42	2.14
	Cell 3	0.64	0.72	1.02	2.75

Similarly, for the US06 profile at 25°C, the estimated SOC and SOE results for all the considered battery Cells with the correct initial SOC are depicted in Figure 6.11. Figure 6.11 (a) shows the estimated SOC and measured SOC for Cell 1 from both DFFAEKF and DEKF. It also shows the SOC error for Cell 1 from both DFFAEKF and DEKF. Figure 6.11 (b) shows the estimated SOE and measured SOE for Cell 1 from both DFFAEKF and DEKF. Also shows the SOE error for Cell 1 from both DFFAEKF and DEKF. Figures 6.11 (a) and 6.11 (b) indicate that the estimated SOC and SOE from DEKF is less accurate and diverging as compared to DFFAEKF. The value of recorded RMSE of estimated SOC and SOE for Cell 1 with DFFAEKF is less than 0.30 % as listed in Table 6.3 and Table 6.4. For Cell 2, Figure 6.11 (c) shows the estimated SOC from both DFFAEKF and DEKF and measured SOC. It also shows the SOC error for Cell 2 from both DFFAEKF and DEKF. Figure 6.11 (d) shows the estimated SOE and measured SOE from both DFFAEKF and DEKF. It also shows the SOE error for Cell 2 from both DFFAEKF and DEKF. Figures 6.11 (c) and 6.11 (d) indicate that the estimated SOC and SOE from DEKF is less accurate as compared to DFFAEKF. The value of recorded

RMSE of estimated SOC and SOE for Cell 2 with DFFAEKF is less than 0.35 % as listed in Table 6.3 and Table 6.4. Similarly, for Cell 3, Figure 6.11 (e) shows the estimated SOC from both DFFAEKF and DEKF and measured SOC. It also shows the SOC error for Cell 3 from both DFFAEKF and DEKF. Figure 6.11 (f) shows the estimated SOE from both DFFAEKF and DEKF and measured SOE. Also indicates the SOE error for Cell 3 from both DFFAEKF and DEKF. Figures 6.11 (e) and 6.11 (f) indicate that the estimated SOC and SOE from DEKF is less accurate and diverging as compared to DFFAEKF. The value of recorded RMSE of estimated SOC and SOE for Cell 2 with DFFAEKF is less than 0.65 % as listed in Table 6.3 and Table 6.4. Further, for all the considered battery cells, the values MaxAE of estimated SOC from DFFAEKF is very low (less than 1.3 %) in comparison to DEKF as listed in Table 6.3.

Table 6.4: Results of SOE estimation under DST and US06 profile with correct initial SOC condition

Dynamic Profile	Battery Cells	SOE RMSE (%)		SOE MaxAE (%)	
		DFFAEKF	DEKF	DFFAEKF	DEKF
DST	Cell 1	0.34	1.23	0.18	3.01
	Cell 2	0.41	0.68	0.70	1.26
	Cell 3	0.56	0.72	1.09	2.11
US06	Cell 1	0.27	1.29	0.15	3.03
	Cell 2	0.31	1.26	0.29	1.81
	Cell 3	0.62	0.73	0.98	2.58

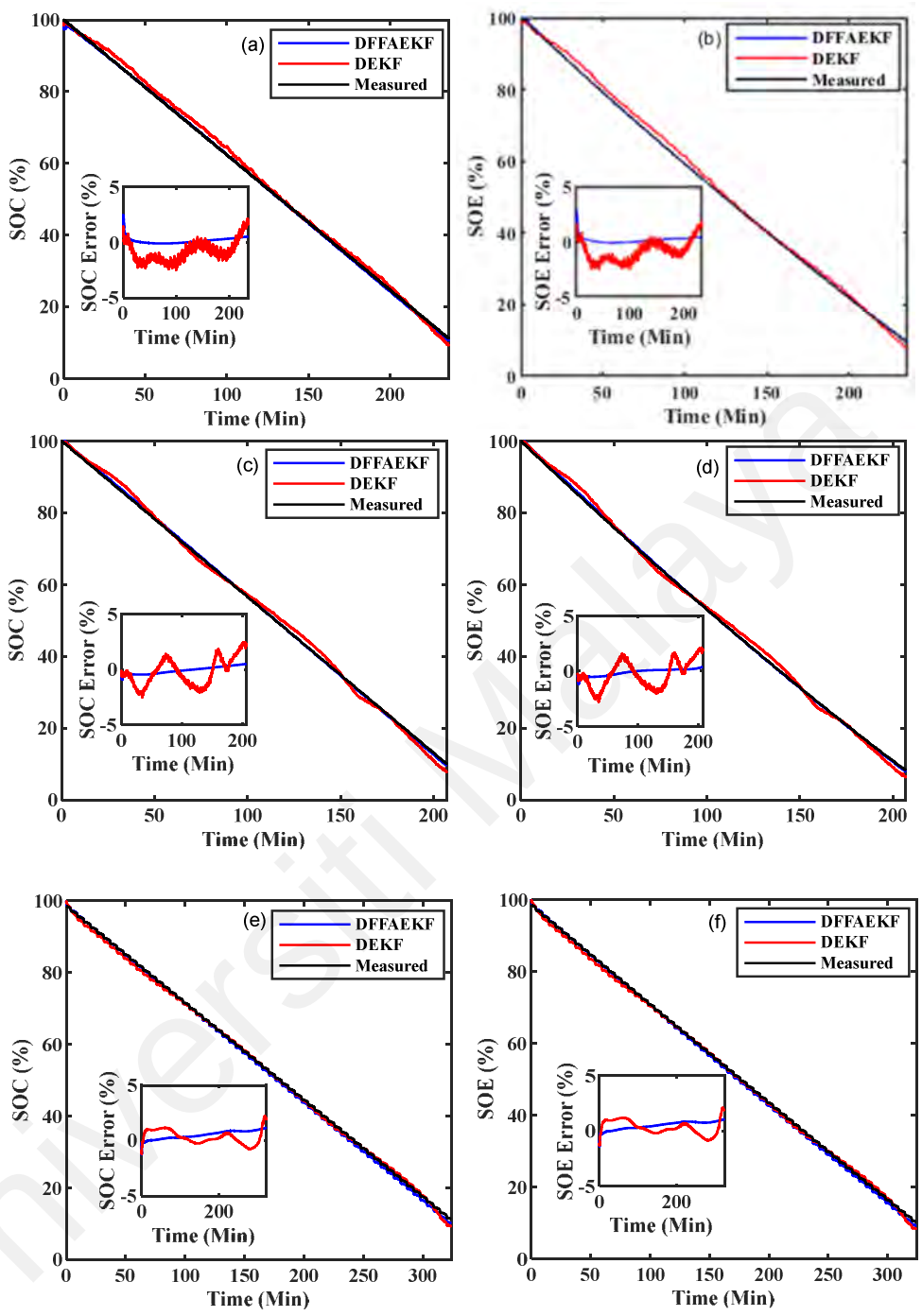

Figure 6.11: SOC and SOE estimation results with correct initial SOC value under US06 profile: (a) estimated SOC of Cell 1 (b) estimated SOE of Cell 1 (c) estimated SOC of Cell 2 (d) estimated SOE of Cell 2 (e) estimated SOC Cell 3 (f) estimated SOE of Cell 3

As indicated in Figures 6.10 and 6.11, under correct initial SOC condition, the estimated SOC and SOE using the proposed co-estimation method for SOC and SOE using DFFAEKF closely follow the measured values irrespective of the change in the battery cell chemistry and dynamic load profiles.

6.2.3.2 With incorrect initial SOC value (80% SOC)

The RMSE of the estimated SOC and SOE based on the proposed method using DFFAEKF with incorrect initial SOC are listed in Table 6.5. The incorrect initial SOC is set to 80 %. With the DST profile at room temperature, the RMSE of the estimated SOC and SOE using the DFFAEKF for all the considered battery cells is less than 0.9 %. With the US06 profile at 25°C, the value RMSE of the estimated SOC and SOE for all the considered battery cells is less than 1.0 %. Besides, for the same erroneous initial SOC condition, the RMSE of estimated SOC and SOE using DEKF for all the considered battery cells is about 1.7 % under the DST profile at 25°C. With the US06 profile at 25°C, the RMSE of the estimated SOC, and SOE is about 1.5 % for all the considered battery cells with the erroneous initial SOC set to 80 %. The results indicate that the proposed co-estimation method for battery SOC and SOE using DFFAEKF is less sensitive to erroneous initial SOC conditions due to the availability of adaptability features as compared to the co-estimation for battery SOC and SOE using DEKF.

Table 6.5: RMSE (%) of estimated SOC and SOE with incorrect initial SOC (80%) value

Dynamic Profile	Battery Cells	SOC RMSE (%)		SOE RMSE (%)	
		DFFAEKF	DEKF	DFFAEKF	DEKF
DST	Cell 1	0.45	1.62	0.48	1.64
	Cell 2	0.63	1.38	0.69	1.39
	Cell 3	0.83	1.16	0.82	1.16
US06	Cell 1	0.56	1.13	0.62	1.40
	Cell 2	0.89	1.37	0.95	1.44
	Cell 3	0.94	1.14	0.93	1.17

6.2.3.3 Convergence speed comparison

Apart from the accuracy, the evaluation of the convergence speed is also an important factor in the performance analysis. In this paper, the considered convergence threshold is less than 5 % for SOC and SOE error. The true initial SOC and SOE value is 100 %. Figure 6.12 and Figure 6.13 shows the comparison of convergence time of SOC and SOE estimation results under different initial SOC conditions for the DST and US06 profile for all the considered battery cells, respectively. The value of convergence time under different incorrect SOC conditions with DST and US06 profiles for all the considered battery cells are listed in Table 6.6.

As shown in Figure 6.12, for all the considered battery cells, the SOC and SOE estimation results from DFFAEKF converged at a faster rate towards true values as compared to estimation results obtained from DEKF under incorrect initial SOC condition. As listed in Table 6.6, with the DST profile for Cell 1, the SOC and SOE estimation convergence time using DFFAEKF is less than 30 % of the convergence time in the estimation of SOC and SOE by using DEKF for the incorrect initial SOC set to 90 %. Similarly, for Cell 2 with the incorrect initial SOC set to 90 %, the SOC and SOE estimation convergence time

using DFFAEKF is less than the convergence time in the estimation of SOC and SOE by using DEKF. With the DST profile, the SOC and SOE estimation convergence time of DFFAEKF is 50% of the convergence time in the estimation of SOC and SOE by using DEKF for Cell 3 with the incorrect initial SOC set to 90 %, as listed in Table 6.6.

Similarly, for the US06 profile at 25°C, for all the considered battery cells, the SOC and SOE estimation results from DFFAEKF converged at a fast rate towards true values as compared to estimation results obtained from DEKF under incorrect initial SOC condition as presented in Figure 6.13. This implies that the application of the DFFAEKF for combined SOC and SOE estimation is more robust to the incorrect initial SOC conditions as compared to the DEKF irrespective of the chemistry of the battery cells. The convergence time increases with the increase in the error but the convergence rate of DFFAEKF remains high as compared to DEKF.

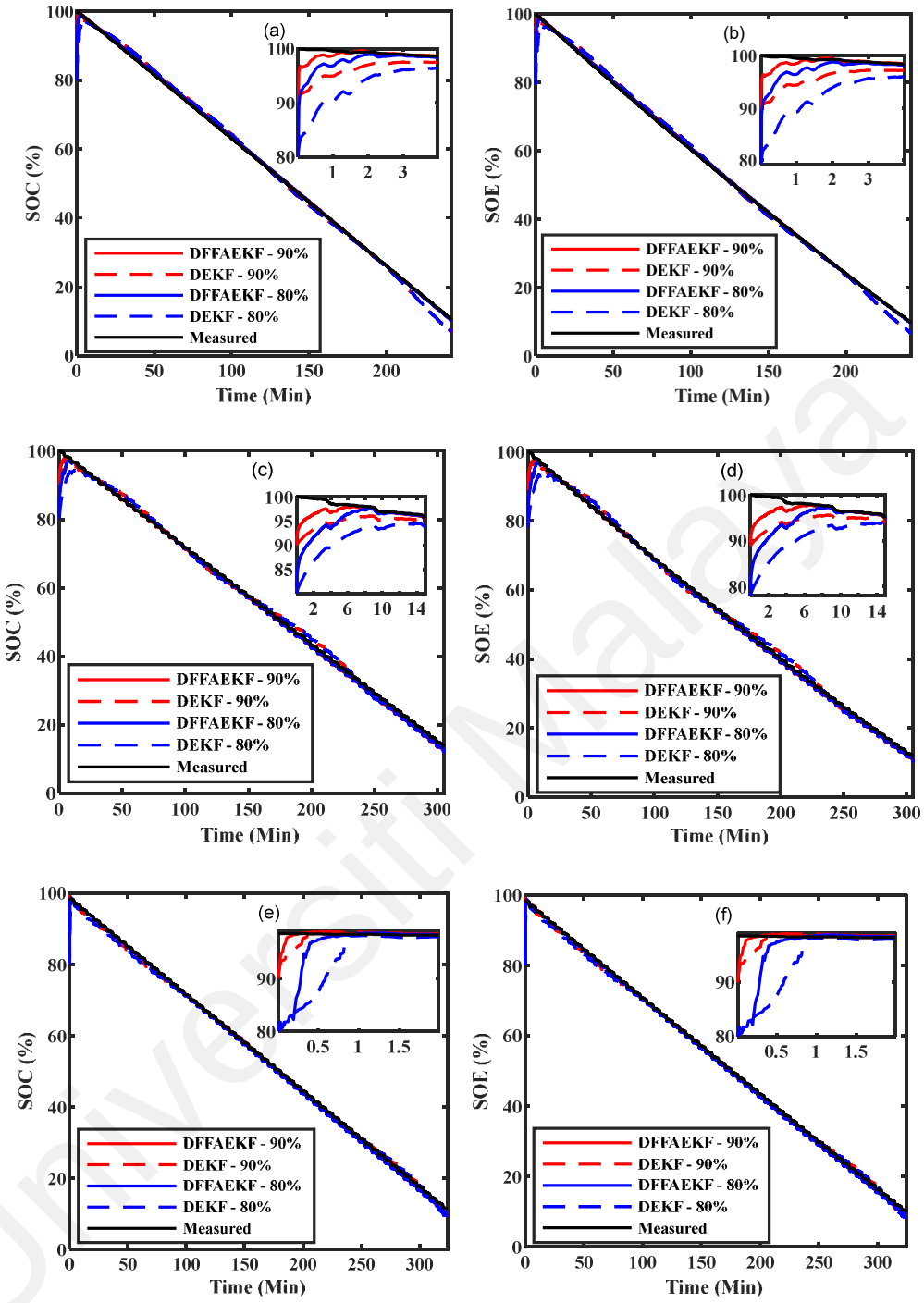

Figure 6.12: SOC and SOE estimation results with incorrect initial SOC values under DST test profile: (a) SOC of Cell 1 (b SOE of Cell 1 (c) SOC of Cell 2 (d) SOE of Cell 2 (e) SOC of Cell 3 (f) SOE of Cell 3

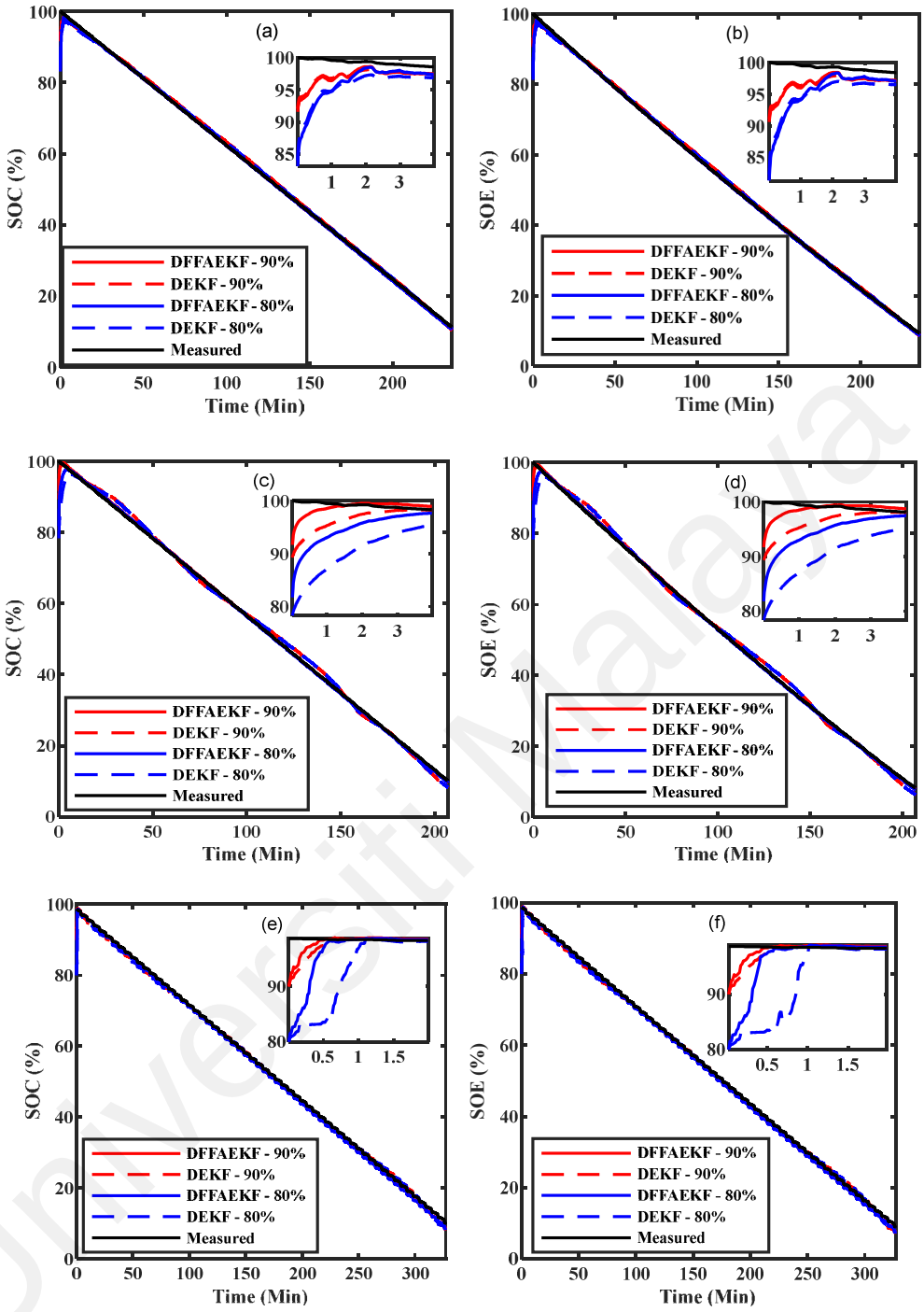

Figure 6.13: SOC and SOE estimation results with incorrect initial SOC values under US06 test profile: (a) SOC of Cell 1 (b SOE of Cell 1 (c) SOC of Cell 2 (d) SOE of Cell 2 (e) SOC of Cell 3 (f) SOE of Cell 3

Table 6.6: Comparison of convergence time of SOC and SOE estimation with incorrect SOC values under DST and US06 test profile

Battery Cells	Initial SOC (%)	Convergence Time (in seconds)							
		DST Profile				US06 Profile			
		DFFAEKF		DEKF		DFFAEKF		DEKF	
		SOC	SOE	SOC	SOE	SOC	SOE	SOC	SOE
Cell 1	90	28.20	25.02	124.02	151.02	45	54	46.01	50.5
	80	68.02	79.02	251	271.98	76.8	91.8	93	94.8
Cell 2	90	109.98	112.02	130.98	144	33	33.1	39.6	39.8
	80	163.8	172.02	216	223.02	67.98	68	70.02	70.05
Cell 3	90	19.88	18.08	31.05	30.1	15.16	16.08	34.05	36.1
	80	29.02	39.60	48.96	49.8	31.02	35.6	42.96	43.8

6.2.3.4 Comparison of computational cost and big O notation complexity

Furthermore, the mean execution time and big O notation complexity are required to evaluate the applicability of the proposed algorithm into the battery management system. Usually, the mean execution time (MET) is utilized to compare the computational cost of SOC estimation algorithms (Lucu et al., 2018). The value of METs are evaluated by using (3.12).

Due to the availability of forgetting factor-based adaptive noise covariance matrices update feature in the proposed DFFAEKF algorithm, the METs of the DFFAEKF algorithm are slightly higher than the DEKF algorithm for both DST and US06 profiles, as described in Table 6.7. For the correct initial SOC condition, the calculated METs for DFFAEKF are 1.60 s (DST profile) and 1.44 s (US06 profile), whereas for METs for DEKF are 1.53 s (DST profile) and 1.39 s (US06 profile).

Table 6.7: Comparison of mean execution time (MET) of DFFAEKF and DEKF

Dynamic Profile	MET (in seconds)	
	DFFAEKF	DEKF
DST	1.60	1.53
US06	1.44	1.39

Table 6.8: Big O complexity of DEKF and DFFAEKF algorithm depending on n, m and P

Steps		DEKF	DFFAEKF	DEKF O (.)	DFFAEKF O (.)
Parameter prediction	1	$\hat{\theta}_k^-$	$\hat{\theta}_k^-$	0	0
	2	$P_{\tilde{\Theta},k}^-$	$P_{\tilde{\Theta},k}^-$	n^2	n^2
Parameter correction	1	r_k^Θ	r_k^Θ	$2m(n+m+p)$	$2m(n+m+p)$
	2	L_k^Θ	L_k^Θ	$4n^2m/4m^2n$	$4n^2m/4m^2n$
	3	$\hat{\theta}_k^+$	$\hat{\theta}_k^+$	$2mn$	$2mn$
	4	$P_{\tilde{\Theta},k}^+$	$P_{\tilde{\Theta},k}^+$	$2n^3/2m^2n$	$2n^3/2m^2n$
	5	e_k^Θ	e_k^Θ	$2m(n+m+p)$	$2m(n+m+p)$
FF based parameter noise covariance update	1	—	$P_{w,k}^\Theta$	—	$2n^2+2n$
	2	—	$P_{v,k}^\Theta$	—	$5n^2+n$

‘ Table 6.8 continued’

Steps		DEKF	DFFAEKF	DEKF O (.)	DFFAEKF O (.)
State prediction	1	$\hat{x}_k^-$	x_k^-	$2n^2$	$2n^2$
	2	$P_{\hat{x},k}^-$	$P_{x,k}^-$	$4n^2$	$4n^2$
State correction	1	r_k^x	r_k^x	$2m(n+m+p)$	$2m(n+m+p)$
	2	L_k^x	L_k^x	$4n^2m/4m^2n$	$4n^2m/4m^2n$
	3	$\hat{x}_k^+$	$\hat{x}_k^+$	$2mn$	$2mn$
	4	$P_{x,k}^+$	$P_{\hat{x},k}^+$	$2n^3/2m^2n$	$2n^3/2m^2n$
	5	e_k^x	e_k^x	$2m(n+m+p)$	$2m(n+m+p)$
FF based state noise covariance update	1	—	$P_{w,k}^x$	—	$2n^2+2n$
	2	—	$P_{v,k}^x$	—	$5n^2+n$

By using the fundamental algorithmic complexity listed in Table 3.4, the big O notation complexity of steps involved in the DEKF algorithm is calculated as presented in Table 6.8. Further, the running time $T(.)$ and worst-case big O notation complexity $O(.)$ of the DFFAEKF and DEKF algorithm are listed in Table 6.9. Due to the employment of additional steps in DFFAEKF, the computed running time $T(.)$ is higher than the DEKF. However, both DFFAEKF and DEKF algorithm have the same worst-case big O complexity of order $8n^3$ as listed in Table 6.9.

Table 6.9: Comparison of the complexity of DEKF and DFFAEKF algorithm

Algorithms	T (.)	O (.)
DFFAEKF	$8n^3 + 8n^2m + 17n^2 + 6m^2 + 6mn + 6mp + 4n$	$8n^3$
DEKF	$8n^3 + 8n^2m + 3n^2 + 6m^2 + 6mn + 6mp$	$8n^3$

With the result of slightly higher computational cost and same order big O complexity of DFFAEKF as compared to DEKF, the high accuracy combined SOC and SOE estimation using DFFAEKF is achieved.

6.2.4 Comparative validation analysis with other methods

The superiority of the proposed combined SOC and SOE estimation using the DFFAEKF method is validated by comparing the error terms of other prominent SOC and SOE estimation methods. Few recent studies of the SOC and/or SOE estimation including dual filter, hybrid LIB model-based analytical method, unscented Particle filter (UPF), forgetting factor-based AEKF, central difference KF (CDKF), unscented KF (UKF), combined SOC and SOE estimation using quantitative relationship, dual H-infinity Filter (DHIF), and dual KF (DKF) are investigated for the comparative analysis, as presented in Table 6.10. For the NCR and NMC chemistry battery cell the value of SOE RMSE is less than 0.42 % under both DST and US06 profiles as listed in Table 6.4.

It is validated that the performance of the proposed combined SOC and SOE estimation method is better than the others under dynamic operating conditions as well as for different chemistry battery cells. The value of SOE RMSE and SOC RMSE of the proposed method with correct initial SOC conditions under both DST and US06 profiles are less than 0.65 %. Whereas, with incorrect initial SOC conditions the value of SOE RMSE and SOC RMSE of the proposed method under both DST and US06 profiles is less than 0.83 % and 0.94 %, respectively.

Table 6.10: Comparative performance assessment of SOC and SOE estimation methods

Method	Ref.	Cell Chemistry	Validation Profile	Temperature	Error (%)
Dual Filter (EKF and PF)	(Dong, Chen, et al., 2016)	LFP	Dynamic current	0°C, 10°C, 25°C, 45°C and 55°C	SOE Error < ±4.0
Hybrid model-based analytical method	(K. Li et al., 2018)	LTO	CCD	5°C, 15°C, 25°C, 35°C, and 45°C	SOC Error < 1.0, SOE Error < 4.7
Unscented Particle Filter (UPF)	(Chang et al., 2020)	LFP	FUDS	5°C, 25°C and 45°C	SOE MaxAE < 1.8
Forgetting factor-based AEKF	(X. Li et al., 2019)	LFP	HPPC, UDDS	10°C, 25°C and 40°C	SOC Error < 3.0
Adaptive fractional-order EKF (AFEKF)	(X. Li et al., 2017)	LFP	FUDS	Room Temperature	SOE Error < ±5.0
Central Difference Kalman Filter (CDKF)	(HongWen He et al., 2015)	LFP and LMO	DST	Room Temperature	SOE Max Error < 1.0
Combined SOC and SOE estimation using quantitative relationship	(L. Zheng et al., 2016a)	LMO	DST	10°C, 25°C and 40°C	SOC Error < 2.0, SOE MaxAE < 3.4
Dual H-infinity Filter (DHIF)	(C. Chen et al., 2018)	LMO, NMC	DST	10°C, 25°C and 45°C	SOC Error < 1.0

‘ Table 6.10 continued’

Method	Ref.	Cell Chemistry	Validation Profile	Temperature	Error (%)
Combined SOC and SOE estimation using DEKF (Benchmark method)	—	NCR, NMC, LFP	DST, US06	5°C, 25°C and 45°C	SOC RMSE < 1.1, SOE RMSE < 1.1
Combined SOC and SOE estimation using DFFAEKF (Proposed Method)	—	NCR, NMC, LFP	DST, US06	5°C, 25°C and 45°C	SOC RMSE < 0.83, SOE RMSE < 0.94

6.3 Results of proposed unified frame of battery states co-estimation method for SOC, SOE, SOP, actual capacity, and maximum available energy

6.3.1 Combined SOC and SOE estimation results

For the performance evaluation of combined SOC and SOE estimation using the DFFAEKF algorithm, two different dynamic load profiles such as US06 and HPPC load profile are considered.

6.3.1.1 Battery model parameters identification results

The 2RC battery model parameters are identified using the DFFAEKF algorithm. The accuracy of the identified model parameters can be verified with the analysis of model terminal voltage errors. The model voltage error values obtained by comparing the model terminal voltage with the measured voltage. For all the considered battery cells, the value of MaxAE, MAE, and RMSE are computed for both the dynamic load profiles.

Table 6.11: Model terminal voltage errors under US06 load profile

Battery Cells	Voltage Error		
	Max AE (mV)	MAE (mV)	RMSE (mV)
Cell 1	132.89	0.21	14.61
Cell 2	55.88	0.11	10.50
Cell 3	61.98	0.20	14.13

Table 6.12: Model terminal voltage errors under HPPC load profile

Battery Cells	Voltage Error		
	Max AE (mV)	MAE (mV)	RMSE (mV)
Cell 1	130.89	0.87	50.74
Cell 2	108.03	0.11	33.65
Cell 3	111.92	0.45	21.41

As listed in Table 6.11, for the US06 drive cycle, the value of model voltage MaxAE for all the considered battery cells is within 133 mV. Whereas the value of voltage MAE and RMSE is less than 0.21 mV and 14.61mV, respectively. For all the considered battery cells under the HPPC test, the value of voltage MAE and RMSE is less than 0.87 mV and 5074 mV, as listed in Table 6.12. The value of model voltage MaxAE for all the considered battery cells is within 130.1 mV. For both the dynamic load profiles, the evaluated voltage RMSE value is lower for cell 3 and highest for cell 1.

6.3.1.2 SOC and SOE estimation results

For all the considered battery cells, the SOC and SOE estimation results under US06 and HPPC profile using combined SOC and SOE estimation algorithm are shown in Figure 14 and Figure 12. In the figures, estimated SOC and SOE with correct initial SOC under US06 and HPPC profile are presented. Under US06 and HPPC profiles, the computed MAE and RMSE of estimated SOC and SOE are listed in Table 6.13 and Table 6.14.

For the US06 profile, the estimated and measured SOC and SOE for cell 1 are shown in Figures 14 (a) and 14 (b), respectively. The value of estimated SOC MAE and RMSE are 0.29 % and 0.37 %, respectively. As listed in Table 6.13, the value of estimated SOE MAE and RMSE are 0.30 % and 0.35 %, respectively. For cell 2, the estimated and

measured SOC and SOE profiles are shown in Figures 14(c) and 14(d). The value of estimated SOC MAE and RMSE are 0.17 % and 0.422 %, respectively. The value of estimated SOE MAE and RMSE are 0.17 % and 0.23 %, respectively. Similarly, for cell 3, the estimated and measured SOC and SOE profiles are shown in Figures 14(e) and 14(f). The value of estimated SOC MAE and RMSE are 0.27 % and 0.31 %. The value of estimated SOE MAE and RMSE are 0.23 % and 0.30 %.

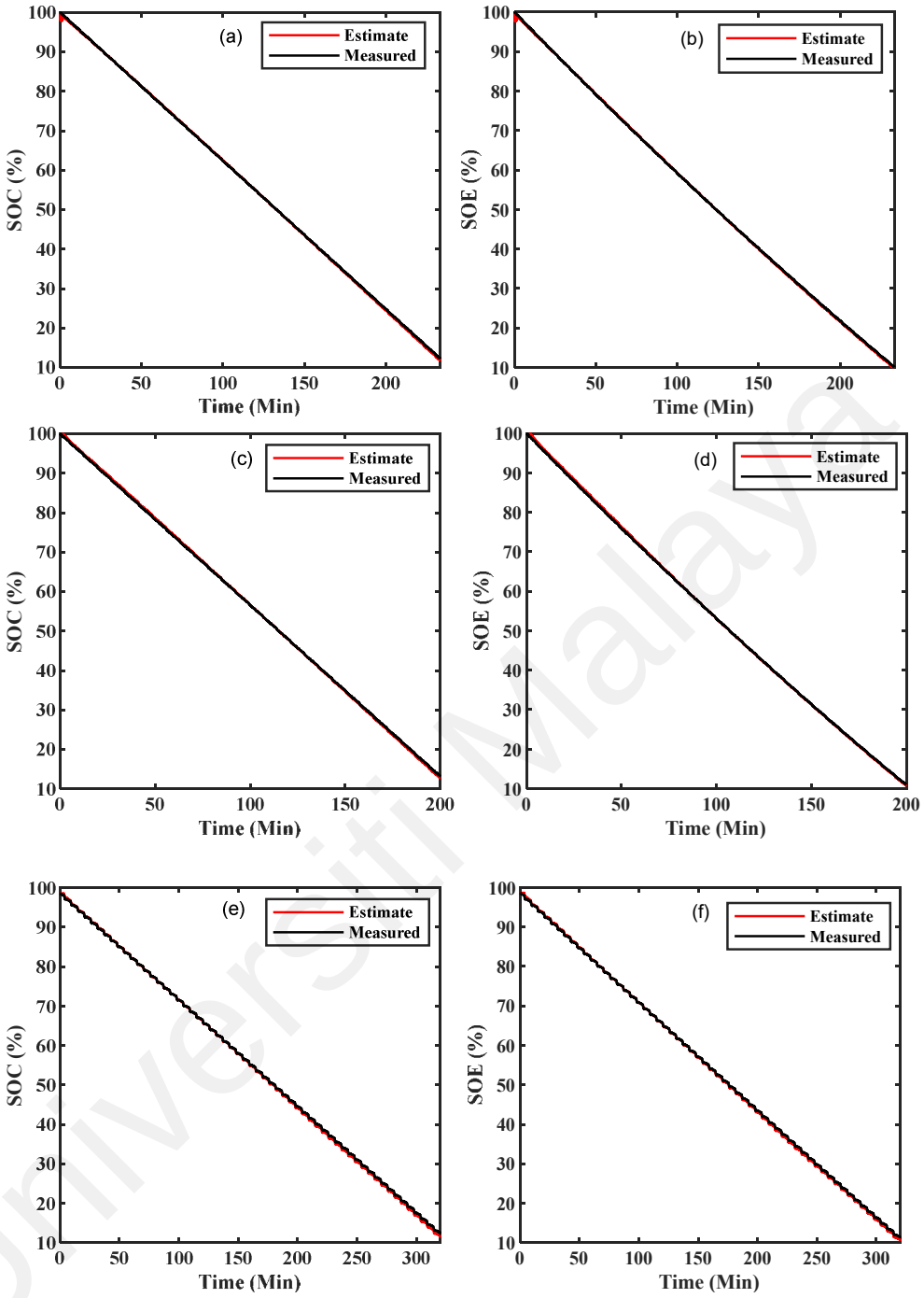

Figure 6.14: Estimated SOC and SOE results under US06 profile: (a) SOC of Cell 1 (b) SOE of Cell 1, (c) SOC of Cell 2 (d) SOE of Cell 2, (e) SOC of Cell 3 (f) SOE of Cell 3

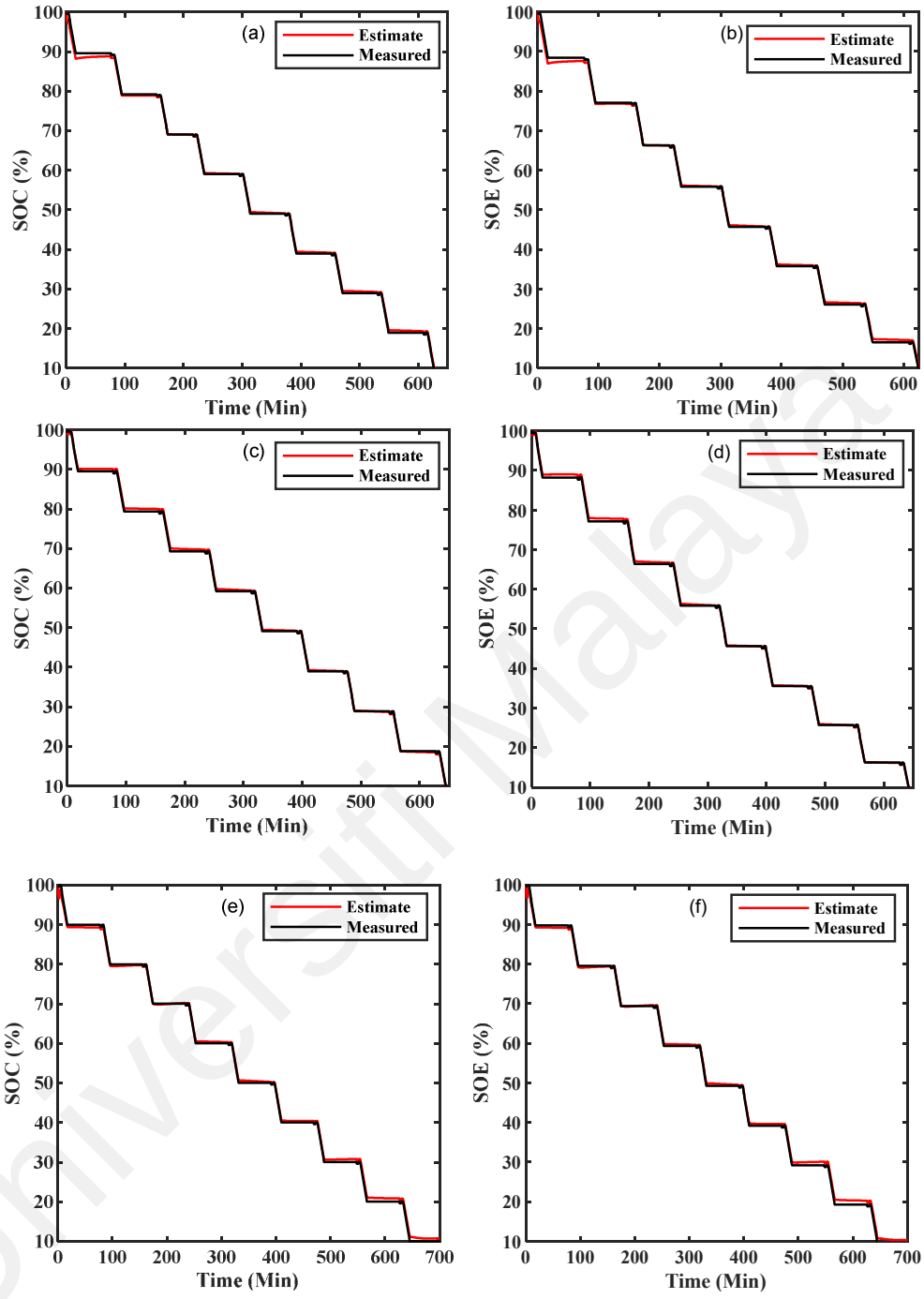

Figure 6.15: Estimated SOC and SOE results under HPPC profile: (a) SOC of Cell 1 (b) SOE of Cell 1, (c) SOC of Cell 2 (d) SOE of Cell 2, (e) SOC of Cell 3 (f) SOE of Cell 3

Table 6.13: SOC and SOE estimation errors under US06 drive cycle profile

Battery Cells	SOC		SOE	
	MAE (%)	RMSE (%)	MAE (%)	RMSE (%)
Cell 1	0.29	0.37	0.30	0.35
Cell 2	0.17	0.22	0.17	0.23
Cell 3	0.27	0.31	0.23	0.30

Table 6.14: SOC and SOE estimation errors under HPPC profile

Battery Cells	SOC		SOE	
	MAE (%)	RMSE (%)	MAE (%)	RMSE (%)
Cell 1	0.54	0.61	0.53	0.63
Cell 2	0.47	0.57	0.48	0.58
Cell 3	0.39	0.41	0.38	0.44

For the HPPC profile, the estimated and measured SOC and SOE for cell 1 are shown in Figures 15 (a) and 15 (b), respectively. The value of estimated SOC MAE and RMSE are 0.54 % and 0.61 %, respectively. As listed in Table 6.14, the value of estimated SOE MAE and RMSE are 0.47 % and 0.57 %, respectively. For cell 2, the estimated and measured SOC and SOE profiles are shown in Figures 15 (c) and 12 (d). The value of estimated SOC MAE and RMSE are 0.47 % and 0.57 %, respectively. The value of estimated SOE MAE and RMSE are 0.48 % and 0.58 %, respectively. Similarly, for cell 3, the estimated and measured SOC and SOE profiles are shown in Figures 15 (e) and 12 (f). The value of estimated SOC MAE and RMSE are 0.39 % and 0.41 %. The value of estimated SOE MAE and RMSE are 0.38 % and 0.44 %. The estimation results verify

that the estimated SOC and SOE follow the measured values with high accuracy under dynamic loading conditions.

6.3.2 SOP estimation results

Finally, for all the considered battery cells, the SOP estimation is performed under the HPPC profile. The Rint model parameters identified by FFRLS are employed to compute the SOP charge/discharge value using (21). For all the considered battery cells, the value of identifying U_{OCV} are presented in Figure 6.16. The identified U_{OCV} for cell 1, cell 2, and cell 3 are presented in Figures 6.16 (a), 6.16 (b), and 6.16 (c), respectively. Since the identified R_{st} values fluctuate in the range, the smoothed curve is obtained by using the cubic smoothing splines method as presented in Figure 6.17. Besides, for all the considered battery cells the battery DC internal charge/discharge resistances are evaluated by HPPC test results are also plotted as a reference in Figure 6.17. For cell 1, cell 2, and cell 3, the identified R_{st} using FFRLS, smoothed curve of R_{st}, and DC resistance charge/discharge evaluated using HPPC test are presented in Figures 6.17 (a), 6.17 (b), and 6.17 (c), respectively.

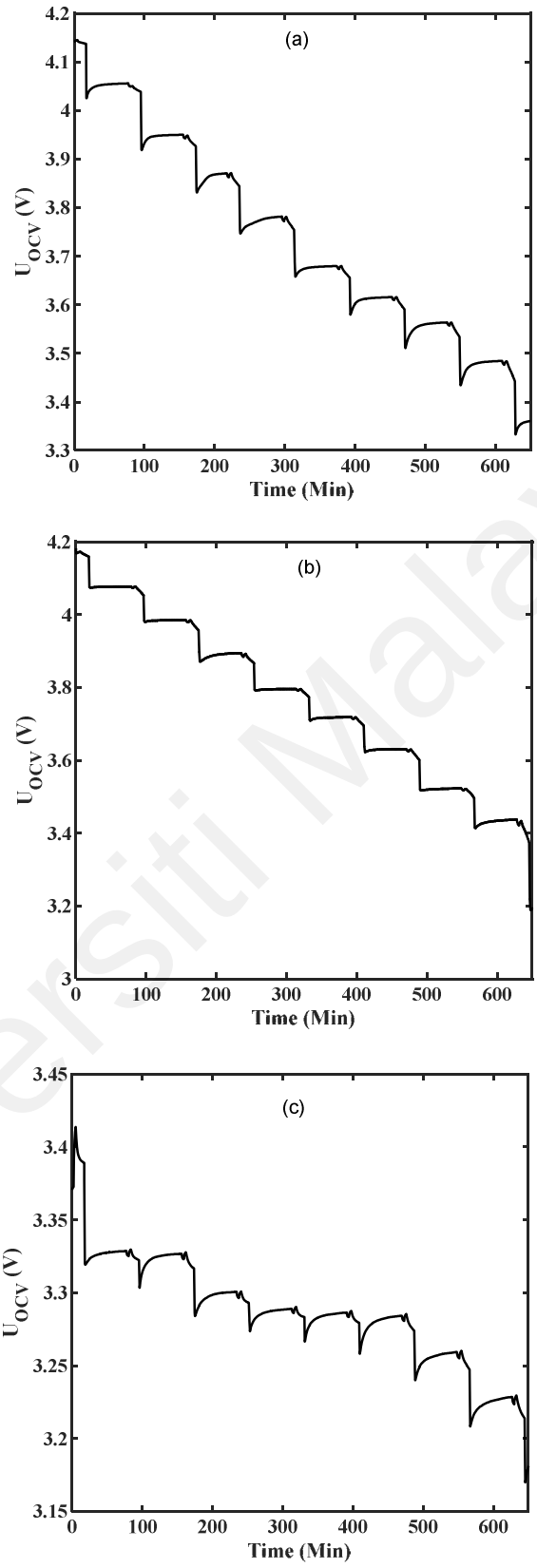

Figure 6.16: Estimated OCV using FFRLS under HPPC test: (a) Cell 1 (b) Cell 2 (c) Cell 3

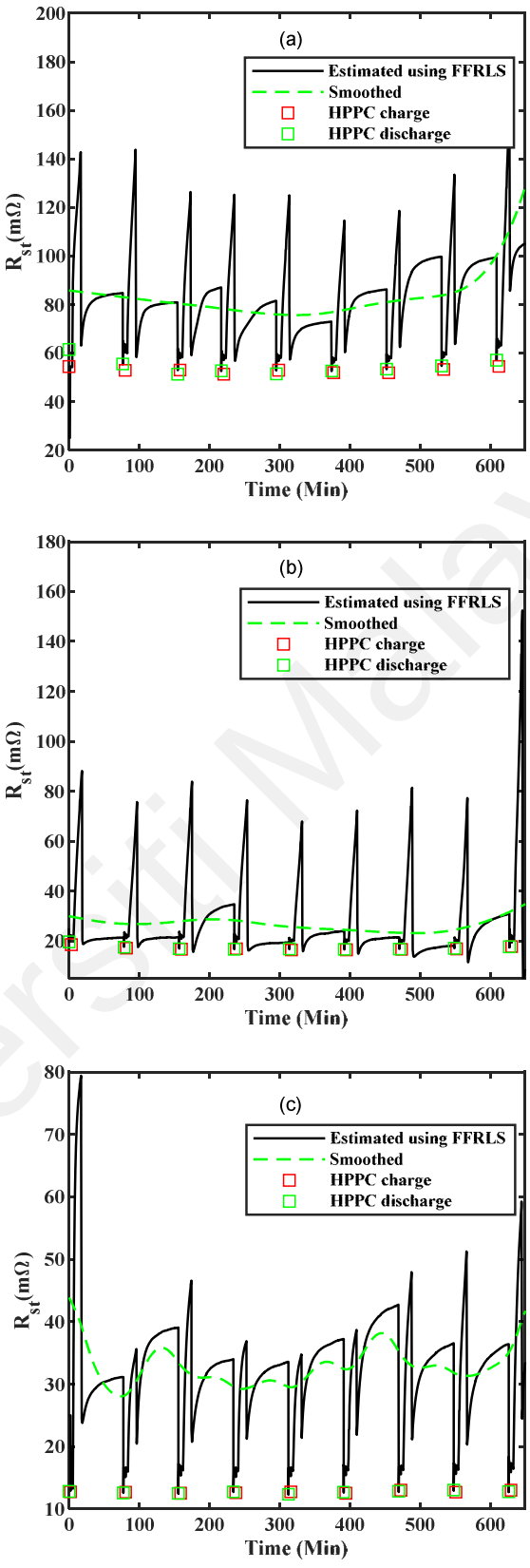

Figure 6.17: Estimated R_{st} using FFRLS under HPPC test: (a) Cell 1 (b) Cell 2 (c) Cell 3

The battery cell design limits such SOC constraints, voltage constraints, and current constraints, the charge/discharge SOP computation is given in Table 6.15. For all the battery cells, the measured SOP is computed from HPPC test results, as shown in Figure 6.18. Based on the battery cells maximum charge/discharge currents using (5.5) to (5.6), the charge/discharge SOP is predicted for all the battery cells using (5.7). As demonstrated in Figure 6.18, the predicted SOP is compared with the SOP obtained from HPPC test results. For cell 1, the value of predicted discharge SOP and charge SOP is presented in Figures 6.18 (a) and 6.18 (b), respectively. For cell 2, the value of predicted discharge SOP and charge SOP is presented in Figures 6.18 (c) and 6.18 (d). Similarly, for cell 3, the value of predicted discharge SOP and charge SOP is presented in Figures 6.18 (e) and 6.18 (f). Due to the high difficulty in finding actual power values, the SOP estimation error is not computed.

Table 6.15: Considered battery design limits of SOC constraints, voltage constraints, and current constraints for all the test battery cells

Battery Cells	Constraints Limits					
	$V_{t,min}$	$V_{t,max}$	I_{chrg}	I_{dis}	SOC_{min}	SOC_{max}
Cell 1	2.5	3.6	-20 C_A	20 C_A	10	100
Cell 2	2.8	4.2	-5C_A	2 C_A	10	100
Cell 3	2.8	4.2	-7 C_A	6 C_A	10	100

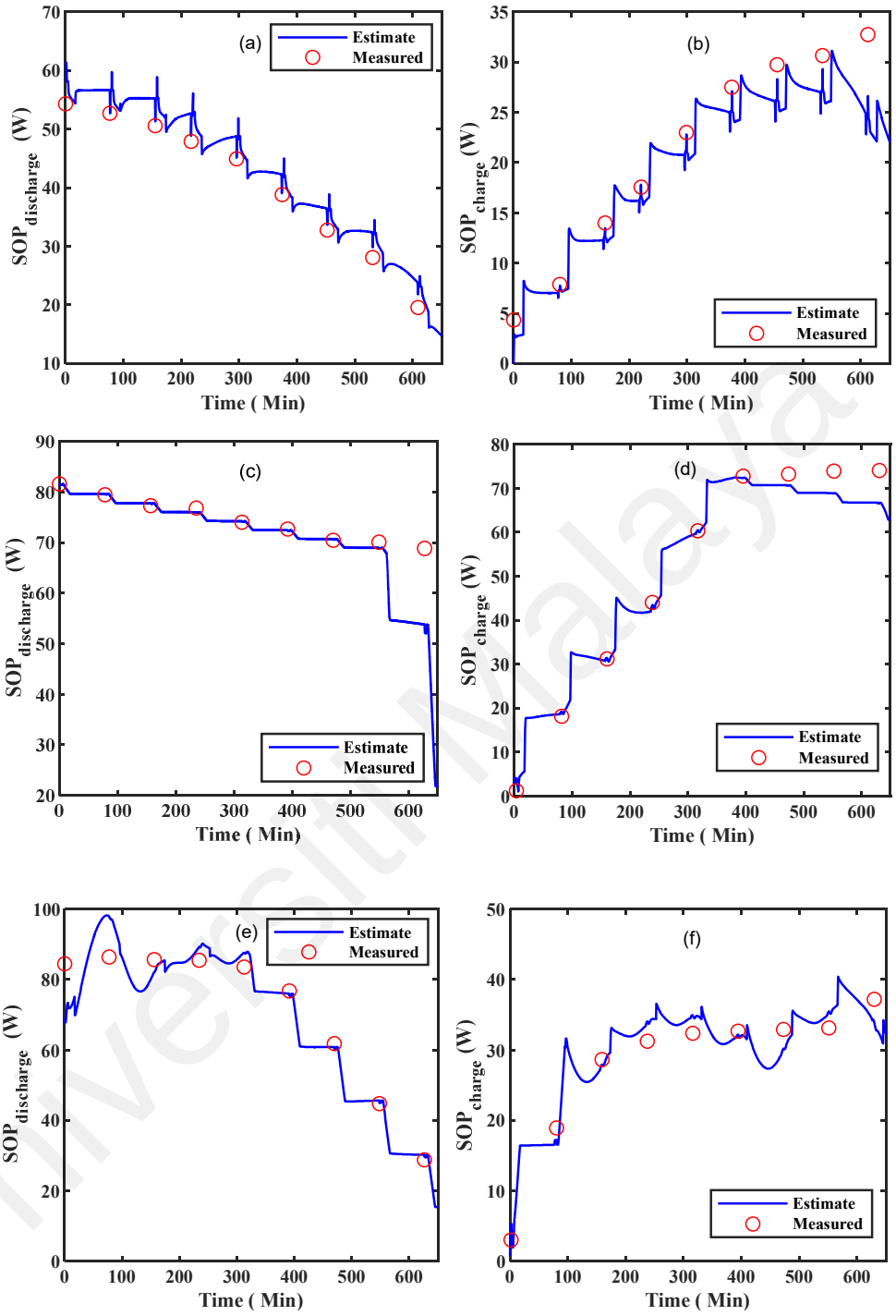

Figure 6.18: Estimated SOP results under HPPC profile: (a) SOP discharge for Cell 1, (b) SOP charge for Cell 1, (c) SOP discharge for Cell 2, (d) SOP charge for Cell 2, (e) SOP discharge for Cell 3, and (f) SOP charge for Cell 3

6.3.3 Actual capacity and maximum available energy estimation results

To compute the performance of Q_n and E_n estimation using SW-AWTLS algorithm, the value of estimated SOC and SOE using DFFAEKF algorithm is employed. The estimated SOC at two different moments of time and respective measured battery current is always required to update the estimated Q_n of the battery cell as expressed by (5.14). Similarly, estimated SOE at two different moments of time and respective measured battery power are always required to update the estimated E_n of the battery cell as expressed by (5.16). The length of the sliding window is selected to 200 to estimate the Q_n and E_n after every 200 seconds. With the application of the DFFAEKF algorithm, the dynamic estimates of the estimated SOC and SOE variance ($\sigma_{SOC,k} = \sigma_{SOE,k} = \sigma_{s,k}$) can be achieved. That ensures the high accuracy of Q_n and E_n estimation using the SW-AWTLS algorithm.

For Q_n and E_n estimation, the uncertainty in the measured current (I_k) and measured voltage (V_k) with zero mean Gaussian noise know variance ($\sigma_{r,k}$) of 0.01 is considered. For all the considered battery cells, the wrong initial value of Q_n and E_n are chosen to 2.0 Ah and 7.5 Wh, respectively.

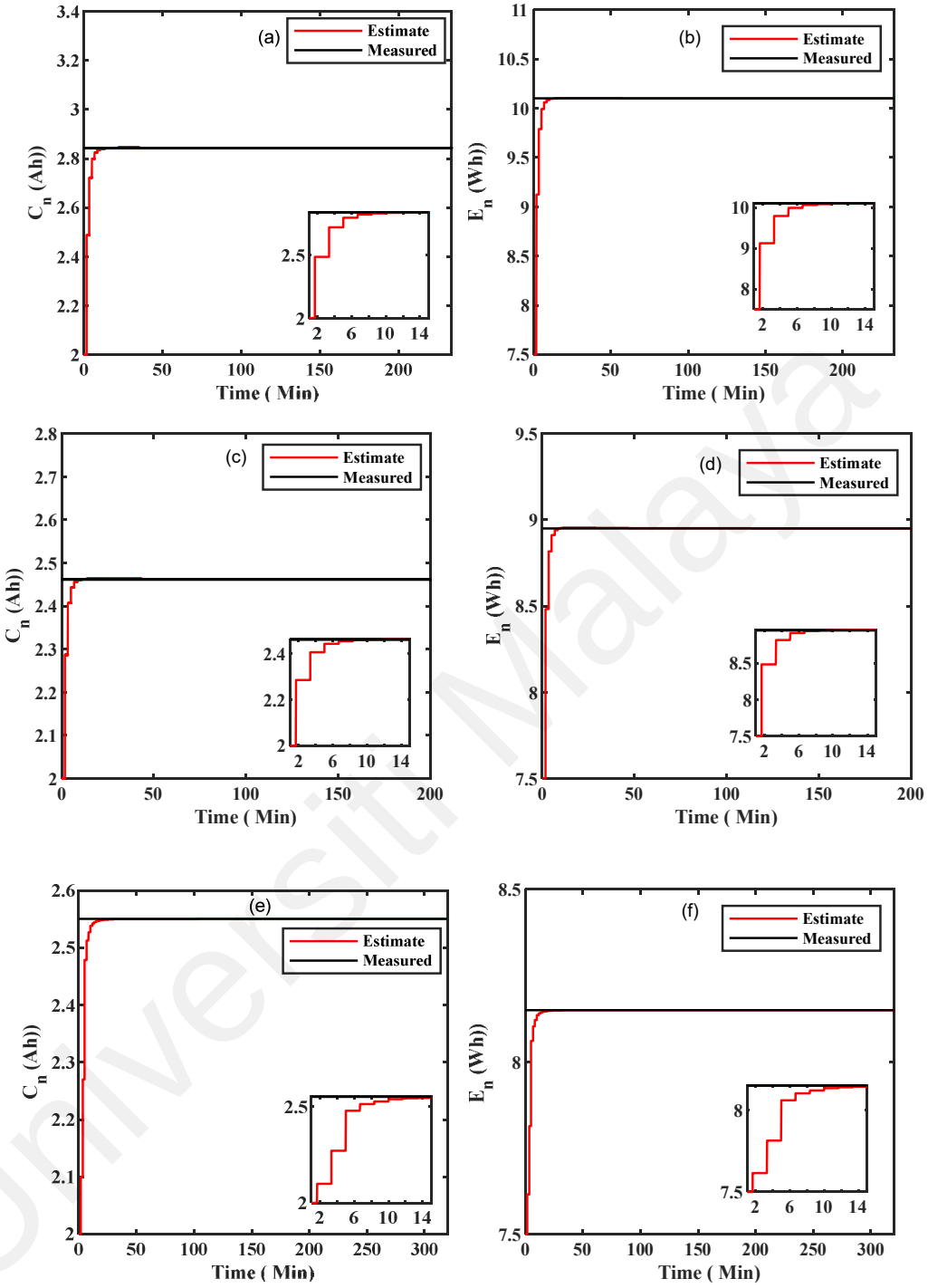

Figure 6.19: Results of estimated C_n and E_n under US06 profile: (a) C_n of Cell 1, (b) E_n of Cell 1, (c) C_n of Cell 2, (d) E_n of Cell 2, (e) C_n of Cell 3 (f) E_n of Cell 3

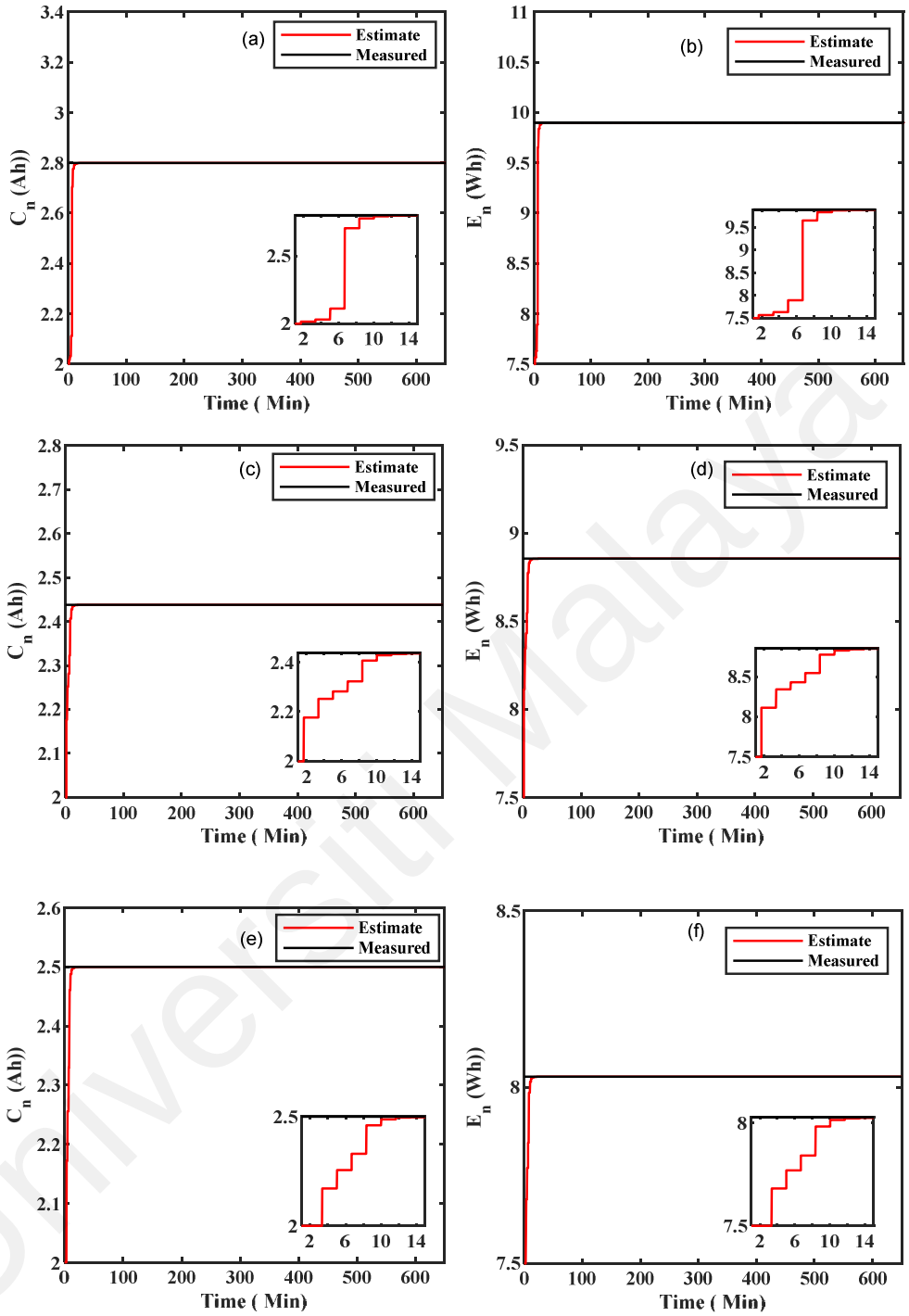

Figure 6.20: Results of estimated C_n and E_n under HPPC test: (a) C_n of Cell 1, (b) E_n of Cell 1, (c) C_n of Cell 2, (d) E_n of Cell 2, (e) C_n of Cell 3 (f) E_n of Cell 3

For the US06 drive cycle, the estimated Q_n for cell 1, cell 2, and cell 3 are shown in Figures 6.19 (a), 6.19 (c), and 6.19 (e). While the estimated E_n for cell 1, cell 2, and cell 3 are shown in Figures 6.19 (b), 6.19 (d), and 6.19 (f). Similarly, for the HPPC profile, the estimated Q_n for cell 1, cell 2, and cell 3 are shown in Figures 6.20 (a), 6.20 (c), and 6.20 (e). Whereas the estimated E_n for cell 1, cell 2, and cell 3 are shown in Figures 6.20 (b), 6.20 (d), and 6.20 (f). As shown in Figures 6.19 and 6.20, the estimated Q_n and E_n are converged towards its true values in the first few minutes irrespective of change in change chemistry and dynamic load profile. Also, with the application of SW-AWTLS, the computational load can be reduced in comparison to the AWTLS algorithm.

Table 6.16: Q_n and E_n estimation errors under US06 load profile after final convergence

Battery Cells	Q_n		E_n	
	MAE (%)	RMSE (%)	MAE (%)	RMSE (%)
Cell 1	9.36e-05	0.096	6.38e-04	0.25
Cell 2	3.73e-05	0.061	5.24e-06	0.23
Cell 3	4.14e-04	0.021	5.16e-02	0.72

For all the considered cells, the value of MAE and RMSE of estimated Q_n and E_n using SW-AWTLS for the final convergence to true values under the US06 drive cycle are listed in Table 6.16. As presented in Figure 3.4, the average of obtained actual capacity and maximum available energy for all the considered battery cells during the capacity test are considered as true values. Under HPPC profile, the value of MAE and RMSE of estimated Q_n and E_n using SW-AWTLS for the final convergence to true values are listed in Table 6.17. The low value of MAEs and RMSEs of estimated Q_n and E_n under both, the considered load profiles prove the robustness and accuracy of the proposed SW-

AWTLS algorithm. Also, with the application of SW-AWTLS, the computational load can be reduced in comparison to the AWTLS algorithm.

Table 6.17: Q_n and E_n estimation errors under HPPC load profile after final convergence

Battery Cells	Q_n		E_n	
	MAE (%)	RMSE (%)	MAE (%)	RMSE (%)
Cell 1	1.74e-04	0.132	1.04e-03	0.32
Cell 2	2.73e-04	0.165	4.21e-03	0.58
Cell 3	3.70e-04	0.192	5.94e-03	0.77

6.3.4 Comparative performance assessment of the proposed unified frame of battery states co-estimation method

To prove the superiority of the proposed unified frame of battery states co-estimation method, the number of states/parameters estimated, and the number of filters/observers utilized are compared. Some of the recent studies on co-estimation are considered. As listed, in Table 6.18, most of the studies introduced a co-estimation method for two battery states/parameters. Only in (P. Shen, Ouyang, Lu, et al., 2018), three different states such as SOC, SOH, and SOP using three filters/observers are estimated by using the developed co-estimation method. Only one chemistry battery cell is considered for the result validation. In the proposed unified frame of battery states co-estimation method, five different battery states/parameters are estimated by using three different filters/observers. Involved fewer filters/observers proves the low computational burden of the proposed method. Furthermore, three battery cells of different chemistries are considered for validation to show the robustness of the proposed method.

Table 6.18: Comparative performance assessment of proposed unified frame of battery states co-estimation method methods

Ref.	Battery Cell Chemistry	Operating condition	Name of battery states/parameters	Name of battery states/parameters estimated	Error (%)
(L. Zheng et al., 2016b)	LMO	DST (10°C, 25°C, and 40°C)	2	SOE and SOP	SOE Error < 2 SOE MaxAE < 3.4
(Yongzhi Zhang et al., 2017)	LMO	UDDS and NN (10°C, 25°C, and varying)	2	SOC and SOE	SOC MAE < 0.91 SOE MAE < 1.09
(X. Hu et al., 2018)	LFP	DST, HPPC, and FUDS (22°C)	2	SOC and SOH	SOC Error < 1 SOH Error < 1
(W. Zhang et al., 2015b)	LFP	FUDS (10°C, 25°C, and 40°C)	2	SOE and SOP	SOE Error < 2
(X. Li et al., 2019)	LMO, NMC	UDDS and HPPC (10°C, and 40°C)	3	Capacity and SOC	SOC MaxAE < 2
(X. Liu et al., 2020)	LFP	FUDS (25°C)	3	SOC and SOP	SOC MaxAE < 1.6

‘ Table 6.18 continued’

Ref.	Battery Cell Chemistry	Validation profile	Number of filters/observers	Name of battery states/parameters estimated	Error (%)
(P. Shen, Ouyang, Lu, et al., 2018)	NMC	DST, HPPC, and FUDS (-5°C, and 25°C)	3	SOC, SOH, and SOP	SOC Error < 1 SOH Error < 0.5
Proposed unified frame of battery states co-estimation method	NCA, NMC, LFP	US06, HPPC (25°C)	3	SOC, SOE, SOP, Actual capacity, and maximum available energy	SOC RMSE < 0.65 SOE RMSE < 0.65 Q_n RMSE < 0.2 E_n RMSE < 0.8

6.4 Summary

In this chapter, the results obtained from the proposed battery states co-estimation methods are presented. The experimental results indicated that the performance of the proposed co-estimation method for SOC and SOE estimation by using the DFFAEKF algorithm is superior as compared to the DEKF algorithm. Under dynamic operating conditions for all the considered battery cells, with the combined estimation method, the recorded RMSE of SOC estimation is less than 0.82 % under the DST profile and less than 0.94 % for the US06 profile. Also, the estimated RMSE of SOE is less than 0.83 % under the DST profile and less than 0.93 % for the US06 profile. The order of worst-case big O notation complexity of the proposed DFFAEKF is equivalent to DEKF. However, the computational cost of the DFFAEKF algorithm is slightly higher than the DEKF algorithm due to the availability of forgetting factor-based adaptive noise covariance matrices update feature in the proposed DFFAEKF algorithm. The proposed co-estimation method for SOC and SOE estimation method by using the DFFAEKF algorithm is less sensitive to the initial error condition and has a fast-converging speed towards the true value as compared to the DEKF algorithm.

Hereafter, the results obtained from the unified frame of battery states co-estimation method for SOC, SOE, SOP, actual capacity, and maximum available energy for EV applications are presented. The correlation between the different battery states is effectively utilized. The proposed unified frame of battery states co-estimation method can reduce the complexity and increase the estimation accuracy as compared to separate estimation algorithms. At a low cost, the SOC and SOE are estimated accurately by using the combined SOC and SOE estimation using the DFFAEKF algorithm. The experimental quantitative relationship between SOC and SOE is employed for SOE estimation. The charge/discharge SOP of the considered battery cells is predicted by using the identified Rint model parameters by FFRLS and the estimated SOC. Also, the predicted SOP

stratifies the battery cell design limits such as SOC, voltage, and current. Lastly, the actual capacity and maximum available energy are estimated by using the new SW-AWTLS algorithm. With the application of the SW method, the computational burden of AWTLS significantly reduce. Furthermore, the estimation results using the SW-AWTLS algorithm demonstrate fast convergence under incorrect initialization. With the features of high accuracy and computationally efficient, the proposed unified frame of battery states co-estimation method can be the best reasonable choice for EV applications.

CHAPTER 7: CONCLUSION AND FUTURE WORK

The conclusion of the thesis reflects the set of objectives discussed in Section 1.4. This chapter summarizes the outcomes of the research and provides suggestions for future work.

The sections of the chapter are arranged in this sequence. In Section 7.1, the re-examination of thesis objectives is provided. In Section 7.2, the contribution of the thesis is discussed. The future work for the researchers is provided in Section 7.3.

7.1 Re-examination of thesis objectives

The first objective of the thesis is to analyze the existing online SOC estimation methods suitable for EV application. To achieve this objective, a state-of-the-art review on different online SOC estimation methods was performed. Several characteristics of model-based online SOC estimation using the KF algorithm were investigated to improve estimation accuracy. In addition, to reduce the overall computational burden and improve the functioning of BMS, the correlation between different battery states was analyzed. The state-of-art review on SOE, SOP, battery actual capacity, and maximum available energy estimation were done. To effectively utilize the correlation between the battery states and for the development of computationally efficient BMS, the different co-estimation methods were investigated.

The second objective is to develop a more accurate online SOC estimation method under under uncertain disturbances and erroneous initial conditions. To achieve this, a new DFFAEKF for SOC estimation was proposed. In which, the benefits of the forgetting factor (high variations in the filter coefficients) together with the features of the DKF algorithm were utilized. The proposed algorithm has the feature of concurrently updating

the battery model parameters with the SOC estimation at high accuracy under different dynamic conditions with the same order big O notation complexity as DEKF.

Finally, the third objective is to develop an accurate and computationally efficient co-estimation method with proper utilization of the correlation among the different battery states. To achieve this, the co-estimation method for battery SOC and SOE using the DFFAEKF algorithm was proposed. The proposed method was capable to estimate the battery SOC and SOE with high accuracy and, strong robustness to the battery model parameter inaccuracy and measurement noise uncertainties. Thereafter, a unified frame of battery states co-estimation method for SOC, SOE, SOP, actual capacity, and maximum available estimation was proposed. The correlation between different battery states was effectively utilized to make the proposed unified frame of battery states co-estimation estimation method more accurate and computationally efficient.

7.2 Conclusion

With the development of LIB technologies, its applications as the main source of the energy storage system in EV and microgrids are significantly increasing. Owing to the highly nonlinear and dynamic nature of LIBs, an effective BMS is continuously required to operate them in a safe operating area. For that purpose, a quick, reliable, and accurate estimation of battery states is always required. However, accurate online battery states such as SOC, SOE, SOP, and SOE estimation are challenging tasks due to the high affectability and complicated internal chemical dynamics of the battery. In the last couple of years, different battery states estimation methods have been investigated by researchers. Nowadays, researchers are focusing on developing the battery states co-estimation that can be easily implementable into the low-cost BMS chips. Interestingly, all the battery states are highly correlated with each other. Hence, there is a need to

develop low computational cost battery states co-estimation method with the proposer utilization of correlation feature for BMS suitable EV applications.

Currently, the MBM for online SOC estimation with battery EECM is more appropriate for EV applications because of its possible benefits, including the capability to deal with unknown noise signals, low complexity, and high accuracy over other modeling methods. Further, the merits of self-correction and low computational burden make KF family algorithms suitable for model-based online SOC estimation. Presently, for online SOC and model parameter identification, the dual extended Kalman filter (DEKF) is extensively utilized by researchers. However, the problem of battery model parameter divergence from the true value greatly affects the estimation accuracy under realistic dynamic loading conditions. To outperform this issue, a new DFFAEKF for SOC estimation is proposed in this thesis. In which, the benefits of the forgetting factor (high variations in the filter coefficients) together with the features of the DKF algorithm are utilized. The proposed DFFAEKF has the feature of concurrently updating the battery model parameters with the SOC estimation at high accuracy under different dynamic conditions with the same order big O notation complexity as DEKF. Further, the co-estimation method for SOC and SOE estimation by using DFFAEKF has been developed to estimate the battery SOC and SOE with high accuracy and, strong robustness to the battery model parameter inaccuracy and measurement noise uncertainties. The different battery discharge tests incorporating dynamic loading profiles on three different chemistry battery cells have been conducted by using the experimental setup developed in the laboratory to validate the effectiveness of the proposed estimation method. The experimental results indicated that the performance of the combined SOC and SOE estimation by using the DFFAEKF algorithm is superior as compared to the DEKF algorithm.

To further improve the performance of the co-estimation method a unified frame of battery states co-estimation for SOC, SOE, SOP, actual capacity, and maximum available energy estimation has been developed. By which, the correlation between the different battery states is effectively utilized. The proposed unified frame co-estimation method can reduce the complexity and increase the estimation accuracy as compared to the separate estimation algorithms. Three battery cells of different chemistries are considered for the validation of the proposed method. As shown in the results, the SOC and SOE are estimated accurately by using the combined SOC and SOE estimation using the DFFAEKF algorithm. The experimental quantitative relationship between SOC and SOE is employed for SOE estimation. Then, the charge/discharge SOP of the considered battery cells is predicted by using the identified Rint model parameters by using FFRLS and the estimated SOC. The predicted SOP satisfied the battery cell design limits such as SOC, voltage, and current. Lastly, the actual capacity and maximum available energy are estimated by using the new SW-AWTLS algorithm. With the application of the SW method, the computational burden of AWTLS was significantly reduced. The estimation results of the SW-AWTLS algorithm demonstrated fast convergence under incorrect initialization. With the high accuracy, robustness, and low computation burden, the proposed battery states co-estimation method can be the best choice for EV applications.

7.3 Future work

The following are the recommendations for future research work based on the research carried out in this thesis:

i. The developed states co-estimation method focuses on the single-cell however due to limited voltage and capacity it has limited use in real applications. The extension of the proposed co-estimation method for the states estimation from cell level to battery pack level can be more meaningful for real-time applications.

ii. Although, the performance of the proposed battery states co-estimation methods has been proved satisfactory, at a controlled operating temperature which is hard to realize in real-time applications. Therefore, the proposed battery states co-estimation methods still need to further verify at dynamic operating temperatures.

iii. Fresh battery cells of different chemistries are utilized for the validation of the proposed batter states co-estimation methods. As the LIB performance does not remain the same, it degrades with aging. Therefore, it would be more useful to consider different aging level battery cells for the further validation of the proposed co-estimation methods.

iv. Due to the prominent features of LIBs, their application as an energy storage system for microgrids and renewable energy systems is also appreciably expanding. It would be interesting to implement the proposed battery states co-estimation methods and validate its performance under an environment other than EV.

REFERENCES

Akhlaghi, S., Zhou, N., & Huang, Z. (2018). Adaptive adjustment of noise covariance in Kalman filter for dynamic state estimation. *IEEE Power and Energy Society General Meeting*, *2018-Janua*, 1–5. https://doi.org/10.1109/PESGM.2017.8273755

Alv, J. C., Nieto, P. J., Juez, F. J. de C., Lasheras, F. S., Viejo, C. B., & Gutierrez, N. R. (2013). Battery State-of-Charge Estimator Using the MARS Technique. *Applied Mathematical Modelling*, *37*(9), 6244–6253. https://doi.org/10.1016/j.apm.2013.01.024

Alvarez Anton, J. C., Garcia Nieto, P. J., Blanco Viejo, C., & Vilan Vilan, J. A. (2013). Support vector machines used to estimate the battery state of charge. *IEEE Transactions on Power Electronics*, *28*(12), 5919–5926. https://doi.org/10.1109/TPEL.2013.2243918

Andre, D., Appel, C., Soczka-Guth, T., & Sauer, D. U. (2013). Advanced mathematical methods of SOC and SOH estimation for lithium-ion batteries. *Journal of Power Sources*, *224*, 20–27. https://doi.org/10.1016/j.jpowsour.2012.10.001

Aung, H., Soon Low, K., & Ting Goh, S. (2015). State-of-Charge Estimation of Lithium-Ion Battery Using Square Root Spherical Unscented Kalman Filter (Sqrt-UKFST) in Nanosatellite. *IEEE Transactions on Power Electronics*, *30*(9), 4774–4783. https://doi.org/10.1109/TPEL.2014.2361755

Baba, A., & Adachi, S. (2013). *Battery SOC estimation device* (Patent No. US 2013/0297243 A1).

Baba, A., & Adachi, S. (2016). *Battery SOC estimation device* (Patent No. US 9,329,240 B2). United States Patent Baba et al. (54).

Barcellona, S., & Piegari, L. (2017a). Lithium Ion Battery Models and Parameter Identification Techniques. *Energies*, *10*(12), 2007. https://doi.org/10.3390/en10122007

Barcellona, S., & Piegari, L. (2017b). Lithium Ion Battery Models and Parameter Identification Techniques. *Energies*, *10*(12), 2007. https://doi.org/10.3390/en10122007

Bartlett, A., Marcicki, J., Onori, S., Rizzoni, G., Xiao Guang Yang, & Miller, T. (2016). Model-based state of charge estimation and observability analysis of a composite electrode lithium-ion battery. *52nd IEEE Conference on Decision and Control*, *24*(2), 7791–7796. https://doi.org/10.1109/CDC.2013.6761126

Bartlett, A., Marcicki, J., Onori, S., Rizzoni, G., Yang, X. G., & Miller, T. (2016). Electrochemical Model-Based State of Charge and Capacity Estimation for a Composite Electrode Lithium-Ion Battery. *IEEE Transactions on Control Systems Technology*, *24*(2), 384–399. https://doi.org/10.1109/TCST.2015.2446947

Batteries, L. (2017). An Adaptive Square Root Unscented Kalman Filter Approach for State of Charge Estimation of Lithium-Ion Batteries. *Energies*, *10*(9), 1345.

https://doi.org/10.3390/en10091345

Berecibar, M., Gandiaga, I., Villarreal, I., Omar, N., Van Mierlo, J., & Van den Bossche, P. (2016a). Critical review of state of health estimation methods of Li-ion batteries for real applications. *Renewable and Sustainable Energy Reviews*, *56*, 572–587. https://doi.org/10.1016/J.RSER.2015.11.042

Berecibar, M., Gandiaga, I., Villarreal, I., Omar, N., Van Mierlo, J., & Van den Bossche, P. (2016b). Critical review of state of health estimation methods of Li-ion batteries for real applications. *Renewable and Sustainable Energy Reviews*, *56*, 572–587. https://doi.org/10.1016/J.RSER.2015.11.042

Buller, S., Thele, M., DeDoncker, R. W. A. A., & Karden, E. (2005). Impedance-Based Simulation Models of Supercapacitors and Li-Ion Batteries for Power Electronic Applications. *IEEE Transactions on Industry Applications*, *41*(3), 742–747. https://doi.org/10.1109/TIA.2005.847280

Buller, Stephan, Thele, M., Karden, E., & De Doncker, R. W. (2003). Impedance-based non-linear dynamic battery modeling for automotive applications. *Journal of Power Sources*, *113*(2), 422–430. https://doi.org/10.1016/S0378-7753(02)00558-X

Cacciato, M., Nobile, G., Scarcella, G., & Scelba, G. (2017). Real-Time Model-Based Estimation of SOC and SOH for Energy Storage Systems. *IEEE Transactions on Power Electronics*, *32*(1), 794–803. https://doi.org/10.1109/TPEL.2016.2535321

Campestrini, C., Heil, T., Kosch, S., & Jossen, A. (2016). A comparative study and review of different Kalman filters by applying an enhanced validation method. *Journal of Energy Storage*, *8*, 142–159. https://doi.org/10.1016/J.EST.2016.10.004

Cao, W., Ming, Z., Wang, X., & Cai, S. (2017). Improved bidirectional extreme learning machine based on enhanced random search. *Memetic Computing*, 1–8. https://doi.org/10.1007/s12293-017-0238-1

Cecile Vacher. (2002). *Method for calculating the parameters of the power battery of an electric motor vehicle* (Patent No. US6788069B2). United States. https://patents.google.com/patent/US6788069B2/en

Chang, J., Chi, M., & Shen, T. (2020). Model based state-of-energy estimation for LiFePO4 batteries using unscented particle filter. *Journal of Power Electronics*, *20*(2), 624–633. https://doi.org/10.1007/s43236-020-00051-5

Chen, C., Xiong, R., & Shen, W. (2018). A Lithium-Ion Battery-in-the-Loop Approach to Test and Validate Multiscale Dual H Infinity Filters for State-of-Charge and Capacity Estimation. *IEEE Transactions on Power Electronics*, *33*(1), 332–342. https://doi.org/10.1109/TPEL.2017.2670081

Chen, L., Wang, Z., Lu, Z., Li, J., Ji, B., Wei, H., & Pan, H. (2018). A Novel State-of-Charge Estimation Method of Lithium-Ion Batteries Combining the Grey Model and Genetic Algorithms. *IEEE Transactions on Power Electronics*, *33*(10), 8797–8807. https://doi.org/10.1109/TPEL.2017.2782721

Chen, X., Shen, W., Dai, M., Cao, Z., Jin, J., & Kapoor, A. (2016). Robust adaptive

sliding-mode observer using RBF neural network for lithium-ion battery state of charge estimation in electric vehicles. *IEEE Transactions on Vehicular Technology*, *65*(4), 1936–1947. https://doi.org/10.1109/TVT.2015.2427659

Chen, Z., Fu, Y., & Mi, C. C. (2013). State of Charge Estimation of Lithium-Ion Batteries in Electric Drive Vehicles Using Extended Kalman Filtering. *IEEE Transactions on Vehicular Technology*, *62*(3), 1020–1030. https://doi.org/10.1109/TVT.2012.2235474

Chin, C. S., & Gao, Z. (2018). State-of-charge estimation of battery pack under varying ambient temperature using an adaptive sequential extreme learning machine. *Energies*, *11*(4). https://doi.org/10.3390/en11040711

Corno, M., Bhatt, N., Savaresi, S. M., & Verhaegen, M. (2015). Electrochemical Model-Based State of Charge Estimation for Li-Ion Cells. *IEEE Transactions on Control Systems Technology*, *23*(1), 117–127.

Cuma, M. U., & Koroglu, T. (2015). A comprehensive review on estimation strategies used in hybrid and battery electric vehicles. *Renewable and Sustainable Energy Reviews*, *42*, 517–531. https://doi.org/10.1016/J.RSER.2014.10.047

Dai, H., Wei, X., & Sun, Z. (2012). Design and Implementation of a UKF-based SOC Estimator for LiMnO2 Batteries Used on Electric Vehicles. *PRZEGLĄD ELEKTROTECHNICZNY (Electrical Review)*, *88*(1b), 57–63.

Dai, H., Wei, X., & Sun, Z. (2009). State and Parameter Estimation of a HEV Li-ion Battery Pack Using Adaptive Kalman Filter with a New SOC-OCV Concept. *2009 International Conference on Measuring Technology and Mechatronics Automation*, 375–380. https://doi.org/10.1109/ICMTMA.2009.333

Das, U. K., Shrivastava, P., Tey, K. S., Bin Idris, M. Y. I., Mekhilef, S., Jamei, E., Seyedmahmoudian, M., & Stojcevski, A. (2020). Advancement of lithium-ion battery cells voltage equalization techniques: A review. *Renewable and Sustainable Energy Reviews*, *134*(August), 110227. https://doi.org/10.1016/j.rser.2020.110227

Dees, D. W., Battaglia, V. S., & Bélanger, A. (2002). Electrochemical modeling of lithium polymer batteries. *Journal of Power Sources*, *110*(2), 310–320. https://doi.org/10.1016/S0378-7753(02)00193-3

Deng, Z., Yang, L., Cai, Y., & Deng, H. (2017). Maximum Available Capacity and Energy Estimation Based on Support Vector Machine Regression for Lithium-ion Battery. *Energy Procedia*, *107*, 68–75. https://doi.org/10.1016/j.egypro.2016.12.131

Dong, G., Chen, Z., Wei, J., Zhang, C., & Wang, P. (2016). An online model-based method for state of energy estimation of lithium-ion batteries using dual filters. *Journal of Power Sources*, *301*, 277–286. https://doi.org/10.1016/j.jpowsour.2015.10.011

Dong, G., Wei, J., & Chen, Z. (2016). Kalman filter for onboard state of charge estimation and peak power capability analysis of lithium-ion batteries. *Journal of Power Sources*, *328*, 615–626. https://doi.org/10.1016/j.jpowsour.2016.08.065

Dong, G., Wei, J., Chen, Z., Sun, H., & Yu, X. (2017). Remaining dischargeable time prediction for lithium-ion batteries using unscented Kalman filter. *Journal of Power Sources*, *364*, 316–327. https://doi.org/10.1016/j.jpowsour.2017.08.040

Dragicevic, T., Sucic, S., & Guerrero, J. M. (2013). Battery state-of-charge and parameter estimation algorithm based on Kalman filter. *Eurocon 2013*, 1519–1525. https://doi.org/10.1109/EUROCON.2013.6625179

El Mejdoubi, A., Oukaour, A., Chaoui, H., Gualous, H., Sabor, J., & Slamani, Y. (2016). State-of-Charge and State-of-Health Lithium-Ion Batteries' Diagnosis According to Surface Temperature Variation. *IEEE Transactions on Industrial Electronics*, *63*(4), 2391–2402. https://doi.org/10.1109/TIE.2015.2509916

Erlangga, G., Perwira, A., & Widyotriatmo, A. (2018). State of charge and state of health estimation of lithium battery using dual Kalman filter method. *2018 International Conference on Signals and Systems (ICSigSys)*, 243–248. https://doi.org/10.1109/ICSIGSYS.2018.8372765

Exclusive: Panasonic aims to boost energy density in Tesla batteries by 20% - executive | Reuters. (n.d.). Retrieved May 13, 2021, from https://www.reuters.com/article/us-panasonic-tesla-exclusive-idUSKCN24V1GB

Fairweather, A. J., Foster, M. P., & Stone, D. A. (2012). Modelling of VRLA batteries over operational temperature range using Pseudo Random Binary Sequences. *Journal of Power Sources*, *207*, 56–59. https://doi.org/10.1016/J.JPOWSOUR.2012.02.024

Fan, L., Wang, P., & Cheng, Z. (2021). A remaining capacity estimation approach of lithium-ion batteries based on partial charging curve and health feature fusion. *Journal of Energy Storage*, *43*(May), 103115. https://doi.org/10.1016/j.est.2021.103115

Farmann, A., & Sauer, D. U. (2016). A comprehensive review of on-board State-of-Available-Power prediction techniques for lithium-ion batteries in electric vehicles. *Journal of Power Sources*, *329*, 123–137. https://doi.org/10.1016/j.jpowsour.2016.08.031

Farmann, A., Waag, W., Marongiu, A., & Sauer, D. U. (2015). Critical review of on-board capacity estimation techniques for lithium-ion batteries in electric and hybrid electric vehicles. *Journal of Power Sources*, *281*, 114–130. https://doi.org/10.1016/j.jpowsour.2015.01.129

Fleischer, C., Waag, W., Bai, Z., & Sauer, D. U. (2013). Adaptive on-line state-of-available-power prediction of lithium-ion batteries. *Journal of Power Electronics*, *13*(4), 516–527. https://doi.org/10.6113/JPE.2013.13.4.516

Gao, S., Liu, Y., Wang, J., Deng, W., & Oh, H. (2016). The Joint Adaptive Kalman Filter (JAKF) for Vehicle Motion State Estimation. *Sensors (Basel, Switzerland)*, *16*(7). https://doi.org/10.3390/s16071103

Gelso, E., & Bryngelsson, H. (2018). *A method and arrangement for determining the State of Charge of a battery pack* (Patent No. WO 2018/127296 Al). World

Intellectual Property Organization.

General Motors recalling nearly 69,000 Bolt EVs for fire risks - The Economic Times. (n.d.). Retrieved May 15, 2021, from https://economictimes.indiatimes.com/news/international/business/general-motors-recalling-nearly-69000-bolt-evs-for-fire-risks/articleshow/79218359.cms?from=mdr

Gou, B., Xu, Y., & Feng, X. (2020). An Ensemble Learning-based Data-Driven Method for Online State-of-Health Estimation of Lithium-ion Batteries. *IEEE Transactions on Transportation Electrification*. https://doi.org/10.1109/TTE.2020.3029295

Gould, C. R., Bingham, C. M., Stone, D. A., & Bentley, P. (2009). New Battery Model and State-of-Health Determination Through Subspace Parameter Estimation and State-Observer Techniques. *IEEE Transactions on Vehicular Technology*, *58*(8), 3905–3916. https://doi.org/10.1109/TVT.2009.2028348

Gould, C., Wang, J., Stone, D., & Foster, M. (2012). EV/HEV Li-ion battery modelling and State-of-Function determination. *International Symposium on Power Electronics Power Electronics, Electrical Drives, Automation and Motion*, 353–358. https://doi.org/10.1109/SPEEDAM.2012.6264616

Guo, H., Wang, Z., Li, Y., Wang, D., & Wang, G. (2017). State of charge and parameters estimation for Lithium-ion battery using dual adaptive unscented Kalman filter. *2017 29th Chinese Control And Decision Conference (CCDC)*, 4962–4966. https://doi.org/10.1109/CCDC.2017.7979374

Guo, X., Kang, L., Yao, Y., Huang, Z., & Li, W. (2016). Joint estimation of the electric vehicle power battery state of charge based on the least squares method and the Kalman filter algorithm. *Energies*, *9*(100), 1–16. https://doi.org/10.3390/en9020100

Hametner, C., & Jakubek, S. (2013). State of charge estimation for Lithium Ion cells: Design of experiments, nonlinear identification and fuzzy observer design. *Journal of Power Sources*, *238*, 413–421. https://doi.org/10.1016/J.JPOWSOUR.2013.04.040

Han, X., Ouyang, M., Lu, L., & Li, J. (2014). A comparative study of commercial lithium ion battery cycle life in electric vehicle: Capacity loss estimation. *Journal of Power Sources*, *268*, 658–669. https://doi.org/10.1016/j.jpowsour.2014.06.111

Han, X., Ouyang, M., Lu, L., & Li, J. (2015a). Simplification of physics-based electrochemical model for lithium ion battery on electric vehicle. Part I: Diffusion simplification and single particle model. *Journal of Power Sources*, *278*, 802–813. https://doi.org/10.1016/J.JPOWSOUR.2014.12.101

Han, X., Ouyang, M., Lu, L., & Li, J. (2015b). Simplification of physics-based electrochemical model for lithium ion battery on electric vehicle. Part II: Pseudo-two-dimensional model simplification and state of charge estimation. *Journal of Power Sources*, *278*, 814–825. https://doi.org/10.1016/J.JPOWSOUR.2014.08.089

Hannan, M. A., Hoque, M. M., Mohamed, A., & Ayob, A. (2017a). Review of energy storage systems for electric vehicle applications: Issues and challenges. *Renewable*

and Sustainable Energy Reviews, *69*(November 2016), 771–789. https://doi.org/10.1016/j.rser.2016.11.171

Hannan, M. A., Hoque, M. M., Mohamed, A., & Ayob, A. (2017b). Review of energy storage systems for electric vehicle applications: Issues and challenges. In *Renewable and Sustainable Energy Reviews* (Vol. 69, pp. 771–789). Elsevier Ltd. https://doi.org/10.1016/j.rser.2016.11.171

Hannan, M. A., Lipu, M. S. H., Hussain, A., & Mohamed, A. (2017). A review of lithium-ion battery state of charge estimation and management system in electric vehicle applications: Challenges and recommendations. *Renewable and Sustainable Energy Reviews*, *78*, 834–854. https://doi.org/10.1016/J.RSER.2017.05.001

He, Hongwen, Qin, H., Sun, X., & Shui, Y. (2013). Comparison study on the battery SoC estimation with EKF and UKF algorithms. *Energies*, *6*(10), 5088–5100. https://doi.org/10.3390/en6105088

He, Hongwen, Xiong, R., & Fan, J. (2011a). Evaluation of lithium-ion battery equivalent circuit models for state of charge estHe, H., Xiong, R., & Fan, J. (2011). Evaluation of lithium-ion battery equivalent circuit models for state of charge estimation by an experimental approach. Energies, 4(4),. *Energies*, *4*(4), 582–598. https://doi.org/10.3390/en4040582

He, Hongwen, Xiong, R., & Fan, J. (2011b). Evaluation of Lithium-Ion Battery Equivalent Circuit Models for State of Charge Estimation by an Experimental Approach. *Energies*, *4*(4), 582–598. https://doi.org/10.3390/en4040582

He, Hongwen, Xiong, R., & Guo, H. (2012a). Online estimation of model parameters and state-of-charge of LiFePO4batteries in electric vehicles. *Applied Energy*, *89*(1), 413–420. https://doi.org/10.1016/j.apenergy.2011.08.005

He, Hongwen, Xiong, R., & Guo, H. (2012b). Online estimation of model parameters and state-of-charge of LiFePO4 batteries in electric vehicles. *Applied Energy*, *89*(1), 413–420. https://doi.org/10.1016/J.APENERGY.2011.08.005

He, HongWen, Zhang, Y., Xiong, R., & Wang, C. (2015). A novel Gaussian model based battery state estimation approach: State-of-Energy. *Applied Energy*, *151*, 41–48. https://doi.org/10.1016/J.APENERGY.2015.04.062

He, J., Wei, Z., Bian, X., & Yan, F. (2020). State-of-Health Estimation of Lithium-Ion Batteries Using Incremental Capacity Analysis Based on Voltage-Capacity Model. *IEEE Transactions on Transportation Electrification*, *6*(2), 417–426. https://doi.org/10.1109/TTE.2020.2994543

He, Z., Liu, Y., Gao, M., & Wang, C. (2012). A Joint Model and SOC Estimation Method for Lithium Battery Based on the Sigma Point KF. *2012 IEEE Transportation Electrification Conference and Expo (ITEC)*, 1–5. https://doi.org/10.1109/ITEC.2012.6243505

Hongwen He, Rui Xiong, Xiaowei Zhang, Fengchun Sun, JinXin Fan, Hongwen, H., Rui, X., Xiaowei, Z., Fengchun, S., & JinXin, F. (2011). State-of-Charge Estimation of the Lithium-Ion Battery Using an Adaptive Extended Kalman Filter Based on an

Improved Thevenin Model. *Vehicular Technology, IEEE Transactions On*, *60*(4), 1461–1469. https://doi.org/10.1109/TVT.2011.2132812

Hossain Lipu, M. S., Hannan, M. A., Hussain, A., Ayob, A., Saad, M. H. M., Karim, T. F., & How, D. N. T. (2020). Data-driven state of charge estimation of lithium-ion batteries: Algorithms, implementation factors, limitations and future trends. *Journal of Cleaner Production*, *277*. https://doi.org/10.1016/j.jclepro.2020.124110

Hossain Lipu, M. S., Hannan, M. A., Karim, T. F., Hussain, A., Saad, M. H. M., Ayob, A., Miah, M. S., & Indra Mahlia, T. M. (2021). Intelligent algorithms and control strategies for battery management system in electric vehicles: Progress, challenges and future outlook. In *Journal of Cleaner Production* (Vol. 292, p. 126044). Elsevier Ltd. https://doi.org/10.1016/j.jclepro.2021.126044

Hu, J. N., Hu, J. J., Lin, H. B., Li, X. P., Jiang, C. L., Qiu, X. H., & Li, W. S. (2014). State-of-charge estimation for battery management system using optimized support vector machine for regression. *Journal of Power Sources*, *269*, 682–693. https://doi.org/10.1016/J.JPOWSOUR.2014.07.016

Hu, X., Yuan, H., Zou, C., Li, Z., & Zhang, L. (2018). Co-Estimation of State of Charge and State of Health for Lithium-Ion Batteries based on Fractional-order Calculus. *IEEE Transactions on Vehicular Technology*, *67*(11), 10319–10329. https://doi.org/10.1109/TVT.2018.2865664

Huang, C., Wang, Z., Zhao, Z., Wang, L., Lai, C. S., & Wang, D. (2018). Robustness Evaluation of Extended and Unscented Kalman Filter for Battery State of Charge Estimation. *IEEE Access*, *6*, 1–1. https://doi.org/10.1109/ACCESS.2018.2833858

Huang, G.-B., & Chen, L. (2008). Enhanced random search based incremental extreme learning machine. *Neurocomputing*, *71*(16–18), 3460–3468. https://doi.org/10.1016/J.NEUCOM.2007.10.008

Huria, T., Ludovici, G., & Lutzemberger, G. (2014). State of charge estimation of high power lithium iron phosphate cells. *Journal of Power Sources*, *249*, 92–102. https://doi.org/10.1016/J.JPOWSOUR.2013.10.079

IEA International Energy Agency. (2018). *Global EV Outlook 2018*. https://doi.org/10.1787/9789264302365-en

Jokar, A., Rajabloo, B., Désilets, M., & Lacroix, M. (2016a). Review of simplified Pseudo-two-Dimensional models of lithium-ion batteries. *Journal of Power Sources*, *327*, 44–55. https://doi.org/10.1016/J.JPOWSOUR.2016.07.036

Jokar, A., Rajabloo, B., Désilets, M., & Lacroix, M. (2016b). Review of simplified Pseudo-two-Dimensional models of lithium-ion batteries. *Journal of Power Sources*, *327*, 44–55. https://doi.org/10.1016/J.JPOWSOUR.2016.07.036

JR, E. D. T., Verbrugge, M. W., Brian J. Koch, B., & Damon R. Frisch, T. (2005). *Generalized electrochemical cell state and parameter estimator* (Patent No. US 2005/0057255A1). United States Patent Application Publication.

Kim, I. (2008). Nonlinear State of Charge Estimator for Hybrid Electric Vehicle Battery.

IEEE Transactions on Power Electronics, *23*(4), 2027–2034. https://doi.org/10.1109/TPEL.2008.924629

Kim, J., & Cho, B. H. (2011). State-of-charge estimation and state-of-health prediction of a Li-Ion degraded battery based on an EKF combined with a per-unit system. *IEEE Transactions on Vehicular Technology*, *60*(9), 4249–4260. https://doi.org/10.1109/TVT.2011.2168987

KIM, J., SONG, T. W., & KIM, S. (2018). *Method and apparatus for estimating state of battery based on error correction* (Patent No. EP 3 327 456 A1). EUROPEAN PATENT APPLICATION.

Kim, T., Wang, Y., Fang, H., Sahinoglu, Z., Wada, T., Hara, S., & Qiao, W. (2015). Model-based condition monitoring for lithium-ion batteries. *Journal of Power Sources*, *295*, 16–27. https://doi.org/10.1016/J.JPOWSOUR.2015.03.184

Klass, V., Behm, M., & Lindbergh, G. (2015a). Capturing lithium-ion battery dynamics with support vector machine-based battery model. *Journal of Power Sources*, *298*, 92–101. https://doi.org/10.1016/J.JPOWSOUR.2015.08.036

Klass, V., Behm, M., & Lindbergh, G. (2015b). Capturing lithium-ion battery dynamics with support vector machine-based battery model. *Journal of Power Sources*, *298*, 92–101. https://doi.org/10.1016/J.JPOWSOUR.2015.08.036

Lai, X., Zheng, Y., & Sun, T. (2018). A comparative study of different equivalent circuit models for estimating state-of-charge of lithium-ion batteries. *Electrochimica Acta*, *259*, 566–577. https://doi.org/10.1016/J.ELECTACTA.2017.10.153

Lashway, C., & Mohammed, O. (2016). Adaptive Battery Management and Parameter Estimation through Physics Based Modeling and Experimental Verification. *IEEE Transactions on Transportation Electrification*, *PP*(99), 1. https://doi.org/10.1109/TTE.2016.2558843

Lee, J. L., Aldrich, L. L., Stetzel, K. D., & Plett, G. L. (2014). Extended operating range for reduced-order model of lithium-ion cells. *Journal of Power Sources*, *255*, 85–100. https://doi.org/10.1016/J.JPOWSOUR.2013.12.134

Lee, J. L., Chemistruck, A., & Plett, G. L. (2012a). Discrete-time realization of transcendental impedance models, with application to modeling spherical solid diffusion. *Journal of Power Sources*, *206*, 367–377. https://doi.org/10.1016/J.JPOWSOUR.2012.01.134

Lee, J. L., Chemistruck, A., & Plett, G. L. (2012b). One-dimensional physics-based reduced-order model of lithium-ion dynamics. *Journal of Power Sources*, *220*, 430–448. https://doi.org/10.1016/J.JPOWSOUR.2012.07.075

Lee, J. L., Chemistruck, A., & Plett, G. L. (2012c). One-dimensional physics-based reduced-order model of lithium-ion dynamics. *Journal of Power Sources*, *220*, 430–448. https://doi.org/10.1016/J.JPOWSOUR.2012.07.075

Lee, S., Kim, J., Lee, J., & Cho, B. H. (2008). State-of-charge and capacity estimation of lithium-ion battery using a new open-circuit voltage versus state-of-charge. *Journal*

of Power Sources, *185*(2), 1367–1373. https://doi.org/10.1016/J.JPOWSOUR.2008.08.103

Lee, T.-K. (2015). *Method and system for estimating battery model parameters to update battery models used for controls* (Patent No. US 2015/0355283 A1).

Lee, T.-K. (2017). *Method and system for battery state of charge estimation* (Patent No. US 9,581,988 B2).

Leng, F., Tan, C. M., Yazami, R., & Le, M. D. (2014). A practical framework of electrical based online state-of-charge estimation of lithium ion batteries. *Journal of Power Sources*, *255*, 423–430. https://doi.org/10.1016/j.jpowsour.2014.01.020

Li, B., Peng, K., & Li, G. (2018). technique State-of-charge estimation for lithium-ion battery using the Gauss-Hermite particle filter technique. *Journal of Renewable and Sustainable Energy*, *10*, 014105. https://doi.org/10.1063/1.5020028

Li, C., Xiao, F., & Fan, Y. (2019). An approach to state of charge estimation of lithium-ion batteries based on recurrent neural networks with gated recurrent unit. *Energies*, *12*(9). https://doi.org/10.3390/en12091592

Li, D., Ouyang, J., Li, H., & Wan, J. (2015). State of charge estimation for LiMn2O4 power battery based on strong tracking sigma point Kalman filter. *Journal of Power Sources*, *279*, 439–449. https://doi.org/10.1016/J.JPOWSOUR.2015.01.002

Li, G., Peng, K., & Li, B. (2018). State-of-charge estimation for lithium-ion battery using a combined method. *Journal of Power Electronics*, *18*(1), 129–136. https://doi.org/10.6113/JPE.2018.18.1.129

Li, Jiahao, Klee Barillas, J., Guenther, C., & Danzer, M. A. (2013). A comparative study of state of charge estimation algorithms for LiFePO4 batteries used in electric vehicles. *Journal of Power Sources*, *230*, 244–250. https://doi.org/10.1016/J.JPOWSOUR.2012.12.057

Li, Junfu, Lai, Q., Wang, L., Lyu, C., & Wang, H. (2016). A method for SOC estimation based on simplified mechanistic model for LiFePO4 battery. *Energy*, *114*, 1266–1276. https://doi.org/10.1016/J.ENERGY.2016.08.080

Li, Junfu, Wang, L., Lyu, C., & Pecht, M. (2017). State of charge estimation based on a simplified electrochemical model for a single LiCoO2 battery and battery pack. *Energy*, *133*, 572–583. https://doi.org/10.1016/J.ENERGY.2017.05.158

Li, K., Wei, F., Tseng, K. J., & Soong, B. H. (2018). A Practical Lithium-Ion Battery Model for State of Energy and Voltage Responses Prediction Incorporating Temperature and Ageing Effects. *IEEE Transactions on Industrial Electronics*, *65*(8), 6696–6708. https://doi.org/10.1109/TIE.2017.2779411

Li, W., Sengupta, N., Dechent, P., Howey, D., Annaswamy, A., & Sauer, D. U. (2021a). Online capacity estimation of lithium-ion batteries with deep long short-term memory networks. *Journal of Power Sources*, *482*, 228863. https://doi.org/10.1016/j.jpowsour.2020.228863

Li, W., Sengupta, N., Dechent, P., Howey, D., Annaswamy, A., & Sauer, D. U. (2021b). Online capacity estimation of lithium-ion batteries with deep long short-term memory networks. *Journal of Power Sources*, *482*, 228863. https://doi.org/10.1016/j.jpowsour.2020.228863

Li, X., Pan, K., Fan, G., Lu, R., Zhu, C., Rizzoni, G., & Canova, M. (2017). A physics-based fractional order model and state of energy estimation for lithium ion batteries. Part II: Parameter identification and state of energy estimation for LiFePO4battery. *Journal of Power Sources*, *367*, 202–213. https://doi.org/10.1016/j.jpowsour.2017.09.048

Li, X., Wang, Z., & Zhang, L. (2019). Co-estimation of capacity and state-of-charge for lithium-ion batteries in electric vehicles. *Energy*, *174*, 33–44. https://doi.org/10.1016/j.energy.2019.02.147

Li, X., Xu, J., Hong, J., Tian, J., & Tian, Y. (2021). State of energy estimation for a series-connected lithium-ion battery pack based on an adaptive weighted strategy. *Energy*, *214*, 118858. https://doi.org/10.1016/j.energy.2020.118858

Li, Z., Huang, J., Liaw, B. Y., & Zhang, J. (2017a). On state-of-charge determination for lithium-ion batteries. *Journal of Power Sources*, *348*, 281–301. https://doi.org/10.1016/j.jpowsour.2017.03.001

Li, Z., Huang, J., Liaw, B. Y., & Zhang, J. (2017b). On state-of-charge determination for lithium-ion batteries. *Journal of Power Sources*, *348*, 281–301. https://doi.org/10.1016/J.JPOWSOUR.2017.03.001

Liao, X., Yu, J., & Gao, L. (2012). Electrochemical study on lithium iron phosphate/hard carbon lithium-ion batteries. *Journal of Solid State Electrochemistry*, *16*(2), 423–428. https://doi.org/10.1007/s10008-011-1387-7

LIM, J. H., & JIN, S. (2012). *The method of measuring SoC of a battery in a battery management system and the apparatus thereof* (Patent No. EP 2 233 939 B1). European Patent Office.

Lin, C., Mu, H., Xiong, R., & Cao, J. (2017). Multi-model probabilities based state fusion estimation method of lithium-ion battery for electric vehicles: State-of-energy. *Applied Energy*, *194*, 560–568. https://doi.org/10.1016/j.apenergy.2016.05.065

Lin, C., Tang, A., & Wang, W. (2015). A review of SOH estimation methods in Lithium-ion batteries for electric vehicle applications. *Energy Procedia*, *75*, 1920–1925. https://doi.org/10.1016/j.egypro.2015.07.199

Liu, F., Liu, T., & Fu, Y. (2015). An Improved SoC Estimation Algorithm Based on Artificial Neural Network. *2015 8th International Symposium on Computational Intelligence and Design (ISCID)*, 152–155. https://doi.org/10.1109/ISCID.2015.2

Liu, K., Li, K., Peng, Q., & Zhang, C. (2019). A brief review on key technologies in the battery management system of electric vehicles. In *Frontiers of Mechanical Engineering* (Vol. 14, Issue 1, pp. 47–64). Higher Education Press. https://doi.org/10.1007/s11465-018-0516-8

Liu, S., Zhao, H., Tan, M., Hu, Y., Shu, X., Zhang, M., Chen, B., & Liu, X. (2017). Er-Doped LiNi0.5Mn1.5O4 Cathode Material with Enhanced Cycling Stability for Lithium-Ion Batteries. *Materials*, *10*(8), 859. https://doi.org/10.3390/ma10080859

Liu, X., Wu, J., Zhang, C., & Chen, Z. (2014). A method for state of energy estimation of lithium-ion batteries at dynamic currents and temperatures. *Journal of Power Sources*, *270*, 151–157. https://doi.org/10.1016/j.jpowsour.2014.07.107

Liu, X., Zheng, C., Wu, J., Meng, J., Stroe, D. I., & Chen, J. (2020). An improved state of charge and state of power estimation method based on genetic particle filter for lithium-ion batteries. *Energies*, *13*(2). https://doi.org/10.3390/en13020478

Liu, Y., He, Z., Gao, M., Li, Y., & Liu, G. (2012). Dual estimation of lithium-ion battery internal resistance and SOC based on the UKF. *2012 5th International Congress on Image and Signal Processing*, 1639–1643. https://doi.org/10.1109/CISP.2012.6469649

Liu, Zhengyu, Zhao, J., Wang, H., & Yang, C. (2020). A new lithium-ion battery SOH estimation method based on an indirect enhanced health indicator and support vector regression in PHMs. *Energies*, *13*(4). https://doi.org/10.3390/en13040830

Liu, Zhentong, & He, H. (2015). Sensor fault detection and isolation for a lithium-ion battery pack in electric vehicles using adaptive extended Kalman filter. *Applied Energy*. https://doi.org/10.1016/j.apenergy.2015.10.168

Liye Wang, Lifang Wang, Chenglin Liao, Jun Liu, Wang, L. L., Wang, L. L., Liao, C., & Liu, J. (2009). Sigma-point Kalman filter application on estimating battery SOC. *5th IEEE Vehicle Power and Propulsion Conference, VPPC '09*, *3*, 1592–1595. https://doi.org/10.1109/VPPC.2009.5289604

Lopez Sanz, J., Moreno Eguilaz, M., Alvarez-Florez, J., Ruiz-Mansilla, R., Lux, G., Kalmus, J., Graber, M., & Ocampo-Martinez, C. (2016). Nonlinear Model Predictive Control for Thermal Management in Plug-in Hybrid Electric Vehicles. *IEEE Transactions on Vehicular Technology*, *9545*(c), 1–1. https://doi.org/10.1109/TVT.2016.2597242

Lu, J., Chen, Z., Yang, Y., & Lv, M. (2018a). Online Estimation of State of Power for Lithium-Ion Batteries in Electric Vehicles Using Genetic Algorithm. *IEEE Access*, *6*, 20868–20880. https://doi.org/10.1109/ACCESS.2018.2824559

Lu, J., Chen, Z., Yang, Y., & Lv, M. (2018b). Online Estimation of State of Power for Lithium-Ion Batteries in Electric Vehicles Using Genetic Algorithm. *IEEE Access*, *6*, 20868–20880. https://doi.org/10.1109/ACCESS.2018.2824559

Lu, J., Chen, Z., Yang, Y., & Lv, M. (2018c). Online Estimation of State of Power for Lithium-Ion Batteries in Electric Vehicles Using Genetic Algorithm. *IEEE Access*, *6*, 20868–20880. https://doi.org/10.1109/ACCESS.2018.2824559

Lu, L., Han, X., Li, J., Hua, J., & Ouyang, M. (2013). A review on the key issues for lithium-ion battery management in electric vehicles. *Journal of Power Sources*, *226*, 272–288. https://doi.org/10.1016/j.jpowsour.2012.10.060

Lucu, M., Martinez-Laserna, E., Gandiaga, I., & Camblong, H. (2018). A critical review on self-adaptive Li-ion battery ageing models. *Journal of Power Sources*, *401*(May), 85–101. https://doi.org/10.1016/j.jpowsour.2018.08.064

Luo, Z., Li, Y., & Lou, Y. (2015). An adaptive kalman filter to estimate state-of-charge of lithium-ion batteries. *2015 IEEE International Conference on Information and Automation*, 1227–1232. https://doi.org/10.1109/ICInfA.2015.7279474

Ma, L., Hu, C., & Cheng, F. (2021). *State of Charge and State of Energy Estimation for Lithium-Ion Batteries Based on a Long Short-Term Memory Neural Network*. *37*(December 2020). https://doi.org/10.1016/j.est.2021.102440

Ma, Y., Duan, P., Sun, Y., & Chen, H. (2018). Equalization of Lithium-ion Battery Pack based on Fuzzy Logic Control in Electric Vehicle. *IEEE Transactions on Industrial Electronics*, *PP*(99), 1. https://doi.org/10.1109/TIE.2018.2795578

Mao, X., & Tang, X. (2014). *Battery State of Charge observer* (Patent No. US 8,922,217 B2).

Mastali, M., Vazquez-Arenas, J., Fraser, R., Fowler, M., Afshar, S., & Stevens, M. (2013). Battery state of the charge estimation using Kalman filtering. *Journal of Power Sources*, *239*, 294–307. https://doi.org/10.1016/j.jpowsour.2013.03.131

Meng, J., Luo, G., & Gao, F. (2016). Lithium Polymer Battery State-of-Charge Estimation Based on Adaptive Unscented Kalman Filter and Support Vector Machine. *IEEE Transactions on Power Electronics*, *31*(3), 2226–2238. https://doi.org/10.1109/TPEL.2015.2439578

Meng, J., Luo, G., Ricco, M., Swierczynski, M., Stroe, D.-I., & Teodorescu, R. (2018). Overview of Lithium-Ion Battery Modeling Methods for State-of-Charge Estimation in Electrical Vehicles. *Applied Sciences*, *8*(5), 659. https://doi.org/10.3390/app8050659

Meng, J., Ricco, M., Acharya, A. B., Luo, G., Swierczynski, M., Stroe, D. I., & Teodorescu, R. (2018). Low-complexity online estimation for LiFePO4battery state of charge in electric vehicles. *Journal of Power Sources*, *395*(May), 280–288. https://doi.org/10.1016/j.jpowsour.2018.05.082

Meng, J., Ricco, M., Luo, G., Swierczynski, M., Stroe, D. I., Stroe, A. I., & Teodorescu, R. (2018). An Overview and Comparison of Online Implementable SOC Estimation Methods for Lithium-Ion Battery. *IEEE Transactions on Industry Applications*, *54*(2), 1583–1591. https://doi.org/10.1109/TIA.2017.2775179

Meng, J., Stroe, D. I., Ricco, M., Luo, G., & Teodorescu, R. (2019). A simplified model-based state-of-charge estimation approach for lithium-ion battery with dynamic linear model. *IEEE Transactions on Industrial Electronics*, *66*(10), 7717–7727. https://doi.org/10.1109/TIE.2018.2880668

Mesbahi, T., Khenfri, F., Rizoug, N., Chaaban, K., Bartholomeüs, P., & Le Moigne, P. (2016). Dynamical modeling of Li-ion batteries for electric vehicle applications based on hybrid Particle Swarm–Nelder–Mead (PSO–NM) optimization algorithm. *Electric Power Systems Research*, *131*, 195–204.

https://doi.org/10.1016/j.epsr.2015.10.018

Miao, Y., Hynan, P., Von Jouanne, A., & Yokochi, A. (2019). Current li-ion battery technologies in electric vehicles and opportunities for advancements. *Energies*, *12*(6), 1–20. https://doi.org/10.3390/en12061074

Mousavi G., S. M., & Nikdel, M. (2014). Various battery models for various simulation studies and applications. *Renewable and Sustainable Energy Reviews*, *32*, 477–485. https://doi.org/10.1016/J.RSER.2014.01.048

Mu, H., Xiong, R., Zheng, H., Chang, Y., & Chen, Z. (2017). A novel fractional order model based state-of-charge estimation method for lithium-ion battery. *Applied Energy*, *207*, 384–393. https://doi.org/10.1016/J.APENERGY.2017.07.003

Nabi Akpolat, A., Yang, Y., Blaabjerg, F., Dursun, E., & Emin Kuzucuoglu, A. (2020, September 1). Li-ion-based battery pack designing and sizing for electric vehicles under different road conditions. *SEST 2020 - 3rd International Conference on Smart Energy Systems and Technologies*. https://doi.org/10.1109/SEST48500.2020.9203196

Nejad, S., Gladwin, D. T., & Stone, D. A. (2016a). A systematic review of lumped-parameter equivalent circuit models for real-time estimation of lithium-ion battery states. *Journal of Power Sources*, *316*, 183–196. https://doi.org/10.1016/J.JPOWSOUR.2016.03.042

Nejad, S., Gladwin, D. T., & Stone, D. A. (2016b). A systematic review of lumped-parameter equivalent circuit models for real-time estimation of lithium-ion battery states. *Journal of Power Sources*, *316*, 183–196. https://doi.org/10.1016/J.JPOWSOUR.2016.03.042

Newman, J., & Tiedemann, W. (1975). Porous-electrode theory with battery applications. *American Institute of Chemical Engineers*, *1*(1), 1–82. https://doi.org/10.1002/aic.690210103

Ouyang, M., Liu, G., Lu, L., Li, J., & Han, X. (2014). Enhancing the estimation accuracy in low state-of-charge area: A novel onboard battery model through surface state of charge determination. *Journal of Power Sources*, *270*, 221–237. https://doi.org/10.1016/J.JPOWSOUR.2014.07.090

Pai, K. J. (2019). A reformatory model incorporating PNGV battery and three-terminal-switch models to design and implement feedback compensations of LiFePO 4 battery chargers. *Electronics (Switzerland)*, *8*(2), 126. https://doi.org/10.3390/electronics8020126

Pan, R., Wang, Y., Zhang, X., Yang, D., & Chen, Z. (2017). Power capability prediction for lithium-ion batteries based on multiple constraints analysis. *Electrochimica Acta*, *238*, 120–133. https://doi.org/10.1016/j.electacta.2017.04.004

Panday, A., & Bansal, H. O. (2016). Energy management strategy for hybrid electric vehicles using genetic algorithm. *Journal of Renewable and Sustainable Energy*, *8*(1), 015701. https://doi.org/10.1063/1.4938552

Paolo Baruzzi, S. C., Paparrizos, G., & Garcea, G. (2013). *Battery fuel gauge* (Patent No. US 2013/0158916 A1). United States Patent Application Publication.

Park, J., Kim, K., Park, S., Baek, J., & Kim, J. (2021). Complementary Cooperative SOC/Capacity Estimator Based on the Discrete Variational Derivative Combined with the DEKF for Electric Power Applications. *Energy*, *232*, 121023. https://doi.org/10.1016/j.energy.2021.121023

Partovibakhsh, M., & Liu, G. (2012). Online estimation of model parameters and state-of-charge of Lithium-Ion battery using Unscented Kalman Filter. *American Control Conference (ACC), 2012*, 3962–3967. https://doi.org/10.1109/ACC.2012.6315272

Pathuri Bhuvana, V., Unterrieder, C., & Huemer, M. (2013). Battery Internal State Estimation: A Comparative Study of Non-Linear State Estimation Algorithms. *2013 IEEE Vehicle Power and Propulsion Conference (VPPC)*, 1–6. https://doi.org/10.1109/VPPC.2013.6671666

Pei, L., Zhu, C., Wang, T., Lu, R., & Chan, C. C. (2014). Online peak power prediction based on a parameter and state estimator for lithium-ion batteries in electric vehicles. *Energy*, *66*, 766–778. https://doi.org/10.1016/J.ENERGY.2014.02.009

Peng, S., Chen, C., Shi, H., & Yao, Z. (2017). State of charge estimation of battery energy storage systems based on adaptive unscented Kalman filter with a noise statistics estimator. *IEEE Access*, *5*, 13202–13212. https://doi.org/10.1109/ACCESS.2017.2725301

Peters, J. F., Baumann, M., Zimmermann, B., Braun, J., & Weil, M. (2017). The environmental impact of Li-Ion batteries and the role of key parameters – A review. *Renewable and Sustainable Energy Reviews*, *67*, 491–506. https://doi.org/10.1016/J.RSER.2016.08.039

Petzl, M., & Danzer, M. A. (2013). Advancements in OCV measurement and analysis for lithium-ion batteries. *IEEE Transactions on Energy Conversion*, *28*(3), 675–681. https://doi.org/10.1109/TEC.2013.2259490

Plett, G. L. (2003). *Method and apparatus for a battery state of charge estimator* (Patent No. US 6,534,954 B1).

Plett, G. L. (2004a). Extended Kalman filtering for battery management systems of LiPB-based HEV battery packs - Part 3. State and parameter estimation. *Journal of Power Sources*, *134*(2), 277–292. https://doi.org/10.1016/j.jpowsour.2004.02.033

Plett, G. L. (2004b). High-performance battery-pack power estimation using a dynamic cell model. *Vehicular Technology, IEEE Transactions On*, *53*(5), 1586–1593. https://doi.org/10.1109/TVT.2004.832408

Plett, G. L. (2004c). Extended Kalman filtering for battery management systems of LiPB-based HEV battery packs: Part 1. Background. *Journal of Power Sources*, *134*(2), 252–261. https://doi.org/10.1016/J.JPOWSOUR.2004.02.031

Plett, G. L. (2004d). Extended Kalman filtering for battery management systems of LiPB-based HEV battery packs: Part 2. Modeling and identification. *Journal of Power*

Sources, *134*(2), 262–276. https://doi.org/10.1016/J.JPOWSOUR.2004.02.032

Plett, G. L. (2004e). Extended Kalman filtering for battery management systems of LiPB-based HEV battery packs: Part 3. State and parameter estimation. *Journal of Power Sources*, *134*(2), 277–292. https://doi.org/10.1016/J.JPOWSOUR.2004.02.033

Plett, G. L. (2004f). High-performance battery-pack power estimation using a dynamic cell model. *IEEE Transactions on Vehicular Technology*, *53*(5), 1586–1593. https://doi.org/10.1109/TVT.2004.832408

Plett, G. L. (2006a). Sigma-point Kalman filtering for battery management systems of LiPB-based HEV battery packs: Part 1: Introduction and state estimation. *Journal of Power Sources*, *161*(2), 1356–1368. https://doi.org/10.1016/J.JPOWSOUR.2006.06.003

Plett, G. L. (2006b). Sigma-point Kalman filtering for battery management systems of LiPB-based HEV battery packs: Part 1: Introduction and state estimation. *Journal of Power Sources*, *161*(2), 1356–1368. https://doi.org/10.1016/J.JPOWSOUR.2006.06.003

Plett, G. L. (2006c). Sigma-point Kalman filtering for battery management systems of LiPB-based HEV battery packs: Part 2: Simultaneous state and parameter estimation. *Journal of Power Sources*, *161*(2), 1369–1384. https://doi.org/10.1016/J.JPOWSOUR.2006.06.004

Plett, G. L. (2009). *Method and system for joint battery state and parameter estimation* (Patent No. US 7,593,821 B2). United States Patent.

Plett, G. L. (2011). Recursive approximate weighted total least squares estimation of battery cell total capacity. *Journal of Power Sources*, *196*(4), 2319–2331. https://doi.org/10.1016/j.jpowsour.2010.09.048

Plett, G. L. (2012). *State and parameter estimation for an electrochemical cell* (Patent No. US 8,103,485 B2).

Pu Shi, Chunguang Bu, Yiwen Zhao, & Pu Shi. (2005). The ANN models for SOC/BRC estimation of li-ion battery. *IEEE International Conference on Information Acquisition*, 560–564. https://doi.org/10.1109/ICIA.2005.1635151

Quet, P.-F. (2014). *Battery State of Charge management method* (Patent No. US 8,635,037 B2). United States Patent.

Rahimi-Eichi, H., Baronti, F., & Chow, M. Y. (2014). Online adaptive parameter identification and state-of-charge coestimation for lithium-polymer battery cells. *IEEE Transactions on Industrial Electronics*, *61*(4), 2053–2061. https://doi.org/10.1109/TIE.2013.2263774

Rahmoun, A., Biechl, H., & Rosin, A. (2012). SOC estimation for Li-Ion batteries based on equivalent circuit diagrams and the application of a Kalman filter. *2012 Electric Power Quality and Supply Reliability*, 1–4. https://doi.org/10.1109/PQ.2012.6256238

Remmlinger, J., Buchholz, M., Soczka-Guth, T., & Dietmayer, K. (2013). On-board state-of-health monitoring of lithium-ion batteries using linear parameter-varying models. *Journal of Power Sources*, *239*, 689–695. https://doi.org/10.1016/j.jpowsour.2012.11.102

Rivera-Barrera, J., Muñoz-Galeano, N., & Sarmiento-Maldonado, H. (2017). SoC Estimation for Lithium-ion Batteries: Review and Future Challenges. *Electronics*, *6*(4), 102. https://doi.org/10.3390/electronics6040102

Riviere, E., Sari, A., Venet, P., Meniere, F., & Bultel, Y. (2019). Innovative Incremental Capacity Analysis Implementation for C/LiFePO4 Cell State-of-Health Estimation in Electrical Vehicles. *Batteries*, *5*(2), 37. https://doi.org/10.3390/batteries5020037

Romero-Becerril, A., & Alvarez-Icaza, L. (2011). Comparison of discretization methods applied to the single-particle model of lithium-ion batteries. *Journal of Power Sources*, *196*(23), 10267–10279. https://doi.org/10.1016/j.jpowsour.2011.06.091

Roscher, M. A., & Sauer, D. U. (2011). Dynamic electric behavior and open-circuit-voltage modeling of LiFePO4-based lithium ion secondary batteries. *Journal of Power Sources*, *196*(1), 331–336. https://doi.org/10.1016/J.JPOWSOUR.2010.06.098

Rzepka, B., Bischof, S., & Blank, T. (2021). Implementing an Extended Kalman Filter for SoC Estimation of a Li-Ion Battery with Hysteresis : A Step-by-Step Guide. *Energies*, *14*.

S. Grewal, M., & P. Andrews, A. (2001). Kalman Filtering: Theory and Practice Using MATLAB. In *Theory and Practice* (2nd ed.). John Wiley & Sons, Inc. https://doi.org/10.1007/1-4020-0613-6

Safwat, I. M., Li, W., & Wu, X. (2017). A Novel Methodology for Estimating State-Of-Charge of Li-Ion Batteries Using Advanced Parameters Estimation. *Energies*, *10*, 1751. https://doi.org/10.3390/en10111751

Salkind, A. J., Fennie, C., Singh, P., Atwater, T., & Reisner, D. E. (1999). Determination of state-of-charge and state-of-health of batteries by fuzzy logic methodology. *Journal of Power Sources*, *80*(1), 293–300. https://doi.org/10.1016/S0378-7753(99)00079-8

Sanguesa, J. A., Torres-Sanz, V., Garrido, P., Martinez, F. J., & Marquez-Barja, J. M. (2021). A Review on Electric Vehicles: Technologies and Challenges. *Smart Cities*, *4*(1), 372–404. https://doi.org/10.3390/smartcities4010022

Sangwan, V., Kumar, R., & Rathore, A. K. (2017). State-of-charge estimation for li-ion battery using extended Kalman filter (EKF) and central difference Kalman filter (CDKF). *2017 IEEE Industry Applications Society Annual Meeting*, 1–6. https://doi.org/10.1109/IAS.2017.8101722

Seo, B., Nguyen, T. H., Lee, D., Lee, K., & Kim, J. (2012). Condition Monitoring of Lithium Polymer Batteries Based on a Sigma-Point Kalman Filter. *Journal of Power Electronics*, *12*(5), 778–786.

Sepasi, S., Ghorbani, R., & Liaw, B. Y. (2014a). A novel on-board state-of-charge estimation method for aged Li-ion batteries based on model adaptive extended Kalman filter. *Journal of Power Sources*, *245*, 337–344. https://doi.org/10.1016/j.jpowsour.2013.06.108

Sepasi, S., Ghorbani, R., & Liaw, B. Y. (2014b). Improved extended Kalman filter for state of charge estimation of battery pack. *Journal of Power Sources*, *255*, 368–376. https://doi.org/10.1016/j.jpowsour.2013.12.093

Shao, S., Bi, J., Yang, F., & Guan, W. (2014). On-line estimation of state-of-charge of Li-ion batteries in electric vehicle using the resampling particle filter. *Transportation Research Part D: Transport and Environment*, *32*, 207–217. https://doi.org/10.1016/J.TRD.2014.07.013

Shehab El Din, M., Hussein, A. A., & Abdel-Hafez, M. F. (2018). Improved Battery SOC Estimation Accuracy Using a Modified UKF With an Adaptive Cell Model Under Real EV Operating Conditions. *IEEE Transactions on Transportation Electrification*, *4*(2), 408–417. https://doi.org/10.1109/TTE.2018.2802043

Shehab El Din, M., Hussein, A. A., Abdel-Hafez, M. F., El Din, M. S., Hussein, A. A., Abdel-Hafez, M. F., Shehab El Din, M., Hussein, A. A., & Abdel-Hafez, M. F. (2018). Improved Battery SOC Estimation Accuracy Using a Modified UKF with an Adaptive Cell Model under Real EV Operating Conditions. *IEEE Transactions on Transportation Electrification*, *4*(2), 408–417. https://doi.org/10.1109/TTE.2018.2802043

Shen, P., Ouyang, M., Han, X., Feng, X., Lu, L., & Li, J. (2018). Error Analysis of the Model-Based State-of-Charge Observer for Lithium-Ion Batteries. *IEEE Transactions on Vehicular Technology*, *67*(9), 8055–8064. https://doi.org/10.1109/TVT.2018.2842820

Shen, P., Ouyang, M., Lu, L., Li, J., & Feng, X. (2018). The co-estimation of state of charge, state of health, and state of function for lithium-ion batteries in electric vehicles. *IEEE Transactions on Vehicular Technology*, *67*(1), 92–103. https://doi.org/10.1109/TVT.2017.2751613

Shen, Y. (2018). Adaptive extended Kalman filter based state of charge determination for lithium-ion batteries. *Electrochimica Acta*, *283*, 1432–1440. https://doi.org/10.1016/J.ELECTACTA.2018.07.078

Sheng, H., & Xiao, J. (2015). Electric vehicle state of charge estimation: Nonlinear correlation and fuzzy support vector machine. *Journal of Power Sources*, *281*, 131–137. https://doi.org/10.1016/J.JPOWSOUR.2015.01.145

Shi, Q.-S., Zhang, C.-H., & Cui, N.-X. (2008). Estimation of battery state-of-charge using ν-support vector regression algorithm. *International Journal of Automotive Technology*, *9*(6), 759–764. https://doi.org/10.1007/s12239-008-0090-x

Singh, P., Vinjamuri, R., Wang, X., & Reisner, D. (2006). Design and implementation of a fuzzy logic-based state-of-charge meter for Li-ion batteries used in portable defibrillators. *Journal of Power Sources*, *162*(2), 829–836. https://doi.org/10.1016/J.JPOWSOUR.2005.04.039

Smith, K. A. (2006). *Electrochemical Modeling, Estimation and Control of Lithium Ion Batteries* [The Pennsylvania State University]. https://etda.libraries.psu.edu/catalog/7376

Smith, K. A., Rahn, C. D., & Wang, C.-Y. (2007). Control oriented 1D electrochemical model of lithium ion battery. *Energy Conversion and Management*, *48*(9), 2565–2578. https://doi.org/10.1016/J.ENCONMAN.2007.03.015

Song, Z., Hou, J., Li, X., Wu, X., Hu, X., Hofmann, H., & Sun, J. (2020). The sequential algorithm for combined state of charge and state of health estimation of lithium-ion battery based on active current injection. *Energy*, *193*. https://doi.org/10.1016/j.energy.2019.116732

Stetzel, K. D., Aldrich, L. L., Trimboli, M. S., & Plett, G. L. (2015). Electrochemical state and internal variables estimation using a reduced-order physics-based model of a lithium-ion cell and an extended Kalman filter. *Journal of Power Sources*, *278*, 490–505. https://doi.org/10.1016/J.JPOWSOUR.2014.11.135

Sun, F., Xiong, R., & He, H. (2014). Estimation of state-of-charge and state-of-power capability of lithium-ion battery considering varying health conditions. *Journal of Power Sources*, *259*, 166–176. https://doi.org/10.1016/J.JPOWSOUR.2014.02.095

Sun, X., Ji, J., Ren, B., Xie, C., & Yan, D. (2019). Adaptive Forgetting Factor Recursive Least Square Algorithm for Online Identification of Equivalent Circuit Model Parameters of a Lithium-Ion Battery. *Energies*, *12*(12), 2242. https://doi.org/10.3390/en12122242

Tagade, P., Hariharan, K. S., Gambhire, P., Kolake, S. M., Song, T., Oh, D., Yeo, T., & Doo, S. (2016). Recursive Bayesian filtering framework for lithium-ion cell state estimation. *Journal of Power Sources*, *306*, 274–288. https://doi.org/10.1016/J.JPOWSOUR.2015.12.012

Tan, X., Zhan, D., Lyu, P., Rao, J., & Fan, Y. (2021). Online state-of-health estimation of lithium-ion battery based on dynamic parameter identification at multi timescale and support vector regression. *Journal of Power Sources*, *484*, 229233. https://doi.org/10.1016/j.jpowsour.2020.229233

Tanachutiwat, S., Wang, W., & Liu, M. (2010). Cubature Kalman Filtering for Continuous-Discrete. *IEEE TRANSACTIONS ON SIGNAL PROCESSING*, *58*(10), 4977–4993.

Tang, X., Zhang, Y., Baughman, A. C., Koch, B. J., Lin, J., & Frisch, D. R. (2013). *Dynamic Battery Capacity Estimation* (Patent No. US 8,560,257 B2). United States Patent. US 8,560,257 B2

This Is the Dawning of the Age of the Battery - Bloomberg. (n.d.). Retrieved May 15, 2021, from https://www.bloomberg.com/news/articles/2020-12-17/this-is-the-dawning-of-the-age-of-the-battery?srnd=green

Tian, Yong, Rusheng Yan, Jindong Tian, Shijie Zhou, C. H. (2017). Online Estimation of Model Parameters of Lithium- Ion Battery Using the Cubature Kalman Filter. *IOP Conf. Series: Earth and Environmental Science 94*. https://doi.org/10.1088/1755-

1315/94/1/012051

Tong, S., Lacap, J. H., & Park, J. W. (2016). Battery state of charge estimation using a load-classifying neural network. *Journal of Energy Storage*, *7*, 236–243. https://doi.org/10.1016/J.EST.2016.07.002

Topan, P. A., Ramadan, M. N., Fathoni, G., Cahyadi, A. I., & Wahyunggoro, O. (2016). State of Charge (SOC) and State of Health (SOH) estimation on lithium polymer battery via Kalman filter. *2016 2nd International Conference on Science and Technology-Computer (ICST)*, 93–96. https://doi.org/10.1109/ICSTC.2016.7877354

Vaidya, V. G., & Kancharla, T. (2014). *System and Method for Battery Monitoring* (Patent No. US 20140232411A1).

Valade, A., Acco, P., Grabolosa, P., & Fourniols, J. Y. (2017). A study about kalman filters applied to embedded sensors. *Sensors (Switzerland)*, *17*(12), 1–18. https://doi.org/10.3390/s17122810

Valdez, G., & Angel, M. (2016). *Battery Condition Monitoring* (Patent No. PCT/EP2015/073808). World Intellectual Property Organization.

Van der Merwe, R., & Wan, E. A. (2001). The square-root unscented Kalman filter for state and parameter-estimation. *2001 IEEE International Conference on Acoustics, Speech, and Signal Processing. Proceedings (Cat. No.01CH37221)*, *6*, 3461–3464. https://doi.org/10.1109/ICASSP.2001.940586

Waag, W., Fleischer, C., & Sauer, D. U. (2014). Critical review of the methods for monitoring of lithium-ion batteries in electric and hybrid vehicles. *Journal of Power Sources*, *258*, 321–339. https://doi.org/10.1016/J.JPOWSOUR.2014.02.064

Waag, W., Käbitz, S., & Sauer, D. U. (2013). Application-specific parameterization of reduced order equivalent circuit battery models for improved accuracy at dynamic load. *Measurement*, *46*(10), 4085–4093. https://doi.org/10.1016/J.MEASUREMENT.2013.07.025

Waag, W., & Sauer, D. U. (2013). Adaptive estimation of the electromotive force of the lithium-ion battery after current interruption for an accurate state-of-charge and capacity determination. *Applied Energy*, *111*, 416–427. https://doi.org/10.1016/J.APENERGY.2013.05.001

Wang, B. J., Liu, Z. Y., Li, S. E., Moura, S. J., & Peng, H. E. (2017). State-of-Charge Estimation for Lithium-Ion Batteries Based on a Nonlinear Fractional Model. *IEEE Transactions on Control Systems Technology*, *25*(1), 3–11. https://doi.org/10.1109/tcst.2016.2557221

Wang, B., Li, S. E., Peng, H., & Liu, Z. (2015). Fractional-order modeling and parameter identification for lithium-ion batteries. *Journal of Power Sources*, *293*, 151–161. https://doi.org/10.1016/J.JPOWSOUR.2015.05.059

Wang, C. Y., Gu, W. B., & Liaw, B. Y. (1998). Micro-Macroscopic Coupled Modeling of Batteries and Fuel Cells. *Journal of The Electrochemical Society*, *145*(10), 3407.

https://doi.org/10.1149/1.1838820

Wang, Qian, Jiang, B., Li, B., & Yan, Y. (2016). A critical review of thermal management models and solutions of lithium-ion batteries for the development of pure electric vehicles. *Renewable and Sustainable Energy Reviews*, *64*, 106–128. https://doi.org/10.1016/j.rser.2016.05.033

Wang, Qianqian, Kang, J., Tan, Z., & Luo, M. (2018). Electrochimica Acta An online method to simultaneously identify the parameters and estimate states for lithium ion batteries. *Electrochimica Acta*, *289*, 376–388. https://doi.org/10.1016/j.electacta.2018.08.076

Wang, Qianqian, Wang, J., Zhao, P., Kang, J., Yan, F., & Du, C. (2017). Correlation between the model accuracy and model-based SOC estimation. *Electrochimica Acta*, *228*, 146–159. https://doi.org/10.1016/j.electacta.2017.01.057

Wang, S., Verbrugge, M., Wang, J. S., & Liu, P. (2012). Power prediction from a battery state estimator that incorporates diffusion resistance. *Journal of Power Sources*, *214*, 399–406. https://doi.org/10.1016/J.JPOWSOUR.2012.04.070

Wang, W., Wang, X., Xiang, C., Wei, C., & Zhao, Y. (2018). Unscented Kalman Filter-based Battery SOC Estimation and Peak Power Prediction Method for Power Distribution of Hybrid Electric Vehicles. *IEEE Access*, *6*, 35957–35965. https://doi.org/10.1109/ACCESS.2018.2850743

Wang, Y., Tian, J., Sun, Z., Wang, L., Xu, R., Li, M., & Chen, Z. (2020). A comprehensive review of battery modeling and state estimation approaches for advanced battery management systems. In *Renewable and Sustainable Energy Reviews* (Vol. 131, p. 110015). Elsevier Ltd. https://doi.org/10.1016/j.rser.2020.110015

Wang, Y., Zhang, C., & Chen, Z. (2015). A method for state-of-charge estimation of LiFePO4 batteries at dynamic currents and temperatures using particle filter. *Journal of Power Sources*, *279*, 306–311. https://doi.org/10.1016/J.JPOWSOUR.2015.01.005

Wang, Y., Zhang, C., & Chen, Z. (2016). Model-based state-of-energy estimation of lithium-ion batteries in electric vehicles. *Energy Procedia*, *88*, 998–1004. https://doi.org/10.1016/j.egypro.2016.06.125

Wang, Z., Ma, J., & Zhang, L. (2017). State-of-Health Estimation for Lithium-Ion Batteries Based on the Multi-Island Genetic Algorithm and the Gaussian Process Regression. *IEEE Access*, *5*, 21286–21295. https://doi.org/10.1109/ACCESS.2017.2759094

Wassiliadis, N., Adermann, J., Frericks, A., Pak, M., Reiter, C., Lohmann, B., & Lienkamp, M. (2018). Revisiting the dual extended Kalman fi lter for battery state-of-charge and state-of-health estimation : A use-case life cycle analysis. *Journal of Energy Storage*, *19*(July), 73–87. https://doi.org/10.1016/j.est.2018.07.006

Wei, Z., Zhao, J., Zou, C., Mariana, T., & Jet, K. (2018). Comparative study of methods for integrated model identi fi cation and state of charge estimation of lithium-ion

battery. *Journal of Power Sources*, *402*(September), 189–197. https://doi.org/10.1016/j.jpowsour.2018.09.034

Weigert, T., Tian, Q., & Lian, K. (2011). State-of-charge prediction of batteries and battery-supercapacitor hybrids using artificial neural networks. *Journal of Power Sources*, *196*(8), 4061–4066. https://doi.org/10.1016/j.jpowsour.2010.10.075

Westerhoff, U., Kurbach, K., Lienesch, F., & Kurrat, M. (2016). Analysis of Lithium-Ion Battery Models Based on Electrochemical Impedance Spectroscopy. *Energy Technology*, *4*(12), 1620–1630. https://doi.org/10.1002/ente.201600154

Wijewardana, S., Vepa, R., & Shaheed, M. H. (2016). Dynamic battery cell model and state of charge estimation. *Journal of Power Sources*, *308*, 109–120. https://doi.org/10.1016/J.JPOWSOUR.2016.01.072

Won, N., Seok, Y. H., Young-Jo, L., Jabbo, & Seok-suk, C. (2006). *The method of assuming the state of charge of the battery, battery management system using the method and the driving method of the battery management system using the method* (Patent No. KR100804698B1).

Wu, B., Yufit, V., Marinescu, M., Offer, G. J., Martinez-Botas, R. F., & Brandon, N. P. (2013). Coupled thermal–electrochemical modelling of uneven heat generation in lithium-ion battery packs. *Journal of Power Sources*, *243*, 544–554. https://doi.org/10.1016/J.JPOWSOUR.2013.05.164

Xia, B., Lao, Z., Zhang, R., Tian, Y., Id, G. C., Id, Z. S., Wang, W., Sun, W., Lai, Y., Wang, M., & Wang, H. (2018). Online Parameter Identification and State of Charge Estimation of Lithium-Ion Batteries Based Nonlinear Kalman Filter. *Energies*, *11*, 3. https://doi.org/10.3390/en11010003

Xia, B., Sun, Z., Zhang, R., & Lao, Z. (2017). A cubature particle filter algorithm to estimate the state of the charge of lithium-ion batteries based on a second-order equivalent circuit model. *Energies*, *10*(4). https://doi.org/10.3390/en10040457

Xia, B., Wang, H., Tian, Y., Wang, M., Sun, W., & Xu, Z. (2015). State of charge estimation of lithium-ion batteries using an Adaptive Cubature Kalman filter. *Energies*, *8*(6), 5916–5936. https://doi.org/10.3390/en8065916

Xia, B., Wang, H., Wang, M., Sun, W., Xu, Z., & Lai, Y. (2015). A new method for state of charge estimation of lithium-ion battery based on strong tracking cubature kalman filter. *Energies*, *8*(12), 13458–13472. https://doi.org/10.3390/en81212378

Xiaojun Tang, Xiaobei Zhao, & Xubin Zhang. (2008). The square-root spherical simplex unscented Kalman filter for state and parameter estimation. *2001 IEEE International Conference on Acoustics, Speech, and Signal Processing. Proceedings (Cat. No.01CH37221)*, 260–263. https://doi.org/10.1109/ICOSP.2008.4697120

Xing, Y., Ma, E. W. M., Tsui, K. L., & Pecht, M. (2011). Battery management systems in electric and hybrid vehicles. *Energies*, *4*(11), 1840–1857. https://doi.org/10.3390/en4111840

Xiong, R, Cao, J., Yu, Q., He, H., & Sun, F. (2018). Critical Review on the Battery State

of Charge Estimation Methods for Electric Vehicles. *IEEE Access*, *6*, 1832–1843. https://doi.org/10.1109/ACCESS.2017.2780258

Xiong, Rui, He, H., Sun, F., Liu, X., & Liu, Z. (2013). Model-based state of charge and peak power capability joint estimation of lithium-ion battery in plug-in hybrid electric vehicles. *Journal of Power Sources*, *229*, 159–169. https://doi.org/10.1016/J.JPOWSOUR.2012.12.003

Xiong, Rui, He, H., Sun, F., & Zhao, K. (2013). Evaluation on State of Charge estimation of batteries with adaptive extended kalman filter by experiment approach. *IEEE Transactions on Vehicular Technology*, *62*(1), 108–117. https://doi.org/10.1109/TVT.2012.2222684

Xiong, Rui, Sun, F., He, H., & Nguyen, T. D. (2013). A data-driven adaptive state of charge and power capability joint estimator of lithium-ion polymer battery used in electric vehicles. *Energy*, *63*, 295–308. https://doi.org/10.1016/J.ENERGY.2013.10.027

Yang, J., Xia, B., Huang, W., Fu, Y., & Mi, C. (2018). Online state-of-health estimation for lithium-ion batteries using constant-voltage charging current analysis. *Applied Energy*, *212*, 1589–1600. https://doi.org/10.1016/J.APENERGY.2018.01.010

Yang, L., Cai, Y., Yang, Y., & Deng, Z. (2020). Supervisory long-term prediction of state of available power for lithium-ion batteries in electric vehicles. *Applied Energy*, *257*(August 2019), 114006. https://doi.org/10.1016/j.apenergy.2019.114006

Yang, Q., Xu, J., Cao, B., & Li, X. (2017). A simplified fractional order impedance model and parameter identification method for lithium-ion batteries. *PLOS ONE*, *12*(2), 1–13. https://doi.org/10.1371/journal.pone.0172424

Yang, S., Deng, C., Zhang, Y., & He, Y. (2017). State of charge estimation for lithium-ion battery with a temperature-compensated model. *Energies*, *10*(10). https://doi.org/10.3390/en10101560

Ying Shi, Prasad, G., Zheng Shen, & Rahn, C. D. (2011). Discretization methods for battery systems modeling. *2011 American Control Conference*, *4*, 356–361. https://doi.org/10.1109/acc.2011.5990857

Yu, Q., Member, S., Xiong, R., Member, S., & Lin, C. (2017). *Lithium-Ion Battery Parameters and State-of-Charge Joint Estimation Based on H-Infinity and Unscented Kalman Filters*. *66*(10), 8693–8701.

Yu, Z., Huai, R., & Xiao, L. (2015). State-of-charge estimation for lithium-ion batteries using a Kalman filter based on local linearization. *Energies*, *8*(8), 7854–7873. https://doi.org/10.3390/en8087854

Zenati, A., Desprez, P., & Razik, H. (2010). Estimation of the SOC and the SOH of Li-ion batteries, by combining impedance measurements with the fuzzy logic inference. *IEEE IECON*, 1773–1778. https://doi.org/10.1109/IECON.2010.5675408

Zeng, M., Zhang, P., Yang, Y., Xie, C., & Shi, Y. (2019). SOC and SOH joint estimation of the power batteries based on fuzzy unscented Kalman filtering algorithm.

Energies, *12*(16). https://doi.org/10.3390/en12163122

Zeng, Z., Tian, J., Li, D., & Tian, Y. (2018). An online state of charge estimation algorithm for lithium-ion batteries using an improved adaptive Cubature Kalman filter. *Energies*, *11*(1), 59. https://doi.org/10.3390/en11010059

Zhang, Caiping, Jiang, J., Zhang, L., Liu, S., Wang, L., & Loh, P. (2016). A Generalized SOC-OCV Model for Lithium-Ion Batteries and the SOC Estimation for LNMCO Battery. *Energies*, *9*(11), 900. https://doi.org/10.3390/en9110900

Zhang, Cheng, Allafi, W., Dinh, Q., Ascencio, P., & Marco, J. (2018). Online estimation of battery equivalent circuit model parameters and state of charge using decoupled least squares technique. *Energy*, *142*, 678–688. https://doi.org/10.1016/J.ENERGY.2017.10.043

Zhang, Li, Li, K., Du, D., Fei, M., & Li, X. (2017). *State-of-Charge Estimation of Lithium Batteries Using Compact RBF Networks and AUKF* (pp. 396–405). https://doi.org/10.1007/978-981-10-6364-0_40

Zhang, Linchao, & Chen, C. (2011). Electrode materials for lithium ion battery. *Progress in Chemistry*, *23*(2–3), 275–283. https://doi.org/10.1016/j.mset.2018.08.001

Zhang, R., Xia, B., Li, B., Cao, L., Lai, Y., & Zheng, W. (2018a). A Study on the Open Circuit Voltage and State of Charge Characterization of High Capacity Lithium-Ion Battery Under Different Temperature. *Energies*, *11*, 2408. https://doi.org/10.3390/en11092408

Zhang, R., Xia, B., Li, B., Cao, L., Lai, Y., Zheng, W., Wang, H., & Wang, W. (2018b). State of the Art of Lithium-Ion Battery SOC Estimation for Electrical Vehicles. *Energies*, *11*(7), 1820. https://doi.org/10.3390/en11071820

Zhang, S., Guo, X., Dou, X., & Zhang, X. (2020). A rapid online calculation method for state of health of lithium-ion battery based on coulomb counting method and differential voltage analysis. *Journal of Power Sources*, *479*(August), 228740. https://doi.org/10.1016/j.jpowsour.2020.228740

Zhang, S., & Zhang, X. (2021a). Joint estimation method for maximum available energy and state-of-energy of lithium-ion battery under various temperatures. *Journal of Power Sources*, *506*(May), 230132. https://doi.org/10.1016/j.jpowsour.2021.230132

Zhang, S., & Zhang, X. (2021b). A multi time-scale framework for state-of-charge and capacity estimation of lithium-ion battery under optimal operating temperature range. *Journal of Energy Storage*, *35*, 102325. https://doi.org/10.1016/j.est.2021.102325

Zhang, W., Shi, W., & Ma, Z. (2015a). Adaptive unscented Kalman filter based state of energy and power capability estimation approach for lithium-ion battery. *Journal of Power Sources*, *289*, 50–62. https://doi.org/10.1016/J.JPOWSOUR.2015.04.148

Zhang, W., Shi, W., & Ma, Z. (2015b). Adaptive unscented Kalman filter based state of energy and power capability estimation approach for lithium-ion battery. *Journal of*

Power Sources, *289*, 50–62. https://doi.org/10.1016/J.JPOWSOUR.2015.04.148

Zhang, Xiaoqiang, Zhang, W., & Lei, G. (2016). A Review of Li-ion Battery Equivalent Circuit Models. *TRANSACTIONS ON ELECTRICAL AND ELECTRONIC MATERIALS*, *17*(6), 311–316.

Zhang, Xu, Wang, Y., Liu, C., & Chen, Z. (2018). A novel approach of battery pack state of health estimation using artificial intelligence optimization algorithm. *Journal of Power Sources*, *376*, 191–199. https://doi.org/10.1016/J.JPOWSOUR.2017.11.068

Zhang, Xu, Wang, Y., Wu, J., & Chen, Z. (2018). A novel method for lithium-ion battery state of energy and state of power estimation based on multi-time-scale filter. *Applied Energy*, *216*, 442–451. https://doi.org/10.1016/J.APENERGY.2018.02.117

Zhang, Xu, Wang, Y., Yang, D., & Chen, Z. (2016). An on-line estimation of battery pack parameters and state-of-charge using dual fi lters based on pack model. *Energy*, *115*, 219–229. https://doi.org/10.1016/j.energy.2016.08.109

Zhang, Yongzhi, Xiong, R., He, H., & Shen, W. (2017). Lithium-Ion Battery Pack State of Charge and State of Energy Estimation Algorithms Using a Hardware-in-the-Loop Validation. *IEEE Transactions on Power Electronics*, *32*(6), 4421–4431. https://doi.org/10.1109/TPEL.2016.2603229

Zhang, Yun, Shang, Y., Cui, N., & Zhang, C. (2017). Parameters Identification and Sensitive Characteristics Analysis for Lithium-Ion Batteries of Electric Vehicles. *Energies*, *11*(1), 19. https://doi.org/10.3390/en11010019

Zhang, Yun, Shang, Y., Cui, N., & Zhang, C. (2018). Parameters Identification and Sensitive Characteristics Analysis for Lithium-Ion Batteries of Electric Vehicles. *Energies*, *11*, 19. https://doi.org/10.3390/en11010019

Zhang, Z., Jiang, L., Zhang, L., & Huang, C. (2021). State-of-charge estimation of lithium-ion battery pack by using an adaptive extended Kalman filter for electric vehicles. *Journal of Energy Storage*, *37*, 102457. https://doi.org/10.1016/J.EST.2021.102457

Zhao, L., Xu, G., Li, W., Taimoor, Z., & Song, Z. (2013). LiFePO4 battery pack capacity estimation for electric vehicles based on unscented Kalman filter. *2013 IEEE International Conference on Information and Automation (ICIA)*, 301–305. https://doi.org/10.1109/ICInfA.2013.6720314

Zhao, Y., Xu, J., Wang, X., & Mei, X. (2018). The Adaptive Fading Extended Kalman Filter SOC Estimation Method for Lithium-ion Batteries. *Energy Procedia*, *145*, 357–362. https://doi.org/10.1016/J.EGYPRO.2018.04.064

Zheng, L., Zhu, J., Wang, G., He, T., & Wei, Y. (2016a). Novel methods for estimating lithium-ion battery state of energy and maximum available energy. *Applied Energy*, *178*, 1–8. https://doi.org/10.1016/j.apenergy.2016.06.031

Zheng, L., Zhu, J., Wang, G., He, T., & Wei, Y. (2016b). Novel methods for estimating lithium-ion battery state of energy and maximum available energy. *Applied Energy*, *178*, 1–8. https://doi.org/10.1016/j.apenergy.2016.06.031

Zheng, Y., Ouyang, M., Han, X., Lu, L., & Li, J. (2018). Investigating the error sources of the online state of charge estimation methods for lithium-ion batteries in electric vehicles. *Journal of Power Sources*, *377*, 161–188. https://doi.org/10.1016/J.JPOWSOUR.2017.11.094

Zhong, Q., Li, B., Li, H., & Zhao, Y. (2014). *System and method for SOC estimation of a battery* (Patent No. US 2014/0316728 A1).

Zhu, R., Duan, B., Zhang, J., Zhang, Q., & Zhang, C. (2020). Co-estimation of model parameters and state-of-charge for lithium-ion batteries with recursive restricted total least squares and unscented Kalman filter. *Applied Energy*, *277*(July), 115494. https://doi.org/10.1016/j.apenergy.2020.115494

Zou, C., Zhang, L., Hu, X., Wang, Z., Wik, T., & Pecht, M. (2018). A review of fractional-order techniques applied to lithium-ion batteries, lead-acid batteries, and supercapacitors. *Journal of Power Sources*, *390*, 286–296. https://doi.org/10.1016/J.JPOWSOUR.2018.04.033

Zou, Y., Hu, X., Ma, H., & Eben Li, S. (2015). Combined State of Charge and State of Health estimation over lithium-ion battery cell cycle lifespan for electric vehicles. *Journal of Power Sources*, *273*, 793–803. https://doi.org/10.1016/j.jpowsour.2014.09.146

Zou, Y., Hu, X., Ma, H., & Li, S. E. (2015). Combined State of Charge and State of Health estimation over lithium-ion battery cell cycle lifespan for electric vehicles. *Journal of Power Sources*, *273*, 793–803. https://doi.org/10.1016/j.jpowsour.2014.09.146

Zubi, G., Dufo-López, R., Carvalho, M., & Pasaoglu, G. (2018). The lithium-ion battery: State of the art and future perspectives. *Renewable and Sustainable Energy Reviews*, *89*, 292–308. https://doi.org/10.1016/j.rser.2018.03.002